Journal of the Serbian Chemical Society

Available on line at

СХД
1897

www.shd.org.rs/JSCS/

CONTENTS

Available online at shd.org.rs/JSCS/

Polystyrene-supported pyridinium chloroaluminate ionic liquid as a new heterogeneous Lewis acid catalyst for selective synthesis of benzimidazoles

KAVEH PARVANAK BOROUJENI*, ASHKAN ZHIANINASAB
and MINA JAFARINASAB

Department of Chemistry, Shahrekord University, Shahrekord 115, Iran

Abstract: Polystyrene-supported pyridinium chloroaluminate ionic liquid was prepared from the reaction of a Merrifield resin with pyridine followed by reaction with aluminium chloride. This catalyst was used as a new chemo-selective Lewis acid catalyst for the exclusive synthesis of 2-substituted benzimidazoles from the reaction of aldehydes with *o*-phenylenediamines. The catalyst was stable (as a benchtop catalyst) and could easily be recovered and re-used without appreciable change in its efficiency.

Keywords: ionic liquids; chloroaluminate salts; heterogeneous catalysis; polymer-supported ionic liquids; benzimidazoles.

INTRODUCTION

The most common group of ionic liquids (ILs) are chloroaluminate molten salts.[1–3] These compounds, composed of mixtures of aluminium chloride with the corresponding 1,3-dialkylimidazolium or 1-alkylpyridinium chlorides, are liquid at or below ambient temperature over a wide range of compositions. The acidity of the resulting IL can be controlled by varying the relative amounts of $AlCl_3$ and organic chloride. Chloroaluminate melts are designated as basic when the $AlCl_3$ mole fraction is smaller than 0.5 and the melts contain Cl^- and $AlCl_4^-$, a Lewis bases. A melt having an $AlCl_3$ mole fraction of exactly 0.5, where $AlCl_4^-$ is the only anion present, is referred to as a neutral melt. Finally, an acidic chloroaluminate melt is one in which the $AlCl_3$ mole fraction is larger than 0.5. In such acidic melts, $Al_2Cl_7^-$ and $Al_3Cl_{10}^-$ exist, which act as very strong Lewis acids.[2]

Despite the unique physical and chemical properties of chloroaluminate ILs and their widespread application in organic synthesis, either as solvents or acidic

---

catalysts, most of them suffer from one or more of the following drawbacks such as laborious work-up procedures, difficulty in recovery and recycling, disposal of spent catalyst, difficulty in handling and corrosion problems. Most importantly, they are extremely hygroscopic and labile towards hydrolysis.[2] Thus, these shortcomings make them a prime target for heterogenization. Although there are several reports on the immobilization of ILs on solid supports,[4−13] to the best of our knowledge, few examples are known for immobilized chloroaluminate ILs.[9,12]

The benzimidazole and its derivatives constitute a very important, privileged class of nitrogen-containing heterocyclic compounds that show various biological activities, such as anticonvulsant,[14] antidepressant,[15] antihistamine,[16] anti-ulcer,[17] antihypertensive,[18] anticancer,[19] anti-inflammatory,[20] anthelmintic,[21] antiprotozoal[22] and antitumour properties.[23] In addition, benzimidazoles are very important intermediates in organic reactions.[24] Therefore, their preparations have received increasing attention of synthetic organic chemists and biologists. Usually, two different approaches have been performed for the preparation of benzimidazoles. The first is the coupling of *o*-phenylenediamines and carboxylic acids or their derivatives (nitriles, amides, orthoesters and acid chlorides), which often requires strongly acidic conditions, sometimes combined with high temperatures.[25−28] Another synthetic approach is the condensation of aldehydes with *o*-phenylenediamines, which involves a two-step procedure including the oxidative cyclodehydration of aniline Schiff bases, which are often generated *in situ* from the reaction of an aldehyde and *o*-phenylenediamine. Various oxidative and catalytic reagents, such as $Yb(OTf)_3$,[29] $I_2/KI/K_2CO_3$,[30] $In(OTf)_3$,[31] $BF_3 \cdot OEt_2$,[32] H_2O_2/HCl,[33] $TsOH–SiO_2$,[34] NaY zeolite,[35] porphyrinatoiron(III) complex supported on silica,[36] Dess–Martin-periodinane,[37] scolecite,[38] AIKIT-5,[39] $WO_x//ZrO_2$,[40] $H_2O_2/SiO_2–FeCl_3$[41] and Amberlite IR-120[42] have been employed for this purpose. However, many of the above methods suffer from drawbacks such as strong oxidizing nature, the formation of bis-anil and dihydrobenzimidazoles as the main side products, involvement of more than one step in the synthesis of these compounds, the generation of environmentally perilous waste material, tedious work-up, long reaction times, complicated operations and the use of moisture-sensitive, expensive, hazardous, difficult to handle or non-reusable catalysts. In view of these, the search for finding a cost effective, mild and simple chemoselective protocol especially using heterogeneous catalysts for the synthesis of benzimidazoles is still relevant.

In 2001, Hölderich *et al.* reported the synthesis and application of silica gel supported chloroaluminate IL as a heterogeneous Lewis acidic IL.[12] This supported IL was prepared by adding $AlCl_3$ to imidazolium chloride grafted onto the silica surface. The prepared catalyst was used for Friedel-Crafts alkylations. Unfortunately, this catalyst is moisture sensitive and hence demands moisture-free reactants and also must be handled under a dry atmosphere. Hölderich suggested

that the predominant acidic chloroaluminate species in this immobilized IL was $Al_2Cl_7^-$.

In a continuation of research work on the development of synthetic methodologies using solid acid catalysts, herein, the above-mentioned strategy to support pyridinium chloroaluminate IL on a Merrifield resin, and the employment of the obtained polymer catalyst as an effective and highly chemoselective heterogeneous catalyst for the coupling of aldehydes and *o*-phenylenediamines to afford 2-aryl and alkylbenzimidazoles (Scheme 1) are reported.

R_1= Alkyl or Aryl
R_2= H or Me
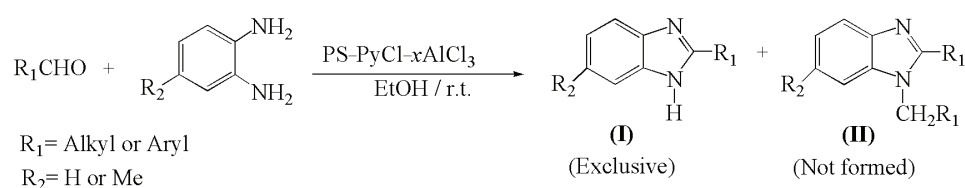
Scheme 1. The coupling reaction of aldehydes and *o*-phenylenediamines to afford 2-aryl and alkyl benzimidazoles, catalyzed by pyridinium chloroaluminate IL supported on a Merrifield resin.

EXPERIMENTAL

Chemicals were either laboratory prepared or purchased from Merck or Fluka. The IR spectra were run on a Shimadzu model 8300 FT-IR spectrophotometer. The ^{1}H-NMR spectra were recorded on a Bruker DPX-300 spectrometer using DMSO-d_6 as solvent and TMS as the internal standard. Melting points were determined on a Fisher–Jones melting-point apparatus and are uncorrected. The capacity of the catalyst was determined by the atomic absorption technique using a Philips atomic absorption instrument. Monitoring of the reaction progress and purity determination of the products were accomplished by GLC or TLC on silica-gel polygram SILG/UV$_{254}$ plates.

Preparation of poly[styrene-co-1-((4-vinylphenyl)methyl)pyridinium chloroaluminate] (PS–PyCl–xAlCl$_3$)

In a round bottomed flask (50 mL) equipped with a reflux condenser, a solution of Merrifield resin (1 g, 2 % divinylbenzene) in pyridine (25 mL) was refluxed for 48 h. Afterwards, the mixture was filtered, washed with distilled water (20 mL) and dried at 80 °C overnight. Then, 1 g of the obtained resin was added to a solution of AlCl$_3$ (0.5 g) in toluene (10 mL) and stirred under reflux condition for 24 h under an N$_2$ atmosphere. Next, AlCl$_3$ (0.4 g) was added again and the mixture was stirred for 24 h and filtered and then the excess of AlCl$_3$ was removed by extraction with ethanol using a Soxhlet apparatus.

Typical procedure for benzimidazole synthesis

To a solution of aldehyde (1 mmol) and *o*-phenylenediamine (1 mmol) in ethanol (5 mL) was added PS–PyCl–xAlCl$_3$ (0.1 mmol), and the resulting mixture was magnetically stirred at room temperature. The progress of the reaction was monitored by TLC. After completion of the reaction, the catalyst was filtered off and washed with EtOH (2×5 mL) and the filtrate was concentrated on a rotary evaporator under reduced pressure to afford the crude product. Whenever required, the products were purified by column chromatography on silica gel (*n*-hexane/EtOAc) or recrystallization from ethanol. The spent catalyst from different experi-

ments was washed with EtOH and reused without further drying. The analytical and spectral data of the obtained compounds are given in the Supplementary material to this paper.

RESULTS AND DISCUSSION

Poly[styrene-*co*-1-((4-vinylphenyl)methyl)pyridinium chloroaluminate], denoted as PS–PyCl–xAlCl$_3$, was prepared by the procedure shown in Scheme 2. In the first stage, commercially available Merrifield resin (2 % divinylbenzene, 2.1 mmol Cl per gram) was reacted with pyridine to give poly[styrene-*co*-1-((4-vinylphenyl)methyl)pyridinium chloride], denoted as PS–PyCl. The obtained material was a cream solid which was analyzed by elemental analysis to quantify the percentage loading of the pyridinium moiety by measuring the nitrogen content, giving 1.89 mmol Py per gram. The PS–PyCl was further treated with excess amounts of AlCl$_3$ in refluxing toluene to form PS–PyCl–xAlCl$_3$. The resulting pale brown solid was reasonably stable to air and moisture and could be kept as a bench-top catalyst for more than 1 year without appreciable change in its efficiency. It is believed that the hydrophobic nature of the polystyrene protects the water-sensitive Lewis acid from hydrolysis by atmospheric moisture until it is suspended in an appropriate solvent where it can be used in a chemical reaction. The atomic absorption technique gave 3.3 mmol Al per g of the catalyst. Considering the aluminium and pyridine contents of PS–PyCl–xAlCl$_3$, it is clear that the AlCl$_3$ mole fraction (AlCl$_3$/AlCl$_3$+Py) in this catalyst was larger than 0.5 and thus it could be imagined that it is the Lewis acid Al$_2$Cl$_7^-$ (as the predominant aluminium species) that plays an important role in the catalytic activity in PS––PyCl–xAlCl$_3$.[2,12]
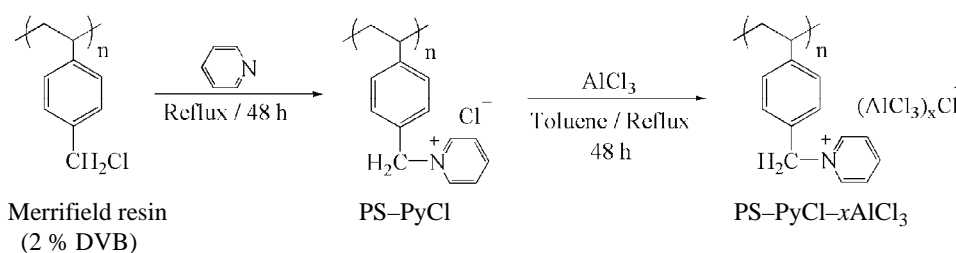
Scheme 2. Preparation procedure to poly[styrene-*co*-1-((4-vinylphenyl)methyl)pyridinium chloroaluminate] (PS–PyCl–xAlCl$_3$).

The successful immobilization of AlCl$_3$ on the polymer was confirmed by FT-IR spectroscopy. The FT-IR spectra of the Merrifield resin, PS–PyCl and PS––PyCl–xAlCl$_3$ are shown in Fig. 1. The IR spectra of the PS–PyCl showed absorption peaks due to the pyridine ring at 3020, 2900, 1640, 1500, 1475, 775 cm^{-1}.[43] As can be seen in the spectrum of PS–PyCl–xAlCl$_3$, when AlCl$_3$ was complexed with PS–PyCl, new peaks appeared at 575, 500, 430, 385 cm^{-1}, which can be assigned to Al–Cl stretching modes of Al$_2$Cl$_7^-$.[43,44]
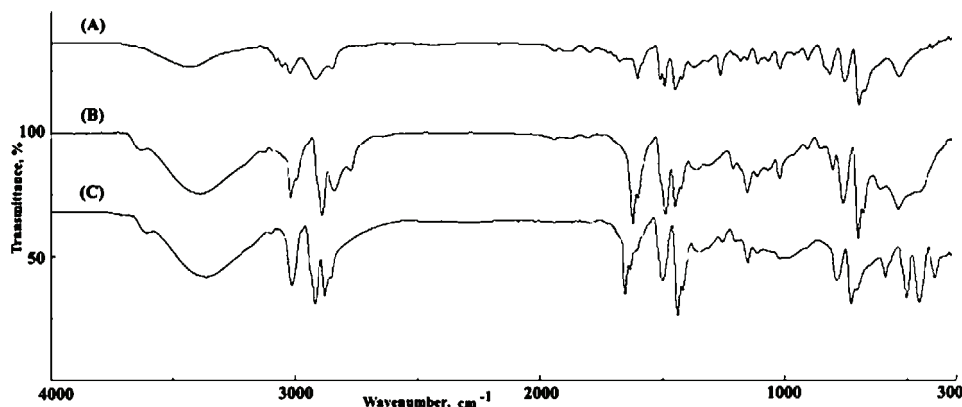
Fig. 1. FT-IR spectra of A) Merrifield resin, B) PS–PyCl and C) PS–PyCl–xAlCl$_3$.

The catalytic activity of PS–PyCl–xAlCl$_3$ was studied in the synthesis of benzimidazoles by the condensation reaction of different aldehydes (aromatic and aliphatic) with o-phenylenediamines (Scheme 1). Initially, to optimize the reaction conditions, the conversion of benzaldehyde (1 mmol) to 2-phenyl-1H--benzimidazole with o-phenylenediamine (1 mmol) and PS–PyCl–xAlCl$_3$ in the presence of a variety of solvents at room temperature was attempted. It was observed that this reaction goes well in ethanol among the commonly used organic solvents, such as acetonitrile, methanol, 1,2-dichloroethane, dichloromethane and tetrahydrofuran. Afterwards, to optimize the quantity of PS–PyCl–xAlCl$_3$, 0.05––0.15 mmol of the catalyst was used in the above reaction. It was found that a 0.1:1 mmol ratio of catalyst:benzaldehyde was sufficient to obtain 2-phenyl-1H--benzimidazole in 94 % yield within 6 min. Then, under the optimal conditions, a wide variety of aromatic aldehydes (containing both electron withdrawing and donating groups) were treated with o-phenylenediamines, and the corresponding 2-substituted benzimidazoles (Scheme 1, I) were obtained exclusively in excellent yields (Table I, entry 1). 2-Naphthaldehyde was also converted to the corresponding benzimidazole in 93 % yield (entry 2). Aliphatic aldehydes required slightly longer times to produce the corresponding benzimidazoles in moderate yields (entries 3–6). It was pleasing to observe that even acid-sensitive aldehydes such as cinnamaldehyde, 2-pyridyl, 2-furyl and 2-thienyl carbaldehyde gave the corresponding benzimidazoles without the formation of any side products, which are normally encountered under acidic conditions (entries 7–10). It is noteworthy that only small activities were observed when PS–PyCl or basic or neutral PS––PyCl–xAlCl$_3$ were used as the catalyst.[45,46] To assess the feasibility of applying this method on the preparative scale, the condensation of benzaldehyde with o-phenylenediamine in a 30-mmol scale in ethanol at room temperature in the presence of PS–PyCl–xAlCl$_3$ was performed. The reaction proceeded smoothly and 2-phenyl-1H-benzimidazole was obtained in 90 % yield after 15 min.

BOROUJENI, ZHIANINASAB and JAFARINASAB

TABLE I. PS–PyCl–xAlCl$_3$ catalyzed synthesis of 2-substituted benzimidazoles in the reactions of aldehydes with o-phenylenediamines; ratio of aldehyde:o-phenylenediamine was 1:1. Unless otherwise noted, all reactions were performed in the presence of 0.1 mmol of PS––PyCl–xAlCl$_3$
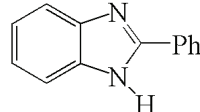
Entry	Aldehyde	R$_2$	Time, min	Yield[a], %
1	X—⟨⟩—CHO	–	–	–
1a	X = H	H	6(7)[b]	94(93)[b]
1b	X = H	Me	10	90
1c	X = 4-CH$_3$	H	7	93
1d	X = 4-CH$_3$	Me	11	91
1e	X = 4-OCH$_3$	H	6(6)[b]	94(92)[b]
1f	X = 4-Cl	H	9	95
1g	X = 4-Cl	Me	15	90
1h	X = 2-Cl	H	10	93
1i	X = 4-Br	H	10	94
1j	X = 3-NO$_2$	H	11	92
1k	X = 4-NO$_2$	H	13	91
1l	X = 2-OH	H	14	91
1m	X = 4-OH	H	16	93
1n	X = 3-OH	H	16	91
1o	X = 4-CN	H	14	92
2	naphthyl–CHO	H	16	93
3	⟨⟩–CH$_2$CHO	H	21(20)[b]	89(88)[b]
4	⟨⟩–CH$_2$CHO	Me	30	83
5	cyclohexyl–CHO	H	21	89
6	CH$_2$CH$_2$CH$_2$CH$_2$–CHO	H	30	82
7	⟨⟩–CH=CH–CHO	H	11(10)[b]	93(90)[b]
8	pyridyl–CHO	H	11	94
9	furyl–CHO	H	11	92
10	thienyl–CHO	H	11	92

[a]Isolated yields. All products are known compounds and were identified by comparison of their physical and spectral data with those of the authentic samples;[32,35,36,39,40] [b]value in parenthesis when the reaction was performed in the presence of 1-butylpyridinium chloroaluminate ionic liquid (1-BuPyCl–xAlCl$_3$; x is the mole fraction of AlCl$_3$ which is equal to 0.7)[46] at 40 °C. Molar ratio of aldehyde:o-phenylenediamine:1-BuPyCl––xAlCl$_3$ was 1:1:0.15

In order to confirm the true heterogeneity of the catalytic system (*i.e.*, the absence of leaching of the AlCl$_3$ into the reaction mixture), PS–PyCl–*x*AlCl$_3$ was added to ethanol and the mixture was stirred at room temperature for 2 h. Then, the catalyst was filtered off and the filtrate was analyzed for its aluminium content, which showed a negligible release of AlCl$_3$. The filtrate was found to be inactive for the condensation reaction of *o*-phenylenediamines with aldehydes. These observations indicate that PS–PyCl–*x*AlCl$_3$ is stable under the reaction conditions, and there was no leaching of acid moieties during the reactions.

PS–PyCl–*x*AlCl$_3$ recovered after a reaction can be washed with ethanol and used again at least five times without any noticeable loss of catalytic activity (Table II).

TABLE II. Recovery of PS–PyCl–*x*AlCl$_3$

PhCHO (1 mmol) $\xrightarrow[\text{EtOH / r.t. / 6 min}]{\begin{array}{c}\text{PS–PyCl–}x\text{AlCl}_3\ (0.1\ \text{mmol})\\ o\text{-Phenylenediamine (1 mmol)}\end{array}}$ 2-phenyl-1H-benzimidazole–Ph

Use	1	2	3	4	5
Isolated yield, %	94	93	91	91	90

A comparison of the present procedure using PS–PyCl–*x*AlCl$_3$ with selected previously known protocols is collected in Table III. As can be seen, in addition to having the general advantages attributed to solid supported catalysts, PS––PyCl–*x*AlCl$_3$ has a good efficiency compared to other recently reported catalysts in the synthesis of benzimidazoles by the condensation of aldehydes with *o*-phenylenediamines.

TABLE III. Comparison of the efficiencies of a number of different reported catalysts with that of PS–PyCl–*x*AlCl$_3$ for the synthesis of 2-phenyl-1*H*-benzimidazole from the condensation of benzaldehyde with *o*-phenylenediamine

Entry	Reaction conditions	Time, min	Yield[a], %
1	Yb(OTf)$_3$, solvent free, r.t.	30	93[29]
2	(I$_2$/KI/K$_2$CO$_3$), H$_2$O, 90 °C	30	90[30]
3	In(OTf)$_3$, solvent free, r.t.	30	95[31]
4	BF$_3$·OEt$_2$, solvent free, r.t.	30	90[32]
5	(H$_2$O$_2$/HCl), CH$_3$CN, r.t.	35	97[33]
6	TsOH–SiO$_2$, solvent free, 70 °C	15	32[34]
7	NaY zeolite, EtOH, r.t.	48	50[35]
8	T(*o*-Cl)PPFe^{III}Cl[b], EtOH, r.t.	90	95[36]
9	DMP[c], dioxane, r.t.	10	89[37]
10	Scolecite, EtOH, 70 °C	55	89[38]

TABLE III. Continued

Entry	Reaction conditions	Time, min	Yield[a], %
11	AlKIT-5, CH$_3$CN, reflux	240	95[39]
12	(WOx/ZrO$_2$), dioxane, 100 °C	300	92[40]
13	FeCl$_3$–SiO$_2$, H$_2$O$_2$, 150 °C	30	95[41]
14	Amberlite IR-120, solvent free, MW	4	92[42]
15	PS-PyCl-XAlCl$_3$, EtOH, r.t.	6	94

[a]Isolated yields; [b]porphyrinatoiron(III) complex supported on silica gel; [c]Dess-Martin-periodinane

CONCLUSIONS

In conclusion, polymer-supported pyridinium chloroaluminate IL was synthesized as a new heterogeneous Lewis acid catalyst that favourably combines the properties of ILs and advantages of solid supports. This polymer catalyst has an activity in the synthesis of 2-substituted benzimidazoles comparable to that of 1-butylpyridinium chloroaluminate IL as far as was tested but offers its own advantages originating from being supported on a polymeric matrix, enhanced stability (as a bench-top catalyst), easier handling, high chemoselectivity, simple product workup, separation and isolation, as well as reuse of the catalyst at least five times without significant change in its catalytic activity.

SUPPLEMENTARY MATERIAL

Physical and spectral data of the obtained compounds are available electronically from http://www.shd.org.rs/JSCS/, or from the corresponding author on request.

ИЗВОД

ЈОНСКА ТЕЧНОСТ ПИРИДИНИЈУМ-ХЛОРОАЛУМИНАТ НА ПОЛИСТИРЕНУ КАО ЛУИСОВА КИСЕЛИНА И НОВ ХЕТЕРОГЕНИ КАТАЛИЗАТОР ЗА СЕЛЕКТИВНУ СИНТЕЗУ БЕНЗИМИДАЗОЛА

KAVEH PARVANAK BOROUJENI, ASHKAN ZHIANINASAB и MINA JAFARINASAB

Department of Chemistry, Shahrekord University, Shahrekord 115, Iran

Јонска течност пиридинијум-хлороалуминат на полистирену добијена је од Мерифилдове смоле и пиридина, након чега следи реакција са алуминијум-хлоридом. Овај катализатор је коришћен за хемоселективну катализу као Луисова киселина за добијање 2-супституисаних бензимидазола као једних производа из реакције алдехида са *o*-фенилдиаминима. Катализатор је стабилан и може се лако изоловати и поново користити без уочљивог губитка ефикасности.

REFERENCES

1. J. P. Hallett, T. Welton, *Chem. Rev.* **111** (2011) 3508
2. P. Wasserscheid, W. Keim, *Angew. Chem. Int. Ed.* **39** (2000) 3772
3. T. Welton, *Chem. Rev.* **99** (1999) 2071

4. N. Fontanals, S. Ronka, F. Borrull, A. W. Trochimczulk, R. M. Marce, *Talanta* **80** (2009) 250

5. Q. Bao, K. Qiao, D. Tomida, C. Yokoyama, *Catal. Commun.* **10** (2009) 1625

6. S. S. Shinde, B. S. Lee, D. Y. Chi, *Tetrahedron Lett.* **49** (2008) 4245

7. D. W. Kim, H. J. Jeong, S. T. Lim, M. H. Sohn, D. Y. Chi, *Tetrahedron* **64** (2008) 4209

8. R. Alleti, W. S. Oh, M. Perambuduru, C. V. Ramana, V. P. Reddy, *Tetrahedron Lett.* **49** (2008) 3466

9. H. W. Bae, J. S. Han, S. Jung, M. Cheong, *Appl. Catal., A* **331** (2007) 34

10. D. W. Kim, D. Y. Chi, *Angew. Chem. Int. Ed.* **43** (2004) 483

11. C. P. Mehnert, R. A. Cook, N. C. Dispenziere, M. J. Afeworki, *J. Am. Chem. Soc.* **124** (2002) 12932

12. M. H. Valkenberg, C. De Castro, W. F. Hölderich, *Top. Catal.* **14** (2001) 139

13. C. DeCastro, E. Sauvage, M. H. Valkenberg, W. F. Hölderich, *J. Catal.* **196** (2000) 86

14. A. G. Borel, F. S. Abbott, *Drugs Metab. Dispos.* **21** (1993) 415

15. R. Lisciani, A. Baldini, *Arzneim. Forsch.* **28** (1978) 417

16. T. Seppala, *Curr. Ther. Res.* **31** (1982) 638

17. T. Güngör, A. Fouquet, J. M. Teulon, D. Provost, M. Cazes, A. Cloarec, *J. Med. Chem.* **35** (1992) 4455

18. V. Shibouta, Y. Inada, M. Ojima, T. Wada, M. Noda, T. Sanada, K. Kubo, Y. Kohara, T. Naka, K. Nishikawa, *J. Pharmacol. Exp. Ther.* **266** (1993) 114

19. M. Akio, M. Yuki, T. Hidetoshi, E. Hajime (JP Patent), 11189594 (1999); *CA* 1999, 131, 87912u

20. S. Hideji, M. Taro, N. Toshio (JP Patent), 2000026430 (2000); *CA* 2000, 132, 122619y

21. T. M. Craig, T. Qureshi, D. K. Miller, C. G. Wade, J. A. Rogers, *Am. J. Vet. Res.* **53** (1992) 1170

22. D. Valdez-Padilla, S. Rodríguez-Morales, A. Hernández-Campos, F. Hernández-Luis, L. Yépez-Mulia, A. Tapia-Contreras, R. Castillo, *Bioorg. Med. Chem.* **17** (2009) 1724

23. W. A. Denny, G. W. Rewcastle, B. C. Baguley, *J. Med. Chem.* **33** (1990) 814

24. P. N. Preston, in *Chemistry of Heterocyclic Compounds*, A. Weissberger, E. C. Taylor, Eds., Wiley, New York, 1981

25. M. R. Grimmet, in *Imidazoles and Their Benzo Derivatives*, Vol. 4, A. R. Katritzky, C. W. Ress, Eds., Pergamon, Oxford, 1984, p. 457

26. R. F. Nadaf, S. A. Siddiqui, T. Daniel, R. J. Lahoti, K. V. Srinivasan, *J. Mol. Catal., A* **214** (2004) 155

27. A. K. Chkraborti, S. Rudrawar, G. Kaur, L. Sharma, *Synlett* **9** (2004) 1533

28. S. Gupta, P. K. Agarwal, B. Kundu, *Tetrahedron Lett.* **51** (2010) 1887

29. M. Curini, F. Epifano, F. Montanari, O. Rosati, S. Taccone, *Synlett* **10** (2004) 1832

30. P. Gogoi, D. Konwar, *Tetrahedron Lett.* **47** (2006) 79

31. R. Trivedi, S. K. De, R. A. Gibbs, *J. Mol. Catal., A* **245** (2006) 8

32. R. R. Nagawade, D. B. Shinde, *Chin. Chem. Lett.* **17** (2006) 453

33. K. Bahrami, M. M. Khodaei, I. Kavianinia, *Synthesis* **4** (2007) 547

34. M. Chakrabarty, R. Mukherjee, S. Karmakar, Y. Harigaya, *Monatsh. Chem.* **138** (2007) 1279

35. A. Mobinikhaledi, N. Forughifar, M. Zendehdel, M. Jabbarpour, *Synth. React. Inorg. Metal-Org. Nano-Metal Chem.* **38** (2008) 390

36. H. Sharghi, M. H. Beyzavi, *Eur. J. Org. Chem.* (2008) 4126

37. S. K. Dabhade, R. O. Bora, M. Farooqui, C. H. Gill, *Chin. Chem. Lett.* **20** (2009) 893
38. L. S. Gadekar, B. R. Arbad, M. K. Lande, *Chin. Chem. Lett.* **21** (2010) 1053
39. M. A. Chari, D. Shobha, E. R. Kenawy, S. S. Al-Deyab, B. V. Subba Reddy, A. Vinu, *Tetrahedron Lett.* **51** (2010) 5195
40. R. V. Shingalapur, K. M. Hosamani, *Catal. Lett.* **137** (2010) 63
41. A. Fazlinia, M. H. Mosslemin, H. Sadoughi, *J. Korean Chem. Soc.* **54** (2010) 579
42. M. A. Pasha, A. Nizam, *J. Saudi Chem. Soc.* **16** (2011) 237
43. R. J. Gale, R. A. Osteryoung, *Inorg. Chem.* **19** (1980) 2240
44. M. E. Peach, V. L. Tracy, T. C. Waddington, *J. Chem. Soc., A* (1969) 366
45. The basic and neutral PS–PyCl–xAlCl$_3$ were prepared by slowly mixing weighed amounts of PS–PyCl and AlC1$_3$. For this purpose, PS–PyCl was first prepared. Then, small amounts of AlCl$_3$ were slowly added to PS–PyCl and the Al content of the obtained PS–PyCl–xAlCl$_3$ was monitored by the atomic absorption technique. A neutral PS–PyCl––xAlCl$_3$ is referred to at an AlCl$_3$ mole fraction of 0.5 and a basic PS–PyCl–xAlCl$_3$ is one in which the AlCl$_3$ mole fraction is smaller than 0.5
46. Z. W. Wang, L. S. Wang, *Green Chem.* **5** (2003) 737
47. H. Sharghi, O. Asemani, R. Khalifeh, *Synth. Commun.* **38** (2008) 1128
48. L. H. Du, X. P. Luo, *Synth. Commun.* **40** (2010) 2880.
49. J. M. Wallace, B. C. G. Söderberg, J. W. Hubbard, *Synth. Commun.* **36** (2006) 3425.
50. Z. H. Zhang, L. Yin, Y. M. Wang, *Catal. Commun.* **8** (2007) 1126.

Polystyrene-supported pyridinium chloroaluminate ionic liquid as a new heterogeneous Lewis acid catalyst for selective synthesis of benzimidazoles

KAVEH PARVANAK BOROUJENI*, ASHKAN ZHIANINASAB
and MINA JAFARINASAB

Department of Chemistry, Shahrekord University, Shahrekord 115, Iran

PHYSICAL AND SPECTRAL DATA OF THE OBTAINED COMPOUNDS

*2-Phenyl-1*H*-benzimidazole (1a)*. m.p. 287–289 °C (Lit.[35]** 286–288 °C); IR (KBr, cm^{-1}): 1630 (C=N), 3438 (NH); ^{1}H-NMR (300 MHz, DMSO-d_6, δ / ppm): 7.16–7.27 (2H, *m*, aromatic), 7.51–7.65 (5H, *m*, aromatic), 8.30–8.33 (2H, *d*, *J* = = 7.1 Hz, aromatic), 12.92 (1H, *bs*, NH).

*6-Methyl-2-phenyl-1*H*-benzimidazole (1b)*. m.p. 249–253 °C (Lit.[47] 246 °C); IR (KBr, cm^{-1}): 1625 (C=N), 3424 (NH); ^{1}H-NMR (300 MHz, DMSO-d_6, δ / / ppm): 2.35 (3H, *s*, CH$_3$), 7.09–7.20 (4H, *m*, aromatic), 7.41–7.55 (4H, *m*, aromatic), 12.88 (1H, *bs*, NH).

*2-(4-Methylphenyl)-1*H*-benzimidazole (1c)*. m.p. 265–267 °C (Lit.[40] 261––263 °C); IR (KBr, cm^{-1}): 1630 (C=N), 3430 (NH); ^{1}H-NMR (300 MHz, DMSO-d_6, δ / ppm): 2.30 (3H, *s*, CH$_3$), 7.20–7.36 (4H, *m*, aromatic), 7.49–7.56 (2H, *m*, aromatic), 7.95–8.09 (2H, *m*, aromatic), 12.85 (1H, *bs*, NH).

*6-Methyl-2-(4-methylphenyl)-1*H*-benzimidazole (1d)*: m.p. 102–104 °C (Lit.[36] 101–102 °C); IR (KBr, cm^{-1}): 1620 (C=N), 3420 (NH); ^{1}H-NMR (300 MHz, DMSO-d_6, δ / ppm): 2.31 (3H, *s*, –CH$_3$), 2.40 (3H, *s*, –CH$_3$), 7.09–7.12 (3H, *m*, aromatic), 7.42 (1H, *s*, aromatic), 7.55 (1H, *d*, *J* = 8.0 Hz, aromatic), 8.20 (2H, *d*, *J* = 8.0 Hz, aromatic), 12.70 (1H, *bs*, NH).

*2-(4-Methoxyphenyl)-1*H*-benzimidazole (1e)*. m.p. 228–231 °C (Lit.[30] 223––226 °C); IR (KBr, cm^{-1}): 1615 (C=N), 3430 (NH); ^{1}H-NMR (300 MHz, DMSO-d_6, δ / ppm): 3.72 (3H, *s*, –OCH$_3$), 7.13–7.21 (4H, *m*, aromatic), 7.45

---

* Corresponding author. E-mail: parvanak-ka@sci.sku.ac.ir
** The reference numbers correspond to the Reference list of the native paper: *J. Serb. Chem. Soc.* 78 (2) (2013) 155–164.

(1H, *s*, aromatic), 7.65 (1H, *s*, aromatic), 8.19 (2H, *d*, *J* = 1.7 Hz, aromatic), 12.10 (1H, *bs*, NH).

*2-(4-Chlorophenyl)-1*H-*benzimidazole (1f)*. m.p. 288–290 °C (Lit.[35] 284––286 °C); IR (KBr, cm^{-1}): 1628 (C=N), 3425 (NH); ^{1}H-NMR (300 MHz, DMSO-d_6, δ / ppm): 7.21–7.29 (2H, *m*, aromatic), 7.55–7.64 (4H, *m*, aromatic), 8.22 (2H, *d*, *J* = 8.5 Hz, aromatic), 12.96 (1H, *bs*, NH).

*6-Methyl-2-(4-chlorophenyl)-1*H-*benzimidazole (1g)*. m.p. 227–228 °C (Lit.[48] 224–225 °C); IR (KBr, cm^{-1}): 1630 (C=N), 3430 (NH); ^{1}H-NMR (300 MHz, DMSO-d_6, δ / ppm): 2.41 (3H, *s*, –CH$_3$), 7.31 (1H, *s*, aromatic), 7.64–7.79 (4H, *m*, aromatic), 8.31–8.36 (2H, *d*, *J* = 8.4 Hz, aromatic), 12.89 (1H, *bs*, NH).

*2-(2-Chlorophenyl)-1*H-*benzimidazole (1h)*. m.p. 230–232 °C (Lit.[40] 231–233 °C); IR (KBr, cm^{-1}): 1633 (C=N), 3429 (NH); ^{1}H-NMR (300 MHz, DMSO-d_6, δ / ppm): 7.25–7.30 (2H, *m*, aromatic), 7.51–7.61 (5H, *m*, aromatic), 7.89–7.93 (1H, *m*, aromatic), 12.64 (1H, *bs*, NH).

*2-(4-Bromophenyl)-1*H-*benzimidazole (1i)*. mp: 288–290 °C (Lit.[35] 283–284 °C); IR (KBr, cm^{-1}): 1624 (C=N), 3415 (NH); ^{1}H-NMR (300 MHz, DMSO-d_6, δ / / ppm): 7.22–7.29 (2H, *m*, aromatic), 7.33–7.44 (6H, *m*, aromatic), 12.89 (1H, *bs*, NH).

*2-(3-Nitrophenyl)-1*H-*benzimidazole (1j)*. mp: 209–211 °C (Lit.[35] 207–208 °C); IR (KBr, cm^{-1}): 1340, 1550 (NO$_2$), 1624 (C=N), 3438 (NH); ^{1}H-NMR (300 MHz, DMSO-d_6, δ / ppm): 7.25–7.40 (4H, *m*, aromatic), 7.67–7.80 (4H, *m*, aromatic), 12.89 (1H, *bs*, NH).

*2-(4-Nitrophenyl)-1*H-*benzimidazole (1k)*. m.p. 310–312 °C (Lit.[40] 308–310 °C); IR (KBr, cm^{-1}): 1338, 1516 (NO$_2$), 1625 (C=N), 3418 (NH); ^{1}H-NMR (300 MHz, DMSO-d_6, δ / ppm): 7.32–7.44 (4H, *m*, aromatic), 8.02–8.15 (4H, *m*, aromatic), 12.87 (1H, *bs*, NH).

*2-(2-Hydroxyphenyl)-1*H-*benzimidazole (1l)*. mp: 242–243 °C (Lit.[35] 240––242 °C); IR (KBr, cm^{-1}):1622 (C=N), 3245, 3350, 3410 (NH, OH); ^{1}H-NMR (300 MHz, DMSO-d_6, δ / ppm): 7.67–7.77 (4H, *m*, aromatic), 7.79–7.86 (3H, *m*, aromatic), 7.88 (1H, *s*, aromatic), 12.98 (2H, *bs*, NH, OH).

*2-(4-Hydroxyphenyl)-1*H-*benzimidazole (1m)*. m.p. 257–259 °C (Lit.[36] 254––255 °C); IR (KBr, cm^{-1}): 1625 (C=N), 3250, 3340, 3415 (NH, OH); ^{1}H-NMR (300 MHz, DMSO-d_6, δ / ppm): 7.61–7.71 (4H, *m*, aromatic), 7.73–7.79 (2H, *m*, aromatic), 7.81–7.86 (2H, *m*, aromatic), 9.89 (1H, *bs*, OH), 12.71 (1H, *bs*, NH).

*2-(3-Hydroxyphenyl)-1*H-*benzimidazole (1n)*. m.p. 184–187 °C (Lit.[36] 182––183 °C); IR (KBr, cm^{-1}):1622 (C=N), 3268, 3360, 3418 (NH, OH); ^{1}H-NMR (300 MHz, DMSO-d_6, δ / ppm): 7.57–7.67 (4H, *m*, aromatic), 7.69–7.76 (3H, *m*, aromatic), 7.79 (1H, *s*, aromatic), 9.85 (1H, *bs*, OH), 12.66 (1H, *bs*, NH).

*4-(1*H-*Benzimidazol-2-yl)benzonitrile (1o)*. m.p. 263–265 °C (Lit.[36] 262 °C); IR (KBr, cm^{-1}): 1618 (C=N), 2220 (CN), 3420 (NH); ^{1}H-NMR (300 MHz, DMSO-d_6, δ / ppm): 7.23–7.27 (2H, *m*, aromatic), 7.51–7.65 (2H, *m*, aromatic),

8.02–8.08 (2H, *d*, *J* = 8.4 Hz, aromatic), 8.40–8.46 (2H, *d*, *J* = 8.4 Hz, aromatic), 13.09 (1H, *bs*, NH).

*2-(2-Naphthyl)-1*H-*benzimidazole (2)*. m.p. 218–219 °C (Lit.[36] 217 °C); IR (KBr, cm^{-1}): 1625 (C=N), 3430 (NH); ^{1}H-NMR (300 MHz, DMSO-d_6, δ / ppm): 7.25–7.29 (2H, *m*, aromatic), 7.49–7.57 (4H, *m*, aromatic), 8.02–8.11 (3H, *m*, aromatic), 8.37–8.41 (1H, *dd*, J_1 = 8.1, J_2 = 2.2 Hz, aromatic), 8.85 (1H, *s*, aromatic), 13.10 (1H, *bs*, NH).

*2-Benzyl-1*H-*benzimidazole (3)*. m.p. 185–188 °C (Lit.[39] 184–186 °C); IR (KBr, cm^{-1}): 1623 (C=N), 3427 (NH); ^{1}H-NMR (300 MHz, DMSO-d_6, δ / ppm): 4.20 (2H, *s*, –CH$_2$–), 7.17–7.20 (2H, *d*, *J* = 7.3 Hz, aromatic), 7.25–7.27 (1H, *m*, aromatic), 7.36–7.41 (4H, *m*, aromatic), 7.45–7.47 (1H, *d*, *J* = 6.4 Hz, aromatic), 7.55–7.57 (1H, *d*, *J* = 8.9 Hz, aromatic), 12.27 (1H, *bs*, NH).

*6-Methyl-2-benzyl-1*H-*benzimidazole (4)*. m.p. 144–147 °C (Lit.[49] 139–140 °C); IR (KBr, cm^{-1}): 1625 (C=N), 3430 (NH); ^{1}H-NMR (300 MHz, DMSO-d_6, δ / ppm): 4.15 (2H, *s*, –CH$_2$–), 7.15–7.18 (2H, *d*, *J* = 7.3 Hz, aromatic), 7.36––7.41 (5H, *m*, aromatic), 7.55–7.57 (1H, *d*, *J* = 8.9 Hz, aromatic), 12.31 (1H, *bs*, NH).

*2-Cyclohexyl-1*H-*benzimidazole (5)*. m.p. 284–286 °C (Lit.[32] 282–283 °C); IR (KBr, cm^{-1}): 1630 (C=N), 3420 (NH); ^{1}H-NMR (300 MHz, DMSO-d_6, δ / / ppm): 1.30–1.51 (2H, *m*, cyclohexyl ring), 1.66–1.77 (2H, *m*, cyclohexyl ring), 1.83–1.87 (2H, *m*, cyclohexyl ring), 2.05–2.15 (3H, *m*, cyclohexyl ring), 2.89––2.99 (2H, *m*, cyclohexyl ring), 7.15–7.20 (2H, *m*, aromatic), 7.53–7.59 (2H, *m*, aromatic), 11.55 (1H, *bs*, NH).

*2-Butyl-1*H-*benzimidazole (6)*. m.p. 149–152 °C (Lit.[50] 148–149 °C); IR (KBr, cm^{-1}): 1630 (C=N), 3438 (NH); ^{1}H-NMR (300 MHz, DMSO-d_6, δ / ppm): 1.01–1.03 (3H, *t*, *J* = 7.3 Hz, CH$_3$), 1.44–1.46 (2H, *sext*, *J* = 7.0 Hz, –CH$_2$–), 1.89–1.91 (2H, *quin*, *J* = 7.0 Hz, –CH$_2$–), 2.95–2.98 (2H, *t*, *J* = 7.0 Hz, –CH$_2$–), 7.29–7.36 (4H, *m*, aromatic), 9.44 (1H, *bs*, NH).

*2-Styryl-1*H-*benzimidazole (7)*. m.p. 200–202 °C (Lit.[31] 201–203 °C); IR (KBr, cm^{-1}): 1620 (C=N), 3425 (NH); ^{1}H-NMR (300 MHz, DMSO-d_6, δ / ppm): 7.20–7.30 (4H, *m*, aromatic), 7.31–7.33 (1H, *d*, *J* = 16.8 Hz, CH), 7.59–7.69 (5H, *m*, aromatic), 7.71–7.73 (1H, *d*, *J* = 16.8 Hz, CH), 12.99 (1H, *bs*, NH).

*2-(2-Pyridyl)-1*H-*benzimidazole (8)*. m.p. 220–221 °C (Lit.[30] 216–219 °C); IR (KBr, cm^{-1}): 1625 (C=N), 3435 (NH); ^{1}H-NMR (300 MHz, DMSO-d_6, δ / / ppm): 7.20–7.25 (2H, *m*, aromatic), 7.51–7.60 (3H, *m*, aromatic), 8.05–8.10 (1H, *dd*, J_1 = 7.5, J_2 = 1.6 Hz, aromatic), 8.25–8.27 (1H, *m*, aromatic), 8.76–8.79 (1H, *d*, *J* = 6.4 Hz, aromatic), 13.07 (1H, *bs*, NH).

*2-(2-Furyl)-1*H-*benzimidazole (9)*. m.p. 289–291 °C (Lit.[36] 287–288 °C); IR (KBr, cm^{-1}): 1625 (C=N), 3425 (NH); ^{1}H-NMR (300 MHz, DMSO-d_6, δ / ppm): 6.78 (2H, *s*, aromatic), 7.50 (1H, *s*, aromatic), 7.60–7.70 (4H, *m*, aromatic), 12.89 (1H, *bs*, NH).

*2-(2-Thienyl)-1*H-*benzimidazole (**10**).* m.p. 327–329 °C (Lit.[30] 330 °C); IR (KBr, cm^{-1}): 1624 (C=N), 3445 (NH); ^{1}H-NMR (300 MHz, DMSO-d_6, δ / ppm): 7.15–7.22 (3H, *m*, aromatic), 7.52–7.61 (2H, *m*, aromatic), 7.79–7.86 (2H, *m*, aromatic), 12.97 (1H, *bs*, NH).

Synthesis of some novel 7-(1*H*-benzimidazol-2-ylazo)-1,3-dimethyl-6,8-disubstituted-1*H*-pyrimido[4,5-*b*][1,4]diazepine-2,4-diones as potential anti-anxiety agents

KANTI SHARMA* and RENUKA JAIN

Department of Chemistry, University of Rajasthan, Jaipur 302 004, India

Abstract: An efficient and mild method for the synthesis of some novel 7-(1*H*-benzimidazol-2-ylazo)-1,3-dimethyl-6,8-disubstituted-1*H*-pyrimido[4,5-*b*]-[1,4]diazepine-2,4-diones in water has been developed. This method is a good option to obtain the title compounds in quantitative yields in a simple and inexpensive manner. Further, the NH of the title compounds was replaced by various substituents in an ionic liquid, [bmim]PF$_6$, a recyclable and environmentally benign solvent. The synthesized compounds were characterized by analytical and spectral (IR, ^{1}H-NMR, ^{13}C-NMR and FAB mass) data and have been screened for their anti-anxiety activity in mice.

Keywords: 2-aminobenzimidazole, diketones, benzimidazolyl-pyrimido-diazepines, aqueous/ionic liquid mediated synthesis; anti-anxiety activity.

INTRODUCTION

Nitrogen-containing heterocycles represent the central framework of many biologically active compounds. Benzimidazoles show antifungal,[1] anti-inflammatory,[1] analgesic,[1] CNS depressant,[2] antitubercular,[3] anticancer,[4] anti-HIV,[5] *etc*. activities. Pyrimidines exhibit varied activities, such as anticancer[6] and antibacterial.[7] 5-Fluorouracil is a well-known anticancer agent. Diazepine derivatives are used as tranquilizers,[8] anticonvulsant, anxiolytic, analgesics, sedatives, antidepressives and hypnotic agents.[9] 1,5-Benzodiazepine shows anti-anxiety,[10] analgesic,[11] anticonvulsant[11] and anti-inflammatory[11] activities.

Due to their wide range of pharmacological activity and industrial applications, the development of mild and efficient protocols for the preparation of diazepines continues to be challenging endeavor in synthetic organic chemistry. The common procedure for the synthesis of these compounds is a one-pot condensation between *o*-phenylenediamines and carbonyl compounds.[12] However, a

---

large number of modified methods reported in the literature[13] suffer from several drawbacks, such as the use of a large amount of catalysts, unsatisfactory product yield and critical product isolation procedures. These disadvantages requires the development of an efficient and practically useful process of preparation.[14]

In continuation of work on bioactive heterocycles,[15–17] reported herein is for the first time a rapid efficient, clean and environmentally benign exclusive synthesis of 7-(1*H*-benzimidazol-2-ylazo)-1,3-dimethyl-6,8-disubstituted-1*H*-pyrimido[4,5-*b*][1,4]diazepine-2,4-diones **4a**–**c** by the reaction of 2-[(1*H*-benzimidazol--2-yl)hydrazono]-1,3-disubstituted-1,3-dione **3a**–**c** and 5,6-diamino-1,3-dimethyl-2,4(1*H*,3*H*)-pyrimidinedione hydrochloride in aqueous medium in excellent yields (92–97 %). The use of water as a solvent for organic transformations offers green chemistry benefits[18] and is widely used to enable and expedite the synthesis of diverse heterocycles. Compounds **3a**–**c** were prepared by coupling reaction[19] of a diazonium salt, formed by the diazotization of 2-aminobenzimidazole **1** and 1,3-diketones **2** in presence of sodium acetate and ethanol. Further, the NH of title compounds was substituted by various substituents by reacting with methyl iodide, benzyl chloride, chloroacetyl chloride, formaldehyde and secondary amines, trifluoroacetic anhydride in [bmim]PF$_6$, an ionic liquid to give the *N*-substituted derivatives **5a**–**i** (Scheme 1). The synthesized compounds **4a**–**c** and **5a**–**i** were screened for their anti-anxiety activity in mice and they exhibited excellent results.

EXPERIMENTAL

Melting points are uncorrected and were taken in open glass capillaries using a Gallenkamp melting point apparatus. The IR spectra were recorded on a Shimadzu FTIR-8400S spectrophotometer in KBr pellets and band positions are recorded in wavenumbers (cm^{-1}). The ^{1}H- and ^{13}C-NMR spectra were recorded on a Bruker DRX-300 instrument at 300.15 and 75 MHz, respectively. CDCl$_3$ was used as the solvent and TMS as internal reference. The mass spectra were recorded on a JEOL, SX 102 (FAB) mass spectrometer. The mass spectra and elemental analyses were performed at the Central Drug Research Institute, Lucknow, India. All employed chemicals were of analytical reagent grade, purchased from Acros and used without further purification.

General method for the synthesis of compounds 3a–c

2-Aminobenzimidazole (0.02 mol) was dissolved in a mixture of conc. HCl and water (20 mL; 1:1), then cooled to 0 °C and a cold aqueous solution of sodium nitrite (0.02 mol; 1.3 g in 10 mL water) was added slowly maintaining the temperature between 0–2 °C. The cold diazotized solution was added dropwise to a cooled mixture of 1,3-diketone (0.02 mol) and sodium acetate (10 g) in 20 mL of 50 % ethanol. The stirring was continued for 1 h and the crystals that separated were filtered, washed with water, dried and crystallized from ethanol to yield **3a**–**c**.

Water mediated synthesis of compounds 4a–c

A solution of 5,6-diamino-1,3-dimethyl-2,4(1*H*,3*H*)-pyrimidinedione hydrochloride (0.01 mol) in water (200 mL) was neutralized with ammonia to pH 7 then **3a**–**c** (0.01 mol),

was added and the mixture heated under reflux for 30 min. The crystalline product, which started to separate out just after cooling the reaction mixture, was washed with water and found to be pure by TLC with no need for further purification. All compounds were synthesized similarly to yield **4a–c**.
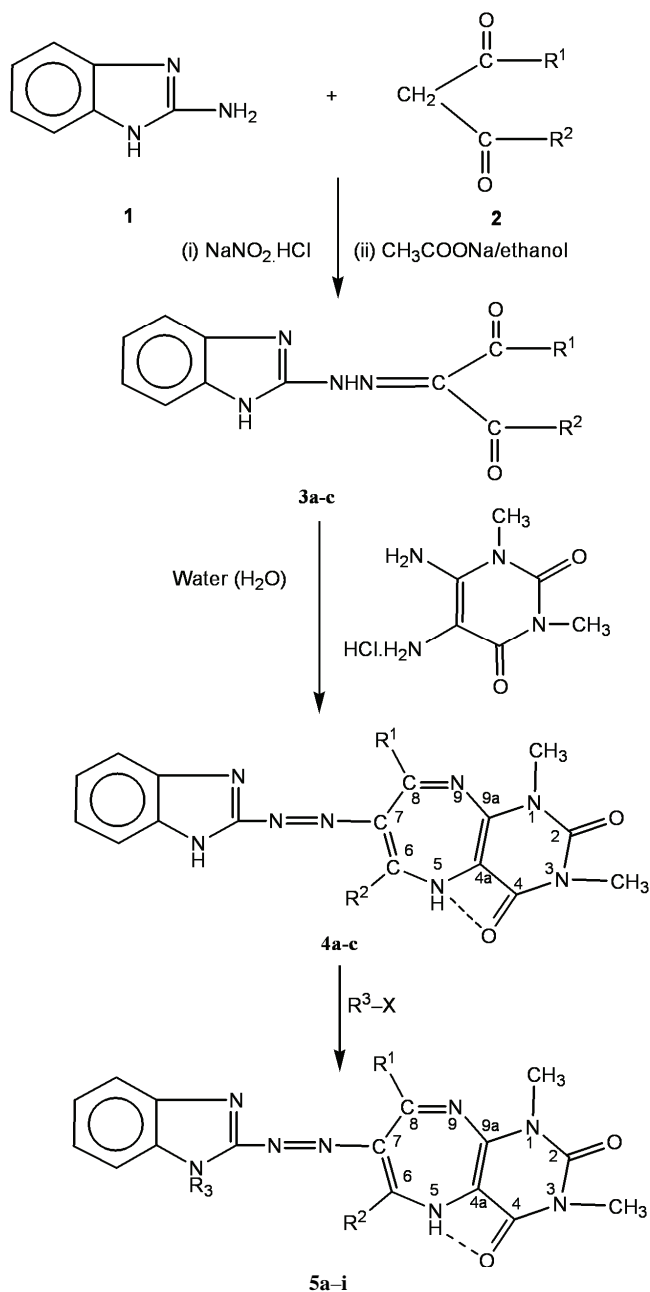
Compound	R^1	R^2	R^3	Compound	R^1	R^2	R^3
3a	CH_3	CH_3	–	**5c**	CH_3	CH_3	CH_2Ph
3b	CH_3	C_6H_5	–	**5d**	CH_3	C_6H_5	CH_2Ph
3c	CF_3	C_6H_5	–	**5e**	CH_3	CH_3	$COCH_2Cl$
4a	CH_3	CH_3	–	**5f**	CH_3	C_6H_5	CH_2NMe_2
4b	CH_3	C_6H_5	–	**5g**	CH_3	C_6H_5	CH_2NEt_2
4c	CF_3	C_6H_5	–	**5h**	CH_3	CH_3	$COCF_3$
5a	CH_3	CH_3	CH_3	**5i**	CF_3	C_6H_5	$COCF_3$
5b	CH_3	C_6H_5	CH_3				

Scheme 1. Synthesis of compounds **3a**–**c**, **4a**–**c** and **5a**–**i**.

*Ionic liquid mediated synthesis of compounds **5a**–**i***

A mixture of **4a**–**c** (0.01 mol), methyl iodide/benzoyl chloride/chloroacetyl chloride//formaldehyde and secondary amine (1:1) or trifluoroacetic anhydride (0.01 mol) and ionic liquid [bmim]PF_6 (5 mL) were taken in a round bottom flask and heated at 60–70 °C under N_2 protection for 1 h. The progress of the reaction was monitored by TLC. After completion of reaction, the mixture was extracted with diethyl ether (6×10 mL). The organic extract was washed with 5 % Na_2CO_3 (40 mL) and water (40 mL), dried with anhydrous sodium sulfate and evaporated under vacuum. The residual product was purified by recrystallization from AcOEt/petroleum ether (60–80 °C) or by column chromatography (silica gel, 60–120 mesh, eluent petroleum ether/AcOEt = 4:1) to give **5a**–**i** (the ionic liquid layer was washed with water (3×5 mL) and kept for 2 h. at 80–85 °C under reduced pressure, the ionic liquid was recycled).

Anti-anxiety activity in mice

Synthesized compounds **4a**–**c** and **5a**–**i** were screened for their anti-anxiety activity in mice on a plus maze apparatus devised by Crawley and Godwin[20] modified by Kilfoil[21] using sodium pentabarbitone as the standard.

The apparatus consisted of a Plexiglas base (102 cm×53 cm×53 cm) divided into two chambers by a black Plexiglas partition. The box was placed within a layer of a soundproof box, which was equipped with a one-way observation window. The partition dividing the sub chamber had a 33 cm×13 cm opening, through which animal could easily pass. The dark chamber (36 cm×53 cm×53 cm) was made up of dark Plexiglas except for the side ferry observation window. This side was clear and covered with black plastic. The testing was performed between 12.00 noon to 6.00 p.m. in an isolated darkened laboratory.

Mice weighing 25 g were chosen and were sorted into five animals in a group. They were allowed free access to food and water *ad libitum*. Animals were given 60 min to acclimatize to the environment prior to the administration of the drug. Drugs or test samples in DMF were given at a dose of 20 mg kg^{-1} body weight, after which each animal was individually placed in the centre of the light area of the apparatus and observed for 10 min. The total amount of time spent in the dark area was measured.

RESULTS AND DISCUSSION

2-Aminobenzimidazole (**1**) was reacted with sodium nitrite and HCl at 0–5 °C. The so-formed diazonium salt was further reacted with 1,3-diketones (**2**) and sodium acetate in ethanol to afford 2-[(1*H*-benzimidazole-2-yl)hydrazono]-1,3--disubstituted 1,3-diones **3a**–**c**. The formation of compound **3** was confirmed by

their IR spectra, in which band appeared at 3200, 3030, 1680 and 1620 cm^{-1} due to –NH benzo, NH hydrazono, C=O and C=N, respectively. The ^{1}H-NMR spetra showed peaks at δ 10.62 and 9.52 ppm due to the NH hydrazono and NH of benzimidazolyl moieties, respectively. The ^{13}C-NMR spectra showed peaks at δ 178.2, 180.1 and 162.4 ppm due to two C=O and the C=N, respectively. Further, the mass spectrum shows M$^+$ at m/z 244 (**3a**).

The advantage of using water as a solvent is its cost, safety (it is non-inflammable and is devoid of any carcinogenic effects) and simple operation. It has the highest specific heat value of all substances as well as unique enthalpic and entropic properties, which have led us to its use. Water has abnormally low volatility because its molecules are associated with each other by means of hydrogen bonding.

In view of this, compounds **3a**–**c** were reacted with 5,6-diamino-1,3-dimethyl-2,4(1H,3H)-pyrimidinedione hydrochloride in aqueous medium to afford 7-(1H-benzimidazol-2-ylazo)-1,3-dimethyl-6,8-disubstituted-1H-pyrimido[4,5-b]-[1,4]diazepine-2,4-diones **4a**–**c**.

The formation of compounds **4** was confirmed by their IR spectra, which showed the disappearance of the peaks due to the hydrazono group and the ketonic group of the 1,3-diketone part with the appearance of a peak due to the NH of diazepine at 3340 cm^{-1} and at 1720 and 1700 cm^{-1} due to the C=O of the pyrimidine ring. The ^{1}H-NMR spectra showed peaks at δ 9.51 and 8.46 ppm due to the NH of benzimidazole and diazepine moiety, respectively. The NCH$_3$ methyl groups present at the positions 4 and 6 appeared at δ 3.20 and 3.62 ppm, respectively. The ^{13}C-NMR spectra showed peaks at δ 33.5 and 34.8 ppm due to the two NCH$_3$ groups of the pyrimidine ring, while two C=O groups appeared at δ 190.2 and 195.1 ppm. Further, the mass spectrum shows M$^+$ at m/z 378 (**4a**).

In recent years ionic liquids[22] (ILs) have emerged, which are organic salts the ions of which do not pack well and remain liquid at room temperature. They have unique properties, such as, for example, a wide liquid range, good solvency, tunable polarity, high thermal stability, negligible vapor pressure and recyclability. Ionic liquids could be recycled and reused as opposed to traditional solvent catalyst systems.

In view of the above, compounds **4a**–**c** were reacted with: *i*) methyl iodide, *ii*) benzyl chloride, *iii*) chloroacetyl chloride, *iv*) formaldehyde and a secondary amine and *v*) trifluoroacetic anhydride in the ionic liquid [bmim]PF$_6$ to give *N*-benzimidazolyl substituted derivatives **5a**–**i**.

Although compounds **4a**–**c** have two NH groups, one in the benzimidazolyl moiety and another in the diazepine ring, it was observed that only NH of benzimidazolyl moiety was replaced by various substituents. The NH of the diazepine moiety could not be replaced due to hydrogen bonding with the C=O of the pyrimidine ring.

The formation of compounds **5a**–**i** were confirmed by the disappearance of peak due to the NH of the benzimidazolyl moiety and the appearance of a peak due to N-substituent in their IR, ^{1}H-NMR and ^{13}C-NMR spectra. The mass spectrum also shows M[+] at *m/z* 392 (**5a**).

Anti-anxiety activity in mice

Synthesized compounds **4a**–**c** and **5a**–**i** were screened for their anti-anxiety activity in mice on a plus maze apparatus devised by Crawley and Godwin[20] modified by Kilfoil.[21] The less time a mouse spent in the dark space, the greater was the anti-anxiety activity of the drug. The results of the anti-anxiety activity of the compounds are given in Table I. Compounds **4c**, **5b**, **5e**, **5h** and **5i** showed better activity than the standard, sodium pentabarbitone, and the other compounds were moderately active. The good activity of these compounds is due to presence of trifluoromethyl, chloro and trifluoroacetyl groups, which enhance their activity.

TABLE I. Results of anti-anxiety activity in mice of compounds **4a**–**c** and **5a**–**i**

Compound	R^1	R^2	R^3	Time spent in dark space, s
4a	CH$_3$	CH$_3$	–	300±9.2
4b	CH$_3$	C$_6$H$_5$	–	298±8.4
4c	CF$_3$	C$_6$H$_5$	–	291±8.2
5a	CH$_3$	CH$_3$	CH$_3$	304±10.5
5b	CH$_3$	C$_6$H$_5$	CH$_3$	294±10.2
5c	CH$_3$	CH$_3$	CH$_2$Ph	314±9.2
5d	CH$_3$	C$_6$H$_5$	CH$_2$Ph	318±10.8
5e	CH$_3$	CH$_3$	COCH$_2$Cl	294±12.0
5f	CH$_3$	C$_6$H$_5$	CH$_2$NMe$_2$	318±11.7
5g	CH$_3$	C$_6$H$_5$	CH$_2$NEt$_2$	321±10.5
5h	CH$_3$	CH$_3$	COCF$_3$	292±9.20
5i	CF$_3$	C$_6$H$_5$	COCF$_3$	290±9.82
Control				401.6±25.0
Pentabarbitone				295±11.50

CONCLUSIONS

Novel 7-(1*H*-benzimidazol-2-ylazo)-1,3-dimethyl-6,8-disubstituted-1*H*-pyrimido[4,5-*b*][1,4]diazepine-2,4-diones **4a**–**c** were synthesized in aqueous medium by the reaction of 2-[(1*H*-benzimidazol-2-yl)hydrazono]-1,3-disubstituted-1,3-diones **3a**–**c** and 5,6-diamino-1,3-dimethyluracil hydrochloride. Further, the title compounds were reacted with various reagents/reactants in [bmim]PF$_6$ to determine whether all NH groups of the title compounds could be substituted. It was observed that only monosubstitution was possible yielding **5a**–**i** as the diazepine NH is involved in hydrogen bonding with the C=O of the pyrimidine ring. Compounds **4a**–**c** and **5a**–**i** were screened for their anti-anxiety activity in

mice and the data revealed that the compounds showed good to moderate activity. Some of the compounds were more active than the standard and could act as potential anti-anxiety agents.

SUPPLEMENTARY MATERIAL

Analytical and spectral data for the compounds **3a**–**c**, **4a**–**c** and **5a**–**i** are available electronically from http://www.shd.org.rs/JSCS/, or from the corresponding author on request.

И З В О Д

СИНТЕЗА НОВИХ 6,8-ДИСУПСТИТУИСАНИХ 7-(1*H*-БЕНЗИМИДАЗОЛ-2-ИЛАЗО)-1,3--ДИМЕТИЛ-1*H*-ПИРИМИДО[4,5-*b*][1,4]ДИАЗЕПИН-2,4-ДИОНА КАО ПОТЕНЦИЈАЛНИХ ЛЕКОВА ПРОТИВ АНКСИОЗНОСТИ

KANTI SHARMA и RENUKA JAIN

Department of Chemistry, University of Rajasthan, Jaipur 302 004, India

Развијен је ефикасан поступак синтезе нових 6,8-дисупституисаних 7-(1*H*-бензими-дазол-2-илазо)-1,3-диметил-1*H*-пиримидо[4,5-*b*][1,4]диазепин-2,4-диона, у води под благим реакционим условима. Описани поступак је добра алтернатива за синтезу ових деривата, у квантитативном приносу на једноставан и економски приступачан начин. Осим тога, NH-група производа дериватизована је различитим супституентима, реакцијом у јонској течности, [bmim]PF_6, растварачу који може да се рециклира и еколошки је прихватљив. Синтетисана једињења су окарактерисана аналитичким и спектроскопским методама (IC, ^{1}H-NMR, ^{13}C-NMR и FAB масена спектрометрија) и испитана је њихова антианксиозна активност на мишевима.

(Примљено 9. априла, ревидирано 29. јула 2012)

REFERENCES

1. B. G. Mohamed, A. Abdel, M. A. Hussein, *Acta Pharm.* **56** (2006) 31
2. G. Akula, B. Srinivas, M. Vidyasagar, S. Kandikonda, *Int. J. Pharm. Tech. Res.* **3** (2011) 360
3. J. Camacho, A. Barazarte, N. Gamboa, J. Rodrigues, R. Rojas, A. Vaisberg, R. Gilman, J. Charris, *Bioorg. Med. Chem.* **19** (2011) 2023
4. A. Gellis, H. Kovacic, N. Boufatah, P. Vanelle, *Eur. J. Med. Chem.* **43** (2008) 1858
5. J. F. Miller, E. M. Turner, K. S. Gudmundsson, S. Jenkinson, A. Spaltenstein, M. Thomson, P. Wheelan, *Bioorg. Med. Chem. Lett.* **20** (2010) 2125
6. S. Sridhar, Y. Rajendra Prasad, S. C. Dinda, *Int. J. Pharm. Sci. Res.* **2** (2011) 2562
7. O. A. Fathalla, I. F. Zeid, M. E. Haiba, A. M. Soliman, S. I. Abd-Elmoez, W. S. El-Serway, *World J. Chem.* **4** (2009) 127
8. G. Oster, D. M. Huse, S. F. Adams, J. Imbimbo, M. W. Russell, *Am. J. Public Health* **80** (1990) 1467
9. H. Schutz, *Benzodiazepines*, Springer, Heidelberg, Germany, 1982

10. R. A. Kusams, M. Ghate, M. V. Kulkarni, *J. Chem. Sci.* **116** (2004) 265
11. S. A. Said, A. E. Amr, N. M. Sabry, M. M. Abdalla, *Eur. J. Med. Chem.* **44** (2009) 4787
12. M. Fodili, M. Amari, B. Kolli, A. Robert, M. Baudy-Floch, P. Le Grel, *Synthesis* **5** (1999) 811
13. R. Kaoua, N. Bennamane, S. Bakhta, S. Benadji, C. Rabia, B. Nedjar-Kolli, *Molecules* **16** (2011) 92
14. M. M. Heravi, S. Sadjadi, H. A. Oskooie, *J. Chin. Chem. Soc.* **55** (2008) 842
15. K. Sharma, R. Jain, *Phosphorus, Sulfur Silicon Relat. Elem.* **186** (2011) 2086
16. R. Jain, K. Sharma, D. Kumar, *Tetrahedron Lett.* **53** (2012) 1993
17. R. Jain, K. Sharma, D. Kumar, *Tetrahedron Lett.* **53** (2012) 6236
18. P. T. Anatas, J. C. Warner, *Green Chemistry Theory and Practice*, Oxford University Press, New York, 2000
19. K. Sharma, V. Sareen, V. Khatri, *Indian J. Heterocycl. Chem.* **14** (2004) 161
20. J. N. Crawley, F. K. Godwin, *Pharm. Biochem. Behav.* **13** (1980) 167
21. T. Kilfoil, A. Michel, D. Montgomony, *Psychol. Pharmacol.* **28** (1988) 901
22. R. Jain, T. Yadav, M. Kumar, A. K. Yadav, *J. Heterocycl. Chem.* **47** (2010) 603.

SUPPLEMENTARY MATERIAL TO

Synthesis of some novel 7-(1*H*-benzimidazol-2-ylazo)-1,3-dimethyl-6,8-disubstituted-1*H*-pyrimido[4,5-*b*][1,4]diazepine-2,4-diones as potential anti-anxiety agents

KANTI SHARMA* and RENUKA JAIN

Department of Chemistry, University of Rajasthan, Jaipur 302 004, India

ANALYTICAL AND SPECTRAL DATA FOR THE COMPUNDS **3a–c**, **4a–c** AND **5a–i**

*3-[(1*H*-Benzimidazol-2-yl)hydrazono]pentane-2,4-dione (3a).* Yield: 94 %; m.p. 160–162 °C; Anal. Calcd. for $C_{12}H_{12}N_4O_2$: C, 59.01; H, 4.91; N, 22.95 %. Found: C, 59.03; H, 4.95; N, 22.91 %; IR (KBr, cm^{-1}): 1620 (C=N), 1680 (C=O), 3205 (NH benz.), 3050 (NH-hydrazono); ^{1}H-NMR (300 MHz, CDCl$_3$, δ / / ppm): 1.56 (3H, *s*, CH$_3$), 1.75 (3H, *s*, CH$_3$), 7.12–8.56 (4H, *m*, Ar–H), 9.51 (1H, *s*, NH benz.), 10.52 (1H, *s*, NH hydrazono); ^{13}C-NMR (75 MHz, CDCl$_3$, δ / ppm): 29.8 (CH$_3$), 30.5 (CH$_3$), 116.5–135.8 (Ar-C), 162.4 (C=N), 178.2 (C=O), 180.1 (C=O); MS (*m/z*): 244 (M$^+$).

*2-[(1*H*-Benzimidazol-2-yl)hydrazono]-1-phenylbutane-1,3-dione (3b).* Yield: 95 %; m.p. 182–183 °C; Anal. Calcd. for $C_{17}H_{14}N_4O_2$: C, 66.66; H, 4.57; N, 18.30 %. Found: C, 66.70; H, 4.53; N, 18.34 %; IR (KBr, cm^{-1}): 1610 (C=N), 1685 (C=O), 3080 (NH-hydrazono), 3215 (NH benz.); ^{1}H-NMR (300 MHz, CDCl$_3$, δ / ppm): 1.65 (3H, *s*, –CH$_3$), 6.95–8.09 (9H, *m*, Ar–H), 9.45 (1H, *s*, NH benz.), 10.62 (1H, *s*, NH hydrazono); ^{13}C-NMR (75 MHz, CDCl$_3$, δ / ppm): 31.2 (CH$_3$), 115.2–137.6 (Ar-C), 160.4 (C=N), 175.0 (C=O), 182.3 (C=O); MS (*m/z*): 306 (M$^+$).

*2-[(1*H*-Benzimidazol-2-yl)hydrazono]-4,4,4-trifluoro-1-phenyl-butane-1,3-dione (3c)* Yield: 92 %; m.p. 145–147 °C; Anal. Calcd. for $C_{17}H_{11}N_4O_2F_3$: C, 56.66; H, 3.05; N, 15.55 %. Found: C, 56.69; H, 3.08; N, 15.58 %; IR (KBr, cm^{-1}): 1618 (C=N), 1690 (C=O), 3200 (NH benz.), 3020 (NH-hydrazono); ^{1}H-NMR (300 MHz, CDCl$_3$, δ / ppm): 6.85–8.02 (9H, *m*, Ar–H), 9.46 (1H, *s*, NH benz.), 10.54 (1H, *s*, NH hydrazono); ^{13}C-NMR (75 MHz, CDCl$_3$, δ / ppm): 115.4 (CF$_3$), 116.2–137.8 (Ar-C), 164.2 (C=N), 175.3 (C=O), 181.4 (C=O); MS (*m/z*): 360 (M$^+$).

---

* Corresponding author. E-mail: drkanti@gmail.com

*7-(1*H*-Benzimidazol-2-ylazo)-1,3,6,8-tetramethyl-1*H*-pyrimido[4,5-*b*][1,4]-diazepine-2,4(3*H,5*H*)-dione (4a)*. Yield: 92 %; m.p. 220–222 °C; Anal. Calcd. for $C_{18}H_{18}N_8O_2$: C, 57.14; H, 4.76; N, 29.62 %. Found: C, 57.18; H, 4.80; N, 29.60 %; IR (KBr, cm^{-1}): 1560 (N=N), 1626 (C=N), 1700 (C=O), 1720 (C=O), 3220 (NH benz.), 3340 (NH diazepine); ^{1}H-NMR (300 MHz, CDCl$_3$, δ / ppm): 1.54 (3H, *s*, CH$_3$), 1.68 (3H, *s*, CH$_3$), 3.32 (3H, *s*, NCH$_3$), 3.63 (3H, *s*, NCH$_3$), 6.89–7.86 (4H, *m*, Ar–H), 8.46 (1H, *s*, NH diazepine), 9.51 (1H, *s*, NH benz.); ^{13}C-NMR (75 MHz,CDCl$_3$, δ / ppm): 28.4 (CH$_3$), 30.2 (CH$_3$), 33.5 (NCH$_3$), 34.9 (NCH$_3$), 115.6–138.4 (Ar-C), 190.2(C=O), 195.1 (C=O); MS (*m/z*): 378 (M$^+$).

*7-(1*H*-Benzimidazol-2-ylazo)-1,3,8-trimethyl-6-phenyl-1*H*-pyrimido[4,5--b][1,4]diazepine-2,4(3*H,5*H*)-dione (4b)*. Yield: 95 %; m.p. 239–240 °C; Anal. Calcd. for $C_{23}H_{20}N_8O_2$: C, 62.72; H, 4.54; N, 25.45 %. Found: C, 62.75, H, 4.58, N, 25.48 %; IR (KBr, cm^{-1}): 1540 (N=N), 1628 (C=N), 1700 (C=O), 1725 (C=O), 3212 (NH benz.), 3350 (NH diazepine); ^{1}H-NMR (300 MHz, CDCl$_3$, δ / / ppm): 1.60 (3H, *s*, CH$_3$), 3.26 (3H, *s*, NCH$_3$), 3.78 (3H, *s*, NCH$_3$), 6.56–7.84 (9H, *m*, Ar–H), 8.39 (1H, *s*, NH diazepine), 9.53 (1H, *s*, NH benz.); ^{13}C-NMR (75 MHz, CDCl$_3$, δ / ppm): 29.3 (CH$_3$), 33.6 (NCH$_3$), 34.8 (NCH$_3$), 115.8–137.9 (Ar-C); 189.4 (C=O), 194.3 (C=O); MS (*m/z*): 440 (M$^+$).

*7-(1*H*-Benzimidazol-2-ylazo)-1,3-dimethyl-6-phenyl-8-(trifluoromethyl)-1*H*--pyrimido[4,5-*b*][1,4]diazepine-2,4(3*H,5*H*)-dione (4c)*. Yield: 94 %; m.p. 189––191 °C; Anal. Calcd. for $C_{23}H_{17}N_8O_2F_3$: C, 55.87; H, 3.44; N, 22.67 %. Found: C, 55.83; H, 3.47; N, 22.70 %; IR (KBr, cm^{-1}): 1560 (N=N), 1630 (C=N), 1710 (C=O), 1730, 3205 (NH benz.), 3345 (NH diazepine); ^{1}H-NMR (300 MHz) CDCl$_3$, δ / ppm): 3.25 (3H, *s*, NCH$_3$), 3.80 (3H, *s*, NCH$_3$), 6.59–7.78 (9H, *m*, Ar–H), 8.42 (1H, *s*, NH diazepino), 9.48 (1H, *s*, NH benz.); ^{13}C-NMR (75 MHz, CDCl$_3$, δ / ppm): 34.1 (NCH$_3$), 35.2 (NCH$_3$), 115.2 (CF$_3$), 116.2–138.5 (Ar-C), 185.5 (C=O), 196 .2 (C=O); MS (*m/z*): 494 (M$^+$).

*1,3,6,8-Tetramethyl-7-[(1-methyl-1*H*-benzimidazol-2yl)azo]-1*H*-pyrimido-[4,5-*b*][1,4]diazepine-2,4(3*H,5*H*)-dione (5a)*. Yield: 92 %; m.p. 170–172°C; Anal. Calcd. for $C_{19}H_{20}N_8O_2$: C, 58.16; H, 5.10; N, 28.57 %. Found: C, 58.20; H, 5.13; N, 28.53 %; IR (KBr, cm^{-1}): 1560 (N=N), 1610 (C=N), 1695 (C=O), 1720 (C=O), 3320 (NH diazepine); ^{1}H-NMR (300 MHz, CDCl$_3$, δ / ppm): 1.73 (3H, *s*, CH$_3$), 1.86 (3H, *s*, CH$_3$), 3.38 (3H, *s*, NCH$_3$), 3.52 (3H, *s*, NCH$_3$), 3.69 (3H, *s*, NCH$_3$), 6.56–7.92 (4H, *m*, Ar–H), 8.61 (1H, *s*, NH diazepine); ^{13}C-NMR (75 MHz, CDCl$_3$, δ / ppm): 28.2 (CH$_3$), 30.6 (CH$_3$), 33.3 (NCH$_3$), 34.8 (NCH$_3$), 35.6 (NCH$_3$), 117.2–139.2 (Ar-C), 189.4 (C=O), 194.2 (C=O); MS (*m/z*): 392 (M$^+$).

*1,3,8-Trimethyl-7-[(1-methyl-1*H*-benzimidazol-2-yl)azo]-6-phenyl-1*H*-pyrimido[4,5-*b*][1,4]diazepine-2,4(3*H,5*H*)-dione (5b)*. Yield: 92 %; m.p. 191–192 °C; Anal. Calcd. for $C_{24}H_{22}N_8O_2$: C, 63.43; H, 4.894; N, 24.66 %. Found: C, 63.40; H, 4.82; N, 24.70 %; IR (KBr, cm^{-1}): 1550 (N=N), 1610 (C=N), 1705

(C=O), 1730 (C=O), 3360 (NH diazepine); ^{1}H-NMR (300 MHz, CDCl$_3$, δ / ppm): 1.68 (3H, s, CH$_3$), 3.41 (3H, s, NCH$_3$), 3.56 (3H, s, NCH$_3$), 3.72 (3H, s, NCH$_3$), 6.78–8.02 (9H, m, Ar–H), 8.47 (1H, s, NH diazepine); ^{13}C-NMR (75 MHz, CDCl$_3$, δ / ppm): 28.6 (CH$_3$), 33.7 (NCH$_3$), 34.6 (NCH$_3$), 35.8 (NCH$_3$), 116.2––138.6 (Ar-C), 190.3 (C=O), 193.6 (C=O); MS (m/z): 454 (M$^+$).

*7-[(1-Benzyl-1*H-*benzimidazol-2-yl)azo]-1,3,6,8-tetramethyl-1*H-*pyrimido[4,5--b][1,4]diazepine-2,4(3*H,5H)*-dione (5c)*. Yield: 95 %; m.p. 126–128 °C; Anal. Calcd. for C$_{25}$H$_{24}$N$_8$O$_2$: C, 64.10; H, 5.12; N, 23.93 %. Found: C, 64.14; H, 5.15; N, 23.90 %; IR (KBr, cm^{-1}): 1560 (N=N), 1620 (C=N), 1720 (C=O), 1735 (C=O), 3310 (NH diazepine); ^{1}H-NMR (300 MHz, CDCl$_3$, δ / ppm): 1.69 (3H, s, CH$_3$); 1.78 (3H, s, CH$_3$), 3.31 (3H, s, NCH$_3$), 3.59 (3H, s, NCH$_3$), 4.02 (2H, s, CH$_2$), 6.75–7.86 (9H, m, Ar–H), 8.68 (1H, s, NH diazepine); ^{13}C-NMR (75 MHz, CDCl$_3$, δ / ppm): 28.4 (CH$_3$), 30.5 (CH$_3$), 33.8 (NCH$_3$), 34.5 (NCH$_3$), 43.8(NCH$_2$Ph), 115.8–138.7 (Ar-C), 186.5 (C=O), 192.4 (C=O); MS (m/z): 468 (M$^+$).

*7-[(1-Benzyl-1*H-*benzimidazol-2-yl)azo]-1,3,8-trimethyl-6-phenyl-1*H-*pyrimido[4,5*-b]*[1,4]diazepine-2,4(3*H,5H)*-dione (5d)*. Yield: 94 %; m.p. 139–140 °C; Anal. Calcd. for C$_{30}$H$_{26}$N$_8$O$_2$: C, 67.92; H, 4.90; N, 21.13 %. Found: C, 67.90; H, 4.94; N, 21.17 %; IR (KBr, cm^{-1}): 1580 (N=N), 1625 (C=N), 1710 (C=O), 1730 (C=O), 3315 (NH diazepine); ^{1}H-NMR (300 MHz, CDCl$_3$, δ / ppm): 1.80 (3H, s, CH$_3$), 3.34 (3H, s, NCH$_3$), 3.68 (3H, s, NCH$_3$), 4.12 (2H, s, CH$_2$), 6.69–8.02 (14H, m, Ar–H), 8.92 (1H, s, NH diazepine); ^{13}C -NMR (75 MHz, CDCl$_3$, δ / ppm): 29.2 (CH$_3$), 33.5 (NCH$_3$), 34.8 (NCH$_3$), 43.4 (NCH$_2$Ph) 116.2–137.8 (Ar-C), 190.8 (C=O), 197.2 (C=O); MS (m/z): 530 (M$^+$).

*7-{[1-(Chloroacetyl)-1*H-*benzimidazol-2-yl]azo}-1,3,6,8-tetramethyl-1*H-*pyrimido[4,5*-b]*diazepine-2,4(3*H,5H)*-dione (5e)*. Yield: 93 %; m.p. 143–145 °C; Anal. Calcd. for C$_{20}$H$_{19}$N$_8$O$_3$Cl: C, 52.80; H, 4.18; N, 24.64 %. Found: C, 52.84; H, 4.14; N, 24.68 %; IR (KBr, cm^{-1}): 1540 (N=N), 1625 (C=N), 1680 (C=O), 1710 (C=O), 1725 (C=O), 3320 (NH diazepine); ^{1}H-NMR (300 MHz, CDCl$_3$, δ / ppm): 1.65 (3H, s, CH$_3$), 1.70 (3H, s, CH$_3$), 3.42 (3H, s, NCH$_3$), 3.64 (3H, s, NCH$_3$), 4.23 (2H, s, CH$_2$Cl), 6.78–7.78 (9H, m, Ar–H), 8.92 (1H, s, NH diazepine); ^{13}C-NMR (75 MHz, CDCl$_3$, δ / ppm): 28.6 (CH$_3$), 30.8 (CH$_3$), 33.5 (NCH$_3$), 34.9 (NCH$_3$), 46.4 (CH$_2$Cl), 116.5–137.6 (Ar-C), 182.2 (C=O), 190.4 (C=O), 196.3 (C=O); MS (m/z): 454.5 (M$^+$).

*7-{[1-(Dimethylamino)methyl-1*H-*benzimidazol-2-yl]azo}-1,3,8-trimethyl-6--phenyl-1*H-*pyrimido[4,5*-b]*-[1,4]-diazepine-2,4(3*H,5H)*-dione (5f)*. Yield: 92 %; m.p. 128–130 °C; Anal. Calcd. for C$_{26}$H$_{27}$N$_9$O$_2$: C, 62.77; H, 5.43; N, 25.35 %. Found: C, 62.79; H, 5.41; N, 25.38 %; IR (KBr, cm^{-1}): 1580 (N=N), 1630 (C=N), 1705 (C=O), 1720 (C=O), 3330 (NH diazepine); ^{1}H-NMR (300 MHz, CDCl$_3$, δ / ppm): 1.76 (3H, s, CH$_3$), 3.40 (3H, s, NCH$_3$), 3.52 (6H, s, N(CH$_3$)$_2$), 3.69 (3H, s, NCH$_3$), 4.21 (2H, s, NCH$_2$–N), 6.75–7.98 (9H, m, Ar–H), 8.96 (1H, s,

NH diazepine); ^{13}C-NMR (75 MHz, CDCl$_3$, δ / ppm): 29.5 (CH$_3$), 33.4 (NCH$_3$), 34.7 (–NCH$_3$), 35.4 (N(CH$_3$)$_2$), 116.8–137.8 (Ar-C), 191.5 (C=O), 194.3 (C=O), 168.2 (NCH$_2$N); MS (*m/z*): 497 (M$^+$).

*7-{[1-(Diethylamino)methyl-1*H-*benzimidazol-2-yl]azo}-1,3,8-trimethyl-6-*
*-phenyl-1*H-*pyrimido[4,5-*b*][1,4]-diazepine-2,4(3*H,5*H)-dione (5g)*. Yield: 94 %; m.p. 135–136 °C; Anal. Calcd. for C$_{28}$H$_{31}$N$_9$O$_2$: C, 64.00; H, 5.90; N, 24.00 %. Found: C, 64.04; H, 5.92; N, 24.03 %; IR (KBr, cm^{-1}): 1560 (N=N), 1628 (C=N), 1710 (C=O), 1725 (C=O), 3318 (NH diazepine); ^{1}H-NMR (300 MHz CDCl$_3$, δ / / ppm): 1.26 (6H, *t*, *J* = 7.0 Hz, N(CH$_2$C**H**$_3$)$_2$), 1.60 (3H, *s*, CH$_3$), 3.50 (4H, *q*, *J* = 7.0 Hz, N(C**H**$_2$CH$_3$)$_2$), 3.62 (3H, *s*, NCH$_3$), 3.79 (3H, *s*, NCH$_3$), 4.42 (2H, *s*, NCH$_2$–N), 6.68–7.89 (9H, *m*, Ar–H), 8.67 (1H, *s*, NH diazepine); ^{13}C-NMR (75 MHz, CDCl$_3$, δ / ppm): 28.4 (N(CH$_2$**C**H$_3$)$_2$), 29.2 (CH$_3$), 34.3 (NCH$_3$), 34.9 (NCH$_3$), 116.5–137.8 (Ar-C), 126.2 (N(**C**H$_2$CH$_3$)$_2$), 169.8 (N–CH$_2$–N), 189.8 (C=O), 193.2 (C=O); MS (*m/z*): 525 (M$^+$).

*1,3,6,8-Tetramethyl-7-{[1-trifluoroacetyl)-1*H-*benzimidazol-2-yl]azo}-1*H-*py-*
*rimido[4,5-*b*][1,4]-diazepine-2,4(3*H,5*H)-dione (5h)*. Yield: 95 %; m.p. 120–122 °C; Anal. Calcd. for C$_{20}$H$_{17}$N$_8$O$_3$F$_3$: C, 50.63; H, 3.58; N, 23.62 %. Found: C, 50.65; H, 3.54; N, 23.64 %; IR (KBr, cm^{-1}): 1565 (N=N), 1620 (C=N), 1680 (**CO**CF$_3$), 1700 (C=O), 1720 (C=O), 3310 (NH diazepine); ^{1}H-NMR (300 MHz, CDCl$_3$, δ / ppm): 1.75 (3H, *s*, CH$_3$), 1.85 (3H, *s*, CH$_3$), 3.50 (3H, *s*, NCH$_3$), 3.67 (3H, *s*, NCH$_3$), 6.58–7.87 (4H, *m*, Ar–H), 8.86 (1H, *s*, NH diazepine); ^{13}C-NMR (75 MHz, CDCl$_3$, δ / ppm): 28.2 (CH$_3$), 30.4 (CH$_3$), 34.8 (–NCH$_3$), 35.6 (NCH$_3$), 116.2 (CF$_3$), 116.8–138.2 (Ar-C), 187.6 (**C**OCF$_3$), 190.3 (C=O), 193.2 (C=O); MS (*m/z*): 474 (M$^+$).

*1,3,8-Trimethyl-6-phenyl-7-{[1-trifluoroacetyl)-1*H-*benzimidazol-2-yl]azo}-*
*-1*H-*pyrimido[4,5-*b*][1,4]-diazepine-2,4(3*H,5*H)-dione (5i)*. Yield: 97 %; m.p. 108–109 °C; Anal. Calcd. for C$_{25}$H$_{19}$N$_8$O$_3$F$_3$: C, 55.97; H, 3.54; N, 20.89 %. Found: C, 55.94; H, 3.52; N, 20.86 %; IR (KBr, cm^{-1}): 3300 (NH diazepine), 1545 (N=N), 1625 (C=N), 1685 (**CO**CF$_3$), 1710 (C=O), 1725 (C=O); ^{1}H-NMR (300 MHz, CDCl$_3$, δ / ppm): 1.79 (3H, *s*, CH$_3$), 3.52 (3H, *s*, NCH$_3$), 3.68 (3H, *s*, NCH$_3$), 6.56–7.88 (9H, *m*, Ar–H), 8.88 (1H, *s*, NH diazepine), ^{13}C-NMR (75 MHz, CDCl$_3$, δ / ppm): 29.4 (CH$_3$), 34.4 (NCH$_3$), 35.2 (NCH$_3$), 116.0 (CF$_3$), 116.4–138.9 (Ar-C), 187.2 (**C**OCF$_3$), 190.2 (C=O), 194.0 (C=O); MS (*m/z*): 536 (M$^+$).

SHORT COMMUNICATION

In situ generated hypoiodous acid in an efficient and heterogeneous catalytic system for the homo-oxidative coupling of thiols

ARASH GHORBANI-CHOGHAMARANI*, MOHSEN NIKOORAZM
and GOUHAR AZADI

*Department of Chemistry, Faculty of Science, Ilam University,
P. O. Box 69315516, Ilam, Iran*

Abstract: Supported hydrogen peroxide on polyvinylpolypyrrolidone (PVPP––H_2O_2), silica sulfuric acid (SiO$_2$–OSO$_3$H) and catalytic amounts of potassium iodide (KI) was developed as a heterogeneous medium for the rapid oxidative coupling of thiols into symmetrical homodisulfides. This oxidizing system proceeds under extremely mild conditions and gives no other oxidized side products.

Keywords: supported hydrogen peroxide on polyvinylpolypyrrolidone; potassium iodide; silica sulfuric acid.

INTRODUCTION

In recent years, supported reagents on polymeric structures have become increasingly popular in organic synthesis,[1–5] because of their mild and heterogeneous nature together with advantages of easy work-up of the products. The conversion of thiols to the corresponding disulfides is an important and interesting transformation in organic chemistry due to the central importance of this functional group in diverse areas of chemistry and biology,[6–11] and oxidation is the most common methodology used for their preparation because of the commercial availability of thiols. A variety of oxidants have been reported for the conversion of thiols into disulfides, such as tributylammonium halochromates//silica gel,[12] Fe(HSO$_4$)$_3$ or Fe(HSO$_4$)$_3$/DMSO,[13] Al(NO$_3$)$_3$·9H$_2$O/SiO$_2$–OSO$_3$H,[14] (C$_3$H$_7$)$_3$NH[CrO$_3$X], (X = F or Cl)/Al$_2$O$_3$,[15] *N*-bromosuccinimide,[16] poly(4-vinylpyridinium nitrate),[17] H$_2$O$_2$/NaI,[18] urea–hydrogen peroxide/maleic anhydride,[19] ethylenebis(*N*-methylimidazolium) chlorochromate,[20] manganese(III)


173

Schiff-base complexes,[21] Au/CeO$_2$,[22] Co(II) and Mn(II) salts of 4-aminobenzoic acid supported on silica gel[23] and Zn(II)–Al(III) double layer hydroxide with intercalated [Mo^{VI}O$_2$(O$_2$CC(S)Ph$_2$)$_2$]$^{2-}$.[24] Some of these procedures suffer from one or more disadvantages, such as long reaction times, overoxidation, tedious work-up, low yields of the products, heavy metal contamination, harsh conditions, and expensive reagents or catalysts.

Hydrogen peroxide (H$_2$O$_2$) is a powerful oxidizing agent that has been used as an oxidant for the oxidation of different types of organic moieties,[25,26] and in order to avoid the hazards connected with the use of concentrated solutions of hydrogen peroxide, this compound has been used supported on a carrier.[25,27,28] In this regard, polyvinylpolypyrrolidone-supported hydrogen peroxide (PVPP–H$_2$O$_2$) has proved to be one of the most popular choices with its advantages of insolubility in organic solvents, easy work-up of products, non-toxic content and mild oxidizing properties. Therefore, it was decided to study the application of this polymeric reagent for the oxidative homocoupling of thiols in conjunction with silica sulfuric acid (SiO$_2$–OSO$_3$H) and catalytic amounts of potassium iodide (KI).
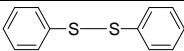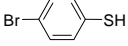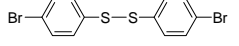
RESULTS AND DISCUSSION
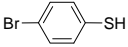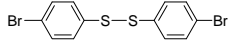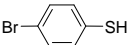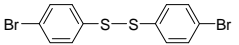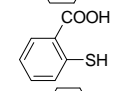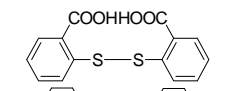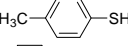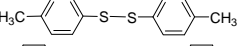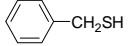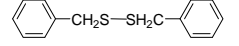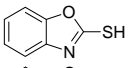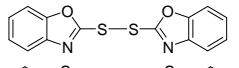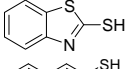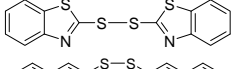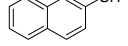
In connection with an ongoing program related to the application of new reagents or reagent systems for organic functional group transformations,[29–35] the preparation of polyvinylpolypyrrolidone-supported hydrogen peroxide (PVPP–H$_2$O$_2$) and its application to the synthesis of symmetrical disulfides from the corresponding thiols were considered of interest.

Therefore, in this study it was decided to design an efficient catalytic system including polyvinylpolypyrrolidone-supported hydrogen peroxide (PVPP–H$_2$O$_2$), silica sulfuric acid and potassium iodide (as catalyst) for the *in situ* generation of hypoiodous acid (IOH), as the active oxidant. A variety of aliphatic and aromatic thiols **1** were converted to the corresponding disulfides **2** using polyvinylpolypyrrolidone-supported hydrogen peroxide (PVPP–H$_2$O$_2$) and silica sulfuric acid (SiO$_2$–OSO$_3$H) in the presence of catalytic amounts of potassium iodide (KI) in dichloromethane or ethyl acetate (as solvent) at room temperature (Scheme 1). The results of this transformation are summarized in Table I.
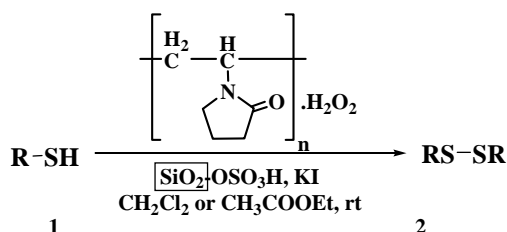
Scheme 1. Oxidative coupling of thiols.

TABLE I. Oxidative coupling of thiols into disulfides using PVPP–H_2O_2 and SiO_2–OSO_3H in the presence of a catalytic amount of KI at room temperature

Entry	Substrate	Product[a]	Time, min	Yield, %[b]	Melting point, °C Found	Melting point, °C Reported	Ref.
1	C6H5–SH	C6H5–S–S–C6H5	40	99	55–58	59–61	34
2	Br–C6H4–SH	Br–C6H4–S–S–C6H4–Br	15	99	91–93	89–92	17
3	Br–C6H4–SH	Br–C6H4–S–S–C6H4–Br	1440	54[c]	91–93	89–92	17
4	Br–C6H4–SH	Br–C6H4–S–S–C6H4–Br	1440	91[d]	91–93	89–92	17
5	2-HOOC–C6H4–SH	2-HOOC–C6H4–S–S–C6H4–COOH-2	60	86	288–292	273–285	17
6	H3C–C6H4–SH	H3C–C6H4–S–S–C6H4–CH3	30	99	40–43	39–42	17
7	C6H5–CH2SH	C6H5–CH2S–SH2C–C6H5	30	83	–	–	19
8	benzoxazole-2-thiol	bis(benzoxazol-2-yl) disulfide	30	97	93–98	84–88	17
9	benzothiazole-2-thiol	bis(benzothiazol-2-yl) disulfide	40	95	174–177	177–179	17
10	naphthalen-2-thiol	bis(naphthalen-2-yl) disulfide	40	99	135–138	141–144	17
11	$HSCH_2CH_2OH$	$HOCH_2CH_2S$–SCH_2CH_2OH	20	82	/[e]	/	34
12	$HSCH_2COOH$	$HOOCCH_2S$–SCH_2COOH	20	98	/	/	17

[a]Substrate/PVPP–H_2O_2/SiO_2–OSO_3H/KI = 1 mmol/0.175 g/0.1 g/0.02 mmol; [b]isolated yield; [c]in the absence of KI; [d]in the absence of silica sulfuric acid; [e]oil

All of the coupling reactions were realized under completely heterogeneous conditions in which the product was easily obtained by simple filtration, washing the filtrate with an organic solvent and evaporation. Subsequent TLC and ^{1}H-NMR spectroscopic analysis of the residue in each case revealed purity to be > 95 %.

In order to demonstrate the role of potassium iodide as catalyst in the described system, it was decided to design a reaction in the absence of this compound. Therefore, 4-bromothiophenol was reacted with polyvinylpolypyrrolidone-supported hydrogen peroxide and silica sulfuric acid in the absence of potassium iodide. As is evident from Table I (entry 3), 1,2-bis(4-bromophenyl)-disulfane was obtained in 54 % yield after 24 h, which is much less efficient than with the potassium iodide (15 min, 99 % yield) . In addition, in order to study the role of the acid, 4-bromothiophenol (as a typical example) was subjected to oxidative coupling by PVPP–H_2O_2 and catalytic amounts of KI in the absence of silica sulfuric acid. In this case, it was observed that the reaction time was increased to 24 h and 1,2-bis(4-bromophenyl)disulfane was obtained in 91 % yield (Table I, entry 4). Thus, it was concluded that the presence of both the acid and potassium iodide was necessary for the rapid and efficient conversion of a thiol

into the corresponding disulfide by polyvinylpolypyrrolidone-supported hydrogen peroxide (PVPP–H_2O_2). A range of thiols were converted and a range of functional groups are chemoselectively tolerated (HO, CO_2H, heteroaromatic).

A plausible mechanism for this conversion is outlined in the catalytic cycle shown in Scheme 2 based on previously reported work.[18,31,32,36] The key is the production of hypoiodous acid (HOI) as the active oxidant to form a sulfenyl iodide RSI as an intermediate. Coupling of this with another molecule of thiol produces the homodisulfide with formation of HI, which exchanges with the potassium salt of silica–sulfuric acid (Scheme 2) to regenerate KI. In this way, HI is not built up in the reaction.
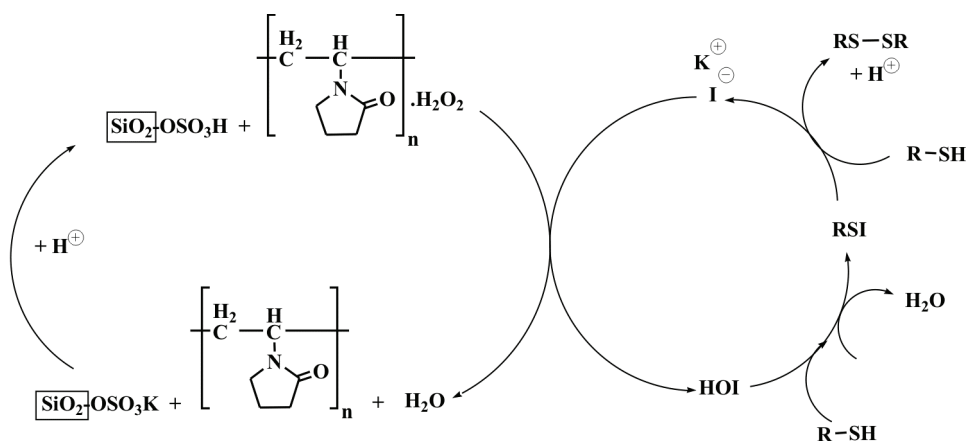
Scheme 2. Mechanism of coupling of thiols by *in situ* generated iodine.

EXPERIMENTAL

Materials and methods

All chemicals and solvents were purchased from Fluka, Merck or Aldrich and were used without further purification. Polyvinylpolypyrrolidone-supported hydrogen peroxide (PVPP––H_2O_2) was prepared *via* the procedure reported by Pourali and Ghanei.[37,38] Silica sulfuric acid was prepared *via* the procedure by reported Zolfigol.[39] All the prepared disulfides are known and were characterized by comparison of their spectral (IR, ^{1}H-NMR or ^{13}C-NMR) and physical data with those of authentic samples.

General procedure for the oxidative coupling of thiols using PVPP–H_2O_2/SiO_2–OSO_3H/KI

To a suspension of polyvinylpolypyrrolidone-supported hydrogen peroxide (0.175 g), silica sulfuric acid (0.1 g) and potassium iodide (0.02 mmol) in dichloromethane or ethyl acetate (5 mL) was added a thiol (1 mmol), and the mixture was stirred at room temperature for the specified time (Table I). The progress of the reaction was monitored by TLC. After completion of the reaction, the reaction mixture was filtered and the residue washed with CH_2Cl_2 (20 mL), (the residue of entry 5 was washed with ethanol). Finally, the organic solvent was evaporated and pure product was obtained as judged by TLC and ^{1}H-NMR spectroscopy.

CONCLUSIONS

In summary, it was demonstrated in this research that polyvinylpolypyr-rolidone-supported hydrogen peroxide (PVPP–H_2O_2) is a practical and versatile oxidizing polymer, which is able to convert a variety of thiols into disulfides in the presence of an acid and iodide salt. The presence of silica sulfuric acid and potassium iodide was found to be critical for the conversion, and the isolation of the product was facile.

ИЗВОД

IN SITU СТВАРАЊЕ ХИПОЈОДАСТЕ КИСЕЛИНЕ У ЕФИКАСНОМ ХЕТЕРОГЕНОМ КАТАЛИТИЧКОМ СИСТЕМУ ЗА ХОМО-ОКСИДАТИВНО КУПЛОВАЊЕ ТИОЛА

ARASH GHORBANI-CHOGHAMARANI, MOHSEN NIKOORAZM и GOUHAR AZADI

Department of Chemistry, Faculty of Science, Ilam University, P. O. Box 69315516, Ilam, Iran

Развијен је хетероген систем који садржи водоник-пероксид на поливинилполи-пиролидину (PVPP–H_2O_2), сумпорну киселину на силика-гелу (SiO$_2$–OSO$_3$H) и катали-тичку количину калијум-јодида (KI). Овакав хетероген систем успешно генерише ката-литичке количине хипојодасте киселине за брзо оксидативно купловање тиола до симет-ричних хомодисулфида. Оксидациони систем је ефикасан при благим реакционим ус-ловима и не производи друге спередне производе оксидације.

(Примљено 23. фебруара, ревидирано 17. маја 2012)

REFERENCES

1. M. A. Karimi-Zarchi, B. F. Mirjalili, Z. Shamsi-Kahrizsangi, M. Tayefi, *J. Iran. Chem. Soc.* **7** (2010) 455
2. A. Ghorbani-Choghamarani, Z. Chenani, S. Mallakpour, *Synth. Commun.* **39** (2009) 4264
3. M. A. Chari, K. Syamasundar, *Catal. Commun.* **6** (2005) 67
4. N. Iranpoor, B. Tamami, K. Niknam, *Can. J. Chem.* **75** (1997) 1913
5. V. Mirkhani, M. Moghadam, S. Tangestaninejad, S. Hajibagheri, *J. Iran. Chem. Soc.* **7** (2010) 641
6. J. M. Herrmann, F. Kauff , H. E. Neuhaus, *Biochim. Biophys. Acta – Mol. Cell Res.* **1793** (2009) 71
7. B. A. Maron, Y. Y. Zhang, D. E. Handy, A. Beuve, S. S. Tang, J. Loscalzo, J. A. Leopold, *J. Biol. Chem.* **284** (2009) 7665
8. S. Fukuzawa, E. Shimizu, Y. Atsuumi, M. Haga, K. Ogata, *Tetrahedron Lett.* **50** (2009) 2374
9. Y. H. Seoa, K. S. Carroll, *Proc. Natl. Acad. Sci. USA* **106** (2009) 16163
10. C. Tidei, M. Piroddi, F. Galli, C. Santi, *Tetrahedron Lett.* **53** (2012) 232
11. D. Witt, *Synthesis* (2008) 2491
12. M. K. Mohammadi, S. Ghammamy, S. Zarrinabadi, M. H. Farjam, B. Sabayan, *Chin. J. Chem.* **28** (2010) 2199
13. H. Eshghi, M. Bakavoli, H. Moradi, A. Davoodnia, *Phosphorus Sulfur Silicon Relat. Elem.* **184** (2009) 3110

14. A. Ghorbani-Choghamarani, M. Nikoorazm, H. Goudarziafshar, B. Tahmasbi, *Bull. Korean Chem. Soc.* **30** (2009) 1388

15. A. HassaniJoshaghani, S. Ghammamy, S. Bagi, A. Moghimi, Z. Javanshir, *Phosphorus Sulfur Silicon Relat. Elem.* **184** (2009) 164

16. H. Ghafuri, M.M. Hashemi, *J. Sulfur Chem.* **30** (2009) 578

17. A. Ghorbani-Choghamarani, S. Sardari, *J. Sulfur Chem.* **32** (2011) 63

18. M. Kirihara, Y. Asai, S. Ogawa, T. Noguchi, A. Hatano, Y. Hirai, *Synthesis* (2007) 3286

19. B. Karami, M. Montazerozohori, M. H. Habibi, *Molecules* **10** (2005) 1358

20. R. Hosseinzadeh, M. Tajbakhsh, H. Khaledi, K. Ghodrati, *Monatsh. Chem.* **138** (2007) 871

21. H. Golchoubian, F. Hosseinpoor, *Catal. Commun.* **8** (2007) 697

22. A. Corma, T. Rodenas, M. J. Sabater, *Chem. Sci.* **3** (2012) 398.

23. M. M. Hashemi, Z. Karimi-Jaberi, *Monatsh. Chem.* **135** (2004) 41.

24. A. Cervilla, A. Corma, V. Fornes, E. Llopis, P. Palanca, F. Reyy, A. Ribera, *J. Am. Chem. Soc.* **116** (1994) 1595.

25. S. P. Mardur, G. S. Gokavi, *J. Iran. Chem. Soc.* **7** (2010) 441

26. A. Hasaninejad, M. A. Zolfigol, G. Chehardoli, M. Mokhlesi, *J. Serb. Chem. Soc.* **75** (2010) 307

27. M. A. Zolfigol, P. Salehi, S. E. Mallakpour, M. Torabi, *Bull. Chem. Soc. Japan* **76** (2003) 1673

28. B. Karimi, D. Zareyee, *J. Iran. Chem. Soc.* **5** (2008) S103

29. G. Chehardoli, M. A. Zolfigol, *Phosphorus Sulfur Silicon Relat. Elem.* **185** (2010) 193

30. A. Ghorbani-Choghamarani, M. Hajjami, H. Goudarziafshar, M. Nikoorazm, S. Mallakpour, F. Sadeghizadeh, G. Azadi, *Monatsh. Chem.* **140** (2009) 607

31. A. Ghorbani-Choghamarani, M. Abbasi, *Chin. Chem. Lett.* **22** (2011) 114

32. H. Goudarziafshar, A. Ghorbani-Choghamarani, M. Nikoorazm, Z. Naserifar, *Chin. J. Chem.* **27** (2009) 1801

33. A. Ghorbani-Choghamarani, M. Nikoorazm, H. Goudarziafshar, L. Shiri, Z. Chenani, *Bull. Korean Chem. Soc.* **30** (2009) 972

34. A. Ghorbani-Choghamarani, H. Goudarziafshar, S. Rezaee, S. S. Mortazavi, *Chin. Chem. Lett.* **20** (2009) 415

35. A. Ghorbani-Choghamarani, M. A. Zolfigol, M. Hajjami, S. Rastgoo, S. Mallakpour, *Lett. Org. Chem.* **7** (2010) 249

36. A. Ghorbani-Choghamarani, S. Sardari, *Chin. J. Catal.* **31** (2010) 1347

37. R. Ozen1, F. Aydin, *Monatsh. Chem.* **137** (2006) 307

38. A. R. Pourali, M. Ghanei, *Bull. Korean Chem. Soc.* **27** (2006) 1674

39. M. A. Zolfigol, *Tetrahedron* **57** (2001) 9509.

The effects of ethanol on paracetamol-induced oxidative stress in mice liver

DUŠAN MLADENOVIĆ[1], MILICA NINKOVIĆ[2], DANIJELA VUČEVIĆ[1],
MIODRAG ČOLIĆ[2], MARJAN MICEV[3], VERA TODOROVIĆ[4],
MILENA N. STANKOVIĆ[1] and TATJANA RADOSAVLJEVIĆ[1]*

[1]*Department of Pathophysiology, Faculty of Medicine, University of Belgrade, Serbia,*
[2]*Institute for Medical Research, Military Medical Academy, Belgrade, Serbia,* [3]*Institute for Digestive Diseases, Clinical Centre of Serbia, Belgrade, Serbia and* [4]*Faculty of Stomatology Pančevo, University of Business Academy, Novi Sad, Serbia*

Abstract: The aim of this study was to investigate the effects of binge drinking on paracetamol-induced oxidative stress in mice liver. Male Swiss mice were divided into groups: control; ethanol-treated group (E) in five sequential doses of 2 g kg^{-1}, administered through an orogastric tube; paracetamol-treated group (P) in a dose of 300 mg kg^{-1}, intraperitoneally and a group that received paracetamol 12 h after the last dose of ethanol (PE). Blood and liver samples were collected for the determination of oxidative stress parameters 6, 24 and 48 h after treatment. Prior binge drinking potentiated the paracetamol-induced increase in the liver malondialdehyde level 48 h after treatment in comparison with the P and E groups (17.14±1.98 *vs.* 13.14±0.82 and 12.99±1.18 μmol L^{-1}, respectively, $p < 0.01$). Ethanol and paracetamol in combination induced a more pronounced decrease in the liver GSH level than either of the individual substances alone at all time intervals ($p < 0.01$). Total liver superoxide dismutase (SOD) activity was significantly lower in PE 48 h after treatment in comparison with the P and E groups (251.73±80.63 *vs.* 707.62±179.92 and 1179.62±147.94 U mg^{-1} protein, respectively, $p < 0.01$). The lowest MnSOD activity in the PE group was detected 48 h after treatment (86.52±28.31; 41.13±11.07 and 23.16±5.18 U mg^{-1} protein in the P, E and PE groups, respectively, $p < 0.05$). Prior binge ethanol drinking potentiates paracetamol-induced reduction of antioxidative capacity of hepatocytes due to GSH depletion and SOD activity reduction, simultaneously increasing lipid peroxidation caused by paracetamol.

Keywords: ethanol; paracetamol; oxidative stress; liver; mice.

---

* Corresponding author. E-mail: tanjamm@med.bg.ac.rs

179

INTRODUCTION

Paracetamol (acetaminophen), a widely used antipyretic and analgetic, is found to exert hepatotoxic effects in humans and rodents. When used in high doses, it produces centrilobular hepatic necrosis that can be fatal.[1,2] The mechanisms of paracetamol hepatotoxicity are still poorly understood. The main mechanism responsible for its toxicity is considered to be its metabolic activation in the liver.[3] The toxic metabolite *N*-acetyl-*p*-benzoquinone imine (NAPQI), produced by the CYP2E1 isoenzyme of cytochrome P450-dependent monooxygenase, induces liver injury by forming acetaminophen–protein adducts[1,4] and by inducing mitochondrial permeability transition.[5] A reduced glutathione content in the liver potentiates the toxic effects of paracetamol since glutathione is a major component involved in NAPQI detoxication.[6] Additional mechanisms apparently involved in paracetamol toxicity are oxidative,[7–11] nitrosative stress[12–15] and activation of Kupffer cells with the release of various pro-inflammatory cytokines.[16] It has been postulated that paracetamol increases the production of superoxide anion and hydrogen peroxide, as well as nitrotyrosine formation in the liver.

Ethanol, when chronically ingested, is known to induce liver injury. Among various mechanisms involved in ethanol-induced liver injury are the production of reactive oxygen species, the formation of acetaldehyde–protein adducts that induce an immune response and the release of gut endotoxin.[17–19] The main source of reactive oxygen species is CYP2E1, an inducible enzyme involved in ethanol metabolism.[17–19] In the presence of iron, which is increased during chronic ethanol consumption, more powerful oxidants, including hydroxyl radicals, ferryl species and 1-hydroxyethyl radical, are produced.[20] An additional source of reactive oxygen species in the liver are Kupffer cells, activated by increased release of endotoxin from gut lumen into portal circulation.[21] In contrast to chronic effects, the mechanisms of acute ethanol-induced liver injury are still not fully understood.

It has been suggested that chronic ethanol consumption potentiates paracetamol hepatotoxicity.[22] Various studies indicated that chronic alcoholics are more susceptible to therapeutic doses of paracetamol than non-alcoholics.[22–24] Most studies regarding these interactions were focused on the metabolic interaction between ethanol and paracetamol. It was suggested that ethanol potentiates paracetamol-induced liver injury by CYP2E1 and CYP3A induction, which are enzymes involved in NAPQI production,[25,26] However, another study did not confirm these interactions.[27]

The effects of acute ethanol intoxication on paracetamol hepatotoxicity are even more blurred. These effects are of great importance, since it is usual for adolescents to take paracetamol or other non-steroidal anti-inflammatory drugs for the treatment of headache caused by binge drinking. Some clinical studies

suggest a protective effect of ethanol pretreatment on paracetamol hepatotoxicity.[28] Interactions between paracetamol and ethanol during acute toxicity cannot be entirely explained by metabolic changes in the liver, since ethanol does not induce CYP2E1 acutely. Possible interactions should be explained by other mechanisms involved in their toxicity. Since reactive oxygen species are postulated to mediate hepatotoxic effects of ethanol and paracetamol, the aim of our study was to investigate the effects of binge drinking on paracetamol-induced oxidative stress in rat liver.

EXPERIMENTAL

Animals

The experiment was performed on adult male Swiss mice weighing 25–30 g, raised at the Military Medical Academy, Belgrade. The animals were kept under standard laboratory conditions (temperature 22±2 °C, relative humidity 50±10 %, 12/12 light–dark cycle with lights turned on at 9 a.m.) and had free access to tap water and standard pelleted LM2 food (Veterinary Institute "Subotica", Subotica, Serbia). The diet, which had a metabolizable energy of at least 11.5 MJ kg^{-1}, was composed of a maximum of 7 % cellulose and a minimum of 19 % protein. On the day prior to sacrifice, the mice were fasted overnight. The study was performed according to the Guidelines for Animal Study No. 282-12/2002 and was approved by the Ethic Committee of the Military Medical Academy for animal experiments.

All animals ($n = 96$) were randomly divided into the following groups: 1) control, saline-treated group (0.9 % NaCl) ($n = 24$); 2) ethanol-treated group (E; $n = 24$) in five subsequent doses of 2 g kg^{-1}, administered every 12 h by an orogastric tube; 3) paracetamol-treated group (P; $n = 24$) in a dose of 300 mg kg^{-1} intraperitoneally (i.p.); 4) group that received paracetamol and ethanol (PE; $n = 24$). Ethanol was administered to the PE group in five repetitive doses in the same manner as it was administered to the E group. Paracetamol was i.p administered to these animals in a dose of 300 mg kg^{-1}, 12 h after the last dose of ethanol. Animals from P and E group received saline instead of ethanol and paracetamol, respectively. For oral administration, the ethanol was dissolved in distilled water in concentration of 30 % v/v. Paracetamol was dissolved in saline (0.9 % NaCl) before i.p. administration.

The mice were sacrificed by cervical dislocation 6, 24 and 48 h after paracetamol administration (or saline for E and the control group). Eight animals from each group were sacrificed at all time intervals. Blood samples for the determination of the oxidative stress parameters were collected from the right side of the heart. For the same purpose, the livers were excised and stored as described below.

Analysis

Liver samples for biochemical analysis were homogenized on ice, in cold buffered 0.25 M sucrose medium (Serva, Heidelberg, New York), 10 mM phosphate buffer (pH 7.0) and 1 mM EDTA (Sigma, St. Louis, USA). The homogenates were centrifuged at 2000×g for 15 min at 4 °C. The crude sediments were dissolved in a sucrose medium and centrifuged. The supernatants were transferred into the tubes and centrifuged at 3200×g for 30 min at 4 °C. The obtained sediments were dissolved in deionized water. After one hour of incubation, the samples were centrifuged at 3000×g for 15 min at 4 °C, and the supernatants were stored at –70 °C. The contents of proteins were determined by the Lowry method using bovine serum albumin as the calibrant.[29]

Biochemical evaluation of liver injury was performed by quantifying the serum activity of alanine aminotransferase (ALT) and aspartate aminotransferase (AST). Their activities were determined spectrophotometrically using Sigma test kits (Sigma, St. Louis, USA) on a BTS-330 photometer, according to the manufacturer's instructions.

The total superoxide dismutase (EC1.15.1.1.; SOD) activity in the liver was measured spectrophotometrically, as the inhibition of epinephrine auto-oxidation at 480 nm. After addition of 10 mM epinephrine (Sigma, St. Louis, USA), the analysis was performed in sodium carbonate buffer (50 mM, pH 10.2; Serva, Heidelberg, New York) containing 0.1 mM EDTA (Sigma, St. Louis, USA). Samples for manganese SOD were previously treated with 8 mM KCN (Sigma, St. Louis, USA) and then analyzed as previously described.[30]

Lipid peroxidation in the plasma and liver homogenates was measured as malondialdehyde (MDA) production, assayed in the thiobarbituric acid reaction as described by Girotti *et al.* [31] The results are expressed as μmol L^{-1} in plasma or nmol mg^{-1} protein in the liver homogenates.

The concentration of nitrites + nitrates (NO_x), as a measure of nitric oxide (NO) production, was determined using the Griess reagent. After reduction of the nitrates, the total nitrites were reacted with sulfanilamide and *N*-(1-naphthyl)ethylenediamine to produce an azo dye, which was measured spectrophotometrically at 492 nm.[32]

Reduced glutathione (GSH) was determined by reaction of aliphatic thiol compounds in Tris–HCl buffer (0.4 mol, pH 8.9) with 5,5-dithiobis-2-nitrobenzoic acid (DTNB, 36.9 mg in 10 mL of methanol), thereby producing the yellow-colored *p*-nitrophenol anion that was measured at 412 nm. The intensity of the formed chemical compound was proportional to the GSH concentration.[33]

Chemicals

All reagents and chemicals were of analytical grade or higher purity. Ethanol was purchased from Merck (Darmstadt, Germany). Paracetamol was obtained from Sigma (St. Louis, MO, USA).

Statistical analysis

Results are expressed as means ± *SD*. Since the normal distribution of the data was confirmed by the Kolmogorov–Smirnov test, multifactorial analysis of variance (multifactorial ANOVA) with Tukey's *post hoc* test were used for testing the difference among the groups. The difference was considered statistically significant if $p < 0.05$. The SPSS15.0 program was used for the statistical analysis.

RESULTS

The activities of the serum aminotransferases (ALT and AST) were significantly elevated at all times after paracetamol administration ($p < 0.01$). Additionally, ethanol induced a significant increase in their activities when administered either alone or in combination with paracetamol ($p < 0.01$) (Table I). The study also showed that the serum MDA concentration was significantly higher in all groups that received either ethanol or paracetamol at all times when blood samples were collected (Table I). A significant rise in the MDA concentration was found 6 h after paracetamol administration in the control group ($p < 0.01$). A similar increase was found after ethanol administration (4.78±0.69 μmol L^{-1}) ($p < 0.01$). Concomitant administration of ethanol and paracetamol did not induce a

significant change in serum MDA concentration in comparison with the ethanol- and paracetamol-treated groups ($p > 0.05$). Neither was a significant change found within 48 h after treatment ($p > 0.05$). However, a significant increase in the liver MDA concentration was found in the PE group 48 h after paracetamol administration, in comparison with the P and E groups ($p < 0.01$). A progressive increase in the liver MDA levels was also found within 48 h in all the experimental groups (Table I). The highest level of liver MDA was measured 48 h after paracetamol or ethanol administration in comparison with the same group of animals 6 and 24 h after treatment ($p < 0.01$ and $p < 0.05$, respectively).

TABLE I. Activities of serum aminotransferases and parameters of lipid peroxidation in the plasma and liver of the experimental animals. Results are expressed as means ± SD. For statistical evaluation, multifactorial ANOVA with Tukey's post hoc test were used (*$p < 0.05$, **$p < 0.01$ *vs.* the control group, #$p < 0.05$, ##$p < 0.01$ in comparison with the group on the same experimental protocol 6 (a) and 24 h (b) after treatment); abbreviations: C_6, C_{24}, C_{48}, control group 6, 24 and 48 h after treatment; P_6, P_{24}, P_{48}, paracetamol-treated group 6, 24 and 48 h after administration; E_6, E_{24}, E_{48}, ethanol-treated group 6, 24 and 48 h after treatment; PE_6, PE_{24}, PE_{48}, group that received paracetamol and ethanol 6, 24 and 48 h after treatment

Group	Serum ALT U L^{-1}	Serum AST U L^{-1}	Conc. serum MDA μmol L^{-1}	Liver MDA level nmol mg^{-1} prot.
C_6	41±5	52±10	3.33±0.71	7.67±1.65
C_{24}	39±3	55±7	3.13±0.64	7.86±0.87
C_{48}	43±7	51±7	3.86±1.73	7.31±0.82
P_6	1924±74**	2197±102**	4.83±1.05**	9.45±0.81*
P_{24}	2025±68**	2297±97**	5.25±1.39**	11.50±0.38** a#
P_{48}	2028±81**	2274±80**	5.10±1.34*	13.14±0.82** b#
E_6	1789±57**	2562±93**	4.78±0.69**	9.56±0.32*
E_{24}	1785±78**	2734±107**	4.89±0.94**	11.47±0.80** a#
E_{48}	1702±71**	2672±76**	5.21±0.50*	12.99±1.18** b#
PE_6	1942±134**	2431±86**	5.11±2.04**	9.23±0.30*
PE_{24}	2145±101**	2497±94**	4.25±1.66**	11.31±0.77** a#
PE_{48}	2108±96**	2503±111**	4.95±1.25*	17.14±1.98** b##

The liver NO_x concentration was significantly higher in the paracetamol-treated group (1.24±0.41 μmol L^{-1}) than in the control group (0.34±0.06 μmol L^{-1}) 6 h after treatment ($p < 0.01$) (Fig. 1). After this period, its concentration showed a progressive rise and maximal values were attained 48 h after paracetamol administration (2.86±0.21 μmol L^{-1}). Similar to paracetamol, ethanol had also induced a rise in the liver NO_x concentration 6 h after treatment (1.04±0.33 μmol L^{-1}) ($p < 0.01$). However, this level remained relatively unchanged within 24 h after administration of the last dose of ethanol (0.97±0.24 μmol L^{-1}) ($p > 0.05$). After this period, ethanol induced an additional increase in the NO_x concentration, and its level was significantly higher 48 h after treatment (2.90±0.32 μmol L^{-1}) than after 6 h ($p < 0.01$). When administered sequentially, ethanol and para-

cetamol also induced a progressive rise in the NO_x concentration within the first 48 h with the highest level being observed at the end of this interval (2.98 ± 0.05 $\mu mol\ L^{-1}$) (Fig. 1). However, no significant change in the NO_x concentration was found in the PE *vs.* the P group at all times ($p > 0.05$).
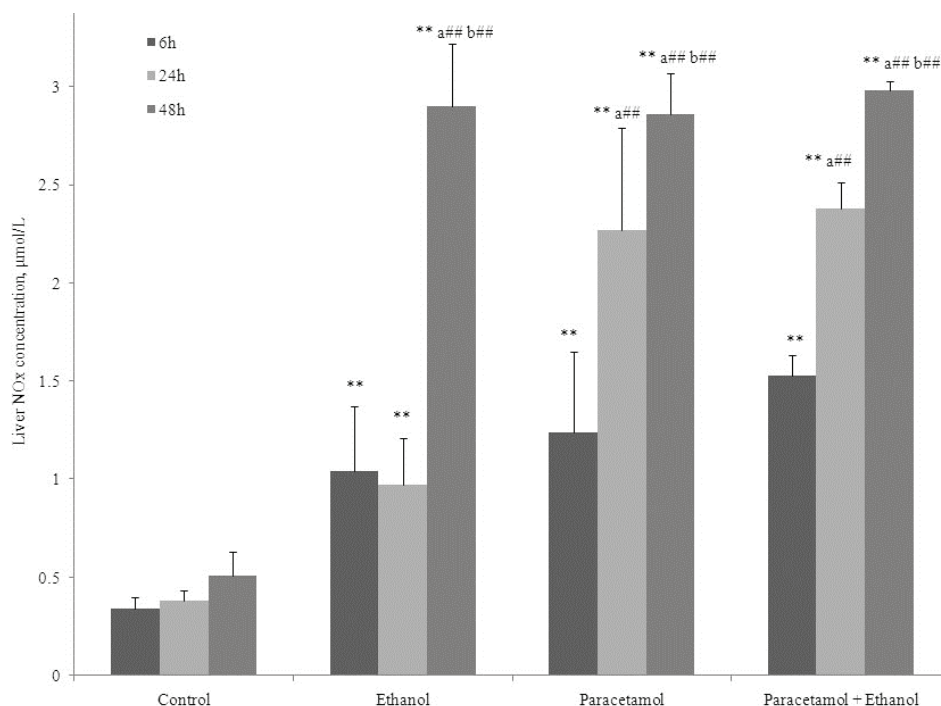
Fig. 1. Liver concentration of nitrites and nitrates (NO_x) in the experimental groups. The NO_x values were determined at 6, 24 and 48 h after treatment. For statistical evaluation, multi-factorial ANOVA with the Tukey's *post hoc* test were used (**$p < 0.01$ *vs.* control group, ##$p < 0.01$ in comparison with the group on the same experimental protocol 6 (a) and 24 h (b) after treatment). Abbreviations: C – control group, E – ethanol-treated group, P – paracetamol-treated group, PE – group that received paracetamol 24 h after the last dose of ethanol.

The liver GSH content was significantly lower in ethanol- and paracetamol-treated groups (0.58 ± 0.05 and 0.75 ± 0.06 nmol mg^{-1} protein, respectively) in comparison with control group (1.03 ± 0.12 nmol mg^{-1} protein) 6 h after treatment ($p < 0.01$), Fig. 2. Within the next 18 h, its content returned to the control range in the ethanol-treated group (0.99 ± 0.09 nmol mg^{-1} protein) and remained approximately constant within the next 24 h (1.05 ± 0.11 nmol mg^{-1} protein) ($p > 0.05$). In contrast to ethanol, paracetamol had induced a significant increase in the liver GSH content 24 h after its administration (1.57 ± 0.18 *vs.* 1.04 ± 0.10 nmol mg^{-1} protein in the P and control group, respectively, $p < 0.01$). After this period,

a progressive decline in the GSH content was observed in the P group and 48 h after paracetamol administration, its content (0.56±0.05 nmol mg^{-1} protein) was significantly lower in comparison with that of the control group (1.11±0.14 nmol mg^{-1} protein) and P group 24 h after treatment ($p < 0.05$ and $p < 0.01$, respectively). Subsequent administration of paracetamol to ethanol-treated animals induced a more pronounced decline in the liver GSH content than administration of paracetamol or ethanol alone ($p < 0.01$). The lowest level of liver GSH in the PE group was detected 6 h after paracetamol administration (0.12±0.01 nmol mg^{-1} protein). After this period, its level gradually increased but was still significantly lower than in P and E groups within 48 h (0.24±0.03 nmol mg^{-1} protein), Fig. 2.
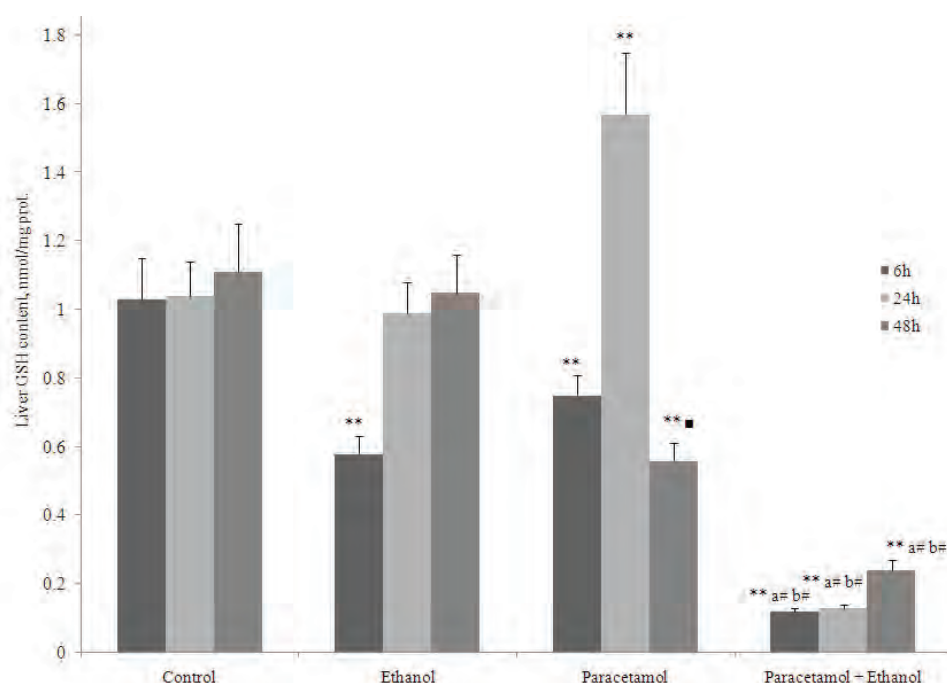
Fig. 2. The level of the reduced glutathione (GSH) in liver samples of treated animals. The GSH levels were determined 6, 24 and 48 h after the appropriate treatment. For statistical evaluation, multifactorial ANOVA with Tukey's *post hoc* test were used (**$p < 0.01$ *vs.* the control group, $^{\blacksquare}p < 0.01$ *vs.* the paracetamol-treated group 24 h after its administration, $^{\#}p < 0.01$ in comparison with ethanol- (a) and paracetamol-treated group (b) at the corresponding times). Abbreviations as in Fig. 1.

Ethanol and paracetamol were found to induce a decrease in the liver SOD activity at all time intervals when administered alone or in combination (Fig. 3). However, the most intensive decrease was observed in the PE group. Prior ethanol administration did not significantly potentiate the paracetamol-induced decrease in SOD activity within the first 24 h after treatment (723.75±102.86 and

784.61±70.19 U mg^{-1} protein after 6 h, 645.35±70.56 and 768.88±143.31 U mg^{-1} protein after 24 h in the PE and P groups, respectively). However, the total SOD activity was significantly lower 48 h after treatment in the PE group (251.73± ±80.63 U mg^{-1} protein) in comparison with the P (707.62±179.92 U mg^{-1} protein) and E groups (1179.62±147.94 U mg^{-1} protein, $p < 0.01$).
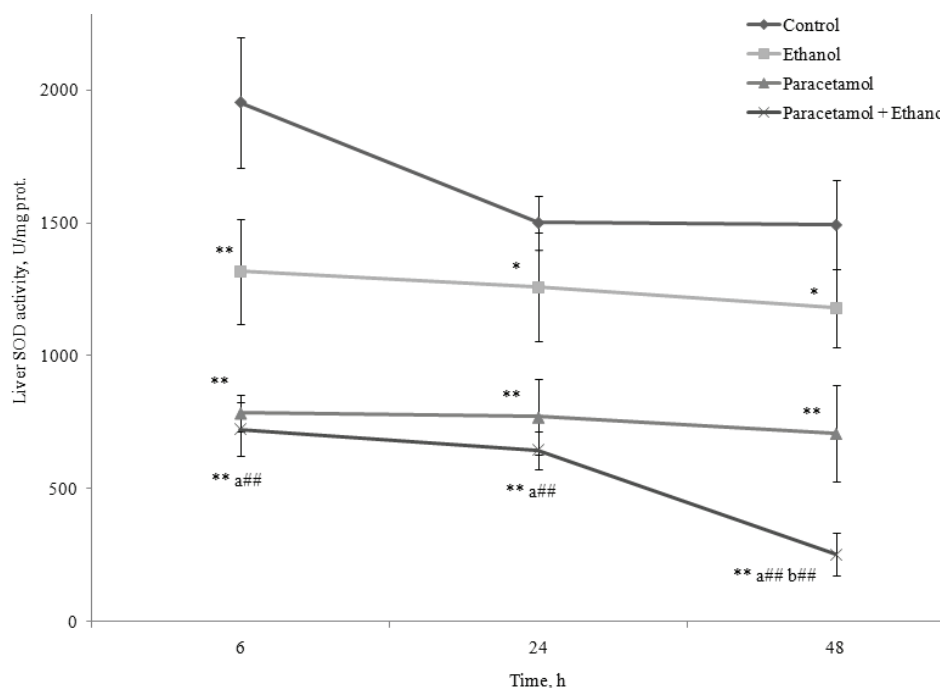
Fig. 3. Total superoxide dismutase (SOD) activity in the liver of treated animals. Liver samples for measuring SOD activity were collected 6, 24 and 48 h after the appropriate treatment. For statistical evaluation, multifactorial ANOVA with Tukey's *post hoc* test were used (*$p < 0.05$, **$p < 0.01$ *vs*. the control group, ##$p < 0.01$ in comparison with the ethanol-treated group (a) and the paracetamol-treated group (b) at the same time intervals).

In contrast to the total SOD activity, the mitochondrial SOD activity was higher after 6 h in all treated groups in comparison with the control group (Fig. 4). Subsequently, the MnSOD activity began to fall and reached its lowest level 48 h after treatment in all experimental groups. The MnSOD activity was significantly lower in the PE group in comparison with the P and E groups at all time when its activity was measured. The lowest MnSOD activity was detected 48 h after treatment (86.52±28.31, 41.13±11.07 and 23.16±5.18 U mg^{-1} protein in the P, E and PE groups, respectively, $p < 0.05$).
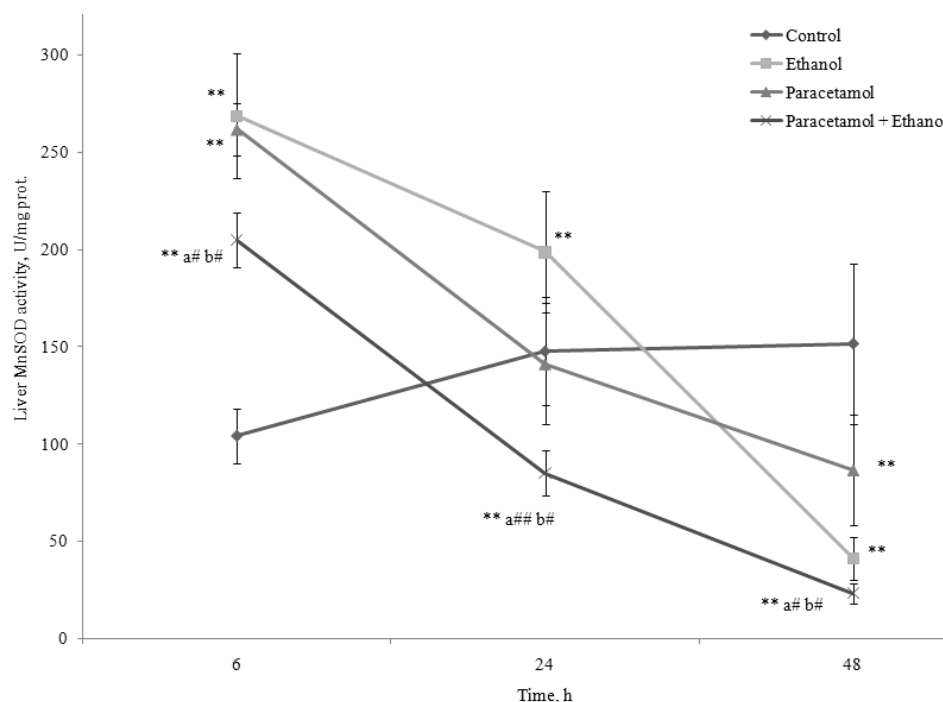
Fig. 4. Activity of mitochondrial (manganese) superoxide dismutase (MnSOD) in the liver of the experimental animals. The MnSOD activity was measured in the mitochondrial liver fraction 6, 24 and 48 h after the experimental protocols. For statistical evaluation, multi-factorial ANOVA with Tukey's *post hoc* test were used (**$p < 0.01$ *vs*. the control group, #$p < 0.05$, ##$p < 0.01$ in comparison with animals treated with ethanol (a) or paracetamol (b) alone).

DISCUSSION

The obtained results showed that the serum aminotransferase activity was significantly elevated after paracetamol or ethanol administration. This indicates that paracetamol and ethanol induce liver injury in the early phase of acute into-xication and that this injury persists for at least 48 h. In addition, the serum and liver MDA concentrations were significantly higher in all groups treated with pa-racetamol or ethanol in comparison with those of the control group. Based on these data, it could be suggested that lipid peroxidation may be an important me-chanism of paracetamol- and ethanol-induced hepatotoxicity, even when admi-nistered acutely. Lipid peroxidation was confirmed to be an important mecha-nism of paracetamol-induced liver injury at different doses in various stu-dies.[7,8,34–36] Paracetamol was found to increase the serum MDA level 4 h after administration[35] and this elevation persisted for 7 days.[34] The role of lipid pe-roxidation was also confirmed by the protective effects of L-carnitine and some medicinal plants on hepatocyte injury caused by paracetamol.[8,34,35] This pro-

tection can, at least partly, be explained by their ability to inhibit MDA production. Similarly, earlier studies showed that a vitamin E-rich diet reduces lipid peroxidation in hepatocytes due to paracetamol toxicity.[37] Vitamin E was found to protect animals on a Wendel diet against paracetamol hepatotoxicity,[37,38] while it had no effect on injury in animals on a standard diet.[39]

It is well known that oxidative stress is a major contributor of ethanol-induced liver injury. Lipid peroxidation, as an important consequence of oxidative stress, was detected in various models of acute and chronic ethanol intoxication.[40–43] Previous binge drinking was found to potentiate paracetamol-induced lipid peroxidation 48 h after paracetamol treatment. These results suggest that ethanol, when acutely administered, has synergistic effects with paracetamol related to lipid peroxidation and this can be one potential mechanism of aggravation of paracetamol-induced liver injury by ethanol.

Liver nitrites and nitrates, markers of NO production, were increased in all groups treated with either paracetamol or ethanol. Their maximal level was reached 48 h after paracetamol or ethanol administration. These findings suggest that reactive nitrogen species are also involved in acute paracetamol- and ethanol-induced liver injury. The role of nitrosative stress in acute paracetamol intoxication, detected as an increase in nitrotyrosine production, was suggested in various studies.[12,14,15,44] Nitrotyrosine immunoreactivity was found to be increased 4 h after paracetamol treatment in mouse liver.[12,44] Similarly, it was found that ethanol is also an inductor of NO synthesis,[45] although its role in ethanol-induced liver injury is not completely understood. In low concentrations NO exerts hepatoprotective effects, while in high concentrations, NO in the presence of superoxide anion leads to peroxynitrite formation, which is known to be a potent oxidant in cells.[41,46] Normally, peroxynitrite is detoxified by GSH/GSH peroxidase, especially in the mitochondria.[47] It has been postulated that GSH depletion induced by paracetamol or ethanol leads to peroxynitrite accumulation, thus aggravating nitrosative stress.[48] The present results are in accordance with these data, since a significant GSH depletion was found in the P and E groups 48 h after treatment, at the same time when the liver nitrite + nitrate level reached its maximal value. However, the increase in the liver nitrite + nitrate level was accompanied by GSH elevation 24 h after treatment. This suggests that ethanol- and paracetamol-induced NO production surpassed the GSH capacity to detoxify reactive nitrogen species in first 24 h.

In the present study, it was found that the liver nitrite + nitrate concentration was not significantly different in the PE group to that in the P group. Based on these results, it appears that prior binge drinking exerts neither a synergistic nor a protective effect on paracetamol-induced nitrite/nitrate production. On the contrary, studies in mice using a chronic alcoholism model found that alcohol pretreatment increased nitrotyrosine formation induced by paracetamol.[25] However,

within a few hours after treatment, the nitrotyrosine formation was found to be decreased when the animals had been pretreated with ethanol.[25] This indicates that interaction between ethanol and paracetamol depends on the exposition time.

The liver GSH content was found to be decreased in the ethanol-treated animals 6 h after its administration. After this period, its level tended to rise and reached the control level within 24 h. This indicates that GSH depletion could represent a contributory mechanism to acute ethanol-induced oxidative injury within a few hours after intoxication. The role of GSH depletion in ethanol-induced liver injury is supported by other studies that confirmed a protective role of *N*-acetylcysteine and L-2-oxothiazolidine-4-carboxylic acid in animal models of alcoholic liver disease.[49,50] Recent studies showed that silymarin and betaine, also exerted protective effects on binge-drinking mice.[40,42] Among the various mechanisms involved in their protective effects, reduction of GSH depletion was suggested to play an important role.

In the present study, paracetamol was found to have decreased the GSH content in the liver 6 h after its administration. Various studies suggested that GSH depletion plays a contributory role in paracetamol hepatotoxicity.[13,51] *N*-Acetylcysteine, a GSH precursor, was found to reduce paracetamol toxicity in mice and this effect was pronounced in the first hours after paracetamol treatment.[52] Similarly, pretreatment with α-lipoic acid reduced GSH depletion induced by high doses of paracetamol (2.5 g kg^{-1}) and protected markedly against its hepatotoxicity.[53] Studies in mice showed that the GSH level was decreased by approximately 90 % at 1- and 2-hour intervals after paracetamol treatment.[13] In addition, *in vitro* studies confirmed a profound GSH depletion after a paracetamol overdose.[54] This is not surprising since the major mechanism involved in early paracetamol hepatotoxicity is inactivation of sulfhydryl groups of various cellular compounds due to NAPQI detoxification.[44] Glutathione-*S*-transferase (GST) is an enzyme that enables detoxification of NAPQI, as well as other electrophilic substrates (products of xenobiotic metabolism) by binding to GSH.[55] However, the contribution of this enzyme to GSH depletion and liver injury in paracetamol intoxication remains controversial. *In vitro* studies suggested that π class GST consumes the majority of GSH for NAPQI detoxication in mice and possibly ameliorates liver injury.[56] Although π class GST was found at high levels in mice liver, *mGstp1/2-/-* mice (knockout mice for π-GST gene) challenged with an overdose of paracetamol exhibited a markedly decreased, not increased hepatotoxicity when compared to *mGstp1/2+/+* mice.[57] The role of GST in mediating the toxic effects of paracetamol in humans is even more blurred, since π class GST is absent or expressed at low levels in the human liver.[55]

After an initial decline, the GSH level returned or became closer to the normal values depending on the administered dose within the next few hours.[13] in the present study, a significant increase in the GSH level in the liver was found

24 h after paracetamol administration in comparison with the control group. Higher doses of paracetamol were found not to induce any rise in the liver GSH content.[58] The increase found in the present study may possibly be explained by an increased expression of glutamate cysteine ligase, the key enzyme in the synthesis of GSH, which is known to be induced by oxidative stress *via* the nuclear factor kappaB (NF-κB), activator protein-1 (AP-1) and other transcription factors.[59] After this period, GSH level fell again and within the following 24 h reached its lowest level, even lower than in the first 6 h. This decrease may be a result of GSH consumption in ROS/RNS detoxification in the liver. According to the results of the present study, it could be suggested that paracetamol induces a triphasic change in the liver GSH level. This finding is supported by the two-phase theory of paracetamol hepatotoxicity. According to this theory, in the first metabolic phase, NAPQI, a reactive metabolite of paracetamol, leads to GSH depletion and covalent binding to various proteins.[60,61] This mechanism may have been involved in the initial fall in the GSH level. In the second oxidative phase, a mitochondrial permeability transition occurs that contributes to the toxic effects of paracetamol. The ROS involved in mitochondrial permeability transition may also be involved in the late GSH consumption.[62]

It was found in some studies that prior ethanol binge drinking in five doses of 4 g kg^{-1} potentiated paracetamol-induced GSH depletion in mice liver.[62] According to the present study, even smaller doses of ethanol (5×2 g kg^{-1}) appeared to potentiate this effect of paracetamol. This potentiation was clearly observed at all time intervals. Additionally, an adaptive increase in GSH level was not observed in the PE group. This indicates that paracetamol and ethanol exert synergistic effects on the liver GSH level.

Liver SOD activity was decreased after administration of either paracetamol or ethanol at all time intervals. Paracetamol was found to induce a more pronounced decrease in SOD activity than ethanol. However, this effect was not the same for both fractions of SOD. While Cu/Zn SOD activity was lower in both paracetamol- and ethanol-treated groups, the activity of mitochondrial MnSOD was higher in the P and E groups 6 h after treatment compared with the control group. After this period, the MnSOD activity progressively decreased and reached its lowest level 48 h after treatment. According to other studies, the effects of ethanol on the SOD activity are inconclusive and depended on dose and route of administration. Some studies found that ethanol induced MnSOD after acute administration.[63,64] A single dose of ethanol was found to increase liver MnSOD activity by about 30 % three hours after administration, with a further increase up to about 50 % in the subsequent 6 h.[63] In the present study, an even more pronounced increase in its activity of approximately by 150 % six hours after binge drinking was found. This increase may be a result of an adaptive response to the increased production of ROS. Since mitochondria are the major source of ROS,[41]

it is not surprising that mitochondrial SOD isoenzyme activity was increased after binge drinking. The subsequent decrease in the MnSOD activity indicates the consumption of this enzyme in the detoxification of ROS. Similar to the present results, the Cu/Zn SOD activity and its immunoreactivity in the liver were found to decrease in various studies using the enteral alcohol model.[65,66]

Paracetamol was found to decrease liver SOD activity in various experimental models.[34,67] Even smaller doses (150 mg kg^{-1}) were found to reduce its activity by about 30 % sixteen hours after paracetamol administration.[67] The precise role of SOD in paracetamol-induced hepatotoxicity is not completely understood. Although it is to be expected that SOD overexpression would have a protective antioxidant effect in the liver, some studies found that deletion of Cu/Zn SOD (SOD1) genes decreased susceptibility to paracetamol.[68] This finding was explained by the fact that SOD1 deletion reduces hepatic protein nitration and CYP2E1 activity by approximately 50 %.[68] In the present study, paracetamol induced a drastic decrease in Cu/Zn SOD activity, which could represent a possible autoprotective mechanism in acute paracetamol overdose. However, many studies suggest a protective role of SOD in acetaminophen-induced liver injury.[67,69,70] In contrast to the total SOD activity, paracetamol had induced a significant increase in the MnSOD activity 6 h after treatment, thus suggesting an adaptive response of the hepatocyte mitochondria to increased production of ROS. On the other hand, Agarwal *et al.*[71] found that the MnSOD activity was decreased 1 h and remained significantly decreased at 2 h in mice that had been treated i.p with 300 mg kg^{-1} of paracetamol. These decreases in MnSOD activity were explained by an increased production of ROS in the mitochondria, which react with nitric oxide, leading to increased levels of reactive nitrogen species.

Paracetamol and ethanol were found to have synergistic effects on the SOD activity in the present study. Within the first 24 h, the liver SOD activity in the PE group was similar to its activity in the P group, thus indicating that prior binge drinking did not potentiate paracetamol-induced reduction in the total SOD activity at this time interval. However, within the next 24 h, ethanol and paracetamol induced a more pronounced decline in the SOD activity when administered together than either of the substances alone. This suggests that reduction in hepatic SOD activity is not an early event in possible synergistic hepatotoxic effects of ethanol and paracetamol. Within the first 6 h, the MnSOD activity was increased to a lesser extent in the PE group than in the P and E groups. Additionally, subsequent administration of paracetamol after ethanol caused a more pronounced decrease in the MnSOD activity than either of these substances alone within 48 h after treatment. This indicates that ethanol and paracetamol induce oxidative stress synergistically and the more pronounced decrease in MnSOD and SOD activity may be explained by increased consumption of this enzyme in ROS detoxication.

CONCLUSIONS

According to this study, it can be concluded that prior binge ethanol drinking may potentiate the paracetamol-induced decrease in the antioxidative capacity of hepatocytes due to GSH depletion and reduction in SOD activity. In addition, paracetamol-induced lipid peroxidation is aggravated by prior ethanol administration within 48 h. However, the formation of reactive nitrogen species is not influenced by paracetamol ingestion. Based on the obtained results, a possible protective effect of ethanol on paracetamol hepatotoxicity cannot be attributed to alleviation of oxidative stress. Other mechanisms involved in this possible protective effect should be further investigated.

И З В О Д

ДЕЈСТВО ЕТАНОЛА НА ОКСИДАТИВНО ОШТЕЋЕЊЕ ЈЕТРЕ МИШЕВА ИЗАЗВАНО ПАРАЦЕТАМОЛОМ

ДУШАН МЛАДЕНОВИЋ[1], МИЛИЦА НИНКОВИЋ[2], ДАНИЈЕЛА ВУЧЕВИЋ[1], МИОДРАГ ЧОЛИЋ[2], МАРЈАН МИЦЕВ[3], ВЕРА ТОДОРОВИЋ[4], МИЛЕНА СТАНКОВИЋ[1] и ТАТЈАНА РАДОСАВЉЕВИЋ[1]

[1]*Инсȴиȴуȴ за ȳаȴолошку физиолоīију, Медицински факулȴеȴ, Универзиȴеȴ у Беоīраду, Др Субоȴиȶа 9,* [2]*Инсȴиȴуȴ за Медицинска исȴраживања, Војно медицинска академија, Беоīрад, Црноȴравска 17,* [3]*Инсȴиȴуȴ за болесȴи диīесȴивноī сисȴема, Клинички ценȴар Србије, Беоīрад и* [4]*Сȴомаȴолошки факулȴеȴ Панчево, Универзиȴеȴ Привредна академија у Новом Саду, Панчево*

Циљ наше студије је био да се испита ефекат викенд пијанства на оксидативно оштећење јетре мишева изазвано парацетамолом. У експерименту су коришћени мишеви, мужјаци *Swiss* соја подељени у следеће групе: 1. контрола; 2. животиње третиране етанолом (5 појединачних доза од по 2 g kg⁻¹ путем орогастричне сонде) (Е); 3. група третирана парацетамолом (појединачна доза од 300 mg kg⁻¹ интраперитонеално) (П); 4. животиње које су примиле парацетамол 12 сати после последње дозе етанола (ПЕ). За одређивање параметара оксидативног стреса узимани су узорци крви и јетре, 6, 24 и 48 сати након третмана. Када су администрирани у комбинацији, етанол и парацетамол изазивају значајно повећање нивоа малондиалдехида (MDA) у јетри 48 сати након третмана у поређењу са П и Е групом (17,14±1,98 *vs.* 13,14±0,82 и 12,99±1,18 nmol mg⁻¹ protein, *p* < 0,01). Такође, етанол и парацетамол у комбинацији доводе до значајног смањења нивоа глутатиона у јетри у свим временским интервалима, у поређењу са П и Е групом (*p* < 0,01). Укупна активност супероксид-дисмутазе (SOD) била је значајно смањена у ПЕ групи 48 сати након третмана у поређењу са П и Е групама (251,73±80,63; 707,62±179,92 и 1179,62±147,94 U mg⁻¹ protein, *p* < 0,01). Најнижа активност манган SOD (MnSOD) нађена је у ПЕ групи 48 сати након третмана (86,52±28,31; 41,13±11,07 и 23,16±5,18 U mg⁻¹ protein у П, Е и ПЕ групама, *p* < 0.05). На основу наших резултата може се закључити да акутна администрација етанола потенцира дејство парацетамола путем смањења антиоксидативног капацитета хепатоцита, услед смањења нивоа глутатиона и активности SOD, уз истовремено повећање липидне пероксидације изазване парацетамолом.

REFERENCES

1. D. Bartlett, *J. Emerg. Nurs.* **30** (2004) 281
2. L. J. Chun , M. J. Tong , R. W. Busuttil, J. R. Hiatt, *J. Clin. Gastroenterol.* **43** (2009) 342
3. G. G. Graham, K. F. Scott, R. O. Day, *Drug Safety* **28** (2005) 227
4. F. J. Gonzalez, *Mutat. Res.* **569** (2005) 101
5. Y. Masubuchi, C. Suda, T. Horie, *J. Hepatol.* **42** (2005) 110
6. B. H. Lauterburg, *Am. J. Ther.* **9** (2002) 225
7. A. D. Grypioti, M. Mykoniatis, C. A. Demopoulos, G. Kostopanagiotou, *Dig. Dis. Sci.* **52** (2006) 192
8. M. Anoush, M. A. Eghbal, F. Fathiazad, H. Hamzeiy, N. S. Kouzehkonani, *Pak. J. Biol. Sci.* **12** (2009) 765
9. J. Das, J. Ghosh, P. Manna, P. C. Sil, *Free Radical Res.* **44** (2010) 340
10. T. Radosavljević, D. Mladenović, D. Vucević, R. J. Vukićević, *Med. Pregled* **63** (2010) 827 (in Serbian)
11. K. Nithianantham, M. Shyamala, Y. Chen, L. Y. Latha, S. L. Jothy, S. Sasidharan, *Molecules* **16** (2011) 10134
12. T. R, Knight, A. Kurtz, M. L. Bayt, J. A. Hinson, H. Jaeschke, *Toxicol. Sci.* **62** (2001) 212
13. L. P. James, S. S. McCullough, T. R. Knight, H. Jaeschke, J. A. Hinson, *Free Radical Res.* **37** (2003) 1289
14. A. S. Burke, L. A. MacMillan-Crow, J. A. Hinson, *Chem. Res. Toxicol.* **23** (2010) 1286
15. A. LoGuidice, U. A. Boelsterli, *Hepatology* **54** (2011) 969
16. H. Jaeschke, C. D. Williams, A. Ramachandran, M. L. Bajt, *Liver Int.* **32** (2012) 8
17. E. Albano, *Proc. Nutr. Soc.* **65** (2006) 278
18. D. Wu, A. I. Cederbaum, *Semin. Liver Dis.* **29** (2009) 141
19. A. I. Cederbaum, *Dig. Dis.* **28** (2010) 802
20. G. N. Ioannou, J. A. Dominitz, N. S. Weiss, P. J. Haegerty, K. V. Wowdley, *Gastroenterology* **126** (2004) 1293
21. S. Yamashina, Y. Takei, K. Ikejima, N. Enomoto, T. Kitamura, N. Sato, *Alcohol Clin. Exp. Res.* **21** (2005) S246
22. H. J. Zimmerman, W. C. Maddrey, *Hepatology* **22** (1995) 767 (Corrigenda, *Hepatology* **22** (1995) 1898)
23. E. Tanaka, K. Yamazaki, S. Misawa, *J. Clin. Pharm. Ther.* **25** (2000) 325
24. O. Kučera, T. Roušar, P. Staňková, L. Haňáčková, H. Lotková, M. Podhola, Z. Cervinková, *J. Gastroenterol. Hepatol.* **27** (2012) 323
25. H. C. Yohe, K. A. O'Hara, J. A. Hunt, T. J. Kitzmiller, S. G. Wood, J. L. Bement, W. J. Bement, J. G. Szakacs, S. A. Wrighton, J. M. Jacobs, V. Kostrubsky, P. R. Sinclair, J. F. Sinclair, *Am. J. Physiol.* **290** (2006) G1269
26. K.K. Wolf, S. G. Wood, J. L. Allard, J. A. Hunt, N. Gorman, B. W. Walton-Strong, J. G. Szakacs, S. X. Duan, Q. Hao, M. H. Court, L. L. von Moltke, D. J. Greenblatt, V. Kostrubsky, E. H. Jeffery, S. A. Wrighton, F. J. Gonzalez, P. R. Sinclair, J. F. Sinclair, *Drug Metab. Dispos.* **35** (2007) 1223
27. C. F. Seifert, D. C. Anderson, *Pharmacotherapy* **27** (2007) 1473
28. W. S. Waring, A. F. Stephen, A. M. Malkowska, O. D. Robinson, *Acad. Emerg. Med.* **15** (2008) 54
29. O. H. Lowry, N. J. Rosenbrough, A. L. Farr, R. J. Randall. *J. Biol. Chem.* **193** (1951) 265
30. M. Sun, S. Zigman, *Anal. Biochem.* **90** (1978) 81

31. M. Girotti, N. Khan, B. McLellan, *J. Trauma* **31** (1991) 32
32. J. B. Hibbs, R. Taintor, Z. Vavrin, E. Rachlin, *Biochem. Biophys. Res. Commun.* **157** (1989) 87
33. M. E. Anderson, in *The DTNB–GSSG reductase recycling assay for total glutathione (GSH + 1/2 GSSG)*, R. A. Greenwald, Ed., CRC Press, Boca Raton, FL, 1986, p. 317
34. M. T. Olaleye, B. T. J. Rocha, *Exp. Toxicol. Pathol.* **59** (2008) 319
35. K. Yapar, A. Kart, M. Karapehlivan, O. Atakisi, R. Tunca, S. Erginsoy, M. Citil, *Exp. Toxicol. Pathol.* **59** (2007) 121
36. D. Mladenović, T. Radosavljević, M. Ninković, D. Vucević, R. Jesić-Vukićević, V. Todorović, *Food Chem. Toxicol.* **47** (2009) 866
37. A. Wendel, H. Jaeschke, C. Kleinwaechter, in *Lipid peroxidation in biological systems*, A. Sevanian, Ed., AOCS Press, Champaign, IL, 1988, p. 71
38. H. Jaeschke, C. Kleinwaechter, A. Wendel, *Chem. Biol. Interact.* **81** (1992) 57
39. H. Jaeschke, T. R. Knight, M. L. Bajt, *Toxicol. Lett.* **144** (2003) 279
40. Z. Song, I. Deaciuc, M. Song, D. Y. Lee, Y. Liu, X. Ji, C. McClain, *Alcohol Clin. Exp. Res.* **30** (2006) 407
41. S. K. Das, D. M. Vasudevan. *Life Sci*. **81** (2007) 177
42. S. J. Kim, Y. S. Jung, Y. do Kwon, Y. C. Kim, *Biochem. Biophys. Res. Commun.* **368** (2008) 893
43. T. Radosavljević, D. Mladenović, M. Ninković, D. Vučević, I. Boričić, R. Ješić-Vukićević, T. Šljivančanin, S. Lopičić, V. Todorović, *J. Serb. Chem. Soc.* **77** (2012) 159
44. L. P. James, P. R. Mayeux, J. A. Hinson, *Drug Metab. Dis.* **31** (2003a) 1499
45. T. Zima, L. Fialova, O. Mestek, M. Janebova, J. Crkovska, I. Malbohan, S. Stipek, L. Mikulikova, P. Popov, *J. Biomed. Sci.* **8** (2001) 59
46. S. E. McKim, E. Gäbele, F. Isayama, J. C. Lambert, L. M. Tucker, M. D. Wheeler, H. D. Connor, R. P. Mason, M. A. Doll, D. W. Hein, G. E. Arteel, *Gastroenterology* **125** (2003) 1834
47. M. Kirsch, M. Lehnig, H. G. Korth, R. Sustmann, H. de Groot, *Chem. Eur. J.* **7** (2001) 3313
48. R. Radi, J. S. Beckman, K. M. Bush, B.A. Freeman. *J. Biol. Chem.* **266** (1991) 4244
49. Y. Iimuro, B. U. Bradford, S. Yamashina, I. Rusyn, M. Nakagami, N. Enomoto, H. Kono, W. Frey, D. Forman, D. Brenner, R. G. Thurman, *Hepatology* **31** (2000) 391
50. M. J. Ronis, A. Butura, B. P. Sampey, K. Shankar, R. L. Prior, S. Korourian, E. Albano, M. Ingelman-Sundberg, D. R. Petersen, T. M. Badger. *Free Radical Biol. Med.* **39** (2005) 619
51. T. R. Knight, Y. S. Ho, A. Farhood, H. Jaeschke, *J. Pharmacol. Exp. Ther.* **303** (2002) 468
52. L. P. James, S. S. McCullough, L. W. Lamps, J. A. Hinson, *Toxicol. Sci*. **75** (2003c) 458
53. A. O. Abdel-Zaher, R. H. Abdel-Hady, M. M. Mahmoud, M. M. Farrag, *Toxicology* **243** (2008) 261
54. X. Ponsoda, R. Jover, M. J. Gómez-Lechón, R. Fabra, R. Trullenque, J. V. Castell, *Toxicology* **70 (**1991) 293
55. M. P. Vaughn, D. Biswal Shinohara, N. Castagna, J. L. Hicks, G. Netto, A. M. De Marzo, T. J. Speed, Z. R. Reichert, B. Kwabi-Addo, C. J. Henderson, C. R. Wolf, S. Yegnasub-ramanian, W. G. Nelson, *PLoS One* **6** (2011) e25707
56. B. Coles, I. Wilson, P. Wardman, J. A. Hinson, S. D. Nelson, B. Ketterer, *Arch. Biochem. Biophys.* **264** (1988) 253
57. C. J. Henderson, C. R. Wolf, N. Kitteringham, H. Powell, D. Otto, B. K. Park, *Proc. Natl. Acad. Sci. USA* **97** (2000) 12741

58. C. Chen, K. W. Krausz, J. R. Idle, F. J. Gonzalez, *J. Biol. Chem.* **283** (2008) 4543
59. S. C. Lu, *Mol. Aspects Med.* **30** (2009) 42
60. J. A. Hinson, A. B. Reid, S. S. McCullough, L. P. James, *Drug Metab. Rev.* **36** (2004) 805
61. C. Saito, H. M. Yan, A. Artigues, M. T. Villar, A. Farhood, H. Jaeschke, *Toxicol. Appl. Pharmacol.* **242** (2010) 182
62. R. S. McCuskey, N. W. Bethea, J. Wong, M. K. McCuskey, E. R. Abril, X. Wang, Y. Ito, L. D. DeLeve, *J. Hepatol.* **42** (2005) 371
63. O. R. Koch, M. E. De Leo, S. Borrello, G. Palombini, T. Galeotti, *Biochem. Biophys. Res. Commun.* **201** (1994) 1356
64. O. R. Koch, G. Pani, S. Borrello, R. Colavitti, A. Cravero, S. Farre, T. Galleoti, *Mol. Aspects Med.* **25** (2004) 191
65. H. Rouach, V. Fattaccioli, M. Gentil, S. W. French, M. Morimoto, R. Nordmann, *Hepatology* **25** (1997) 351
66. R. Polavarapu, D. R. Spitz, J. E. Sim, M. H. Follansbee, L. W. Oberley, A. Rahemtulla, A. A. Nanji, *Hepatology* **27** (1998) 1317
67. H. Gao, Y. W. Zhou, *World J. Gastroenterol.* **11** (2005) 3671
68. X. G. Lei, J. H. Zhu, J. P. McClung, M. Aregullin, C. A. Roneker, *Biochem. J.* **399** (2006) 455
69. P. J. Ferret, R. Hammoud, M. Tulliez, A. Tran, H. Trébéden, P. Jaffray, B. Malassagne, Y. Calmus, B. Weill, F. Batteux, *Hepatology* **33** (2001) 1173
70. M. O. Laukkanen, P. Leppanen, P. Turunen, T. Tuomisto, J. Naarala, S. Yla-Herttuala, *J. Gene Med.* **3** (2001) 321
71. R. Agarwal, L. A. MacMillan-Crow, T. M. Rafferty, H. Saba, D.W. Roberts, E. K. Fifer, L. P. James, J. A. Hinson, *J. Pharmacol. Exp. Ther.* **337** (2011) 110.

Glutathione protects liver and kidney tissue from cadmium- and lead-provoked lipid peroxidation

JASMINA M. JOVANOVIĆ[1]*, RUŽICA S. NIKOLIĆ[1], GORDANA M. KOCIĆ[2], NENAD S. KRSTIĆ[1]# and MILENA M. KRSMANOVIĆ[1]

[1]*Department of Chemistry, Faculty of Science and Mathematics, University of Niš, Višegradska Street 33, P. O. Box 224, 18000 Niš, Serbia and* [2]*Faculty of Medicine, University of Niš, Bulevar dr Zorana Đinđića 81, 18000 Niš, Serbia*

Abstract: Cd and Pb represent a serious ecological problem due to their soluble nature, their mobility and ability to accumulate in the soil. The exposure to these heavy metals can originate from different sources (drinking water, food and air), and they can enter into the human body through the respiratory and digestive systems. The effects of glutathione on Cd and Pb accumulation and lipid peroxidation effects in the liver and kidneys of heavy metal intoxicated rats were investigated. The content of the marker of lipid peroxidation, malondialdehyde, was increased several fold in the tissues of the exposed animals, the effects being more pronounced in the liver. The treatment of intoxicated animals with glutathione drastically suppressed lipid peroxidation. The obtained results imply that the application of glutathione may have a protective role in heavy metal intoxication by inhibiting lipid peroxidation. However, precaution should be exercised when Cd is considered, since it seems that glutathione promotes Cd accumulation in the liver.

Keywords: cadmium; lead; glutathione; lipid peroxidation; malondialdehyde.

INTRODUCTION

Heavy metals are toxic, non-biodegradable and have a very long half-life in the soil.[1] They enter living systems *via* food chains, water or air.[2] For this reason, metals, as polluters in the working and living environment, represent a very serious health and ecological hazard.

Volcanic activity is one of the reasons for the periodical increase in cadmium concentrations in the living environment, primarily in the air. The constant sources of cadmium contamination are related to its application in industry as a

---

corrosion reagent, a stabilizer in PVC products and car tires, colour pigments and nickel–cadmium batteries. Groups which are highly exposed to its effect include not only factory workers, as even the population living within a 2 km radius of a cadmium source are considered to be at a risk of high exposure, whereas people living within a 2 to 10 km radius are considered to be at a risk of medium high exposure.[3] Smoking is a significant source of intoxication, as cadmium is inhaled during the process. Through cigarette smoke, 50 % of cadmium is absorbed into the lungs and transferred into the circulatory system during active smoking.[4] Absorption mainly takes place by means of the respiratory tract, and to a smaller extent *via* the gastro–intestinal tract, while an insignificant amount is absorbed transcutaneously. When it enters the body, cadmium is transported into the bloodstream *via* red blood cells and albumin.[5] Although cadmium is spread through the bloodstream throughout the entire body, it is mostly accumulated in the kidneys and liver. Cadmium excretion from the body is slow and is performed *via* the kidneys and bile, saliva and milk during lactation.[6]

The sources of lead contamination include metallurgic gases which are a part of the non-ferrous extractive metallurgy, the metallurgy of iron and steel and also exhaust gases from the chemical industry and traffic, industrial waste, mine and landfill waters.[7] The most exposed are the workers in lead smelters and foundries, recycling plants, paint, ceramic, glass, battery and ammunition industry. From the atmosphere, soil and water (both surface and underground) lead is introduced and retained in plants, thereby finding its way into human body *via* the food chain and drinking water. Lead can be introduced into the body through the skin and digestive tract.[8] Once it enters the body, lead circulates through it mainly connected to erythrocytes, and to a lesser extent to plasma albumin, and least of all in ionic form or tied to low molecular proteins. It is mostly accumulated in the bones, then the liver, kidneys, spleen, nervous tissue and muscles. From the human body it is usually extracted through urine, slightly less through the mucous membrane of the digestive tract, gall, hair, nails, sweat and milk.

Although cadmium is not a redox active metal and cannot actively participate in Fenton's reaction or the creation of reactive oxygen species (ROS), it indirectly leads to oxidative stress and consequent damage to body structure, due to its ability to bind thiol (–SH) groups which leads to the depletion of the central antioxidant – glutathione (GSH).[9] Recent research has shown that cadmium causes oxidative damage to DNA, proteins and lipids. At the molecular level, the action of lead can be seen in the increased production of reactive oxygen species.[10] The lead(II) ion can accelerate oxidation of oxyhaemoglobin to methaemoglobin (with increased formation of ROS). In addition, lead combines with thiol groups on proteins and, at high concentrations, causes GSH depletion. Lead may directly be attached to a cell membrane, thus increasing the sensitivity of the membrane to the process of lipid peroxidation.

Lipid peroxidation is oxidative damage that affects cell membranes, lipoproteins and other molecules containing lipids under conditions of oxidation stress.[11–13] Lipid peroxidation is a self-propagating chain reaction caused by the reaction of free radicals on unsaturated fatty acids in cell membranes. Lipid peroxidation reduces the fluidity of biological membranes resulting in increased permeability for uni- and divalent ions and deactivation of membrane enzymes.[14,15] The fragmentation of fatty acid chains to the level of intermediates of the aldehyde type and short chain volatile hydrocarbons leads to the loss of membrane integrity, while the rupture of lysosome membranes leads to the release of hydrolysis enzymes which further damage cells.[16] The process of lipid peroxidation initiates the death of cells.[17,18]

Malondialdehyde (MDA) is the final product in the lipid peroxidation process, and may be presented in enol form:

$$CH_2(CHO)_2 \rightarrow HOCH=CH–CHO$$

This compound is a biomarker of oxidative stress in the body or individual organs. MDA has very strong cytotoxic effects. The reaction between proteins, RNA, DNA, or phospholipids may cause the modification of these substrates and damage to cell membranes and intracellular molecules.[19] MDA when attached to DNA creates so-called "DNA radicals", which are responsible for mutation. MDA is a reactive potential mutagen and carcinogen. It also inhibits numerous thiol-dependent enzymes, such as glucose-6-phosphatase, Na^+, K^+-ATP-ase, adenylate cyclase and Ca^{2+}ATP-ase.[13] The degree of lipid peroxidation is evaluated by measuring the level of MDA in different tissues.[20]

GSH is a tripeptide L-γ-glutamyl-cysteinyl-glycine, which makes up 90 % of the overall non-protein sulphate compounds of the cell and is an essential cofactor of some enzymes (glutathioneperoxidase, glutathione S-transferase, glutathione transhydrogenase, glutathione reductase). GSH is a biological redox agent in erythrocyte metabolism and plays a role in the transfer of amino acids.

GSH is widespread in human and animal tissues, and plants and microorganisms. Intra-cell concentrations of 0.1–10 mM make GSH one of the most frequent thiol compounds.[21] GSH as a thiol compound is an antioxidant found within a cell.[22] Based on the results obtained upon defining the content of GSH in mosquitoes, flies, mice, rats and humans, a hypothesis was formed that its concentration reduces with age, which is the possible key to ageing and the appearance of different pathological states.[23]

Herein, the accumulation of Cd and Pb and the related lipid peroxidation in liver and kidney tissue of model animals (albino Wistar rats) is investigated. The study is focused on the effects of GSH on these processes. The protective role of glutathione was examined by measuring the MDA concentrations.

EXPERIMENTAL

The model system. The study was realized on female white (albino) Wistar rats, 2 months old with an approximate weight of 200±20 g. The animals were kept in groups, in metal cages under laboratory conditions with ventilation systems and an environmental temperature of $t = 22\pm2$ °C.[24] The experimental animals were bred under laboratory conditions with procurable water and food *ad libitum*, in vivarium at the Faculty of Medicine in Niš, divided into 6 groups of 6 animals. The groups were designated as Group I, II, III, IV, V and VI.

Heavy metal intoxication and the addition of a supplement. The first group of experimental animals was kept on a normal diet and led a normal life (the control group). The experimental animals from Group II and III were intoxicated by subcutaneous injection with an overall dose of 0.18 mg of cadmium in the form of cadmium(II) chloride in saline solution (0.9 % NaCl).[25] One day following intoxication by cadmium, the animals from Group III received a dose of glutathione in a molar ratio of metal:GSH = 1:2.[26] The animals from Groups IV and V were intoxicated with an overall dose of 21 mg of lead in the form of lead(II) acetate in saline solution in 7 equal doses over a period of 21 days.[27,28] One day following intoxication *via* lead, the animals in Group V received a dose of glutathione in a mol ratio of metal:GSH = 1:2.[26] The animals in Group VI were treated only with glutathione for the duration of the experiment. All the used reagents were of p.a. purity, and manufactured by Sigma–Aldrich (Steinheim, Germany). The experimental procedure was performed in accordance with the ethical scientific work code.

Preparation of the biological material for analysis. Ketalar anaesthesia (35 mg kg^{-1} of body weight) was performed on the rats after a certain number of days. Following laparotomy, the liver and kidneys were removed and, after washing in saline solution, were encapsulated, frozen at –20 °C and later used for making homogenates. Homogenization was performed on ice using a Teflon pestle Ultra Turrax® IKA® Tl8 basic homogenizer (IKA). From 10 % of the liver and kidney tissue homogenates, prepared in ionized water, samples were extracted for the following analyses: the determination of malondialdehyde concentrations and the definition of Cd and Pb concentrations in the organs.

Determination of the concentration of the lipid peroxidation product (TBARS) in the tissue homogenates. The level of lipid peroxidation in the tissues is expressed as the concentration of thiobarbituric acid reactive substances (TBARS) in the tissue homogenates and was defined by means of a spectrophotometric method.[29]

Determination of the metal concentration in the tissue homogenates of the kidneys and liver. The content of toxic metals in the tissue homogenates was determined by potentiometric stripping analysis (PSA).[30]

Statistical analysis. All of the obtained results are presented as average values of all the samples in one group, average ± standard deviation (*SD*). For statistical processing of the results, the Student t-test for independent samples was used. The statistical importance of the tests was defined as $p<0.01$.

RESULTS AND DISCUSSION

The results of the content of lead and cadmium in the analyzed kidney and liver tissue homogenates, with and without the GSH supplementation are shown in Fig. 1. It can be observed that both Cd and Pb accumulate to a higher level in the liver in comparison to kidneys. This can be attributed to a higher lipid content and detoxifying function of liver. GSH showed biased effects on the metal accu-

mulation. It promoted the accumulation of Cd in liver, but suppressed Pb accumulation in both the studied organs. This may be related to the binding of Cd and Pb to GSH, which may alter their metabolism in the blood.

** p<0.05
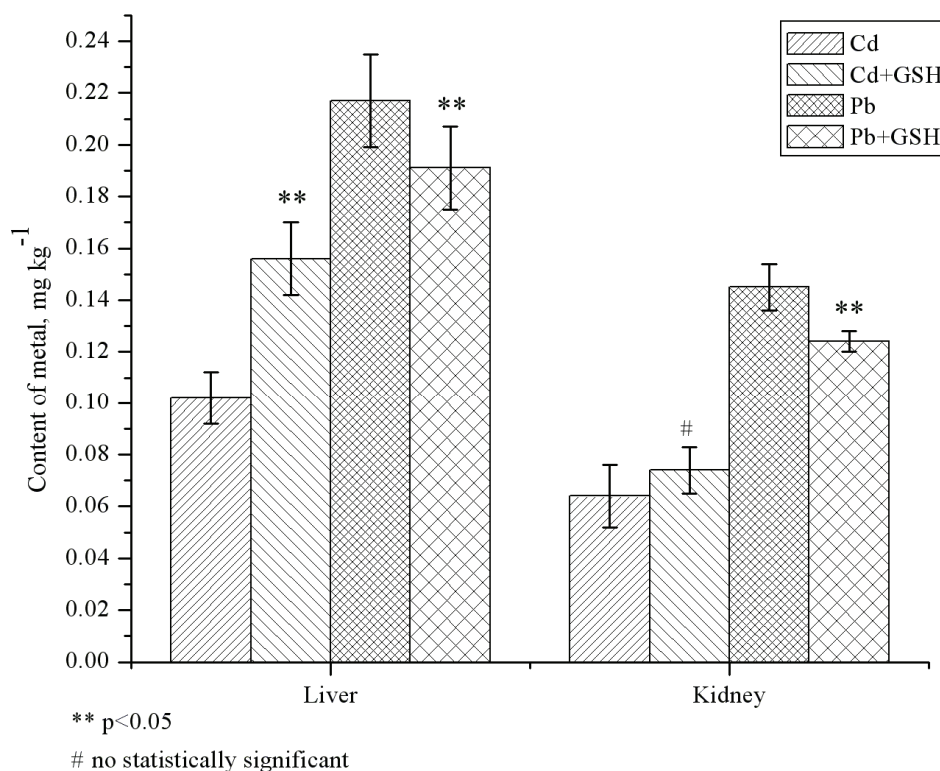# no statistically significant

Fig. 1. The content of Cd and Pb metals in the homogenates of the analyzed liver and kidney samples, in the presence and absence of GSH.

The results obtained from monitoring the toxic effects of cadmium in the analyzed tissue samples obtained through the content of MDA are shown in Fig. 2. The results in Fig. 2 show that under conditions of cadmium intoxication, the level of MDA was increased when compared to the level found in the liver and kidneys of the control group of animals. The results show that after cadmium intoxication, the level of TBARS was significantly increased. A direct consequence of exposure to cadmium *in vivo* is probably the depletion of physiological antioxidants, such as reduced glutathione and proteins which contain –SH groups, as one of the mechanisms of cadmium toxicity. In the experimental group of animals, where along with cadmium, GSH was applied as a supplement, the concentration of MDA was significantly reduced in comparison to the group of animals intoxicated with cadmium. The application of GSH along with cadmium

leads to a reduction in the TBARS level, probably because of the intake of supplements with –SH groups. Cadmium attaches to the active glutathione centre (–SH) and donor atoms (–S, –N and –O), thus reducing its pro-oxidant effect. Based on these research results, it may be concluded that the level of lipid peroxides is significantly reduced in the case when GSH supplement was added one day following intoxication of the rats with cadmium.
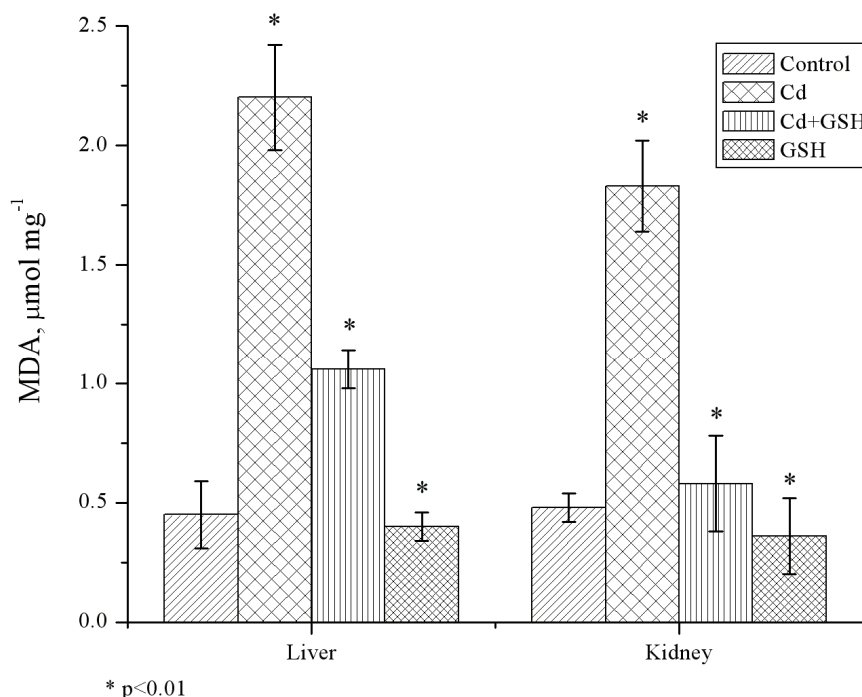

* p<0.01

Fig. 2. The content of MDA in the homogenates of the analyzed tissue samples in the case of acute cadmium intoxication, in the presence and absence of GSH.

As a consequence of chronic Pb intoxication, humans suffer from liver disorders that cause the deactivation of important enzymes with active sulphydryl groups. An entire group of disorders occur in the hepatocytes, including the synthesis of haem. The synthesis disorder of haem creates free radicals which further destroy liver cells. Intoxication with Pb reduces kidney circulation which is caused by changes in the small blood vessels, leading to lead nephropathy.[31] Persons who are exposed to Pb in their line of work suffer from kidney disorders, which lead to increased levels of urea, creatinine and urine acids in their serum, higher than the reference values.

The results of the determination of MDA concentrations in Wistar rats after intoxication by lead are presented in Fig. 3.
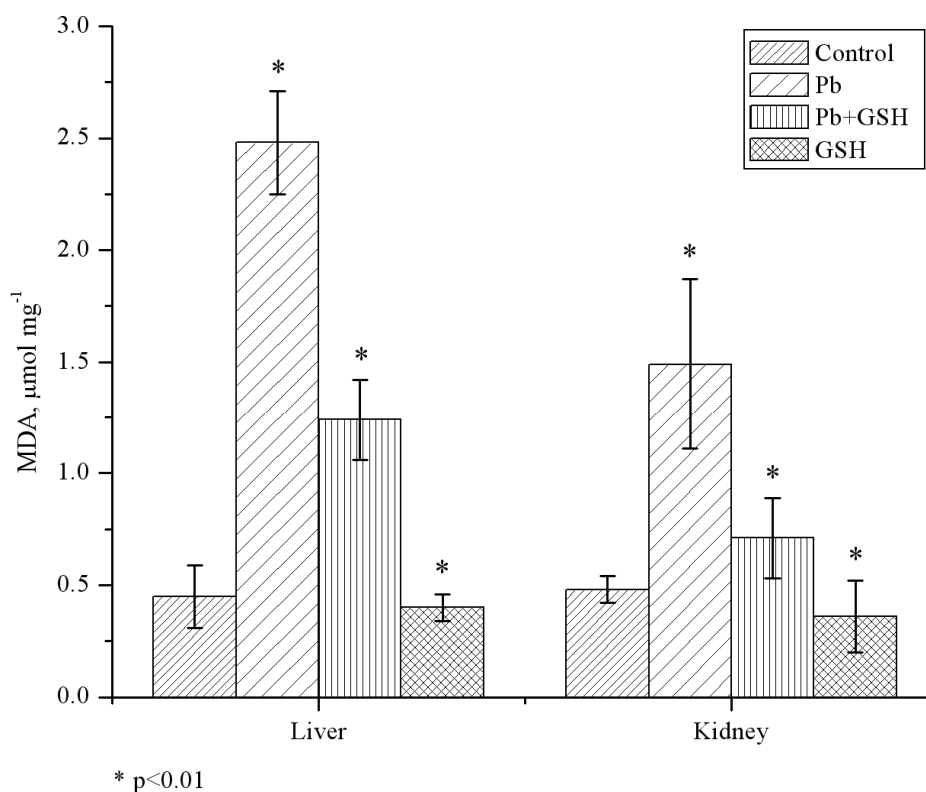
* p<0.01

Fig. 3. The content of MDA in the homogenates of the analyzed tissue samples in the case of acute lead intoxication, in the presence and absence of GSH.

Under lead intoxication, the level of MDA in the liver and kidneys increased as compared to the level in the control group. Lead probably directly or indirectly increases the number of reactive oxygen species and reduces the antioxidative system of cell defence, which causes an imbalance between free radicals and antioxidants. It is known that lead has a toxic influence on cell membranes and its functions (for example mitochondrial membranes, endoplasmic reticulum membranes, lysosome membranes and plasma membrane). The cell membrane, in addition to other chemical compounds, contains fatty acids. The presence of double bonds in them weakens the allylic C–H bond in the =C–H system, which leads to an easier release of H. As a result, fatty acids with <2 double bonds are more resistant to oxidative stress, unlike unsaturated ones with >2 double bonds in their molecule. Upon the exposure of essential fatty acids to lead, the concentration of the final product of oxidative stress, MDA, increases with increasing number of double bonds, Lead may directly be bound to a cell membrane, which results in sensitivity of the membrane to lipid peroxidation.[32]

In the group of experimental animals to which, in addition to lead, glutathione was applied as a supplement, the MDA concentrations were significantly reduced in comparison to the group poisoned by lead, as can be seen in Fig. 3. The reduction of the toxic effect of lead in the presence of GSH is the result of the interaction between Pb^{2+} and donor atoms of GSH, which shows that the time difference between the input of this metal and GSH, one day after intoxication with metal, indicates the possibility that GSH and the food that contains it may be a good supplement for the purpose of reduction of the toxic effects of heavy metal, especially those of lead.

The presence of a GSH supplement significantly reduces the toxic effects caused by Cd and Pb intoxication.

Increased values of MDA, as a biochemical marker of oxidative disorder of cell membranes, indicate an increased process of lipid peroxidation, which was found in the kidney tissue homogenates due to acute cadmium intoxication, just as a reduction in the MDA concentration in cases when the experimental animals were given a glutathione supplement implies decreased lipid peroxidation.

Poisoning by a sub-lethal dose of lead causes a slightly greater production of MDA in the liver in comparison to sub-lethal doses cadmium poisoning, which correlates with the results of the roles of heavy metals in lipid peroxidation.[33] In the case of kidneys, cadmium intoxication causes a slightly greater production of MDA in comparison to lead intoxication, probably due to the difference in their metabolism and rate of excretion.

The kidneys represent the primary organs which enable the extraction of GSH from the peripheral bloodstream.[34,35] GSH is actively synthesized and secreted in the kidneys. In addition to kidneys, other tissue types, for example the lungs and the epithelium of the intestinal tract, participate in the re-synthesis and inter organ flow of GSH. In the case of intense oxidative stress, GSH extraction from the liver into the peripheral bloodstream is increased.[36] In this way the remaining organs have easier access to GSH.

GSH forms low solubility mercaptides with heavy metal ions *via* its –SH group. However, GSH can make complexes of heavy metal ions. The stability of the complex which GSH may create with heavy metal ions (Pb^{2+} and Cd^{2+} in this case) depends on the size of the ions, the acid–base characteristics of the ions as well as the affinity of the –SH group for these ions. Adding GSH, one day after the exposure of experimental animals to these metals during the experiment, partially reduced the effect of their toxic influence.

Metals with a stable valence (Cd and Pb) express an indirect pro-oxidant effect, as do metals with variable valence (Cu, Fe, Hg and Cr), by interacting with bio-elements, *i.e.*, by reacting with metals in the active centre of an enzyme, through interference in the same ion channels and the disturbance of the intercellular homeostasis of ions, thus contributing to the induction and propagation

of the lipid peroxidation process.[37] The bonding with biomolecules is realised *via* the –O, –N or –S donor atoms of these bio-ligands, so that their effective concentration may be reduced together with their availability for interaction under the physiological conditions of the functioning of the human body.

The measured content of metal in the liver was higher in the case of animals which one day after poisoning received the supplement (GSH) which, by bonding with the metal, contributes to its retention in the tissue. In the liver and kidney homogenates, the presence of lead was registered, along with a minor reduction in the concentration of lead in the tissue samples in the presence of the supplement. Even though they are present in the tissue samples, these toxic metals have a lower toxic effect, as measured *via* the MDA concentration levels, which is the result of the partial blocking of toxic metals achieved through bonding through the active centres. GSH as a ligand with a potentially large number of donor atoms (–O from the –COOH group, –N from the –NH$_2$ group, –S from the –SH group) can initiate various interactions with metal ions (Me^{2+}), depending on the radius of the ions of these metals ($r_{Pb^{2+}} > r_{Cd^{2+}}$).[38,39] The donor atoms of GSH that could potentially interact with Me^{2+} are represented in Fig. 4.
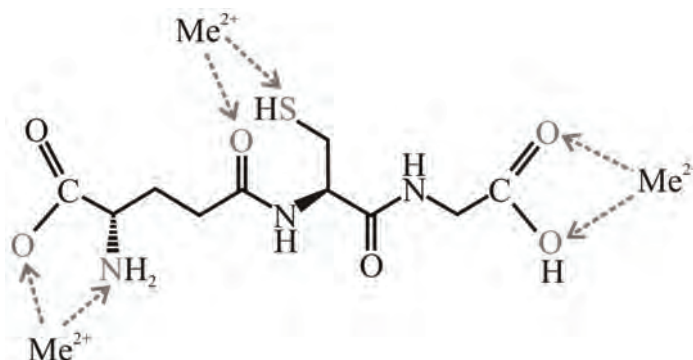
Fig. 4. Donor GSH atoms for the potential interactions with Me^{2+}.

According to the obtained results, GSH more effectively blocks, or reduces, the toxic effect of Cd^{2+}. The results indicate that in the presence of GSH, larger amounts of these metals are accumulated in the analyzed tissue samples, but the negative effect of their presence is lower than in the absence of GSH.

CONCLUSIONS

This study, performed on a model system involving experimental animals intoxicated by sub-lethal doses of Cd and Pb showed that the effects of intoxication, apart from measurement of the toxic metal contents in biological fluids, may also be monitored *via* an indicator of the level of lipid peroxidation, *i.e.*, MDA concentrations. In situations where intoxication *via* these metals occurs,

GSH has a protective role during and also following intoxication. This supplement contains a free –SH group that forms stable associations with the ions of these metals, thus blocking the heavy metals and reducing their toxic effects. The intake of food rich with GSH supplement and of products of a similar structure may have a preventive effect, and significantly reduce the toxic influence of these metals.

ИЗВОД

ЗАШТИТНА УЛОГА ГЛУТАТИОНА У ИНТОКСИКАЦИЈИ КАДМИЈУМОМ И ОЛОВОМ. ПРАЋЕЊЕ ПРЕКО САДРЖАЈА МАЛОНДИАЛДЕХИДА

ЈАСМИНА М. ЈОВАНОВИЋ[1], РУЖИЦА С. НИКОЛИЋ[1], ГОРДАНА М. КОЦИЋ[2], НЕНАД С. КРСТИЋ[1] и МИЛЕНА М. КРСМАНОВИЋ[1]

[1]*Деūарūман за хемију, Природно–маūемаūички факулūеū, Универзиūеū у Нишу, Вишеīрадска 33, 18000 Ниш и* [2]*Медицински факулūеū, Универзиūеū у Нишу, Булевар др Зорана Ђинђића 81, 18000 Ниш*

Тешки метали (Cd и Pb) представљају озбиљан еколошки проблем због њихове растворљивости, покретљивости и акумулацији у земљишту. Изложеност тешким металима, кадмијуму и олову, може бити из различитих извора (вода за пиће, храна, ваздух, итд.), а у организам човека могу доспети преко респираторног и дигестивног система. У раду је испитиван негативан ефекат интоксикације сублеталним дозама олова или кадмијума преко мерења садржаја у хомогенатима јетре и бубрега малондиалдехида, који настаје у процесу липидне пероксидације. Студија је урађена на модел систему експерименталних животиња (албино пацови Wistar соја). Садржај малондиалдехида је одређиван спектрофотометријски. Резултати ове студије су показали да у условима интоксикације овим металима долази до вишеструког повећања садржаја малондиалдехида. Овај ефекат је изразитији у јетри. Глутатион, који се у физиолошким условима синтетише у организму, као потенцијално полидентатни лиганд са већим бројем донор атома може бити суплемент који испољава протективну улогу у случајевима интоксикације овим металима без обзира на акумулацију истих у анализираним ткивима.

(Примљено 14. фебруара, ревидирано 17. априла 2012)

REFERENCES

1. M. S. Ram, L. Singh, M. V. Suryanarayana, S. T. Alam, *Water Air Soil Pollut.* **117** (2000) 305
2. H. J. Hapke, in *Metals and their compounds in the environment, Occurrence analysis, and biological relevance*, VCH-Verlag, Weinheim, 1991, p. 469
3. M. Stoeppler, in *Metals and their compounds in the environment*, E. Merian, Ed., Verlag Chemie, Weinheim, 1991, p. 805
4. S. Satarug, J. R. Baker, S. Urbenjapol, M. Haswell-Elkins, P. E. B. Reilly, D. J. Williams, M. R. Moore, *Toxicol. Lett.* **137** (2003) 65
5. R. Goyer, *Casarett and Doul's toxicology*, Pergamon Press, New York, 1991, p. 623

6. V. Popović, K. Tričković, *Booklet Med. Sci.* **93** (1983) 1
7. US Geological Survey, Data series (2005) 140 http://minerals.usgs.gov/ds/2005/140/
8. A. Fischbein, in: *Environmental and Occupational Medicine*, W. N. Rom, Ed., Little Brown, Boston, 1992, p. 735
9. L.A. Videla, V. Fernandez, G. Tapia, P. Varela, *Biometals* **16** (2003) 103
10. H. Gurer, N. Ercal, *Free Rad. Biol. Med.* **29** (2000) 927
11. B. Halliwell, J. M. C. Gutteridge, in *Free radicals in biology and medicine*, B. Halliwell, J. M. C. Gutteridge, Eds., Clarendon Press, Oxford, UK, 1985, pp. 139–189
12. C. U. Kagan, *Lipid peroxidation in biomembranes*, CRC. Press, Inc. Boca Raton, FL, 1988
13. T. F. Slater, *Biochem. J.* **222** (1984) 1
14. C. Richard, C. W. Thayer, *Biochim. Biophys. Acta* **733** (1983) 216
15. K. Myung-Suk, L. Akera, *Am. J. Physiol.* **525** (1987) 225
16. K. L. Fong, P. B. McCay, J. L. Poyer, *J. Biol. Chem.* **248** (1973) 7792
17. G. L. Nikolson, *Biochim. Biophys. Acta* **457** (1978) 57
18. S. I. Korsmeyer, X. M. Yin, C. E. Oltvai, D. J. Veis-Novack, G. P. Linette, *Biochim. Biophys. Acta* **1271** (1995) 63
19. N. Sreejayan, C. von Ritter, *Pathophysiology* **5** (1999) 225
20. S. J. Yiin, T. H. Lin, *Biol. Trace Elem.* **50** (1995) 167
21. A. Meister, *J. Biol. Chem.* **263** (1988) 17205
22. D. V. Parke, J. K. Piotrowski, *Acta Pol. Toxicol.* **4** (1996) 1
23. R. S. Sohal, R. Weindruch, *Science* **273** (1996) 59
24. A. L. Sayeda, A. Newairy, *Food Chem. Toxicol.* **47** (2009) 813
25. G. Deepti, P. Shabad, K. K. Dua, *J. Food Drug Anal.* **18(6)** (2010) 464
26. H. Fuke, I. Koki, N. Watanabe, S. Kumada, *Folia Pharmacol. Jpn.* **68** (1972) 175
27. A. A. Berrahal, A. Nehdi, N. Hajjaji, N. Gharbi, S. El-Fazaa, *C. R. Biol.* **330** (2007) 581
28. J. C. Ponce-Canchihuaman, O. Perez-Mendez, R. Hernandez-Munoz, P. V. T. Duran, M. A. Juarez-Oropeza, *Lipids Health Dis.* **31** (2010) 9
29. L. Andreeva, L. Kozhemiakin, A. Kishkun, *Lab. delo* **11** (1988) 41 (in Russian)
30. B. Kaličanin, R. Nikolić, in *Wide spectra of quality control*, I. Akyar Ed., In Tech, Rijeka, 2011, p. 211
31. M. Aranđelović, J. Jovanović, in *Occupational Medicine*, M. Višnjić Ed., Faculty of Medicine, Niš, 2009, p. 100 (in Serbian)
32. G. J. Quinlan, B. Halliwell, C. P. Moorhouse, J. M. C. Gutteridge, *Biochim. Biophys. Acta* **962** (1988) 196
33. J. A. Benedet, T. Shibamoto, *Food Chem.* **107** (2008) 165
34. T. M. McIntyre, N. P. Cuthoys, *J. Biol. Chem.* **257** (1983) 11915
35. S. Orrenius, K. Ormstad, H. Thor, S. A. Jewell, *Fed. Proc.* **42** (1983) 3177
36. S. C. Lu, C. Garcia-Ruiz, J. Kuhlenkamp, M. Ookhtens, M. Salas-Prato, N. Kaplowitz, *J. Biol. Chem.* **265** (1990) 16088
37. V. Đorđević, D. Pavlović, *Biochemical markers of oxidative stress in experimental and clinical medicine*, Faculty of Medicine, University of Niš, 2006 (in Serbian)
38. K. Nakamoto, *Infrared and Raman Spectra of Inorganic and Coordination Compounds*, 3rd ed., Wiley, New York, 1978
39. R. R. Crichton, *Biological Inorganic Chemistry. An Introduction*, Elsevier, Amsterdam, 2008.

Chemical composition and insecticidal activities of the essential oil of the flowering aerial parts of *Aster ageratoides*

SHA SHA CHU[1], SHAO LIANG LIU[2], QI ZHI LIU[1], GUO HUA JIANG[3]
and ZHI LONG LIU[1]*

[1]*Department of Entomology, China Agricultural University, Haidian District, Beijing 100193, China,* [2]*Department of Biology, Faculty of Preclinical Medicine, Guang Xi Traditional Chinese Medical University, Nanning 530001, China and* [3]*Analytic and Testing Center, Beijing Normal University, Haidian District, Beijing 100875, China*

Abstract: Water-distilled essential oil from the flowering aerial parts of *Aster ageratoides* Turcz. (Compositae) was analyzed by gas chromatography-mass spectrometry (GC–MS) for the first time. Forty-three compounds, accounting for 96.4 % of the oil, were identified. The main compounds found were *α*-terpineol (10.8 %), *β*-caryophyllene (10.3 %), linalool (7.2 %), D-limonene (6.9 %), spathulenol (6.5 %), bornyl acetate (5.8 %) and bicyclosesquiphellandrene (5.6 %). The essential oil of *A. ageratoides* flowering aerial parts possessed contact toxicity against two grain storage insects *Sitophilus zeamais* and *Tribolium castaneum* adults with LD_{50} values of 27.16 and 8.09 μg per adult, respectively. The essential oil also exhibited fumigant toxicity against *S. zeamais* and *T. castaneum* adults with LC_{50} values of 13.73 and 12.14 mg L^{-1}, respectively. The essential oil showed potential for development as a possible natural fumigant/insecticide for control of insects in stored products.

Keywords: *Aster ageratoides*; *Sitophilus zeamais*; *Tribolium castaneum*; essential oil.

INTRODUCTION

Aster ageratoides Turcz. (Family: Compositae) is a perennial suffrutescent erect herb with long stoloniferous rhizomes that is distributed widely in Siberia, Mongolia, China, South Korea and Japan.[1] Great variations (many types) were observed in this species and 11 varieties (such as var. *ageratoides*; var. *oophyllus*; var. *pilosus*; var. *ovatus*) were suggested. This plant has long been used in traditional Chinese medicine for the treatment of colds, fever, tonsillitis, bronchitis, snake bites and bee stings.[2] Phytochemical analyses of *A. ageratoides* led to the isolation of a number of chlorogenic acids, sesquiterpene lactones, kaurane diter-

---

penoids, diterpene glycosides, pentacyclic triterpenoids and triterpenoid saponins.[3–10] However, the constituents of the essential oil derived from the flowering aerial parts of *A. ageratoides* have not been determined to date. Only the essential oil and headspace constituents from the aerial parts of *A. ageratoides* var. *ovatus* were determined by GC and GC–MS.[11] Moreover, the insecticidal activities of the essential oil of *A. ageratoides* against grain storage insects have not been measured. The present investigation consisted of two parts: determination of chemical composition of the essential oil of the flowering aerial parts of *A. ageratoides* and an evaluation of the essential oil as insecticide/fumigant against two grain storage insect pests.

The maize weevil (*Sitophilus zeamais* Motsch.) and red flour beetle (*Tribolium castaneum* Herbst) are two serious pest species of stored grains worldwide.[12] Infestations not only cause significant losses due to the consumption of grains, but also they result in elevated temperature and moisture conditions that lead to an accelerated growth of molds, including toxigenic species.[13] Infestations of grain storage insect pests could be controlled by using synthetic fumigants or insecticides. However, the heavy use of synthetic insecticides/fumigants has led to problems, such as disturbances of the environment, increasing costs of application, pest resurgence, pest resistance to insecticides and lethal effects on non-target organisms, in addition to direct toxicity to users. Moreover, the use of methyl bromide will be prohibited in the near future because of its ozone depletion potential. These problems have highlighted the need to find new safe, economical and effective fumigants. Fortunately, essential oils or their constituents may provide an alternative to currently used fumigants/pesticides in the control of stored-food insects. Investigations in several countries confirm that some plant essential oils not only repel insects, but possess contact and fumigant toxicity against stored product pests as well as exhibiting feeding inhibition or harmful effects on the reproductive system of insects.[14] The toxicity of a large number of essential oils and their constituents has been evaluated against a number of stored-product insects.[15–18] The purpose of the present study was to ascertain the chemical composition of *A. ageratoides* and to evaluate the effectiveness of its essential oil as a fumigant and contact toxicant against two species of stored-product beetles.

EXPERIMENTAL

Plant material and essential oil extraction

The flowering aerial parts of *A. ageratoides* were collected in August 2009 from Xiaolongmen National Forest Park (39.48° N latitude and 115.25° E longitude, Mentougou District, Beijing 102300). The samples were air-dried and identified by Dr. Q. R. Liu (College of Life Sciences, Beijing Normal University, Beijing 100875, China) and a voucher specimen (ENTCAU-Compositae-10044) was deposited at the Department of Entomology, China Agricultural University (Beijing 100193). The samples were ground to a powder using a grinding

mill (Retsch Mühle, Germany). Each 600 g portion of powder was mixed in 1800 ml of distilled water and soaked for 3 h. The mixture was then boiled in a round-bottom flask, and steam distilled for 6–8 h. Volatile essential oil from the distillation was collected in a flask. Separation of the essential oil from the aqueous layer was performed in a separating funnel, using the non-polar solvent, *n*-hexane. The solvent was evaporated using a vacuum rotary evaporator (Büchi Rotavapor R-124, Switzerland). The sample was dried over anhydrous Na_2SO_4 and kept in a refrigerator (4 °C) for the subsequent experiments.

Insects

S. zeamais and *T. castaneum* were obtained from laboratory cultures maintained in the dark in incubators at 29–30 °C and 70–80 % r.h. The *T. castaneum* were reared on wheat flour mixed with yeast (10:1, w/w) while the *S. zeamais* were reared on whole wheat at 12–13 % moisture content in glass jars (diameter 85 mm, height 130 mm). Unsexed adult weevils//beetles used in all the experiments were about 2 weeks old. All containers housing the insects and the Petri dishes used in the experiments were made escape-proof with a coating of polytetrafluoroethylene (Fluon, Blades Biological, UK).

Gas chromatography–mass spectrometry

The essential oil of *A. ageratoides* was subjected to GC–MS analysis on an Agilent system consisting of a model 6890N gas chromatograph, a model 5973N mass selective detector (EIMS, electron energy 70 eV), and an Agilent ChemStation data system. The GC column was an HP-5MS fused silica capillary with a 5 % phenyl-methylpolysiloxane stationary phase, with a film thickness of 0.25 µm, a length of 30 m and an internal diameter of 0.25 mm. The following GC settings were employed: the initial oven temperature was held at 60 °C for 1 min and increased at 10 °C min^{-1} to 180 °C held for 1 min, and then increased at 20 °C min^{-1} to 280 °C and held for 15 min. The injector temperature was maintained at 270 °C. The sample (1 µL) was injected neat, with a split ratio of 1:10. The carrier gas was helium at a flow rate of 1.0 mL min^{-1}. Spectra were scanned from 20 to 550 *m/z* at two scans s[-1]. Most constituents were identified by gas chromatography by comparison of their retention indices with those in the literature or with those of authentic compounds. The retention indices were determined in relation to a homologous series of *n*-alkanes (C_8–C_{24}) run under the same operating conditions. Further identification was made by comparison of their mass spectra with those stored in the NIST 08 and Wiley 275 libraries or with mass spectra from the literature.[19] Component relative percentages were calculated based on the normalization method without using correction factors.

Fumigant toxicity bioassay

Range-finding studies were run to determine the appropriate testing concentrations of the essential oil. The fumigant toxicity of *A. ageratoides* essential oil was determined using the method of Liu and Ho[20] with some modifications. A serial dilution of the essential oil (5.0–20.0 %, 6 concentrations) was prepared in *n*-hexane. A Whatman filter paper (CAT No. 1001020, diameter 2.0 cm) was placed on the underside of the screw cap of a glass vial (diameter 2.5 cm, height 5.5 cm, volume 24 mL). Ten microliters of an appropriate concentration of the essential oil was added to the filter paper. The solvent was allowed to evaporate for 15 s before the cap was placed tightly on the glass vial (with 10 unsexed insects) to form a sealed chamber. Preliminary experiments demonstrated that 15 s was sufficient for the evaporation of solvents. The vials were upright and the Fluon (ICI America Inc.) coating restricted the insects to the lower portion of the vial to prevent them from reaching the treated filter paper. *n*-Hexane was used as a control. They were incubated at 27–29 °C and 70–80 %

relative humidity for 24 h. Five replicates were performed for all treatments and controls. The insects were considered dead if their appendages did not move when probed with a camel brush. The mortality of the insects was observed and the results from all replicates were subjected to Probit analysis using the PriProbit Program V1.6.3 to determine the LC_{50} values.[21]

Contact toxicity by topical application

Range-finding studies were run to determine the appropriate testing concentrations. A serial dilution of the essential oil (5.0–25.0 %, v/w, 6 concentrations) was prepared in *n*-hexane. Aliquots of 0.5 μL of the dilutions were applied topically to the dorsal thorax of the insects, using a Burkard Arnold microapplicator. Controls were determined using *n*-hexane. Both treated and control insects were then transferred to glass vials (10 insects per vial) with culture media and kept in incubators. The mortality of insects was observed daily until the end-point mortality was reached one week after treatment. The insects were considered dead if their appendages did not move when probed with a camel brush. The LD_{50} values were calculated using Probit analysis.[21]

RESULTS AND DISCUSSION

The yield of the yellow essential oil of the flowering aerial parts of *A. ageratoides* was 0.79 % (vol/wt) and the density of the concentrated essential oil was 0.87 g mL^{-1}. A total of 43 components were identified in the essential oil of the flowering aerial parts of *A. ageratoides*, accounting for 96.4 % of the total oil (Table I). The main compounds found were *α*-terpineol (10.8 %), *β*-caryophyllene (10.3 %), linalool (7.2 %), D-limonene (6.9 %), spathulenol (6.5 %), bornyl acetate (5.8 %) and bicyclosesquiphellandrene (5.6 %) (Table I). Monoterpenoids represented 21 of the 43 compounds, corresponding to 53.6 % of the whole oil while 20 of the 43 constituents were sesquiterpenoids (41.1 % of the crude essential oil).

TABLE I. Chemical constituents of the studied essential oil

Peak No.	Compound	RI[a]	Content, %
1	*α*-Pinene	931	2.3
2	*β*-Pinene	974	1.3
3	*p*-Cymene	1024	0.2
4	D-Limonene	1027	6.9
5	1,8-Cineole	1031	3.6
6	(*Z*)-*β*-Ocimene	1037	1.1
7	(*E*)-*β*-Ocimene	1048	1.2
8	Linalool	1097	7.2
9	*β*-Phenylethanol	1116	0.5
10	Borneol	1167	1.7
11	4-Terpineol	1177	3.7
12	*p*-Cymene-8-ol	1182	1.8
13	*α*-Terpineol	1189	10.8
14	Verbenone	1204	0.7
15	*cis*-Carveol	1222	0.5

TABLE I. Continued

Peak No.	Compound	RI^a	Content, %
16	*cis*-Geraniol	1229	0.2
17	Isothymol methyl ether	1244	0.7
18	*trans*-Geraniol	1252	2.0
19	Perillaldehyde	1274	0.8
20	Bornyl acetate	1285	5.8
21	Cuminic alcohol	1292	0.7
22	Neric acid	1347	0.4
23	Eugenol	1356	1.2
24	Cyclosativene	1364	0.2
25	Ylangene	1372	0.3
26	Copaene	1375	0.6
27	*β*-Bourbonene	1383	0.3
28	*β*-Elemene	1390	1.5
29	10*S*,11*S*-Himachala-3(12), 4-diene	1401	0.5
30	*β*-Caryophyllene	1420	10.3
31	*α*-Ionone	1427	1.2
32	Geranyl acetone	1452	0.5
33	*α*-Caryophyllene	1456	1.3
34	*allo*-Aromadendren	1461	0.9
35	*γ*-Gurjunene	1473	1.5
36	*α*-Selinene	1495	1.3
37	Bicyclosesquiphellandrene	1499	5.6
38	1*ξ*,6*ξ*,7*ξ*-Cadina-4,9-diene	1502	1.9
39	*γ*-Cadinene	1512	1.7
40	*δ*-Cadinene	1523	1.8
41	Ledol	1565	1.7
42	Spathulenol	1578	6.5
43	Caryophyllene oxide	1584	1.5
	Total		96.4

[a]Retention index as determined on a HP-5MS column using a homologous series of *n*-hydrocarbons

No death of insects was observed in the control under the current concentration. The essential oil of the flowering aerial parts of *A. ageratoides* possessed contact toxicity against *S. zeamais* and *T. castaneum* adults with LD_{50} values of 27.16 and 8.09 μg per adult, respectively (Table II). However, the essential oil *A. ageratoides* demonstrated only one-fifth and one-twentieth of the toxicity of a pyrethrum extract against *S. zeamais* and *T. castaneum* (LD_{50} = 4.29 and 0.36 μg per adult, respectively).[22]

The essential oil of the flowering aerial parts of *A. ageratoides* exhibited fumigant toxicity against *S. zeamais* and *T. castaneum* adults with LC_{50} values of 13.73 and 12.14 mg L^{-1}, respectively (Table II). No death of insects was observed in the control under the current concentration. The commercial grain fumigant, methyl bromide (MeBr) exhibited fumigant activity against *S. zeamais* and *T. castaneum* adults with LC_{50} values of 0.67 and 1.75 mg L^{-1}, respectively.[20]

Thus, the toxicity of the essential oil was one-twentieth and one-sixth that of MeBr towards *S. zeamais* and *T. castaneum* adults, respectively. However, compared with other essential oils that were tested in the previous studies using a similar bioassay, the essential oil of the flowering aerial parts of *A. ageratoides* exhibited stronger fumigant toxicity against *S. zeamais* and *T. castaneum* adults than the essential oils of *Caryopteris incana*,[23] *Kadsura heteroclite*,[16] *Illicium fragesii*,[24] *I. simonsii*,[17] *Murraya exotica*[22] and several essential oils from the genus *Artemisia*.[15] Moreover, the three main constituent monoterpenoids, α-terpineol, linalool and D-limonene have been demonstrated to possess fumigant and contact toxicity activity against several stored-product insects.[25–29] The isolation and identification of the bioactive constituent compounds in the essential oil of the flowering aerial parts of *A. ageratoides* are of utmost importance so that their potential application in controlling stored-product pests can be fully exploited.

TABLE II. Contact and fumigant toxicity of *Aster ageratoides* essential oil against *Sitophilus zeamais* and *Tribolium castaneum* adults

| Insect | Treatment | Contact toxicity | | | Fumigant toxicity | | |
		LD_{50} / μg adult^{-1} (95 % confidence limit)	Slope $\pm SE$	χ^2	LC_{50} / μg mL^{-1} air (95 % confidence limit)	Slope $\pm SE$	χ^2
S. zeamais	*A. ageratoides*	27.16 (20.67–26.08)	2.45 ±0.21	12.43	13.73 (11.32–15.12)	3.23 ±0.25	11.26
	Pyrethrum extract[22]	4.29 (3.86–4.72)	–	–	–	–	–
	MeBr[20]	–	–	–	0.67	–	–
T. castaneum	*A. ageratoides*	8.09 (7.89–9.12)	3.23 ±0.32	17.49	12.14 (11.67–13.73)	3.51 ±0.27	16.21
	Pyrethrum extract[22]	0.36 (0.32–0.41)	–	–	–	–	–
	MeBr[20]	–	–	–	1.75	–	–

The present findings suggest that the fumigant activity of the essential oil of the flowering aerial parts of *A. ageratoides* is quite promising considering that the currently used fumigants are synthetic insecticides. The essential oil of the flowering aerial parts of *A. ageratoides* could play an important role in stored grain protection and reduce the need for and the risks associated with synthetic insecticides. However, for the practical application of the essential oil as a novel insecticide/fumigant, further studies on the safety of the essential oil to humans and on development of formulations are necessary to improve the efficacy and stability and to reduce costs.

Life Sciences, Beijing Normal University, Beijing 100875 for the identification of the investigated plant.

И З В О Д

ХЕМИЈСКИ САСТАВ И ИНСЕКТИЦИДНА АКТИВНОСТ ЕТАРСКОГ УЉА НАДЗЕМНИХ ДЕЛОВА У ЦВЕТУ БИЉКЕ *Aster ageratoides*

SHA SHA CHU[1], SHAO LIANG LIU[2], QI ZHI LIU[1], GUO HUA JIANG[3] и ZHI LONG LIU[1]

[1]*Department of Entomology, China Agricultural University, Haidian District, Beijing 100193, China,* [2]*Department of Biology, Faculty of Preclinical Medicine, GuangXi Traditional Chinese Medical University, Nanning 530001, China u* [3]*Analytic and Testing Center, Beijing Normal University, Haidian District, Beijing 100875, China*

Етарско уље надземних делова у цвету биљке *Aster ageratoides* Turcz. (Compositae) је добијено дестилацијом воденом паром и анализирано је методом гасне хроматографије-масене спектрометрије (GC–MS). Идентификована су 43 једињења, што чини 96,4 % уља. Главни састојци су α-терпинеол (10,8 %), β-кариофилен (10,3 %), линалоол (7,2 %), D-лимонен (6,9 %), спатуленол (6,5 %), борнил-ацетат (5,8 %) и бициклосесквифеландрен (5,6 %). Етарско уље надземних делова у цвету биљке *A. ageratoides* испољило је цитотоксичност спрам одраслих инсеката који настањују силосе жита *Sitophilus zeamais* и *Tribolium castaneum*. LD_{50} вредности су биле 27,16 и 8,09 μg po јединки. Етарско уље је, такође, имало фумигантну активност спрам *S. zeamais* и *T. castaneum*. LC_{50} вредности су биле 13,73 и 12,14 mg L^{-1}. Испитивано етарско уље има потенцијал за даљу примену као природни фумигант/инсектицид у контроли инсеката у силосима.

(Примљено 30.јануара, ревидирано 12. априла 2012)

REFERENCES

1. Y. Ling, Y. L. Chen, *Flora Reipublicae Popularis Sinicae*, Vol. 74, Science Press, Beijing, China, 1985, p. 159
2. Jiangsu New Medical College, *A Dictionary of the Traditional Chinese Medicines*, People's Press, Shanghai, 1977, p. 177
3. D. L. Cheng, X. P. Cao, H. X. Wei, L. Yang, *Chin. Chem. Lett.* **4** (1993) 39
4. D. L. Cheng, X. P. Cao, H. X. Wei, L. He, *Phytochemistry* **33** (1993) 1181
5. S. J. Guo, J. P. Katalinic, L. He, D. L. Cheng, *Pharmazie* **53** (1998) 481
6. K. Sakai, T. Nagao, H. Okabe, *Phytochemistry* **51** (1999) 309
7. A. A. Ahmed, A. A. Mahmoud, M. F. Hegazy, P. W. Pare, J. Karchesy, *Pharmazie* **57** (2002) 567
8. F. L. Yan, A. X. Wang, Z. J. Jia, *Pharmazie* **59** (2004) 882
9. M. N. Clifford, Z. Wang, N. Kuhnert, *Phytochem. Anal.* **17** (2006) 384
10. F. L. Yan, S. M. Yao, Y. Zhou, *J. Chin. Chem. Soc.* **54** (2007) 1321
11. M. Miyazawa, J. Kawata, K. Kohno, M. Imai, T. Ono, *J. Essent. Oil Res.* **20** (2007) 9
12. Z. L. Liu, S. H. Goh, S. H. Ho, *J. Stored Prod. Res.* **43** (2007) 290
13. N. Magan, R. Hope, V. Cairns, D. Aldred, *Eur. J. Plant Pathol.* **109** (2003) 723
14. M. B. Isman, *Annu. Rev. Entomol.* **51** (2006) 45
15. Z. L. Liu, Q. R. Liu, S. S. Chu, *Chem. Biodiv.* **7** (2010) 2040
16. H. Q. Li, C. Q. Bai, S. S. Chu, L. Zhou, S. S. Du, Z. L. Liu, Q. Z. Liu, *J. Med. Plants Res.* **5** (2011) 4943

17. C. F. Wang, P. Liu, K. Yang, Y. Zeng, Z. L. Liu, S. S. Du, Z. W. Deng, *Afr. J. Biotechnol.* **10** (2011) 18179
18. Z. L. Liu, S. S. Du, *E-J. Chem.* **8** (2011) 1937
19. R. P. Adams, *Identification of Essential Oil Components by Gas Chromatography/Quadrupole Mass Spectroscopy*, Allured, Carol Stream, IL, USA, 2001
20. Z. L. Liu, S. H. Ho, *J. Stored Prod. Res.* **35** (1999) 317
21. M. Sakuma, *Appl. Entomol. Zool.* **33** (1998) 339
22. W. Q. Li, C. H. Jiang, S. S. Chu, M. X. Zuo, Z. L. Liu, *Molecules* **15** (2010) 5831
23. S. S. Chu, Q. Z. Liu, L. Zhou, S. S. Du, Z. L. Liu, *Afr. J. Biotechnol.* **10** (2011) 8476
24. S. S. Chu, S. L. Liu, G. H. Jiang, Z. L. Liu, *Rec. Nat. Prod.* **4** (2010) 205
25. S. A. M. Abdelgaleil, M. I. E. Mohamed, M. E. I. Badawy, S. A. A. El-Arami, *J. Chem. Ecol.* **35** (2009) 518
26. B. H. Lee, W. S. Choi, S. E. Lee, B. S. Park, *Crop Prot.* **20** (2001) 317
27. S. Karaborklu, A. Ayvaz, S. Yilmaz, M. Akbulut, *J. Econ. Entomol.* **104** (2011) 1212
28. D. Suthisut, P. G. Fields, A. Chandrapatya, *J. Stored Prod. Res.* **47** (2011) 222
29. V. Rozman, I. Kalinovic, Z. Korunic, *J. Stored Prod. Res.* **43** (2007) 349.

Journal of the Serbian Chemical Society

Synthesis, characterization and cytotoxicity of a palladium(II) complex of 3-[(2-hydroxybenzylidene)amino]-2-thioxo-imidazolidin-4-one

BILJANA ŠMIT[1*#], RADOSLAV Z. PAVLOVIĆ[1], ANA RADOSAVLJEVIĆ-
-MIHAILOVIĆ[2], ANJA DOŠEN[2], MILENA G. ĆURČIĆ[1], DRAGANA S. ŠEKLIĆ[1]
and MARKO N. ŽIVANOVIĆ[1]

[1]*Faculty of Science, University of Kragujevac, Radoja Domanovića 12, P. O. Box 60,
34000 Kragujevac, Serbia and* [2]*Vinča Institute of Nuclear Sciences,
P. O. Box 522, 11001 Belgrade, Serbia*

Abstract: The polydentate ligand 3-[(2-hydroxybenzylidene)amino]-2-thioxo-imidazolidin-4-one was synthesized in the intermolecular cyclocondensation reaction of 2-hydroxybenzaldehyde thiosemicarbazone and ethyl chloroacetate. A novel palladium(II) complex was obtained from *cis*-[Pd(DMSO)$_2$Cl$_2$] by nucleophilic substitution of both DMSO ligands with the iminic nitrogen and the thiolactamic sulfur from the ligand. The structures of the compounds were characterized based on their spectral data. The cytotoxic activities of the ligand and the palladium(II) complex were studied on the tumor cell lines: human colon carcinoma HCT-116 and SW-480 cells using the MTT viability test. The results showed that the investigated palladium(II) complex had a significantly greater cytotoxic effect compared to that of the ligand.

Keywords: thiohydantoins; palladium(II) complexes; cytotoxic activity.

INTRODUCTION

Thiohydantoins are sulfur analogs of hydantoins with one or both carbonyl group(s) replaced by a thiocarbonyl group.[1–5] Among the known thiohydantoins, 2-thiohydantoins (2-thioxoimidazolidin-4-ones) are the most well known due to their wide applications as intermediates and reagents as well as therapeutics, herbicides and fungicides. They are traditionally considered as useful intermediates in peptide synthesis and structure determination.[6] 2-Thiohydantoins are also used for other purposes, including textile printing,[7] as catalysts for polymerizations,[8] in the production of resins and plastics[9] and as qualitative reagents for the detec-

tion of some metal ions upon complexation.[10] Thiohydantoins and their derivatives exist in many natural products.[11–13] In the past decades, great efforts have been devoted to introducing thiohydantoins and their derivatives into desirable substrates, such as pharmacophores and synthetic intermediates.[14–17] Compounds containing the thiohydantoin structural motif have been identified to display a wide range of biological activities. For example, many of them exhibit anticonvulsant,[18] anti-epileptic,[19] antimicrobial,[20] antiviral,[21] antineoplastic,[22] hypolipidemic,[23] antithrombotic,[24] and potential antitumor activities,[25,26] *etc*. Several derivatives are employed either as established drugs in clinical practice[2] or as fungicides and herbicides in agriculture.[27]

It is known[28] that coordination of these compounds with transition metal ions sometimes enhances their antiviral and antitumor activities. 2-Thiohydantoin molecules contain a thioamide fragment and can undergo thione–thiol tautomerism,[29] due to which they can be coordinated to metal ions through the lone electron pairs of the nitrogen or sulfur atoms, or both. Coordination with some transition metals was previously studied.[30–35]. The resulting complexes can contain 2-thiohydantoins as either neutral ligands or monoanions, which are formed upon deprotonation of the N–H group.[36–40] Most of the resulting complexes contain four-membered metalla-cycles.

Thiohydantoin molecules containing substituents with an additional donor atom can form chelate[40–43] or supramolecular[44] complexes in which the metal atom is coordinated by one or two thiohydantoin ligands in the neutral or deprotonated form.

The synthesis of coordination compounds that incorporate the thiohydantoin nucleus could have significant impact in the field of drug design and drug delivery.

In this paper, the synthesis and spectroscopic characterization of a palladium(II) complex of 3-[(2-hydroxybenzylidene)amino]-2-thioxoimidazolidin-4--one is described. The cytotoxic activities of the ligand and its palladium(II) complex were studied on two tumor cell lines of human colon carcinoma using the MTT viability test.

<div align="center">EXPERIMENTAL</div>

Starting materials

All chemicals were purchased from commercial sources (Sigma-Aldrich, Fluka or Centrohem) and were used without further purification. Solvents were purified and dried by standard methods. Dimethyl sulfoxide (DMSO) and 3-[4,5-dimethylthiazol-2-yl]-2,5-diphenyltetrazolium bromide (MTT) were obtained from Serva, Germany. Dublecco's modified Eagle medium (DMEM) was obtained from Gibco Invitrogen. Fetal bovine serum (FBS) and trypsin–EDTA were obtained from PAA-The cell culture company, Austria.

Cis-[Pd(DMSO)$_2$Cl$_2$][45] and 2-hydroxybenzaldehyde thiosemicarbazone[46] **1** were synthesized according to literature methods.

Instrumentations

The elemental analyses were performed by standard micro-methods using an Elemental Vario ELIII CHNSO analyzer.

The IR spectra were recorded on a Perkin-Elmer FTIR spectrometer, model Spectrum One.

The ^{1}H- and ^{13}C-NMR spectra were recorded on a Varian Gemini 2000 spectrometer at 200 and 50 MHz, respectively, in DMSO-d_6 solution using TMS as internal standard. D_2O exchange was applied to confirm the assignment of the nitrogen- and oxygen-bound protons.

The UV–Vis spectra were recorded on a Perkin-Elmer Lambda 35 double beam spectrophotometer in 1.00 cm quartz Suprasil cells.

The X-ray powder diffraction (XRPD) patterns were obtained on a Philips PW 1710 automated X-ray powder diffractometer using a Cu tube operated at 40 kV and 35 mA. The instrument was equipped with a diffracted beam curved graphite monochromator and a Xe-filled proportional counter. The diffractometer was calibrated with a silicon standard sample. For the Rietveld profile fitting method, the diffraction data were collected using the step-scanning mode in the 2θ range between 4 and 130° with 0.02° steps. The counting time was fixed to 5 s per step. The collected data were refined using FullProff software.

Ligand synthesis

The procedure for preparation of 3-[(2-hydroxybenzylidene)amino]-2-thioxoimidazo-lidin-4-one **2** was analogous to that described previously.[46] A mixture of 5.100 g **1** (26.15 mmol) and 3.204 g ethyl chloroacetate (26.15 mmol) in absolute methanol (150 cm³) in the presence of 6.433 g fused sodium acetate (78.45 mmol) was heated under reflux for 6 h. The reaction mixture was cooled and poured into water. The precipitate was separated by filtration, washed with cold water and dried. The crude product was recrystallized from hot methanol. Yield: 4.548 g.

Complex synthesis

The synthesis of palladium(II) complex with 3-[(2-hydroxybenzylidene)amino]-2-thio-xoimidazolidin-4-one **3** was achieved by dissolving 0.178 g **2** (0.76 mmol) in 10 cm³ of absolute methanol under reflux until dissolution and then adding 10 cm³ of a methanolic solution of Pd(DMSO)$_2$Cl$_2$ (0.252 g, 0.76 mmol) in three portions. Reaction mixture was heated under reflux for 12 h, cooled to 0 °C and the resulting orange–red precipitate was separated by filtration, washed with hot water, small amount of hot methanol and dried. The complex was recrystallized from hot methanol. Yield: 0.180 g.

Antiproliferative assay

Tumor cell lines were obtained from the American Type Culture Collection. The cells were maintained in DMEM supplemented with 10 % FBS, with 100 units mL^{-1} penicillin and 100 µg mL^{-1} streptomycin. The cells were cultured in a humidified atmosphere with 5 % CO$_2$ at 37 °C. The cells were grown in 75 cm² culture bottles supplied with 15 mL DMEM, and after a few passages, the cells were plated in a 96-multiwell plate (10⁴ cells well^{-1}). All studies were realized with cells at 70 to 80 % confluence. After 24 h of incubation of the cells, the medium was replaced with 100 µL medium containing various doses of **2** and **3** (0.1, 1, 10, 50, 100 and 500 µM) for 24 and 72 h. Untreated cells served as the control. After 24 and 72 h of treatment, the cell viability was determined by the MTT assay.[47] The proliferation test is based on the color reaction of mitochondrial dehydrogenase in living cells with MTT. At the end of the treatment period, MTT (final concentration 5 mg mL^{-1} PBS) was added to each well, which was then incubated at 37 °C in 5 % CO$_2$ atmosphere for 2–4 h. The colored crys-

tals of the produced formazan were dissolved in 150 μL DMSO. The absorbance was measured at 570 nm on Microplate Reader (Elisa 2100C). Cell proliferation was calculated as the ratio of the absorbance of the treated group divided by the absorbance of the control group, multiplied by 100 to give the percentage proliferation.

Biological activity was the result of one individual experiment, performed in triplicate for each dose. The magnitude of correlation between the variables was determined using an SPSS (Chicago, IL) statistical software package (SPSS for Windows, ver. 17, 2008). The effect of each extract are expressed by IC_{50} (inhibitory dose which inhibits 50 % of cell growth) and by the magnitude of maximal effect in exposed cells. The IC_{50} values were calculated from the dose curves using the CalcuSyn computer program.

RESULTS AND DISCUSSION

The polydentate ligand, 3-[(2-hydroxybenzylidene)amino]-2-thioxoimidazolidin-4-one **2**, was obtained by intermolecular cyclocondesation reaction of 2-hydroxybenzaldehyde thiosemicarbazone and ethyl chloroacetate (Scheme 1).[46]

Yield: 74.0 %. Anal. Calcd. for $C_{10}H_9N_3O_2S$: C, 51.05; H, 3.86; N, 17.86 %. Found: C, 51.08; H, 3.88; N, 17.89 %; IR (KBr, cm^{-1}): 3443 (O–H), 3318 (NH), 3173, 3031 (CH Ar), 2987, 2808 (CH$_2$), 1721 (C=O), 1616 (C=N), 1604, 1538, 1490 (C=C Ar), 1464, 1368, 1282, 1266 (C=S), 1202 (C–O), 1112, 1062, 949, 830, 753 (δ CH Ar), 627; ^{1}H-NMR (DMSO-d_6, δ / ppm): 3.97 (2H, s, CH$_2$), 6.94 (2H, m, H1–, H2–Ar), 7.30 (1H, dt, J = 7.8 and 1.8 Hz, H3–Ar), 7.75 (1H, dd, J = 8.0 and 1.9 Hz, H4–Ar), 8.64 (1H, s CH=N), 10.88 (1H, s OH), 12.06 (1H, bs NH); ^{13}C-NMR (50 MHz, DMSO-d_6, δ / ppm = 33.53 (CH$_2$), 116.51, 118.63, 119.69, 130.76, 132.34, 156.60 (Ar), 158.19 (C=N), 174.04 (C=O), 177.94 (C=S); UV–Vis (DMSO, λ_{max} / nm): 305.91, 338.97, 351.14.

The novel palladium(II) complex **3** was obtained by nucleophilic substitution of both DMSO ligands from *cis*-[Pd(DMSO)$_2$Cl$_2$] with the iminic nitrogen and thiolactamic sulfur from ligand **2** (Scheme 2). A non-charged complex was isolated as an orange–red amorphous precipitate. The metal complex was non-hygroscopic, soluble in DMSO, sparingly soluble in methanol and ethanol and insoluble in water. The analytical data revealed 1:1 (metal:ligand) stoichiometry. The structures of the ligand and complex were established by its elemental composition and IR, NMR and electronic spectra.

Yield: 57.7 %. Anal. Calcd. for $C_{10}H_9Cl_2N_3O_2PdS$: C, 29.11; H, 2.22; N, 10.18 %. Found: C, 29.08; H, 2.18; N, 10.16 %; IR (KBr, cm^{-1}) 3436 (O–H), 3153 (NH), 2925 (CH$_2$), 2853, 1719 (C=O), 1602 (C=N), 1533, 1400, 1385, 1332 (C=S), 1254, 1201 (C–O), 1154, 755 (δ CH Ar); ^{1}H-NMR (DMSO-d_6, δ / ppm): 3.16 (2H, s CH$_2$), 6.64 (1H, t, J = 7.0 Hz, H2–Ar), 6.93 (1H, d, J = 8.0 Hz, H1–Ar), 7.29 (1H, dt, J = 8.6 and 1.9 Hz, H3–Ar), 7.48 (1H, dd, J = 7.6 and 1.9 Hz, H4–Ar), 8.10 (1H, s CH=N), 9.78 (1H, s OH), 10.89 (1H, bs NH). ^{13}C-NMR (50 MHz, DMSO-d_6, δ / ppm) 48.77 (CH$_2$), 115.32, 118.12, 119.67, 133.47, 134.26, 148.71 (Ar), 161.31 (C=N), 169.91 (C=O), 193.26 (C=S). UV–Vis (DMSO, λ_{max} / nm): 259.25, 304.72, 340.39, 403.33.
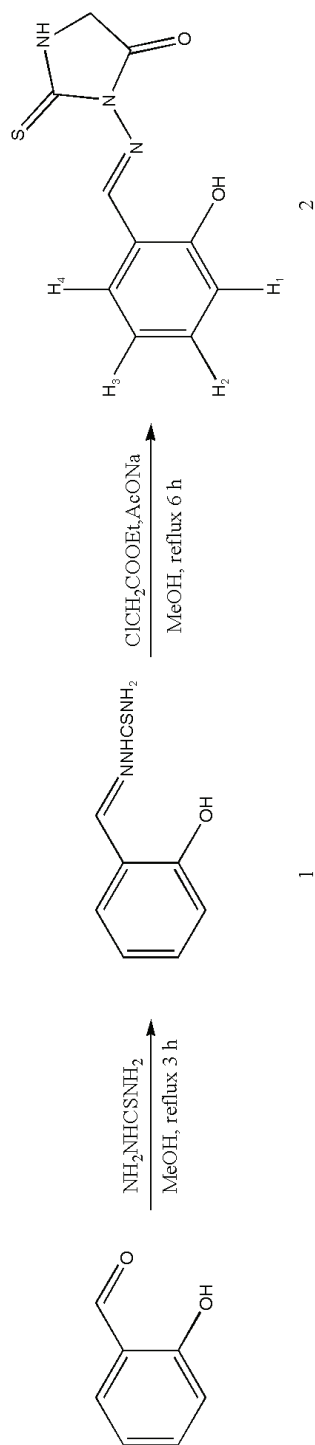
Scheme 1. Synthesis of 3-[(2-hydroxybenzylidene)amino]-2-thioxoimidazolidin-4-one **2**.
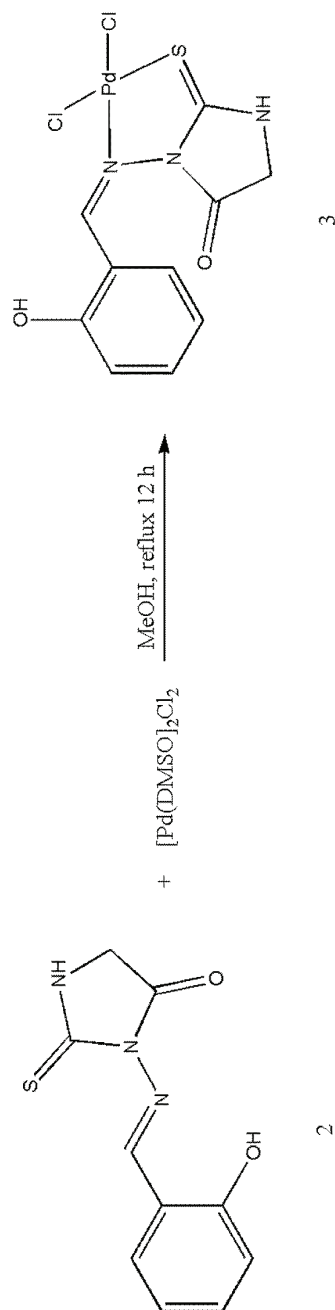
Scheme 2. Synthesis of the palladium(II) complex with 3-[(2-hydroxybenzylidene)amino]-2-thioxoimidazolidin-4-one **3**.

Spectroscopic characterization

In order to confirm complex formation and gain insight into the structure of obtained compounds, the IR spectra of the free ligand and its complex were recorded. The absence of the strong band at ≈ 2500 cm^{-1}, assignable to the ν(S–H) mode, indicate that both compounds exist in the thiono (C=S) form in the solid state. Comparison of vibrational frequencies of the free ligand with those of the complex showed a shift in the C=S band to a higher frequency by 66 cm^{-1}. This is evidence that the thionic sulfur atom was involved in the coordination.[32,48] In addition, the C=N absorption band was shifted to a lower frequency by 14 cm^{-1}. Consequently, the iminic nitrogen atom is also presumably involved in the co-ordination.[49] The non-coordination of O is shown by the C=O band shifting only very slightly upon complexation. The broad band observed in region 3153 cm^{-1} due to N–H stretch was shifted in complex, probably because of an adjustment in the current arising due to coordination of the thionic sulfur.

Further evidence for the coordinating mode of the thiohydantoin **2** was obtained from the NMR spectra in DMSO-d_6. In the ^{1}H-NMR spectrum of the ligand, there is no resonance at *ca*. 4.0 ppm, attributed to the resonance of the –SH proton, while the appearance of a broad peak at 12.06 ppm due to the –NH proton indicates that even in a polar solvent such as DMSO, it remains in the thione form. Such a large chemical shift for an –NH proton was already reported for similar systems.[50] Various types of primary and secondary hydrogen bond interactions are possible in the studied system. The phenolic H-atom could form an intramolecular hydrogen bond with the iminic nitrogen and additionally, as donating bifurcated, with the carbonyl group (Fig. 1). This proposal was confirmed experimentally by recording the ^{1}H-NMR spectrum of ligand **2** in the presence of NaOH. Upon transformation of the ligand into the phenolate form, the OH proton at 10.88 ppm disappeared while the other protons shift upfield (the –NH proton shifted from 12.06 to 10.98 ppm, Fig. 2.) This fact also could explain the upfield shifts of the corresponding signals in complex **3**. It seems that coordination prevented the formation of an intramolecular hydrogen bond because after complexation, iminic nitrogen has no lone electron pair. The –NH proton signal of the thiohydantoin shifted upfield and appeared at 10.89 ppm in complex **3**. The up-
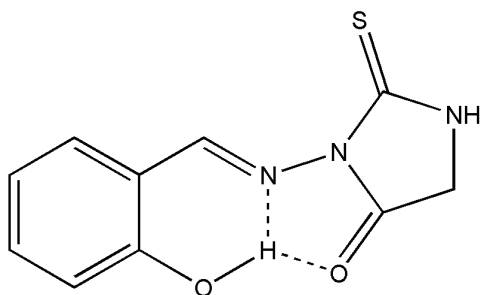

Fig. 1. Intramolecular hydrogen bond interaction in ligand **2**.

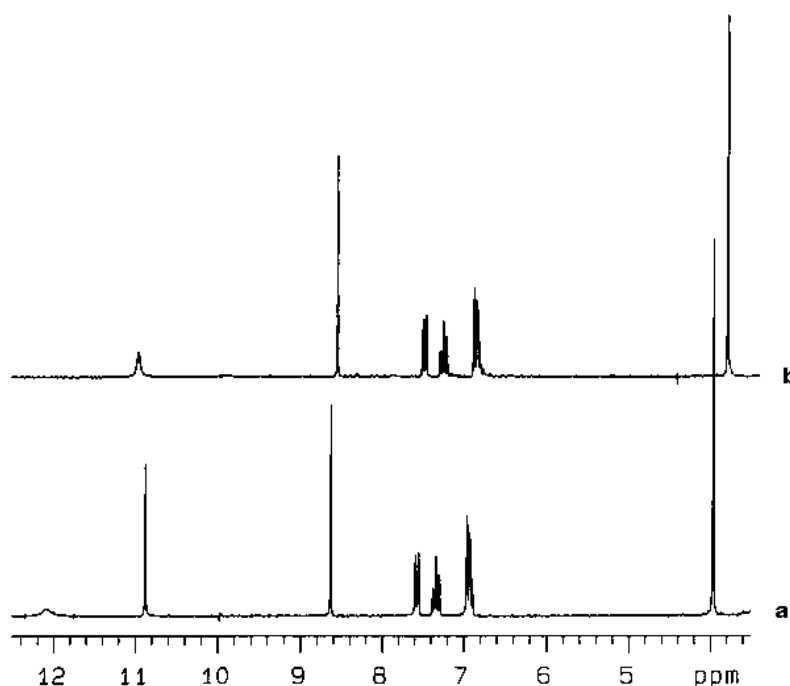field shift of the iminic proton signal by 0.54 ppm is clear evidence for coordination by the iminic nitrogen.

Fig. 2. ^{1}H-NMR spectra of ligand **2** (a) and ligand **2** after the addition of a small amount of solid NaOH (b).

The ^{13}C-NMR chemical shifts of the C=S and C=N resonances reflected the involvement of the sulfur from the thiohydantoin ring and the iminic nitrogen in an intermolecular interaction.

Based on foregoing discussion, the ligand behaves as a neutral NS-bidentate coordinative agent towards the palladium(II) ion.

In the electronic spectra, two intense absorption bands were exhibited at 305.91 and 351.14 nm for the ligand and at 304.72 and 403.33 nm for the complex. Three d–d spin allowed singlet–singlet and three spin forbidden singlet–triplet transitions are predicted for square-planar complexes of palladium(II). However, strong charge-transfer transitions may interfere and prevent the observation of some of the expected bands, especially for complexes containing sulfur donor atoms.[51] The prominent strong band at 403.33 nm was assigned to a combination of intraligand and ligand to metal charge transfer absorptions and d–d bands, which supports the idea of a square-planar environment for the metal ion.

In the XRPD pattern of the ligand **2**, low intensity and fairly broad peaks showed the poor crystallinity of the substance. The low intensities, poorly de-

fined peaks on the XRPD pattern of complex **3** demonstrated its low degree of crystallinity. The broad hump around 10° 2θ indicates the existence of an amorphous phase and might represent extremely poor or partial crystallinity of complex **3**. The existence of an amorphous hump between 6 and 15° 2θ in the pattern of complex **3** is obvious in comparison with the ligand **2**. In addition, there is no clear phase transition, but the metal–ligand complex disrupted the structure, causing the poor crystallinity demonstrated in the diffraction pattern.

Due to the poor solubility of the isolated complex in suitable solvents, no single crystal of sufficient quality could be obtained. Therefore, attention was focused on spectroscopic methods for the structural characterization of complex **3**, which suggested coordination of the ligand to palladium *via* the iminic nitrogen and the thionic sulfur (Scheme 2).

Antiproliferative activity

After seeding in standard DMEM medium, the cells were exposed to different concentrations of ligand **2** and complex **3** for 24 and 72 h at 37 °C. The results obtained with the antiproliferative assays are represented through IC_{50} values (Table I).

Comparing the cytotoxic effect of the complex and ligand, a significant difference was observed. Namely, while the complex exerted extreme cytotoxicity with IC_{50} values for 72-h treatment of 6.51 and 8.89 µM for HCT-116 and SW-480 cell lines respectively (Table I), the ligand did not show a considerable cytotoxic effect, even though decreased cell viability was generated with increasing ligand concentration.

TABLE I. Growth inhibitory effects – IC_{50} values (µM) of the Pd(II) complex and its ligand on HCT-116 and SW-480 cell lines after 24 and 72 h of treatment

Compound	HCT-116		SW-480	
	24 h	72 h	24 h	72 h
Pd(II) complex	16.98±0.21	6.51±0.02	15.73±0.25	8.89±0.36
Ligand	336.75±2.20	>500	>500	366.00±2.55
Cisplatin	293.52±2.36	58.55±1.23	325.19±2.35	49.58±1.54

Complex **3** exerted very high cytotoxic activity, *i.e.*, with increasing complex concentration, the cytotoxicity increased. A statistically significant difference in cytotoxicity after 24 h of treatment was noticed compared to that after 72 h of treatment. Interestingly, studying the complex activity it was shown that sensitivity of investigated cell lines are of similar extent.

Considering the cytotoxicity of the ligand, it was noticed from the IC_{50} values (Table I) and from the measured absorbances that the cytotoxicity increased with increasing applied concentration of the ligand. It was shown that the SW-480 cells exhibited greater sensitivity to the ligand 72 h after treatment (IC_{50} =

366 µM) compared to after 24 h (> 500 µM). Interestingly, the HCT-116 cells show exactly the opposite trend, *i.e*., a greater cytotoxic effect was observed 24 h (IC_{50} = 337 µM) after treatment compared to after 72 h (> 500 µM). This was probably due to the acute effect of the investigated ligand on the SW-480 cells. Although the cytotoxicity of the ligand was quantified and statistically processed, it is important to notice that this cytotoxic effect was certainly not significant, especially in comparison with the activity of the complex.

The results show that the investigated complex had a significantly greater cytotoxicity compared to that of cisplatin and further opened up the possibility for the synthesis of similar complexes of palladium(II).

CONCLUSIONS

A novel palladium(II) complex was synthesized by substitution reaction of *cis*-[Pd(DMSO)$_2$Cl$_2$] with a 2-thiohydantoin type ligand. Based on spectral data, it is proposed that 3-[(2-hydroxybenzylidene)amino]-2-thioxoimidazolidin-4-one acts as a bidentate ligand, making use of the thiolactamic sulfur and iminic nitrogen for coordination to the central metal ion. The cytotoxicity of this complex was investigated on two independent colon cancer cell lines (HCT-116 and SW-480) using the MTT viability test. The complex exhibited very high cytotoxic activity and showed a cytotoxic effect that was much better than that of the ligand. The observed cytotoxicity could be pursued to obtain a potential chemotherapeutic drug.

И З В О Д

СИНТЕЗА, КАРАКТЕРИЗАЦИЈА И ЦИТОТОКСИЧНОСТ ПАЛАДИЈУМ(II) КОМПЛЕКСА СА 3-[(2-ХИДРОКСИБЕНЗИЛИДЕН)АМИНО]-2-ТИОКСОИМИДАЗОЛИДИН-4-ОНОМ

БИЉАНА ШМИТ[1], РАДОСЛАВ З. ПАВЛОВИЋ[1], АНА РАДОСАВЉЕВИЋ-МИХАИЛОВИЋ[2], АЊА ДОШЕН[2], МИЛЕНА Г. ЂУРЧИЋ[1], ДРАГАНА С. ШЕКЛИЋ[1] и МАРКО Н. ЖИВАНОВИЋ[1]

[1]Природно–математички факултет, Универзитет у Крагујевцу, Радоја Домановића 12, п. пр. 60, 34000 Крагујевац и [2]Институт за нуклеарне науке Винча, п. пр. 522, 11001 Београд

Полидентатни лиганд, 3-[(2-хидроксибензилиден)амино]-2-тиоксоимидазолидин-4-он синтетисан је интермолекулском циклокондензацијом 2-хидроксибензалдехидтио-семикарбазона и етил-хлороацетата. Нов паладијум(II) комплекс добијен је нуклео-филном супституцијом оба DMSO лиганда из *cis*-[Pd(DMSO)$_2$Cl$_2$] иминским азотом и тиолактамским сумпором из лиганда. Структуре једињења су окарактерисане на основу њихових спектралних података. Цитотоксична активност лиганда и паладијум(II) ком-плекса испитивана је на туморским ћелијским линијама: хуманог карцинома колона HCT-116 и SW-480 помоћу MTT теста вијабилности. Испитивани паладијум(II) ком-плекс испољава веома висок цитотоксични ефекат, много бољи од лиганда.

(Примљено 25. маја, ревидирано 21. децембра 2012)

REFERENCES

1. T. B. Johnson, L. H. Chernoff, *J. Am. Chem. Soc.* **35** (1913) 1208
2. C. A. López, G. G. Trigo, *Adv. Heterocycl. Chem.* **38** (1985) 177
3. E. Ware, *Chem. Rev.* **46** (1950) 403
4. M. A. Metwally, E. Abdel-Latif, *J. Sulfur Chem.* **33** (2012) 229
5. K. M. Thakar, D. J. Paghdar, P. T. Chovatia, H. S. Joshi, *J. Serb. Chem. Soc.* **70** (2005) 807
6. M. Bodanszky, *Principles of Peptide Synthesis*, Springer-Verlag, Berlin, 1993, p. 95
7. Sociéte pour l'industrie chimique á Bâle, *British patent 330883* (1942)
8. W. D. Stewart, Goodrich Company, US patent *2430591* (1947)
9. H. V. Wood, W. O. Drake, Phillip Petroleum Company, US patent *3560470* (1971)
10. N. M. Turkevich, U. F. Gerlich, *Zh. Analit. Khim.* **11** (1956) 180
11. R. A. Davis, W. Aalbersberg, S. Meo, R. Moreira da Rocha, C. M. Ireland, *Tetrahedron* **58** (2002) 3263
12. L. Kandra, J. Remenyik, G. Batta, L. Somsák, G. Gyémánt, K. H. Park, *Carbohydr. Res.* **340** (2005) 1311
13. N. Roué, J. Bergman, *Tetrahedron* **55** (1999) 14729
14. W. G. Chang, M. V. Kulkarni, C. M. Sun, *J. Comb. Chem.* **8** (2006) 141
15. J. Fuentes, B. A. B. Salameh, M. A. Pradera, F. J. F. Córdoba, C. Gash, *Tetrahedron* **62** (2006) 97
16. E. K. Beloglazkina, A. G. Majouga, R. B. Romashkina, N. B. V. Zyk, *Tetrahedron Lett.* **47** (2006) 2957
17. M. J. Lin, C. M. Sun, *Tetrahedron Lett.* **44** (2003) 8739
18. V. Chazeau, M. Cossac, A. Boucherle, *Eur. J. Med. Chem.* **27** (1992) 615
19. K. Kiec-Kononowich, J. Karolak-Wojciechowska, *Phosphorus Sulfur* **73** (1992) 235
20. G. Lacroix, J.-P. Bascou, J. Perez, A. Gardas, Noranda Mines Limited, US patent *5650519* (2000)
21. A. A. El-Barbary, A. I. Khodair, E. B. Pedersen, C. Nielsen, *J. Med. Chem.* **37** (1994) 73
22. G. W. Peng, V. E. Marquez, J. S. Driscroll, *J. Med. Chem.* **18** (1975) 846
23. J. E. Tompkins, *J. Med. Chem.* **29** (1986) 855
24. D. Kushev, G. Gorneva, V. Enchev, E. Naydenova, J. Popova, S. Taxirov, L. Maneva, K. Grancharov, N. Spassovska, *J. Inorg. Biochem.* **89** (2002) 203
25. A. M. Al-Obaid, H. I. El-Subbagh, A. I. Khodair, M. M. A. Elmazar, *Anti-Cancer Drugs* **7** (1996) 873
26. S. Suzen, E. Buyukbingol, *Farmaco* **55** (2000) 246
27. J. Marton, J. Enisz, S. Hosztafi, T. Timár, *J. Agric. Food. Chem*. **41** (1993) 148
28. J. A. Grim, H. G. Petring, *Cancer Res.* **27** (1967) 1278
29. J. S. Casas, E. E. Castellano, A. Macfas, N. Playa, A. Sanchez, J. Sordo, J. M. Varela, *Polyhedron* **20** (2001) 1845
30. F. A. Nour El-Dien, M. A. Abdel-Aziz, M. A. Zayed, *Thermochim. Acta* **162** (1990) 399
31. M. A. Khalifa, A. M. A. Hassaan, *Sulfur Lett.* **17** (1994) 261
32. E. K. Beloglazkina, A. G. Majouga, I. V. Yudin, N. A. Frolova, N. V. Zyk, V. D. Dolzhikova, A. A. Moiseeva, R. D. Rakhimov, K. P. Butin, *Russ. Chem. Bull.* **55** (2006) 1015
33. A. Ahmedova, P. Marinova, G. Tyuliev, M. Mitewa, *Inorg. Chem. Commun*. **11** (2008) 545

34. S. S. Kandil, G. B. El-Hefnawy, E. A. Baker, *Thermochim. Acta* **414** (2004) 105
35. A. Ahmedova, P. Marinova, K. Paradowska, M. Marinov, I. Wawer, *Polyhedron* **29** (2010) 1639
36. M. Arca, F. Demartin, F. Davillanova, A. Garau, F. Isaia, V. Lippolis, *Inorg. Chem.* **37** (1998) 4164
37. A. M. A. Hassaan, *Sulfur Lett.* **13** (1991) 1
38. R. S. Srivastava, R. R. Srivastava, H. N. Bhargava, *Bull. Soc. Chim. Fr.* **128** (1991) 671
39. M. M. Chowdhry, D. M. Mingos, A. J. White, D. J. Williams, *J. Chem. Soc., Perkin Trans. 1* **20** (2001) 3495
40. J. S. Casas, E. E. Castellano, A. Macfas, N. Playa, A. Sanchez, J. Sordo, J. Zukerman--Schpector, *Inorg. Chim. Acta* **238** (1995) 129
41. J. S. Casas, A. Castineiras, N. Playa, A. Sanchez, J. Sordo, J. M. Varela, E. Vasquez-Lopez, *Polyhedron* **18** (1999) 3653
42. J. S. Casas, E. E. Castellano, M. D. Couce, N. Playa, A. Sanchez, J. Sordo, J. M. Varela, J. Zukerman-Schpector, *J. Coord. Chem.* **47** (1999) 299
43. M. M. Chowdhry, A. Burrows, D. M. Mingos, A. J. White, D. J. Williams, *J. Chem. Soc., Chem. Commun.* (1995) 1521
44. M. M. Chowdhry, D. M. Mingos, A. J. White, D. J. Williams, *J. Chem. Soc., Chem. Commun.* (1996) 899
45. J. H. Price, A. N. Williamson, R. F. Schramm, B. B. Wayland, *Inorg. Chem.* **116** (1972) 1280
46. M. E. Abd El-Fattah, A. H. Soliman, H. H. Abd Allah, in *Proceedings of the 14th International Electronic Conference on Synthetic Organic Chemistry (ECSOC-14)*, CD-ROM, MDPI, Basel, 2010, Abstract No. B024
47. T. Mosmann, *J. Immunol. Meth.* **65** (1983) 55
48. A. Ahmedova, P. Marinova, K. Paradowska, N. Stoyanov, I. Wawer, M. Mitewa, *Inorg. Chim. Acta* **363** (2010) 3919
49. X. Ran, L. Wang, D. Cao, Y. Lin, J. Hao, *App. Organometallic Chem.* **25** (2010) 9
50. J. S. Casas, N. Playa, A. Sanchez, J. Sordo, J. M. Varela, E. M. Vasquez-Lopez, *Polyhedron* **18** (1998) 187
51. A. I. Matesanz, J. M. Perez, P. Navarro, J. M. Moreno, E. Colacio, P. Souza, *J. Inorg. Biochem.* **76** (1999) 29.

Synthesis, characterization of thiosemicarbazone metal complexes and their antioxidant activity in different *in vitro* model systems

DESIREDDY HARIKISHORE KUMAR REDDY[1], SEUNG-MOK LEE[1]*,
KALLURU SESHAIAH[2] and K. RAMESH BABU[3]

[1]*Department of Environmental Engineering, Kwandong University, Gangneung, Republic of Korea,* [2] *Inorganic and Analytical Chemistry Division, Department of Chemistry, Sri Venkateswara University, Tirupati – 517 502, India and* [3] *Department of Biochemistry, Sri Venkateswara University, Tirupati – 517 502, India*

Abstract: The synthesis of bimetallic Cu(II), Co(II), Ni(II), Zn(II) and U(VI) complexes with general stoichiometry $[H_2L\ M(X_2)(H_2O)_2]$ (where H_2L is the di-deprotanated ligand and X is chloride/sulphate) were obtained with the ligand terephthaladehyde bis(thiosemicarbazone) (H_2L) and are discussed. The ligand and its binuclear complexes were characterized by micro analysis (CHNS), ^{1}H-NMR, FT-IR, UV-vis, TG-DTA and conductance measurements. The thermal behaviour of these complexes showed that the hydrated complexes loose water molecules of hydration in the first step, followed immediately by decomposition of the anions and ligand molecules in the subsequent steps. The molar conductance measurements of the complexes in DMF correspond to the non-electrolytic nature of the complexes. Furthermore, the antioxidant activity of the ligand and its complexes were determined *in vitro* by the hydroxyl radical scavenging, DPPH, NO and reducing power methods. The obtained IC_{50} value of the DPPH activity for complex **2** (IC_{50} = 0.254 M) was shown to be the best.

Keywords: thiosemicarbazone; transition metal complexes; spectral analysis; bimetallic complexes; antioxidant activity

INTRODUCTION

Thiosemicarbazones (TSCs) have become the subject of intense research interest with coordination chemists as they are simple to prepare, have excellent complexation ability with both transition and non-transition elements and the complexes have interesting structural characteristics and possible analytical applications. This interest and wide range of applications resulted in a large number

---

* Corresponding author. E-mail: leesm@kwandong.ac.kr

229

of papers and several reviews on TSCs.[1–4] In addition, TSCs have received considerable attention due to their broad profile of pharmacological activity, as they afford a diverse variety of compounds with different activities.[5,6] The mechanism of action of TSCs is due to their ability to inhibit DNA biosynthesis, possibly by blocking the enzyme ribonucleotide diphosphate reductase; binding to the nitrogen bases of DNA, hindering or blocking base replication, or creating lesions in the DNA strands by oxidative rupture.[7,8] The remarkable biological activities of TSCs have provided real impetus to drive developments in their coordination chemistry, which subsequently showed that the biological activity of TSCs is related to their metal complexing ability. In some cases, the highest activity of TSCs is associated with a metal atom, and the biological properties of TSCs are often related to their metal ion coordination. The lipophilicity, which controls the rate of entry of TSCs into the cell, is modified by coordination. Additionally, the metal complexes can be more active than the free ligands, and some of the side effects associated with free ligands may decrease upon complexation. In addition, the complexes may exhibit bioactivities which are not exerted by free ligands.[9] Studies related to new developments in metal-based drugs are both promising and of great interest in the development of therapeutic agents.[10,12]

Atherosclerosis and its associated complications are currently the major causes of cardiovascular morbidity and mortality worldwide. Elevated levels of cholesterol, especially low-density lipoprotein (LDL) and triglycerides, along with free radical oxidative stress are recognized as the leading causes of atherosclerosis and coronary heart disease. Hydroxyl radicals (OH$^\bullet$) are generated by the metal ions present in serum, and changes in their oxidation states result in oxidative damage of LDL and other lipoproteins in plasma, which is responsible for the initiation and progression of atherosclerosis in hyperlipidemic subjects.

Free radicals also interact with proteins in other normal metabolic processes, which can lead to many types of pathologic changes.[13–17] To protect biomolecules against the attack of free radicals and/or to suppress the resultant damage, numerous natural and synthetic free radical scavengers and antioxidants have been developed and studied[18,19] Among them, thiosemicarabazones and their metal complexes have been evaluated for their free radical scavenger activity.[20,21]

The synthesis and characterization of copper(II), cobalt(II) and nickel(II) complexes with terephthalaldehyde bis(thiosemicarbazone) was described by Minghao *et al.*[22] In addition, the coordination polymerization (polycoordination) of terephthalaldehyde bis(thiosemicarbazone) with mercury(II) and cadmium(II) complexes was studied by Marcu *et al.*[23] However, the biological activity of terephthalaldehyde bis(thiosemicarbazone)–metal complexes has not been reported. Given the potential biological activity of thiosemicarbazone and the involvement of metal ions in cell metabolism, a systematic study was undertaken to explore this chemistry, with the development of new biologically active pharmaceuticals

as the final goal. Herein, the preparation and spectroscopic characterization of five metal complexes derived from terepthaladehyde bis(thiosemicarbazone) are reported. The ligand and metal complexes were evaluated for their antioxidant activity. It was envisaged that the thiosemicarbazone could be useful in controlling metabolic disorders by scavenging free radicals.

EXPERIMENTAL

Physical measurements

Melting points were determined by the open capillary method and are uncorrected. The metal content of the complexes was estimated using standard methods. The analysis of CHNS/O contents of ligand and metal complexes were realized on a Euro elemental analyzer. The IR spectra were recorded as KBr pellets using a Perkin–Elmer Fourier-Transform Spectrum RX1 spectrophotometer in the region 4500–450 cm^{-1}. The TG/DTA curves for the complexes were recorded on a Nietzsche thermobalance (model-STA 40g) with a P_t V_s P_t 10 % Rh thermocouple under dynamic air conditions between room temperature (≈20 °C) and 1020 °C (gradient 10 K min^{-1}).

Synthesis of the ligand (1)

The synthesis of terepthaladehyde bis(thiosemicarbazone) (1) was based on the following method: an ethanolic solution (50 mL) of terepthaladehyde (0.2 g) and thiosemicarbazide (0.270 g) in an ethanol–water mixture (50 mL) were mixed and refluxed for 2 h. After cooling to room temperature, the formed yellow solid was isolated and dried under vacuum.

Synthesis of metal complexes (2–6)

In a representative preparation, the complexes were synthesized by refluxing DMF–ethanol (1:1, 20 mL) solution of ligand (5 mmol) with an ethanolic solution (20 mL) of corresponding metal salt (10 mmol) for 12 h at 70 °C. On cooling overnight, the collared complex precipitated out. The precipitate was filtered, washed with cold DMF–ethanol and dried under vacuum. The metal salts used in this study were $CuSO_4\cdot5H_2O$, $CoCl_2\cdot6H_2O$, $NiCl_2\cdot6H_2O$, $ZnSO_4\cdot7H_2O$ and $UO_2(CH_3COO)_2\cdot2H_2O$.

Antioxidant activity

The scavenging effects of compounds 2–6 on the DPPH radical were evaluated using the stable DPPH• as the reagent.[24] In the H_2O_2 scavenging activity experiments, the hydroxyl radical (OH•) in aqueous media was generated through the Fenton Reaction.[25] For determining the nitric oxide (NO) scavenging activity, the absorbance of the chromophore formed during diazotization of nitrite with sulphanilamide and subsequent N-naphthylethylenediamine dihydrochloride was measured at 546 nm.[26,27] The reducing power of the synthesized compounds was determined according to the method of Oyaizu.[28]

RESULTS AND DISCUSSION

Terepthaladehyde was treated with thiosemicarbazide in refluxing methanol to afford terepthaladehyde bis(thiosemicarbazone) (H_2L). The synthetic route to the ligand is shown in Scheme 1. The synthesized ligand was confirmed by ^{1}H--NMR spectra recorded in d_6-dimethylsulphoxide (DMSO-d_6) solution using tetramethylsilane (TMS) as an internal standard. The hydrazinic proton (–N^{2}H) of the free ligand appeared as a broad single peak at 11.46 ppm.[29] The amino group

($-N^1H_2$) showed a signal in the region 8.05 ppm. A singlet in the region 7.99––8.01 ppm was observed which was assigned to the azomethine proton ($-HC=N$). In the region 7.8 ppm, the signals were assigned to chemical shifts of hydrogens on the symmetric aromatic ring of the ligand. Further the metal complexes were prepared with the ligand as described in experimental section. All the synthesized complexes were binuclear with an M:L ratio of 2:1. The molar conductance values in DMF were in the expected range (17–24 S cm^2 mol^{-1}) of non-electrolytes, indicating bonding of chloride and sulphate anions to the metal ions.[30] The complexes were analyzed for carbon, hydrogen, nitrogen, oxygen, sulphur and metals. The analytical results are given in Table I, while the physical, UV/Vis and molar conductance data are listed in Table II. The metal complexes were stable under atmospheric conditions for extended periods, and were easily soluble in dimethylsulphoxide (DMSO) and *N,N*-dimethylformamide (DMF); however, they were insoluble in most common solvents. The composition and coordination geometry of these complexes were established based on the following experimental observations.

Scheme. 1 Synthesis of the ligand H$_2$L.

TABLE I. Analytical data of the compounds

Cmpd.	Molecular formula	FW	Elemental analysis, Calcd. (found), %					
			C	H	N	S	O	M
1	$C_{10}H_{12}N_6S_2$	280.4	42.84 (42.74)	4.31 (4.28)	29.97 (29.88)	22.87 (22.86)	–	–
2	$Cu_2C_{10}H_{14}N_6O_4S_5$	537.54	22.34 (22.01)	2.63 (2.34)	15.63 (15.17)	17.90 (17.24)	17.86 (17.25)	23.64 (23.25)
3	$Co_2C_{10}H_{14}Cl_2N_6O_2S_2$	503.16	23.87 (23.56)	2.80 (2.78)	16.70 (16.64)	12.75 (12.29)	6.36 (6.33)	23.43 (23.33)
4	$Ni_2C_{10}H_{14}Cl_2N_6O_2S_2$	499.87	23.89 (23.80)	2.81 (2.20)	14.11 (14.01)	12.76 (12.32)	6.37 (6.34)	23.35 (23.26)
5	$Zn_2 C_{10}H_{14}N_6O_4S_5$	541.27	22.19 (22.13)	2.61 (2.36)	15.53 (15.22)	17.77 (17.32)	17.74 (17.43)	24.17 (24.02)
6	$U_2C_{10}H_{18}N_6O_8S_2$	890.47	13.49 (13.41)	2.04 (2.01)	9.44 (9.47)	7.20 (7.56)	14.37 (14.22)	53.46 (53.54)

FT-IR spectra

The spectra of the free thiosemicarabzone ligand showed peaks of concern at 3395–3265 (two peaks), 3192 and 1593 cm^{-1}, attributed to the symmetric and asymmetric stretching of NH$_2$, ν(NH) and ν(C=N), respectively. Additionally, no

band due to an SH group was observed between 2600 and 2500 cm^{-1}, which is in agreement with the deprotonated thiolate form of the ligand in the complexes.[31] The strong absorption bands near 3480 and 3440 cm^{-1} in the IR spectra of both the ligand and the complexes were due to N–H stretching vibrations. The intense band at 1680 may be assigned to C=N stretching vibration in the free ligand. It showed a positive shift towards higher frequencies in the spectra of the metal complexes (an additional band was observed near 1700 cm^{-1}). The shifting of the band towards higher frequency region indicates an increase in bond order of the coordinated C=N group due to back donation of π-electrons by the metals. The spectrum of the ligand shows bands at 1358 and 1465 cm^{-1}, which were assigned to C=S and N–C–N stretching, respectively. These bands were shifted to higher values in the complexes, indicates coordination of a thiosemicarbazone to the metal centre. These bands were absent in the spectra of the complexes due to likely changes of C=S to C–S and N–C–N to N–C=N on complexation. It is evident that ligand acts as a binucleating chelating agent coordinating through the thiol sulphur and nitrogen of the (C=N) group of the Schiff base. The complexes also display bands due to coordinated water molecules. The bands in the ranges 749–849 cm^{-1} and 609–633 cm^{-1} appeared in the spectra of the complexes, which may be assigned to ρr(H$_2$O) and ρw(H$_2$O).[33]

TABLE II. Physical, UV/Vis and molar conductance data for the compounds

Cmpd.	Yield, %	Colour	M.p., °C	UV/Vis (DMF), λ / nm	Λ / S cm^2 mol^{-1}
1	92	Yellow	153–156	–	–
2	66	Dark blue	>280	224, 265, 363, 413	19
3	58	Brown	>280	242, 265, 366, 383	21
4	68	Green	>280	265, 366, 383	24
5	65	Black	>280	265, 383, 365	21
6	54	Yellow	>280	265, 382, 365	17

Electronic spectra

With aim to obtain information about the type of the electronic transition and interaction liable to exist in solutions, the electronic spectra of ligand and their complexes were measured in DMF solvent. The recorded spectra of ligand displayed two main absorption bands. The first band was observed in the 260−265 nm range as a broad and/or a shoulder band. This band could be ascribed to π–π* transitions of the benzenoid system of the compounds strongly overlapped with n–π* electronic transitions involving the nonbonding electrons of the azomethine nitrogen atom. The longer wavelength band(s) in the recorded spectra of the ligands observed in the range 316–355 nm can be ascribed to the transition within the whole molecule, essentially as intramolecular charge transfer (CT) interactions. The CT bands seem to originate from the aryl moiety, whereas the positive charged azomethine carbon atom was the acceptor centre. This behaviour sug-

gests an instantaneous complex formation in solution from the reaction of the ligand with each of the employed metal ions. Bands due to the n–π* transition of the C=N chromophores occurred between 260−265 nm as the ligand shifts to lower energy upon complexation.[33] In the ultraviolet region, the bands observed in the range 267–299 nm in spectra of metal complexes can be ascribed to an intraligand electronic transition, because bands in these regions were sensitive enough to the type of metal ion used.

The longer wavelength band(s) of the free ligand at 363–366 nm acquired a red shift on complex formation with a metal ion. A new band was observed at longer wavelengths (in the range of 382–413 nm) in case of the complex solutions. This behaviour can be explained as follows. The longer wavelength band observed in the spectrum of the free ligands can be assigned to an intramolecular CT transition liable to take place within the solute molecule. Thus the red shift observed in the λ_{max} of this band on complex formation with the divalent transition metal ions Mn(II), Co(II), Cu(II) and Zn(II) can be interpreted based on the principle of an expected easier CT transition within the complexed Schiff bases rather than within the free ligand. This is due to the positive charge of the coordinating metal ions. On the other hand, these bands strongly overlap with an intermolecular transition from the ligand molecule to the vacant orbitals localized on the coordinated metal ions, *i.e.*, LMCT.

Thermogravimetric analysis

Thermogravimetric (TG) and differential thermal (DTA) analyses were employed to describe the thermal behaviour of the prepared complexes **2**–**6.** The TG curve of complex **2** showed three mass loss steps. The first mass loss step occurred in the temperature range 160–300 °C, the second one in the temperature range 300–620 °C and the third step between 620–770 °C. The DTA curve showed two exothermic peaks, one at 290 °C and the other at 620 °C. The TG curve of complex **3** showed four mass loss steps. The first step occurred in the temperature range between 260–300 °C. In this temperature range, one small endo effect was observed at 280 °C. The second mass loss step occurred in the temperature range 300–580 °C. In this temperature range, two exothermic peaks were observed at 370 and 520 °C. The third mass loss step occurred in the temperature range 580––750 °C. The fourth decomposition step occurred between 750–880 °C. This range was accompanied by one small endo effect at 870 °C. The TG and DTA study for complex **4** presented two regions of decomposition. In the TG study, the first mass loss step occurred in the temperature range between 260 and 320 °C. In this temp range (260–320 °C), one endothermic peak at 270 °C was observed. The second mass loss step occurred in the temperature range 320–710 °C. In this temperature range, two exothermic peaks were observed, one at 360 °C and the other at 700 °C. The TG and DTA study for complex **5** showed a two-

-step decomposition. The first mass loss step occurred in the temperature range 270–530 °C, while the second decomposition step occurred between 530–650 °C. In the temperature range of the first stage of mass loss, one small endo and one small exo effect can be seen on the DTA curve at 280 and 370 °C, respectively. The second mass loss step was accompanied by two exo effects with maxima at 530 and 630 °C, respectively.

The thermal behaviour of these complexes showed that the hydrated complexes lost water molecules of hydration in the first step followed immediately by decomposition of the anions and ligand molecules in the subsequent steps. The final decomposition steps of the complexes are attributed to complete decomposition of the complexes leaving M residues (M = Cu, Co, Ni, Zn and U).

Antioxidant activities of the ligand and complexes

The antioxidant activities of terepthaladehyde bis(thiosemicarabzone) (**1**) and its metal complexes **2**–**6** were evaluated by several *in vitro* methods in order to compare the results and to establish some structure–antioxidant–activity relationships for each method. The evaluation study was performed at various concentrations and comparative studies were realised with standard antioxidants.

DPPH radical scavenging activity. The percentage activity of DMF solutions of compounds **1**–**6** were examined and compared. The activities of the complexes as a function of concentration are shown in Fig. 1. All the complexes **2**–**5**
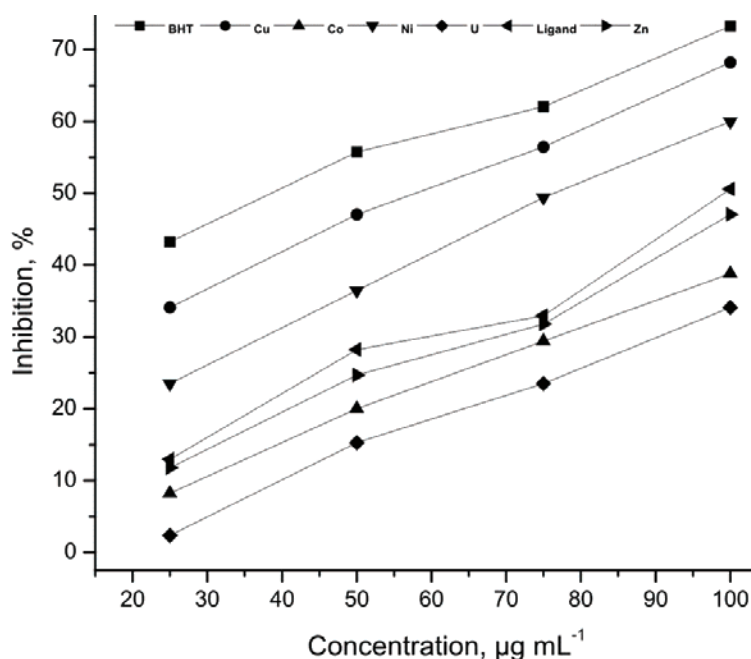

Fig. 1. Scavenging activity of compounds **1**–**6** for DPPH.

showed comparable or slightly lower activity than the standard, butylated hydroxytoluene (BHT). The copper complex **2**, containing an electron donating group showed the dominate DPPH scavenging activity. Nickel complex **3** exhibited slightly lower activity than that of compound **2**. At low concentrations, compound **6** showed negligible DPPH activity The IC_{50} values for all the compounds were calculated.

Reducing power. The reducing power of compounds **2**–**6** as a function of their concentration are shown in Fig. 2. The reducing power of the standard BHT at various concentrations showed a higher absorbance value to those of the newly synthesized compounds. The reducing power of newly synthesized compound solutions in DMF increased with increasing concentration. All the analogues **2**–**6** showed high absorbance values which were comparable or slightly lower than those of the standards. The presence of the lone pair electron in complex **2** resulted in a higher reducing power. The absorbance values for compound **6** were very low, showing the low reducing power of this complex, while compounds **2**–**5** showed higher values indicating their higher reducing power but lower than that of the standards.
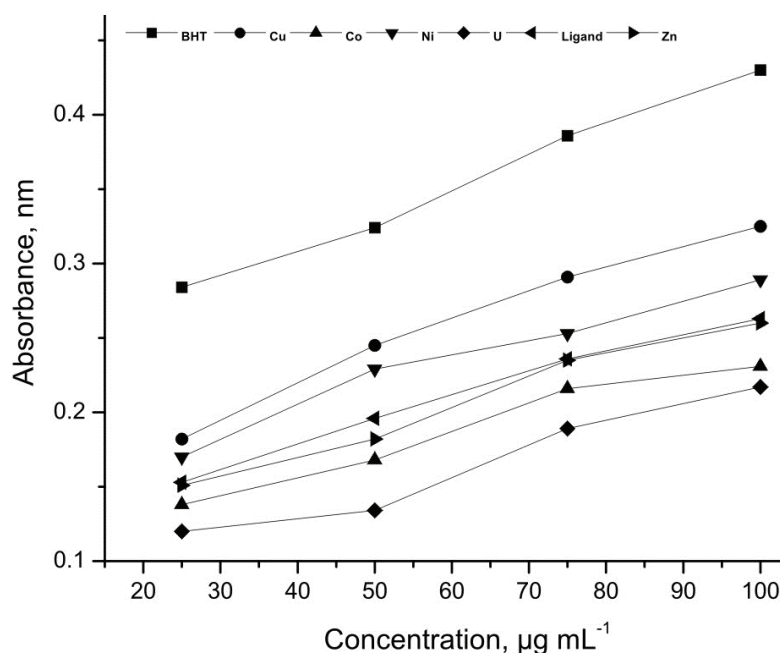

Fig. 2. Reducing power scavenging activity of compounds **1**–**6**.

H_2O_2 *scavenging activity*. The data of the suppression ratio for OH$^\bullet$ are shown in Fig. 3. The inhibitory effect of the compounds tested on OH$^\bullet$ were concentrate dependent and the suppression ratio increased with increasing sample

concentrations in the range tested. The average suppression ratio of the uranium complex (IC_{50} = 144.09 μM) for OH$^\bullet$ was the lowest of all the compounds. The copper(II) complex (IC_{50} = 66.72 μM) was the most effective among all the tested complexes. The order of the suppression ratio of the tested compounds for OH$^\bullet$ was **2** > **4** > **1** > **5** > **3** > **6**.
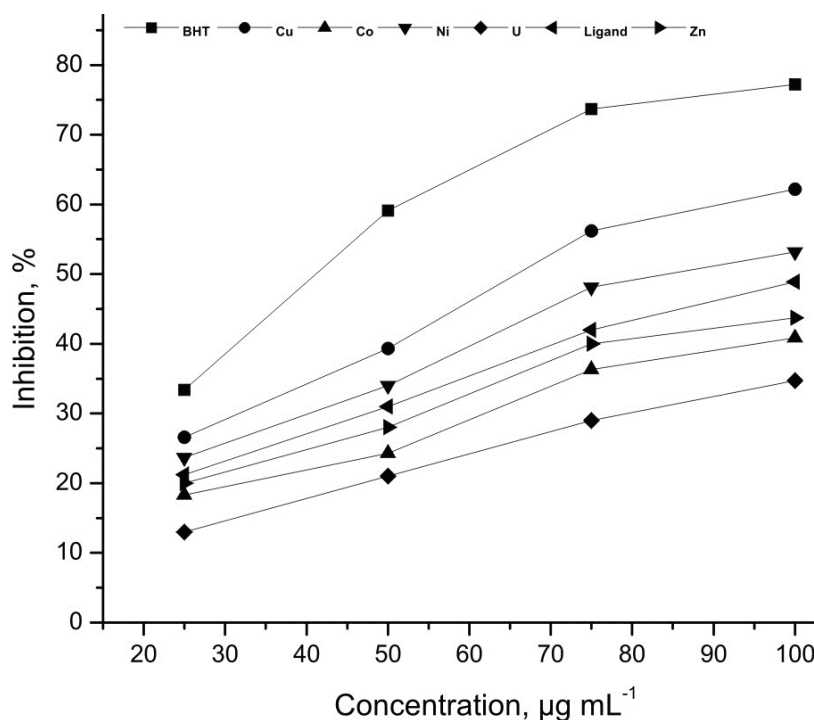

Fig. 3. Scavenging activity of compounds **1**–**6** for H$_2$O$_2$.

Nitric oxide (NO) scavenging activity. Nitric oxide undergoes a facile radical–radical reaction with O$_2^{\bullet-}$ to yield ONOO$^-$, a reaction that is three times faster than the SOD-catalyzed dismutation of O$_2^{\bullet-}$. This diversion of O$_2^{\bullet-}$ through ONOO$^-$ oxidation and decomposition pathways would also limit H$_2$O$_2$ accumulation and subsequent reactions of H$_2$O$_2$ by decreasing the amount of O$_2^{\bullet-}$ available for spontaneous or SOD-catalyzed dismutation. It was find that the inhibitory effects of the compounds tested on NO$^\bullet$ were concentration dependent and the suppression ratio increased with increasing sample concentrations in the range tested (Fig. 4). The average suppression ratio of the uranium complex (IC_{50} = 233.64 μM) for NO$^\bullet$ was the lowest of all the tested compounds. The copper(II) complex (IC_{50} = 134.87 μM) was the most effective among all the complexes. The order of the suppression ratio of the tested compounds for NO$^\bullet$ is **2** > **4** > **1** >**5** > **3** > **6**.
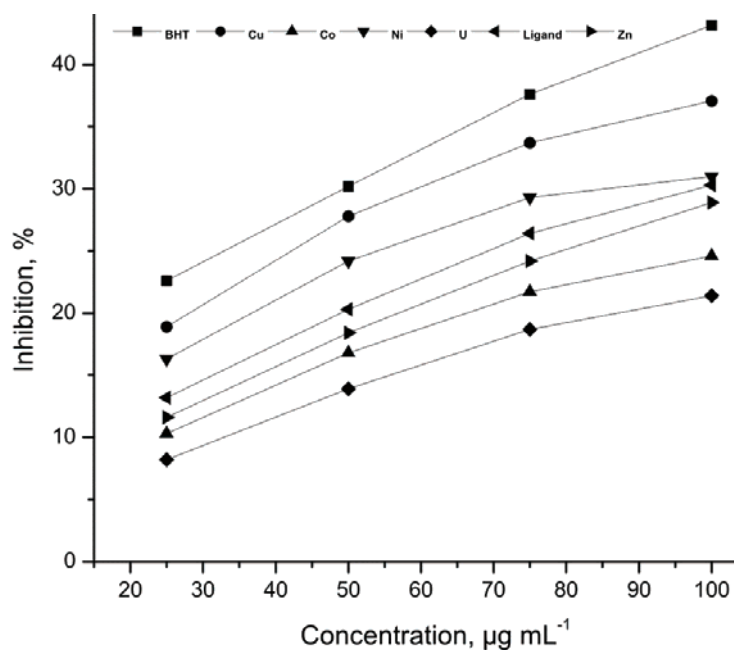
Fig. 4. Scavenging activity of compounds **1**–**6** for NO.

CONCLUSIONS

Based on the above results, the structures of metal complexes shown in Fig. 5 are proposed. The antioxidant properties of the ligand and complexes obtained were evaluated by several methods. Compounds **2**–**5** had enhanced antioxidant activities, which were comparable but slightly lower than that of the standard. The copper complex **2** revealed high DPPH scavenging, reducing power, H_2O_2 inhibition and nitrous oxide inhibition values. As a result, this study provides evidence that the chelation of different copper complexes with terepthaladehyde bis-(thiosemicarbazone) had significant influence on the antioxidant activities in different *in vitro* model systems.
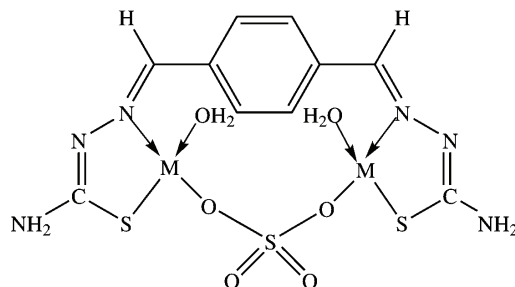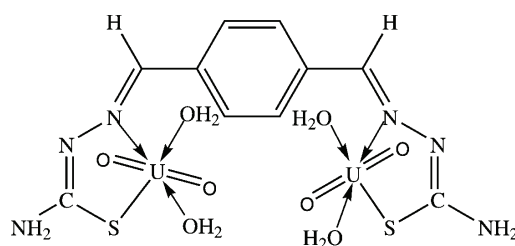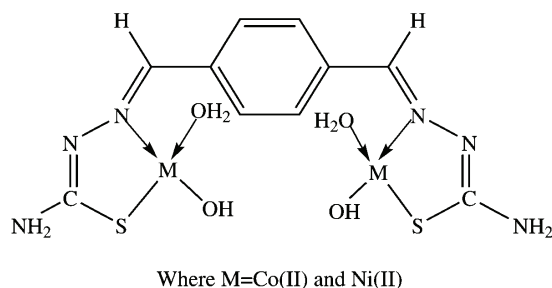

Where M=Cu(II) and Zn(II)

Where M=Co(II) and Ni(II)

Fig. 5. The proposed structure of metal complexes with H_2L ligand.

ИЗВОД

СИНТЕЗА, КАРАКТЕРИЗАЦИЈА КОМПЛЕКСА МЕТАЛА СА
ТИОСЕМИКАРБАЗОНСКИМ ЛИГАНДИМА И ЊИХОВА АНТИОКСИДАТИВНА
АКТИВНОСТ У РАЗЛИЧИТИМ *IN VITRO* УСЛОВИМА

DESIREDDY HARIKISHORE KUMAR REDDY[1], SEUNG-MOK LEE[1], KALLURU SESHAIAH[2] и K. RAMESH BABU[3]

[1]Department of Environmental Engineering, Kwandong University, Gangneung, Republic of Korea, [2]In-organic and analytical Chemistry Division, Department of Chemistry, Sri Venkateswara University, Tirupati – 517 502, India u [3]Department of Biochemistry, Sri Venkateswara University, Tirupati – 517 502, India

Полазећи од терефталалдехидbis(тиосемикарбазона) синтетисани су динуклеарни Cu(II), Co(II), Ni(II), Zn(II) и U(VI) комплекси опште формуле $[H_2LM(X_2)(H_2O)_2]$ (где је H_2L двоструко депротоновани лиганд и X је хлорид/сулфат). Лиганд (H_2L) и одговарајући комплекси су окарактерисани, поред термалне анализе и методе мерења проводљивости, применом ^{1}H-NMR, FT-IR и UV–Vis спектроскопских метода. Термална анализа ових комплекса је показала да, у првој фази, хидратисани комплекси губе молекуле воде, док у наредној фази долази до разлагања хлоридног и сулфатног анјона, као и молекула лиганда. На основу мерења моларне проводљивости у DMF растварачу закључено је да су испитивани комплекси неелектолити. Поред тога, одређена је *in vitro* антиоксидативна активност лиганда и одговарајућих комплекса.

(Примљено 30. априла, ревидирано 3. јула 2012)

REFERENCES

1. N. A. Mangalam, M. R. P. Kurup, *Spectrochem. Acta* **71** (2009) 2040
2. M. C. Rodríguez-Argüelles, E. C. López-Silva, J. Sanmartín, P. Pelagatti, F. Zani, *J. Inorg. Biochem.* **99** (2005) 2231

3. T. S. Lobana, R. Sharma, G. Bawa, S. Khanna, *Coord. Chem. Rev.* **253** (2009) 977
4. D. H. K. Reddy, K. Seshaiah, A. V. R. Reddy, *Orient. J. Chem.* **27** (2011) 1125
5. H. Beraldo, D. Gambino, *Mini Rev. Med. Chem.* **4** (2004) 159
6. A. G. Quiroga, C. N. Ranninger, *Coord. Chem. Rev*. **248** (2004) 119
7. K. C. Agrawal, A. C. Sartorelli, Prog. *Med. Chem.* **15** (1978) 321
8. M. C. Miller, C. N. Stineman, J. R. Vance, D. X. West, H. Hall, *Anticancer Res.* **18** (1998) 4131
9. S. Chandra, S. Raizada, T. Monika, K. S. Praveen, *Spectrochem. Acta* **69** (2008) 816
10. A. Saeed, A. A. Isab, S. Ali, A. R. Al-Arfaj, *Polyhedron* **25** (2006) 1633
11. R. J. Mauthe, E. Sideras-Haddad, K. W. Turteltaub, G. Bench, *J. Pharm. Biomed*. *Anal*. **17** (1998) 651
12. M. Navarro, G. Chiara, L. Messori, D. Gambino, *Drug Discov. Today* **15** (2010) 23
13. M. Valko, D. Leibfritz, J. Moncol, M. Cronin, M. Mazur, J. Telser, *Int. J. Biochem. Cell Biol.* **39** (2007) 44
14. N. Yusaku, S. Kunihiko, S. Katsumi, T. Daisuke, T. Teruhisa, N. Yoshimichi, *Biol. Chem*. **387** (2006) 373
15. S. Stohs, D. Bagchi, *Free Radical Bio. Med.* **18** (1995) 321
16. V. Marian, I. Mario, M. Milan, R. J. Christopher, T. Joshua, *Mol. Cell. Biochem*. **266** (2004) 37
17. H. Sies, *Exp. Physiol.* **82** (1997) 291
18. Y. Byun, D. Darby, K. Cooksey, P. Dawson, S. Whiteside, *Food Chem.* **124** (2011) 615
19. R. M. Wang, J. J. Mao, J. F. Song, C. X. Huo, Y. F. He, *Chin. Chem. Lett.* **18** (2007) 1416
20. D. S. Raja, N. S. P. Bhuvanesh, K. Natarajan, *Eur. J. Med. Chem.* **46** (2011) 4584
21. P. Mariana, D. Bruno, T. Jeanette, B. Lucia, G. Mercedes, C. Hugo, O. A. Claudio, N. Ester, G. Dinorah, O. Lucia, *Eur. J. Med. Chem.* **44** (2009) 4937
22. S. Minghao, W. Di, W. Jingyuan, L. Yaoxian. *Polym. Prepr. (Am. Chem. Soc., Div. Polym. Chem.)* **44** (2003) 751
23. M. M. Marcu, M. Dima, *Rev. Roum. Chim*. **12** (1967) 1353.
24. M. Burits, F. Bucar, *Phytother. Res*. **14** (2000) 323
25. R. J. Ruch, S. J. Cheng, J. E. Klaunig, *Carcinogenesis* **10** (1989) 1003
26. L. C. Green, D. A. Wagner, J. Glogowski, P. L. Skipper, J. S. Wishnok, S. R. Tannenbaum, *Anal. Biochem.* **126** (1982) 131
27. L. Marcocci, J. J. Maguire, M. T. Droy-Lefaix, L. Packer. *Biochem. Biophys. Res. Commun.* **201** (1994) 748
28. M. Oyaizu, *Jpn. J. Nutr.* **44** (1986) 307
29. T. S. Lobana, S. Khanna, R. J. Butcher, A. D. Hunter, M. Zeller, *Polyhedron* **25** (2006) 2755
30. G. G. Mohamed, N. A. Ibrahim, H. A. E. Attia, *Spectrochim. Acta* **72** (2009) 610
31. E. Manoj, M. R. P. Kurup, *Polyhedron* **27** (2008) 275
32. S. Chandra, J. Deeepali, K. S. Amit, *Spectrochem. Acta* **71** (2009) 1712
33. S. Rajeev, N. K. Kaushik, *Spectrochim. Acta* **72** (2009) 691.

Correlation between standard enthalpy of formation, structural parameters and ionicity for alkali halides

ABU NASAR*

Department of Applied Chemistry, Faculty of Engineering & Technology, Aligarh Muslim University, Aligarh – 202002, India

Abstract: The standard enthalpy of formation ($\Delta H^{\ominus}$) is considered to be an interesting and useful parameter for the correlation of various properties of alkali halides. The interrelation between $\Delta H^{\ominus}$ and structural parameters for the halides of Li, Na, K and Rb has been thoroughly analyzed. When the cationic component element is kept constant in a homologous series of alkali halides, the negative value of $\Delta H^{\ominus}$ was observed to decrease linearly with increasing interionic distance (d). Accordingly, the following empirical equation $\Delta H^{\ominus} = \alpha + \beta d$ (where α and β are empirical constants) was established. However, for common anionic series of alkali halides, an opposing non-linear trend was observed, with the exception of common fluorides. The correlation study on the standard enthalpy of formation was extended in term of the radius ratio and also discussed in the light of ionization energy of the metal, electron affinity of the halogen, size of the ions, ionic character of the bond and the lattice energy of the compound.

Keywords: thermodynamic properties; exothermicity; interionic distance; radius ratio; interrelation.

INTRODUCTION

Alkali halides are crystalline ionic solids that are of great interest for both theoretical and experimental studies. In recent years, they have gained increased interest due to their prominent applications in the fabrication of various electronic, optical and optoelectronic devices.[1] They have also received considerable attention due to their potential role in emerging nano-scale technologies and importance in environmental chemistry, such as ozone layer depletion and precipitation.[2] During the past few years, considerable efforts, *e.g.*, see references[3–22], have been made to understand the interrelation between their various structural, optical and electronic properties, such as lattice constants, interionic distance, radius ratio, refractive index, electronic polarizability, dielectric constant, cohe-

---

sive energy, bond energy, magnetic susceptibility, energy gap, bulk modulus, *etc*. Although thermodynamic properties are of considerable importance for an understanding of the nature of a compound against a changing environment, limited attempts have been made to study the interrelation of the thermodynamic properties of alkali halides with their other properties. Shanker *et al*.[23] studied the relationship between solid state parameters and melting parameters for alkali halides and reported that melting temperature and relative change in volume after melting vary in a systematic manner with the ionic character of bond. Kanno[24,25] observed the relationship between enthalpy of fusion, entropy change upon fusion or sublimation upon melting, melting point, electronic polarizability, interionic distance and the ionic radius ratio for some alkali halides. He also developed an empirical relation between the relative volume changes upon melting with the interionic distance.[26] In a relatively recent work of Rozman,[27] correlations between thermodynamic parameters (such as melting point, melting energy and jump in entropy upon melting) and the binding energy of dipolons were established for the halides of lithium, sodium, potassium and rubidium. Ohashi[28] expressed an empirical relation between the heats of formation and the electronegativity of halogen ions. Recently Vasiliu *et al*.[29] predicted the geometric parameters, frequencies, enthalpies of formation and bond dissociation energies for some simple alkali metal compounds by employing the coupled cluster theory. A second order empirical polynomial relation between standard enthalpy of formation and refractive index for all the twenty alkali halides has also been developed.[30]

A literature survey reveals that no systematic effort has hitherto been made to correlate the thermodynamic properties of alkali halides with their structural, physical, optical and electronic properties. The available work in this direction is very limited and scanty. Since structural parameters are basic constants that are involved in most theoretical calculations and also in predicting the behaviour of a compound, it is worth correlating them with the thermodynamic properties of alkali halides. As the enthalpy of formation throws light on the nature of the bond and the intrinsic stability of the compound in the condensed phase, it was decided to study the correlation of the enthalpy of formation with the structural and ionic parameters of alkali halides.

BASIC INPUT DATA AND THEIR TREND IN THE HOMOLOGOUS SERIES OF ALKALI HALIDES

The values of room temperature standard enthalpy of formation[31] and interionic distance[1] are listed in Table I for the common cationic and anionic homologous series of alkali halides. The radius ratio in a crystal having the NaCl structure as presented in Table I is calculated from the effective ionic radii of the cationic and anionic constituent elements of the compound with a coordination number 6.[31] Table I indicates that the negative value of standard enthalpy of formation ($-\Delta H^{\ominus}$), *i.e*., exothermicity, decreases with increasing of

interionic distance (d) and decreasing radius ratio (r^+/r^-) in the homologous series of compounds when the cationic component element is kept constant. On the other hand, for the common anionic homologous series of compounds (Table I), the exothermicity ($-\Delta H^\ominus$) generally increases with increasing of both d and r^+/r^-, with the exception of the common fluorides, which obey the reverse trend.

TABLE I. Standard enthalpy of formation and structural parameters of alkali halides

Compound	$-\Delta H^\ominus$ / kJ mol^{-1}	d / Å	r^+/r^-
Common cationic series			
LiF	616.0	2.0131	0.5714
LiCl	408.6	2.5699	0.4199
LiBr	351.2	2.7508	0.3878
LiI	270.4	3.0060	0.3455
NaF	576.6	2.3164	0.7699
NaCl	411.2	2.8200	0.5635
NaBr	361.1	2.9865	0.5204
NaI	287.9	3.2364	0.4636
KF	567.2	2.6720	1.0376
KCl	436.5	3.1464	0.7624
KBr	393.8	3.2991	0.7041
KI	327.9	3.5327	0.6273
RbF	557.7	2.8258	1.1429
RbCl	435.4	3.2949	0.8398
RbBr	394.6	3.4454	0.7755
RbI	333.8	3.6710	0.6909
Common anionic series			
LiF	616.0	2.0131	0.5714
NaF	576.6	2.3164	0.7699
KF	567.2	2.6720	1.0376
RbF	557.7	2.8258	1.1429
LiCl	408.6	2.5699	0.4199
NaCl	411.2	2.8200	0.5635
KCl	436.5	3.1464	0.7624
RbCl	435.4	3.2949	0.8398
LiBr	351.2	2.7508	0.3878
NaBr	361.1	2.9865	0.5204
KBr	393.8	3.2991	0.7041
RbBr	394.6	3.4454	0.7755
LiI	270.4	3.0060	0.3455
NaI	287.9	3.2364	0.4636
KI	327.9	3.5327	0.6273
RbI	333.8	3.6710	0.6909

DISCUSSION

The values of the room temperature standard enthalpy of formation are plotted against interionic distance for different homologous series of alkali halides in Fig. 1. It could be inferred from Fig. 1 that when the cationic component element

is kept constant in a given homologous series of the compounds, there is almost linear decrease in the negative value of standard enthalpy of formation with increasing d. Thus, the exothermicity of compound formation decreases with increasing anion size. Based on the linear variation between $\Delta H^{\ominus}$ and d, the following empirical relation was established:

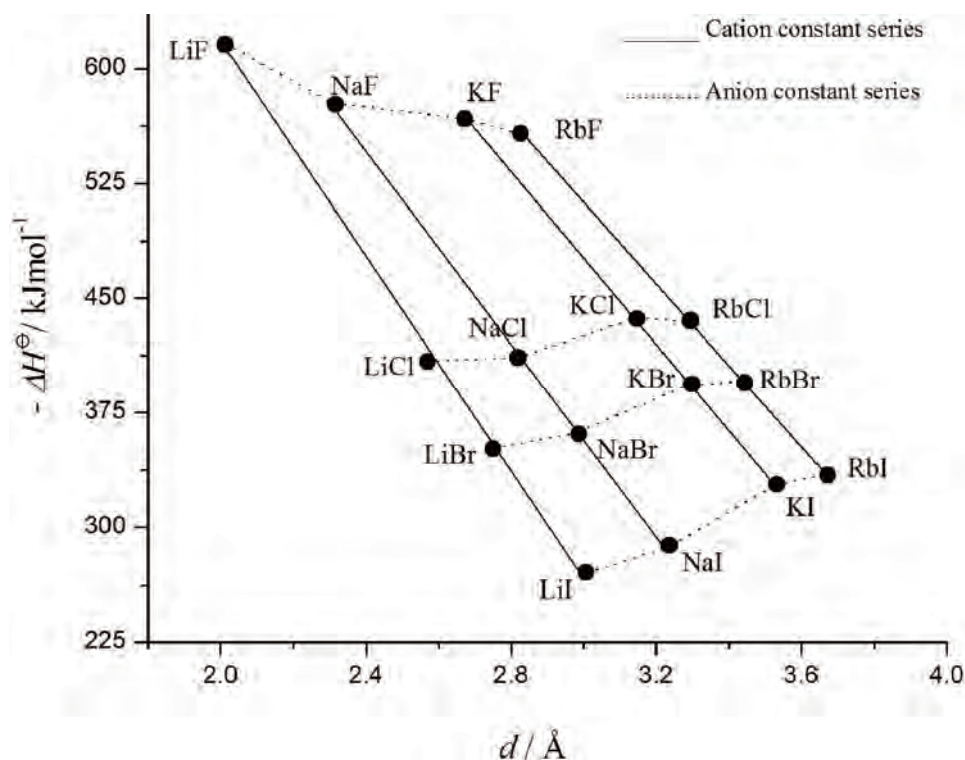$$\Delta H^{\ominus} = \alpha + \beta d \qquad (1)$$

Fig. 1. Plot of the standard enthalpy of formation *vs.* the interionic distance for alkali halides.

where α and β are empirical constants that are presented in Table II for the different cationic series of alkali halides. The values of square of the correlation coefficient, *i.e.*, R^2, which can be used to judge the effectiveness of the correlation equation, are also incorporated in this Table. Table II clearly indicates that the R^2 value (≥ 0.9980) was very satisfactory for each case. The values for standard enthalpy of formation ($\Delta H^{\ominus}_{cal}$) as calculated from Eq. (1) are compared with the known values[31] in Table III. The percent deviations for the different compounds, as obtained using the relation:

$$\text{percent deviation} = 100 \left| \Delta H^{\ominus}_{known} - \Delta H^{\ominus}_{cal} \right| / \Delta H^{\ominus}_{known} \qquad (2)$$

are also incorporated in Table III. This table clearly shows that there is excellent agreement between the calculated and the known values with the percent deviation ranging from 0.04 to 2.33. Moreover, the average percent deviation is only 0.65.

TABLE II. Empirical constants (α and β) for different series of alkali halides (Eq. (1)); X represents F, Cl, Br or I

Compound series	$-\alpha$ / kJ mol^{-1}	β / kJ mol^{-1} Å^{-1}	R^2
LiX	1316.8	350.2	0.9980
NaX	1304.3	315.2	0.9991
KX	1309.7	277.8	1.0000
RbX	1306.1	264.6	0.9999

TABLE III. Known and calculated values of the standard enthalpy of formation of alkali halides

Compound	$-\Delta H^{\ominus}$ / kJ mol^{-1}		Deviation, %
	Literature[31]	Calculated (Eq. (1))	
LiF	616.0	611.8	0.68
LiCl	408.6	416.8	2.01
LiBr	351.2	353.5	0.66
LiI	270.4	264.1	2.33
NaF	576.6	574.2	0.42
NaCl	411.2	415.4	1.02
NaBr	361.1	363.0	0.55
NaI	287.9	284.2	1.29
KF	567.2	567.4	0.04
KCl	436.5	435.6	0.21
KBr	393.8	393.2	0.15
KI	327.9	328.3	0.12
RbF	557.7	558.4	0.13
RbCl	435.4	433.3	0.48
RbBr	394.6	394.4	0.05
RbI	333.8	334.8	0.30

Furthermore, it is very interesting and surprising to note that the value of empirical constant α, listed in Table II, remains the same (average: –1309.2 kJ mol^{-1}) for all the sixteen halides of Li, Na, K and Rb. In fact, this constant is the standard enthalpy of formation of an imaginary compound in the series having zero interionic distance. It is the limiting value and exists only under the hypothetical situation. Although it appears practically impossible for a compound to have zero interionic distance, its implication for future studies cannot be ruled out.

On the other hand, for the common anionic series of compounds, an opposite non-linear trend for the variation of $\Delta H^{\ominus}$ with d was observed with the exception of the common fluorides (Fig. 1). Thus the exothermicity of compound formation increases with increasing size of cationic component element for the common an-

ionic series of alkali halides, except for the fluorides which exhibit the opposite trend. The general increase of exothermic enthalpy of formation with increasing cationic size of chlorides, bromides and iodides is due to the decreasing value of the ionization energy of the metals, which facilitates the formation of the respective cations in the same order. It is also inferred from Table I that the homologous series of same anion do not show any unambiguous general trend for in the $\Delta H^{\ominus}$ values. This observation is consistent with the finding of Shenkin[32] who theoretically showed that only the anion size plays a decisive role in thermodynamic relationships for alkali halides. The anomalous behaviour of fluorides is presumably due to the small size and high electronegativity of fluorine compared to other halogens. In fact, the ionic radius of the fluoride anion is similar to that of the oxide anion; thus, fluorides often resemble oxides while other halides resemble sulphides in many respects.[33]

The anomalous behaviour of fluorides can be explained in the light of the unusually lower value of the electron affinity of fluorine compared to the other higher halogens. The numerical value of electron affinity is 115.0 kJ mol^{-1} lower than the value expected from the linear extrapolation of the plot between electron affinity and ionization energy for other halogens (Fig. 2). The values of electron affinity and ionization energy for the halogens were taken from the literature.[31] In a similar way, a 110.0 kJ mol^{-1} discrepancy was reported Politzer.[34] Thus, fluorides are accompanied by anomalously lower bond energies of about 115.0 kJ mol^{-1} than would be predicted from the trends of the other halides. The lower value of electron affinity for fluorine is due to the small size of the atom as putting an extra electron into a region of space already crowded with electrons offers a significant amount of repulsion. This repulsion decreases the attraction of an incoming electron and accordingly lowers the electron affinity.

Based on the thermodynamic Born–Haber cycle, the standard enthalpy of formation ($\Delta H^{\ominus}$) can be related to the electron affinity (*EA*) of the halogen, the ionization energy (*EI*) of the metal, the enthalpy of atomization (ΔH_{ax}) of the halogen, the enthalpy of atomization (ΔH_{am}) of the metal and the lattice energy (ΔH_l) of the compound by the following equation:

$$\Delta H^{\ominus} = EA + \mathrm{EI} + \Delta H_{ax} + \Delta H_{am} + \Delta H_l \tag{3}$$

Thus, the trend of the lattice energy is expected to be more regular than that of the standard enthalpy of formation because the former is obtained by subtracting the irregular value of the electron affinity along with other parameters from the latter. The plot of lattice energy[35] *vs.* interionic distance for alkali halides shown in Fig. 3 can be best represented by the following second order polynomial equation:

$$\Delta H_l = 1962.9 - 602.7d + 65.2d^2 \; (R^2 = 0.9958) \tag{4}$$
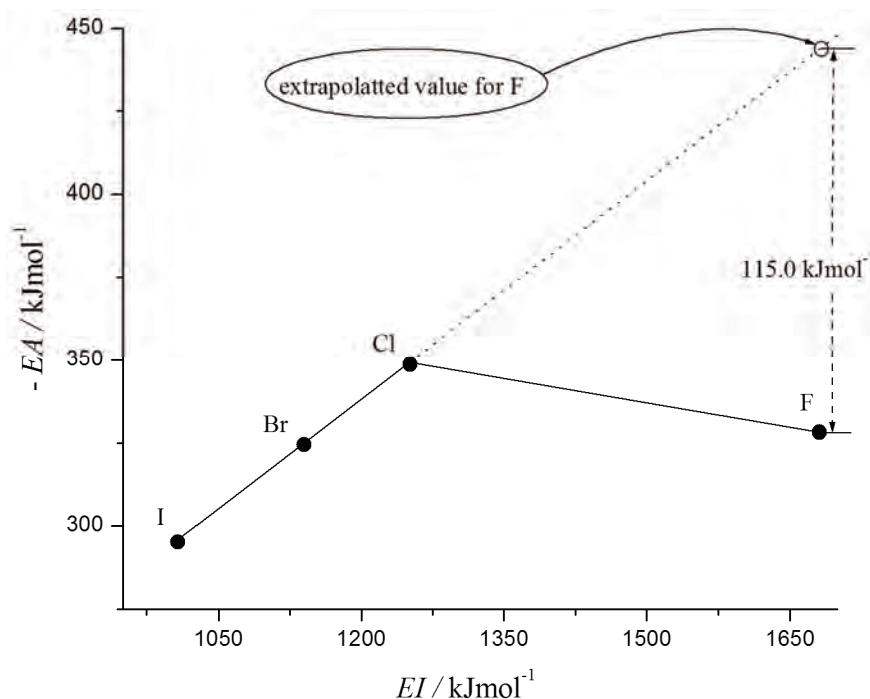
Fig. 2. Plot of electron affinity *vs.* ionization energy of the halogens.

Figure 3 clearly indicates that the variation of lattice energy with interionic distance is very regular and does not show any anomalous or irregular behaviour of fluorides. Thus, the electron affinity plays a dominant role for the anomalous nature of fluorides. However, further work is required in this direction.

The correlation studies of standard enthalpy of formation were extended to the radius ratio (r^+/r^-). The variation plot shown in Fig. 4 indicates that $-\Delta H^\ominus$ increases regularly with increasing radius ratio of the compounds for different homologous series when either of the component elements is fixed, again with the exception of the common fluorides. The common fluorides show a regular decrease in the value of $-\Delta H^\ominus$ with the radius ratio. In fact, the enthalpy of formation of any fluoride is less exothermic than that expected from the extrapolation of linear plot obtained for the other halides. The possible reasons have already been discussed.

Since F is the most electronegative, the fluoride is more ionic in nature than any of the other respective halides. Thus, it appeared quite interesting to study the correlation between the standard enthalpy of formation and the ionic character of the bond. The ionic character of the bond of a particular compound may be calculated from the value of electronegativity difference ($\Delta\chi$) of its constituent elements by employing the Pauling Equation:[36]

Fractional ionic character of bond $(f^i) = 1 - \exp\{-\frac{1}{4}(\Delta\chi)^2\}$ (5)
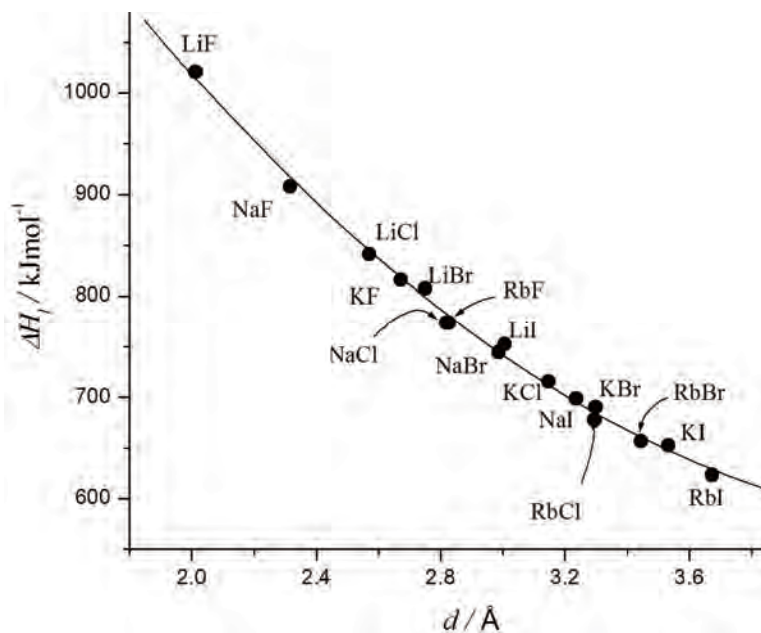

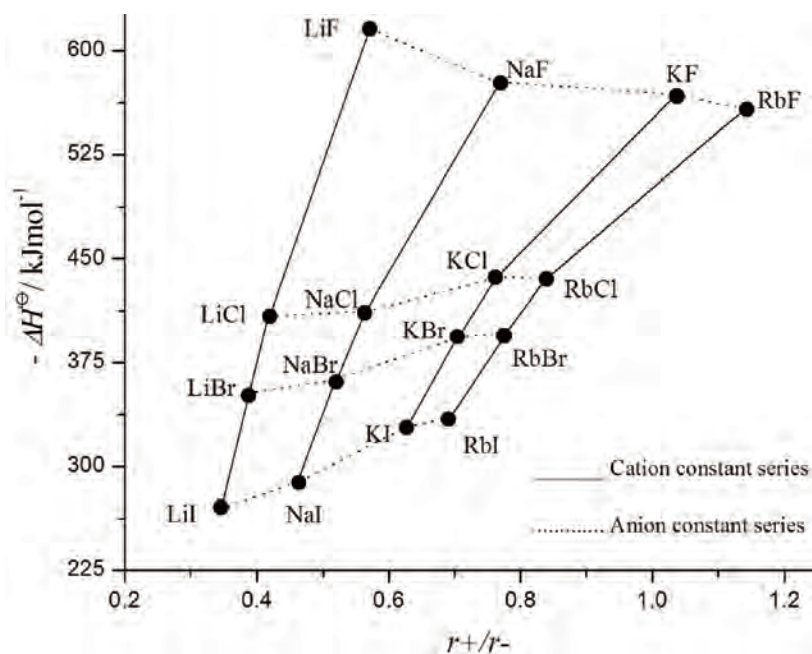Fig. 3. Plot of lattice energy *vs.* interionic distance for the alkali halides.

Fig. 4. Plot of standard enthalpy of formation *vs.* radius ratio for the alkali halides.

The electronegativity values (χ) of atoms are available on a number of scales, including the popular ones Pauling,[36] Pauling revised,[31] Allred and Rochow,[37] Gordy,[38] Sanderson,[39] Allen[40] and Mulliken.[40] These scales are prepared by independent methods and have different values of χ for a particular atom. Since χ is measure of the tendency of an atom to attract bonding electrons towards itself, smaller atoms, as a rule, should have higher values of χ. The electronegativities of alkali metals as proposed by Sanderson, Gordy, Mulliken and Allen are in conformity with the criterion of increase in value with decreasing atomic size and therefore these scales were considered in the calculation of the fractional ionic character of the bond for the different compounds. The values of fractional ionic character of bond for alkali halides as calculated using different electronegativity scales are presented in Table IV. This Table shows that the value of the fractional ionicity for any compound is different for the different scales. However, for any common cationic series of compounds, the trend of the variation with size of the anionic component element remains the same. Hence, for the sake of simplicity, average values were used for further analysis. It can be inferred from Table IV that the fractional ionic character of the bond in a compound decreases with increasing size of the anionic component elements in a common cationic series. However, for the common anionic series of the compounds, an opposite trend was obtained, *i.e.*, the ionicity increases with increasing size of the cationic component elements. Thus the following generalization was established for all the halides of Li, Na, K and Rb: "ionicity increases with decreasing size of the anionic and increasing size of cationic component elements in a given common cationic or anionic series of compounds, respectively".

TABLE IV. Fractional ionic character of the bond in alkali halides

Compound	Gordy[38]	Sanderson[39]	Mulliken[40]	Allen[40]	Average (used)
LiF	0.891	0.937	0.917	0.932	0.919
LiCl	0.647	0.860	0.719	0.616	0.711
LiBr	0.523	0.803	0.615	0.544	0.621
LiI	0.387	0.671	0.472	0.408	0.485
NaF	0.901	0.948	0.926	0.937	0.928
NaCl	0.668	0.880	0.741	0.632	0.730
NaBr	0.547	0.829	0.703	0.562	0.660
NaI	0.431	0.708	0.501	0.426	0.512
KF	0.912	0.957	0.945	0.950	0.941
KCl	0.695	0.899	0.791	0.680	0.766
KBr	0.579	0.854	0.703	0.614	0.688
KI	0.447	0.744	0.574	0.483	0.562
RbF	0.916	0.967	0.948	0.952	0.946
RbCl	0.705	0.918	0.801	0.690	0.779
RbBr	0.591	0.879	0.715	0.624	0.702
RbI	0.460	0.781	0.589	0.495	0.581

The validity of this generalization is very clearly observed in Fig. 5. The plot also indicates that the ionic character of bond increases with increase of radius ratio for the homologous series of compounds when either of the component elements is kept constant. Besides this it is also inferred from this figure that the variation is almost linear for the common anionic and common cationic series of compound with the exception of fluorides.
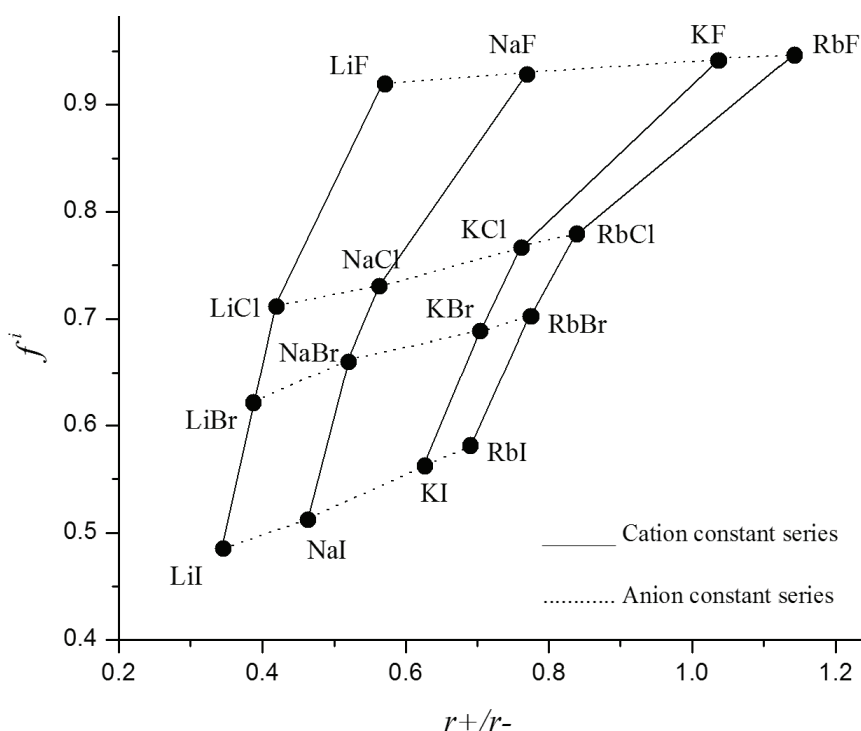

Fig. 5. Plot of fractional ionic character of the bond *vs.* radius ratio for the alkali halides.

The standard enthalpy of formation of a compound throws light on the type of bonding. A large value of exothermic enthalpy of formation of compound indicates that the nature of bonding is different from that in the constituent elements. The exothermicity has been observed to be generally increased with the degree of ionicity of bond. The plot of standard enthalpy of formation with fractional ionic character of bond shown in Fig. 6 indicates that there is a general linear relation between these two parameters and variation may be represented as:

$$\Delta H^\ominus = 74.4 - 686.9 \, f^i \; (R^2 = 0.9629) \tag{6}$$

Since in most cases fluorides exhibit exceptional behaviour, Eq. (6) can be presented in a better way by excluding the fluorides. The empirical equation between $\Delta H^\ominus$ and f^i as obtained for the plot represented by line B in Fig. 6 is:

$$\Delta H^{\ominus} = -3.2 - 561.0 f^{i} \ (R^2 = 0.9878) \tag{7}$$

The linear variation indicates that there exists a very good correlation between standard enthalpy of formation and the ionic character of the bond. Thus, the hypothesis of increasing ionicity with exothermicity is valid for the alkali halides with an NaCl structure. However, this generalization is not valid within the alkali fluorides.
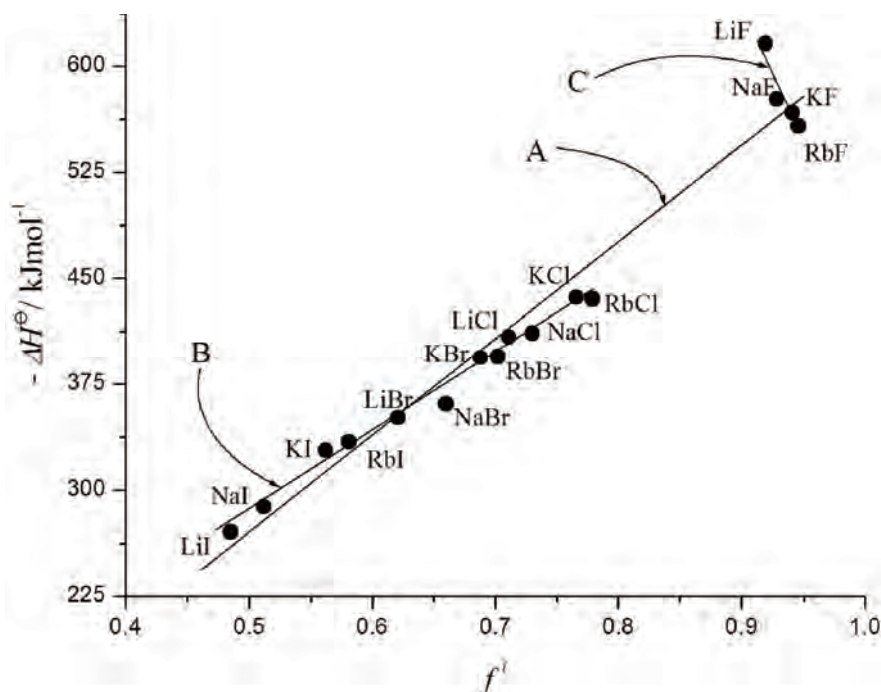

Fig. 6. Plot of the standard enthalpy of formation *vs.* the fractional ionic character of the bond for alkali halides.

CONCLUSIONS

Systematic variation between the standard enthalpy of formation and structural parameters (interionic distance and radius ratio) for all the sixteen halides of Li, Na, K and Rb were observed. It was established that the exothermicity decreases with increasing or decreasing size of the anionic or cationic component element for the common cationic or anionic series of alkali halides. However, common fluorides show the opposite behaviour to that of the other common halides. Empirical relationships between the standard enthalpy of formation and the interionic distance were proposed for the different common cationic series of compounds.

It was found that the ionicity increases with decreasing size of the anionic and increasing size of cationic component elements in a given common cationic or anionic series of the compounds, respectively. Furthermore, a general linear relation between the standard enthalpy of formation and ionicity was observed to exist for the alkali halides, except for the fluorides. It was proposed that the anomalous behaviour of fluorides with respect to other halides is due to the small size of the fluorine atom, which leads to lower values of the electron affinity than those expected from the trend of the other halogens.

И З В О Д

КОРЕЛАЦИЈА ИЗМЕЂУ СТАНДАРДНЕ ЕНТАЛПИЈЕ ФОРМИРАЊА, СТРУКТУРНИХ ПАРАМЕТАРА И ЈОНСКОГ КАРАКТЕРА АЛКАЛНИХ ХАЛОГЕНИДА

ABU NASAR

Department of Applied Chemistry, Faculty of Engineering & Technology, Aligarh Muslim University, Aligarh – 202002, India

Стандардна енталпија формирања ($\Delta H^\ominus$) је значајан и веома користан параметар за корелацију са различитим особинама алкалних халогенида. Веза између $\Delta H^\ominus$ и структурних параметара халогенида Li, Na, K и Rb у овом раду је детаљно анализирана. У случају када је у хомологној серији алкалних халогенида катјонска компонента соли иста, нађено је да се негативна вредност $\Delta H^\ominus$ линеарно смањује са повећањем интерјонског растојања и да се ова релација може изразити следећом емпријском формулом: $\Delta H^\ominus = \alpha + \beta d$ (α и β су емпиријске константе). Међутим, супротан нелинеаран тренд промене негативне вредности $\Delta H^\ominus$ је нађен у солима алкалних халогенида за исту серију халогенидних анјона, осим у случају флуорида. Поред тога, у овом раду дискутована је веза између стандардне енталпије формирања и јонског радијуса, као промене јонизационе енергије алкалног метала, електронског афинитета халогена, величине јона, јонског карактера везе и енергије кристалне решетке јонског једињења.

(Примљено 13. јануара, ревидирано 18. априла 2012)

REFERENCES

1. D. B. Sirdeshmukh, L. Sirdeshmukh, K. G. Subhadra, *Alkali Halides: A Handbook of Physical Properties,* Springer, Berlin, Germany, 2001
2. B. Li, A. Michaelides, M. Scheffler, *Phys. Rev. Lett.* **97** (2006) 046802
3. A. K. Koh, *J. Phys. Chem. Solids* **57** (1996) 51
4. A. K. Koh, *J. Phys. Chem. Solids* **57** (1996) 369
5. H. Neumann, *Cryst. Res. Technol.* **23** (1988) 531
6. N. Dutt, G. G. Agrawal, J. Shanker, *Solid State Commun.* **55** (1985) 993
7. J. Lielmezs, *Thermochim. Acta* **12** (1975) 323
8. R. R. Reddy, Y. N. Ahammed, A. S. Rao, P. M. Reddy, *J. Mol. Struct. (Theochem.)* **339** (1995) 233

9. R. R. Reddy, Y. N. Ahammed, K. R. Gopal, P. A. Azeem, D. V. Raguram, T. V. R. Rao, *J. Magn. Magn. Mater.* **192** (1999) 516
10. R. R. Reddy, Y. N. Ahammed, K. R. Gopal, P. A. Azeem, T. V. R. Rao, *Infrared Phys. Technol.* **42** (2001) 49
11. R. R. Reddy, K. R. Gopal, K. Narsimhulu, L. S. S. Reddy, K. R. Kumar, G. Balakrishnaiah, M. R. Kumar, *J. Alloys Compd.* **473** (2009) 28
12. A. K. Vijh, *J. Mater. Sci.* **9** (1974) 2052
13. V. Kumar, J. K. Singh, *Ind. J. Pure Appl. Phys.* **48** (2010) 571
14. M. A. E. Salem, *Turk. J. Phys.* **27** (2003) 569
15. B. P. Singh, V. S. Baghel, K. S. Baghel, *Ind. J. Pure Appl. Phys.* **48** (2010) 311
16. A. S. Verma, S. R. Bhardwaj, *J. Phys.: Condens. Matter* **18** (2006) 8603
17. R. Heyrovska, *Chem. Phys. Lett.* **436** (2007) 287
18. A. K. Koh, K. N. Ng, *Phys. Status Solidi B* **213** (1999) 11
19. W. Kucharczyk, *Phys. B: Condens. Matt.* **172** (1991) 473
20. J. Shanker, M. P. Verma, *J. Phys. Chem. Solids* **37** (1976) 883
21. H. Schlosser, *J. Phys. Chem. Solids* **53** (1992) 855
22. P. Herve, L. K. J. Vandamme, *Infrared Phys. Technol.* **35** (1994) 609
23. J. Shanker, W. N. Bhende, M. Kumar, *Solid State Commun.* **55** (1985) 479
24. H. Kanno, *Nature* **218** (1968) 765
25. H. Kanno, *Bull. Chem. Soc. Jpn.* **44** ((1971) 559
26. H. Kanno, *Bull. Chem. Soc. Jpn.* **50** (1977) 2799
27. G. A. Rozman, *Phys. Solid State* **46** (2004) 247
28. H. Ohashi, *Thermochim. Acta* **108** (1986) 189
29. M. Vasiliu, S. Li, K. A. Peterson, D. Feller, J. L. Gole, D. A. Dixon, *J. Phys. Chem., A* **114** (2010) 4272
30. A. Nasar, *Int. J. Chem. Sci.* **7** (2009) 2489
31. J. G. Speight, *Lange's Handbook of Chemistry*, 16th ed., McGraw-Hill, New York, USA, 2005
32. Y. S. Shenkin, *Sov. Phys. Solid State* **23** (1981) 1110
33. F. A. Cotton, G. Wilkinson, C. A. Murillo, M. Bochmann, *Advanced Inorganic Chemistry*, 6th ed., Wiley, New York, USA, 1999, p. 554
34. P. Politzer, *J. Am. Chem. Soc.* **91** (1969) 6235
35. D. F. C. Morris, *Acta Cryst.* **9** (1956) 197
36. L. Pauling, *The Nature of the Chemical Bond*, 3rd ed, Cornell University Press, New York, USA, 1960
37. A. L. Allred, E. G. Rochow, *J. Inorg. Nucl. Chem.* **5** (1958) 264
38. W. Gordy, *Phys. Rev.* **69** (1946) 604
39. R. T. Sanderson, *J. Am. Chem. Soc.* **105** (1983) 2259
40. L. C. Allen, *J. Am. Chem. Soc*. **111** (1989) 9003.

Journal of the Serbian Chemical Society

A calorimetric investigation for the bindings of mushroom tyrosinase to *p*-phenylene-bis(dithiocarbamate) and to alkyl xanthates

GHOLAM REZA REZAEI BEHBEHANI[1]*, MELISA MEHRESHTIAGH[1],
LYLA BARZEGAR[2] and ALI AKBAR SABOURY[3]

[1]*Department of Chemistry, Imam Khomeini International University, Qazvin, Iran,*
[2]*Department of Chemistry, Islamk Azad University, Takestan Branch, Takestan, Iran*
and [3]*Institute of Biochemistry and Biophysics, University of Tehran, Tehran, Iran*

Abstract: A comprehensive, simple and rapid thermodynamic study on the interaction of mushroom tyrosinase, MT, with three isoalkyldithiocarbonates (xanthates) as sodium salts, $C_3H_7OCS_2Na$ (**I**), $C_4H_9OCS_2Na$ (**II**), and $C_5H_{11}OCS_2Na$ (**III**), with *p*-phenylene-bis(dithiocarbamate) (**IV**), was performed using isothermal titration calorimetry to clarify the thermodynamics of these bindings as well as structural changes of the enzyme due to its interaction with inhibitors at 300 K in phosphate buffer (10 m mol L^{-1}; pH 6.8). The extended solvation theory was used to elucidate the effect of the inhibitors on the stability of the enzyme. The obtained results indicated that there are two identical and non-cooperative binding sites for these inhibitors.

Keywords: mushroom tyrosinase; isopropyl xanthate; isobutyl xanthate; isopentyl xanthate; *p*-phenylene-bis(dithiocarbamate); extended solvation theory.

INTRODUCTION

Tyrosinase is a bifunctional, copper-containing mono-oxygenase catalysing the *o*-hydroxylation of monophenols to the corresponding catechols and the oxidation of catechols to the corresponding *o*-quinones.[1] *o*-Quinones undergo some reactions that result in the formation of biopolymers such as melanin.[2] Tyrosinase is ubiquitously distributed among animals, plants and fungi. Mushroom tyrosinase (MT) is popular among researchers as it is commercially available and inexpensive.[3] In mushrooms as well as in fruits and vegetables, this enzyme is responsible for browning, a commercially undesirable phenomenon.[4] Therefore, tyrosinase inhibitors have attracted interest recently due to undesired browning in vegetables and fruits in post-harvest handling. Among the inhibitors, a distinction

---

255

can be made between chelators of two Cu^{2+} in the active site.[5] The well-known heavy metal chelators, derivatives of dithiocarbamate, have been found to possess a wide range of biological activities of mushroom tyrosinase. Special interest in the study of metaldithiocarbamates was aroused because of the striking structural features presented by this class of compounds and also because of their diverse applications, such as high pressure lubricants in industry, fungicides and pesticides and as accelerators in vulcanization.[6] Bismuth and chromone dithiocarbamate complexes show antitumor activity.[7,8] The inhibitory effects of xanthates on mushroom tyrosinase was elucidated, which is related to the chelating of the copper ions at the active site by a negative head group (S^-) of the xanthate anion. The inhibitory effects of three synthetic *n*-alkyl xanthates sodium salts with C_3, C_4 and C_5 aliphatic tails were described. Lineweaver–Burk plots showed different patterns of mixed inhibition for *p*-phenylene-bis(dithiocarbamate) and isopropyl xanthate and competitive inhibition for isobutyl and isopentyl xanthate.[4,9] In view of the increasing importance of controlling tyrosinase activities, we applied isothermal titration calorimetry (ITC) was applied in the present study to obtain thermodynamic parameters for the interaction between mushroom tyrosinase and inhibitors.

EXPERIMENTAL

MT was obtained from Sigma and the inhibitors were synthesized. All other materials and reagents were of analytical grade and solutions were made in 10 mmol L^{-1} phosphate buffer (pH 6.8) using double-distilled water.

The isothermal titration calorimetric experiments were performed with a four-channel commercial microcalorimetric system, Thermal Activity Monitor 2277 (Thermometric, Sweden). The microcalorimeter is composed of two identical cells, a reference cell and a sample cell of 1.8 mL in volume, which were made of a highly efficient thermal conducting material surrounded by an idiabetic jacket. The sample cell was loaded with mushroom tyrosinase solution (8.3 µmol L^{-1}) and phosphate buffer solution (10 mmol L^{-1}) and the reference cell contained buffer solution. The titration of MT with isopropyl xanthate (**I**), isobutyl xanthate (**II**), isopentyl xanthate (**III**) or *p*-phenylene-bis(dithiocarbamate) (**IV**) involved 20 consecutive injections and each injection included 20 µL of inhibitor. To correct the thermal effects due to ligand dilution, control experiments were performed in which identical aliquots were injected into the buffer solution with the exception of enzyme. The precision of measured heats were ±0.1 µJ or better.

RESULTS AND DISCUSSION

It was shown previously that the heats of interactions between a biomolecule and ligand in aqueous solvent systems could be analyzed by the following equation:[10–14]

$$q = q_{max} x'_B - \delta^\theta_A (x'_A L_A + x'_B L_B) - (\delta^\theta_B - \delta^\theta_A)(x'_A L_A + x'_B L_B) x'_B \qquad (1)$$

where:

$$x'_B = \frac{px_B}{x_A + px_B} \tag{2}$$

x'_B is the fraction of the inhibitor bound to the binding sites and $x'_A = 1 - x'_B$ is the fraction of unbound inhibitor. x_B can be expressed as the concentration of the inhibitor after each injection, $[L]$, divided by the maximum concentration of the inhibitor, $[L]_{max}$, upon saturation of the entire enzyme.

$$x_B = \frac{[L]}{[L]_{max}} \tag{3}$$

$p = 1$ means that the inhibitor binds at each site independently and that the binding is non-cooperative. L_A and L_B are the relative contributions of unbound and bound inhibitor in the heats of dilution with the exclusion of MT and can be calculated from the heats of dilution of inhibitor in buffer as follows:

$$L_A = q_{dilut} + x_B \left(\frac{\partial q_{dilut}}{\partial x_B} \right), \; L_B = q_{dilut} + x_A \left(\frac{\partial q_{dilut}}{\partial x_B} \right) \tag{4}$$

The agreement between the experimental data and the data calculated *via* Eq. (1) (Fig. 1) supports the extended solvation model. The values of δ_A^θ and δ_B^θ obtained from the coefficients of the second and third terms of Eq. (1) are the
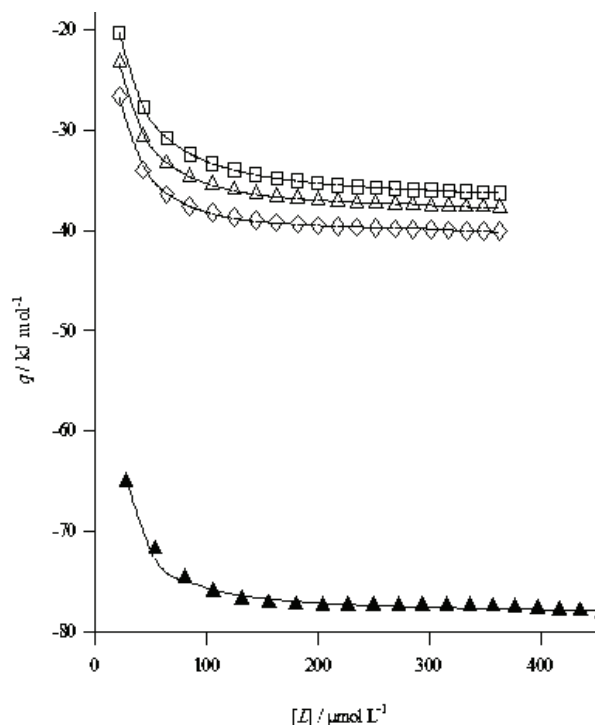
Fig. 1. Comparison between the experimental heats, q, for the interaction of mushroom tyrosinase with isopropyl (□), isobutyl (Δ) and isopentyl (◊) xanthate, and *p*-phenylene-bis(dithiocarbamate) (▲) and the data calculated *via* Eq. (1) (lines).

indexes of MT structural changes due to the reaction with the inhibitor in low and high concentrations, respectively. The superscript θ in all cases refers to the quantities at infinite dilution of the solute. The negative values of δ_A^θ and δ_B^θ show that isopropyl, isobutyl, isopentyl xanthate and *p*-phenylene-bis(dithiocarbamate) destabilize the MT structure.

In competitive inhibition, the amount of enzyme inhibition depends upon the inhibitor concentration; hence, the large changes in the δ_A^θ and δ_B^θ values for isobutyl and isopentyl xanthate with increasing inhibitor concentration can be attributed to the competitive manner of inhibition, which are in good agreement with the kinetic results.

In mixed inhibition, the inhibitor can bind to the enzyme at the same time as its substrate, although, the binding of the inhibitor affects the binding of the substrate, and *vice versa*. This type of inhibition can be reduced, but not overcome, by increasing the concentration of the substrate. Although it is possible for mixed-type inhibitors to bind in the active site, this type of inhibition generally results from an allosteric effect where the inhibitor binds to a different place on the enzyme. Inhibitor binding to this allosteric site changes the conformation of the enzyme so that the affinity of the substrate for the active site is reduced. Mixed inhibition occurs when contributions of competitive and uncompetitive are both available. In mixed inhibition with a predominantly competitive component, the obtained δ_A^θ and δ_B^θ values are different, such as in the inhibition of MT by *p*-phenylene-bis(dithiocarbamate), but when the uncompetitive component is dominant, the obtained δ_A^θ and δ_B^θ values are similar to each other, such as in the mixed mode of inhibition of MT by isopropyl xanthate (Table I). Double reciprocal Lineweaver–Burk plots confirmed the mixed inhibition by *p*-phenylene-bis(dithiocarbamate) and *iso*-propyl xanthate.[4,9]

TABLE I. Thermodynamic parameters for the interaction of isopropyl (**I**), isobutyl (**II**) and isopentyl (**III**) xanthates, and *p*-phenylene-bis(dithiocarbamate) (**IV**) with mushroom tyrosinase. The same values of δ_A^θ and δ_B^θ indicate mixed inhibition with the same contribution of competitive and uncompetitive component of MT by **I** and the different values for **IV** show a larger contribution of the competitive component in the mixed inhibition of MT by **IV**. The great changes of δ_A^θ and δ_B^θ are in good agreement with competitive inhibition of MT by **II** and **III**

Compound	**I**	**II**	**III**	**IV**
p	1	1	1	1
g	2±0.02	2±0.02	2±0.02	2±0.01
K_a / mol^{-1} L	9.07×10^4±24	1.26×10^5±12	1.68×10^5±12	3.3×10^5±56
ΔH / kJ mol^{-1}	–18.70±0.06	–19.30±0.07	–1.16±0.03	–39.23±0.12
ΔG / kJ mol^{-1}	–28.47±0.12	–29.28±0.14	–30.02±0.13	–31.7±0.09
ΔS / kJ mol^{-1} K^{-1}	0.03±0.01	0.03±0.01	0.10±0.02	–0.025±0.002
δ_A^θ	–4.99±0.02	–4.47±0.06	–4.23±0.06	–7.4±0.05
δ_B^θ	–4.23±0.02	–6.58±0.08	–8.66±0.08	–16.7±0.04

For a set of identical and independent binding sites, there are three different methods of ITC data analysis for providing the dissociation-binding constant (K_d). In the first method, using Eq. (5):[15–17]

$$\frac{\Delta q}{q_{max}}[M] = \frac{\Delta q}{q}[L]\frac{1}{g} - \frac{K_d}{g} \tag{5}$$

where $\Delta q = q_{max} - q$. q Represents the heat value at a certain inhibitor and MT concentration, $[M]$ and $[L]$ are the concentrations of MT and the inhibitor, respectively and q_{max} represents the heat value upon saturation of all MT molecules. The obtained results suggest a set of two binding sites ($g = 2$) with non-cooperativity for each inhibitor. The related plot for the binding of MT to p-phenylene--bis(dithiocarbamate) is shown in Fig. 2 as an example of the employment of Eq. (5). The best linear plot was obtained using −1171.5 μJ (equal to −78.4 kJ mol^{-1}). If q and q_{max} are calculated per mole of MT, then the molar enthalpy of binding for each binding site (ΔH) will be:

$$\Delta H = \frac{q_{max}}{g}$$

The calculated K_a ($1/K_d$), g and ΔH are reported in Table I.
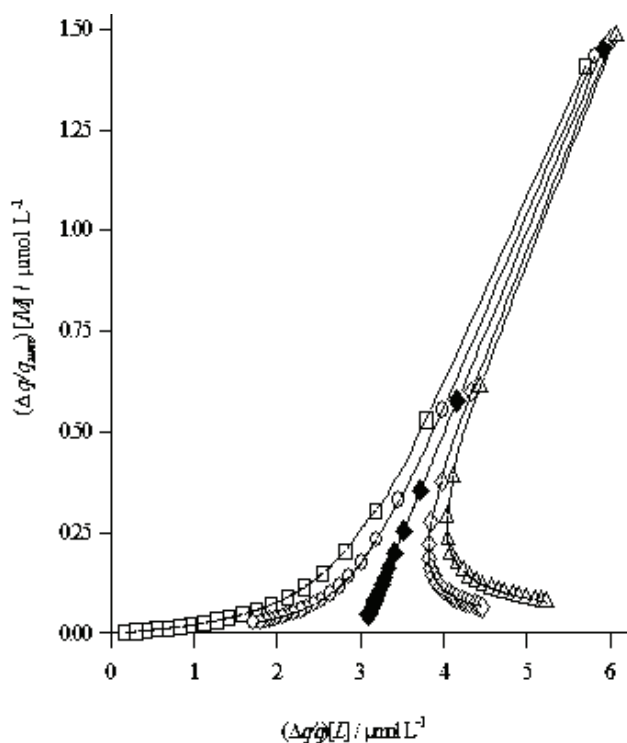
Fig. 2. The best linear plot of ($\Delta q/q_{max}$) [M] *vs.* ($\Delta q/q$) [L], according to Eq. (5), using the values of −1164 μJ ( ), −1168 μJ (○), −1171.5 μJ (♦), −1175 μJ (◊) and −1176 μJ (Δ) for q_{max} to obtain the best correlation coefficient value for a linear plot.

In the second ITC data analysis method, a simple linear plot of $q/[L]$ *vs. q* can be used for the determination of the association equilibrium constant and the molar enthalpy of binding by using Eq. (6):

$$\frac{q}{[L]} = K_a(\Delta H - q) \qquad (6)$$

A plot of $q/[L]$ *vs. q* for *p*-phenylene-bis(dithiocarbamate) is shown Fig. 3 as a typical example. The values of K_a and ΔH obtained from the axis intercept and slope are in good agreement with the results obtained from Eq. (5).
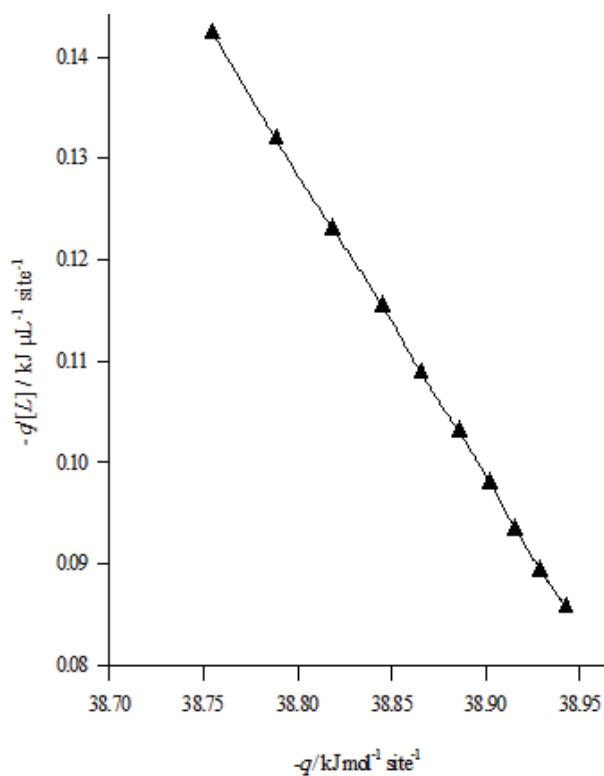

Fig. 3. The linear plot of $q/[L]$ *vs. q* according to Eq. (6) for the interaction between mushroom tyrosinase and *p*-phenylene-bis-(dithiocarbamate).

In third method, by a double reciprocal linear plot of $1/q$ *vs.* $1/[L]$, the values of K_d and ΔH can be calculated from the intercept of the axis using Eq. (7):

$$\frac{1}{q} = \frac{1}{\Delta H} + \frac{K_d}{\Delta H} \times \frac{1}{[L]} \qquad (7)$$

As an example, the plot for *p*-phenylene-bis(dithiocarbamate) is shown in Fig. 4. The obtained results are markedly consistent with the results from the analysis of the ITC data *via* Eqs. (5) and (6).
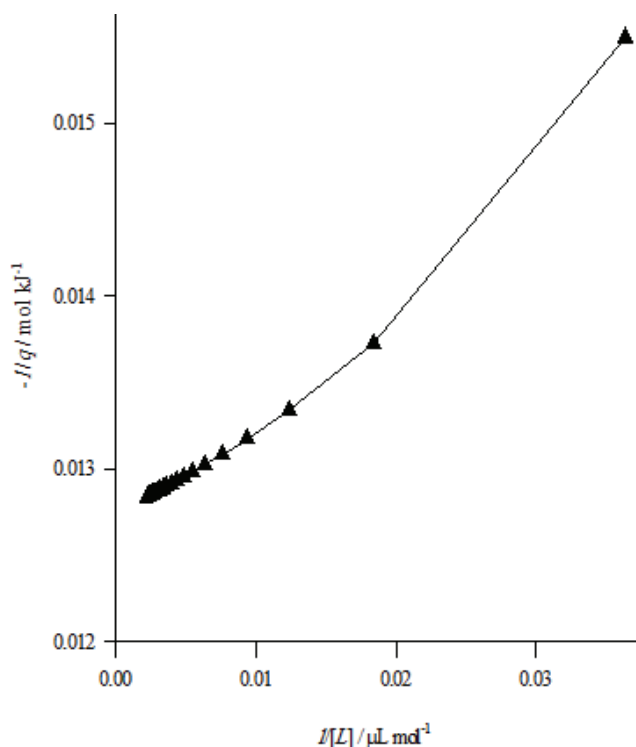
Fig. 4. The double reciprocal linear plot of 1/q *vs.* 1/[L] according to Eq. (7) for the interaction between mushroom tyrosinase and *p*-phenylene-bis(dithiocarbamate).

The change in the standard Gibbs free energy of binding (ΔG) was determined using K_a, the association-binding constant (the inverse of K_d) from the equation:

$$\Delta G = -RT\ln K_a \qquad (8)$$

The change in standard entropy (ΔS) of this binding can be calculated as follows:[18,19]

$$\Delta S = \frac{\Delta H - \Delta G}{T} \qquad (9)$$

The obtained values of ΔG and ΔS are given in Table I.

CONCLUSIONS

The extended solvation theory was used to determine the effects of the studied inhibitors on the thermal stability of MT. The agreements between the experimental heats and the results calculated *via* Eq. (1) are striking and support the extended solvation model. The results of this study also revealed the molar enthalpy and entropy, the standard Gibbs free energy changes and non cooperativity between two identical binding sites on MT for the three xanthates and *p*-phenylene-bis(dithiocarbamate). All the studied binding processes were spon-

taneous ($\Delta G < 0$). The obtained values of δ_A^θ and δ_B^θ were attributed to the type of inhibition. The different values of δ_A^θ and δ_B^θ showed the competitive inhibition of MT by **II**, **III** and **IV**.

И З В О Д

КАЛОРИМЕТРИЈСКО ИСПИТИВАЊЕ ВЕЗИВАЊА ТИРОЗИНАЗЕ ИЗ ПЕЧУРАКА ЗА
p-ФЕНИЛЕН-BIS(ДИТИОКАРБАМАТ) И КСАНТАТ

GHOLAM REZA REZAEI BEHBEHANI[1], MELISA MEHRESHTIAGH[1], LYLA BARZEGAR[2] и ALI AKBAR SABOURY[3]

[1]*Department of Chemistry, Imam Khomeini International University, Qazvin, Iran,* [2]*Department of Chemistry, Islamk Azad University, Takestan branch, Takestan, Iran u* [3]*Institute of Biochemistry and Biophysics, University of Tehran, Tehran, Iran*

Једноставно и брзо термодинамичко испитивање интеракције тирозиназе из печурака, MT, са три изо-алкилдитиокарбоната (ксантата), као соли натријума, $C_3H_7OCS_2Na$ (**I**), $C_4H_9OCS_2Na$ (**II**), $C_5H_{11}OCS_2Na$ (**III**) и *p*-фенилен-бис(дитиокарбамат) (**IV**), применом изотермалне титрационе калориметрије, је урађено са циљем да се објасни термодинамички аспект формираних веза као и структурне промене ензима при интеракцији са инхибиторима на 300 K у фосфатном пуферу (10 m mol L^{-1}; *p*H 6,8). Проширена теорија солватације је коришћена да би се објаснио ефекат инхибитора на стабилност ензима. Добијени резултати указују да постоје два идентична и не-кооперативна везујућа места за испитиване инхибиторе.

(Примљено 5. октобра 2010, ревидирано 12. септембра 2012)

REFERENCES

1. A. Rescigno, F. Sollai, B. Pisu, A. Rinaldi, E. Sanjust, *J. Enzyme Inhib. Med. Chem.* **17** (2002) 207
2. A. A. Saboury, *J. Iran. Chem. Soc.* **6** (2009) 219
3. E. Bourquelot, A. A. Bertrand, *C. R. Soc. Biol.* **47** (1895) 582
4. M. Alijanianzadeh, A. A. Saboury, H. Mansouri-Torshizi, K. Haghbeen, A. A. Moosavi--Movahedi, *J. Enzyme Inhib. Med. Chem.* **22** (2007) 239
5. A. J. M. Schoot-Uterkamp, H. S. Mason, *Proc. Natl. Acad. Sci. U.S.A.* **70** (1973) 993
6. D. Ondrusova, E. Jona, P. Simon, *J. Therm. Anal. Calorim.* **67** (2002) 147
7. H. Li, C. S. Lai, J. Wu, P. C. Ho, D. D. Vos, E. R. T. Tiekink, *J. Inorg Biochem.* **101** (2007) 809
8. W. Huang, Y. Ding, Y. Miao, M. Z. Liu, Y. Li, G. F. Yang, *Eur. J. Med. Chem.* **44** (2009) 3687
9. E. Amin, A. A. Saboury, H. Mansouri-Torshizi, S. Zolghadri, A. Kh. Bordbar, *Acta Biochim. Pol.* **57** (2010) 277
10. G. Rezaei Behbehani, *Chin. Chem. Lett.* **20** (2009) 751
11. G. Rezaei Behbehani, A. Divsalar, A. A. Saboury, F. Faridbod, M. R. Ganjali, *Bull. Korean Chem. Soc.* **30** (2009) 1262
12. M. Saeidfar, H. Masouri-Torshizi, G. Rezaei Behbehani, A. Divsalar, A. A. Saboury, *Bull. Korean Chem. Soc.* **30** (2009) 1951

13. G. Rezaei Behbehani, A. Divsalar, A. A. Saboury, A. A. Hekmat, *J. Solution Chem.* **38** (2009) 219
14. G. Rezaei Behbehani, M. Mirzaie, *J. Therm. Anal. Calorim.* **96** (2009) 631
15. G. Rezaei Behbehani, A. A. Saboury, M. Mohebbian, S. Tahmasbi Sarvestani, M. Poorheravi, *Chin. Chem. Lett.* **20** (2009) 1389
16. G. Rezaei Behbehani, A. A. Saboury, A. Fallah Baghery, A. Abedini, *J. Therm. Anal. Calorim.* **93** (2008) 479
17. A. A. Saboury, E. Poorakbar-Esfahani, G. Rezaei Behbehani, *J. Sci. Islam. Repub. Iran* **21** (2009) 15
18. A. A. Saboury, *J. Therm. Anal. Calorim.* **72** (2003) 93
19. A. A. Saboury, *J. Iran. Chem. Soc.* **3** (2006) 1.

Journal of the Serbian Chemical Society

Ferrate(VI) synthesis at a boron-doped diamond anode

MILAN ČEKEREVAC[1*#], LJILJANA NIKOLIĆ BUJANOVIĆ[1],
ANJA JOKIĆ[2#] and MILOŠ SIMIČIĆ[1]

[1]*IHIS Techno-Experts, Batajnički put 23, 11080 Belgrade, Serbia and* [2]*University of Priština, Faculty of Science, Kosovska Mitrovica, Serbia*

Abstract: The electrochemical synthesis of ferrate(VI) by the oxidation of iron compounds from alkaline 10 M KOH electrolytes on a boron-doped diamond electrode was examined by cyclic voltammetry between the potentials of the hydrogen evolution reaction and the oxygen evolution reaction. It was shown that the anodic current peak that appeared in iron-free electrolyte at a less positive potential than the potential of the oxygen evolution probably coincides with oxidation of hydrogen in $>CH_2$ groups and C-sp^2 graphite impurities with formation of $>C=O$ groups in a C-sp^3 diamond structure. Addition of Fe(III) compounds to the electrolyte provoked the formation of an anodic wave on the cyclic voltammograms in the potential region that correlates with the generation of ferrate(VI). It is concluded that the direct electrochemical synthesis of Fe(VI) at a boron-doped diamond anode is possible because of the less positive potential of ferrate(VI), FeO_4^{2-}, formation with respect to the potential of the oxygen evolution reaction. The presence of ferrate(VI) in the electrolyte, formed after anodic polarization of the boron electrode in 10 M KOH electrolyte saturated with Fe(III) at 0.9 V against Hg/HgO electrode, was proven by UV–Vis spectrometry.

Key words: ferrate(VI); boron-doped diamond electrode; synthesis; alkaline electrolyte; cyclic voltammetry; UV–Vis spectrophotometry.

INTRODUCTION

Ferrate(VI) anion, FeO_4^{2-}, as a strong environmentally friendly oxidant, has already found numerous applications in environment friendly chemistry, particularly in the processes of polluted water treatment.[1,2] The ferrate(VI) aqueous alkaline solutions obtained by chemical or electrochemical synthesis are the most appropriate reactants for a treatment of a large number of water pollutants. However, ferrates (VI) quite rapidly oxidize water even in strong alkaline water solu-

---

tions and decompose to Fe(III), thereby gradually loosing their decontamination capacity. Hence, the direct electrochemical synthesis of ferrate(VI) in the decontaminating reactor by oxidation of Fe(III) compounds at a diamond electrode could solve many technical problems of its practical applications. This could be particularly suitable in cases of the water treatment processes where Fe(II) and Fe(III) salts are used to form Fe(III) hydroxide, an efficient absorbent, coagulant and flocculent, which can be used simultaneously as a reactant for the synthesis of ferrate(VI). The boron-doped diamond (BDD) is one of several suitable dimensionally stable electrode (DSE) materials, which could be utilized for electrochemical synthesis of ferrate(VI) from alkaline solutions of Fe(III) compounds, because of its high chemical and electrochemical stability in aggressive environment over a wide electrode potential range and wide potential difference between the oxygen evolution reaction (OER) and the hydrogen evolution reaction (HER) of more than 3 V and its relatively high electrical conductivity.[3–7]

As a corrosion resistant material, diamond retains its morphology and stability during long-term cycling between the hydrogen and oxygen evolution potentials in very aggressive media, even in acidic fluoride solutions.[7–9]

The BDD surface is also characterized by a low adsorption capacity, so the double-layer capacitance of diamond is up to one order of magnitude lower than that of glassy carbon.[7]

Therefore, conductive diamond is a promising DSE material and in the last decades, it has been used in the development of applications in three broad areas: *i*) electrochemical synthesis of inorganic and organic compounds; *ii*) polluted water treatment, which includes the purification of wastewater and the disinfection of drinking water and *iii*) electro-analysis and sensor technology.[3–21]

The electrochemical generation of ferrate(VI) by the transpassive anodic oxidation of iron in concentrated alkaline solutions has been studied extensively,[1] but the electrochemical generation of ferrate(VI) by oxidation of iron compounds at inert anodes has been much less explored.[12–15] Recently, the electrochemical generation of ferrate(VI) on diamond anodes by the oxidation of ferric and ferrous compounds from the alkaline and acid solutions at high anodic potentials was reported,[12–15,22] but the authors described the ferrate(VI) synthesis mechanism on diamond as a mediated oxidation of Fe(III) to Fe(VI) by electrochemically generated hydroxyl radicals at high anodic potential, because of the chemical inertness of diamond.[12–15]

The possibility of ferrate(VI) generation by a direct anodic oxidation of soluble iron compounds on a diamond electrode from alkaline solutions at lower anodic potentials, which correlates with ferrate(VI) generation by transpassive oxidation of iron, has not hitherto been reported in the relevant literature.

The object of this study was to explore a possibility of ferrate(VI) formation by the direct anodic oxidation of soluble iron(III) compounds on a boron-doped

diamond electrode in alkaline solutions at potentials lower than that of oxygen evolution.

EXPERIMENTAL

The electrode material, a highly boron-doped diamond layer produced by chemical vapor deposition (CVD) of diamond on a p-silicon wafer plate, was purchased from Element Six Ltd., UK. The synthetic diamond layer was 0.6 mm thick, doped with boron in a concentration $[B] > 10^{20}$ atoms cm^{-3} and with specific resistivity of 0.020–0.18 Ω cm.

The working electrode was made by fixing of the p-silicon substrate plate on which the BDD layer had been deposited to a copper plate current collector with conductive silver adhesive to secure electrical contact. The inactive back and lateral surfaces of the electrode are insulated from the electrolyte using chemically resistant epoxy resin. The area of the exposed active surface of the electrode was 1 cm^2.

The BDD electrode surface was washed with ethanol and rinsed with distilled water before each experiment.

The electrode potentials were measured against a red mercuric oxide (Hg|HgO) reference electrode filled with 10 M KOH electrolyte ($E_0 = 0.095$ V $vs.$ SHE) connected to the working electrode via a Luggin capillary electrolyte bridge.

The auxiliary electrode was a coiled platinum wire.

Cyclic voltammetry experiments were performed using a computer-controlled potentiostat–galvanostat PAR 273 and Gamry G300.

The electrolyte was prepared with p.a. grade chemicals in distilled water. Ferrous sulfate was used for electrolyte preparation because of its higher solubility with respect to those of ferric salts.

The electrolyte compositions labeled on the cyclic voltammetry diagrams denote initial electrolyte composition from which a particular electrolyte is prepared according to the following procedure.

The colloid suspension of Fe(OH)$_3$ (pK_s = 38 at 25 °C for [Fe(OH)$_3$] = 10 mM)[23] in concentrated alkaline solution, has been prepared before each experiment by oxidation of 10 M KOH solution saturated with ferrous sulfate by intensive aeration and agitation by means of a laboratory magnetic stirrer. The oxidation of ferrous hydroxide to ferric hydroxide follows change of the solution color from a pale greenish color of Fe(II) to an orange–brown color of Fe(III). Oxidation of the Fe(II) residues in the electrolyte is performed by addition of a stoichiometric quantity of hydrogen peroxide to the previously aerated solution. Finally, the electrolyte was stabilized for at least two hours before electrochemical experiments.

RESULTS AND DISCUSSION

Crystallography of BDD

The crystallography of the BDD electrode was examined by X-ray diffracttion, Fig. 1, recorded on a Philips PW 1710 X-ray analyzer, prior to and after electrochemical experiments to verify its stability in the experimental environment. The X-ray diffraction patterns illustrate that the main crystallographic parameters of the diamond electrode crystal lattice are generally unchanged after 10 h anodic polarization at $j = 100$ mA cm^{-2} in 10 M KOH solution, which confirmed the structural stability of the BDD material. However, both the decrease in

the intensity of the diffraction peaks and the slight increase in the lattice para-
meter indicated consumption of the electrode material after prolonged exploit-
ation, but during the short-time CV experiments used, the BDD electrode could
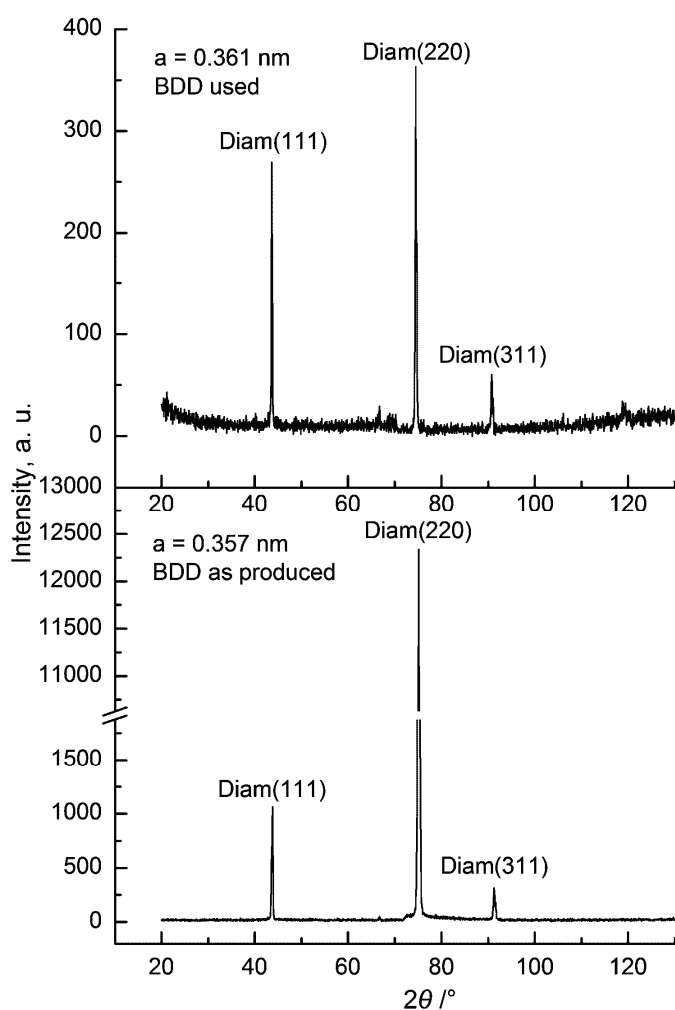be considered as stable.

Fig. 1. X-Ray diffraction pattern of the new and the BDD electrode after 10 h anodic
polarization at $j = 100$ mA cm^{-2}, θ – XRD diffraction angle, a – crystal lattice parameter.

Electrochemical behavior of the BDD electrode in 10 M KOH

The focus of the preliminary experimental work was the behavior of the
BDD electrode in the potential region between the OER and the HER in 10 M
KOH electrolyte free of iron ions.

The cyclic voltammograms in Fig. 2 show a steady decline of the anodic current peak, which appeared before the OER potential in the anodic scan direction. This behavior could be the result of the oxidation of inclusions at the diamond surface, C-sp^2 and >CH$_2$ groups. C-sp^2 groups are usually present in commercial highly boron-doped diamond because of the secondary carbon deposition during the doping process, while the >CH$_2$ groups are formed on the diamond during cathodic polarization.[7,23–27]
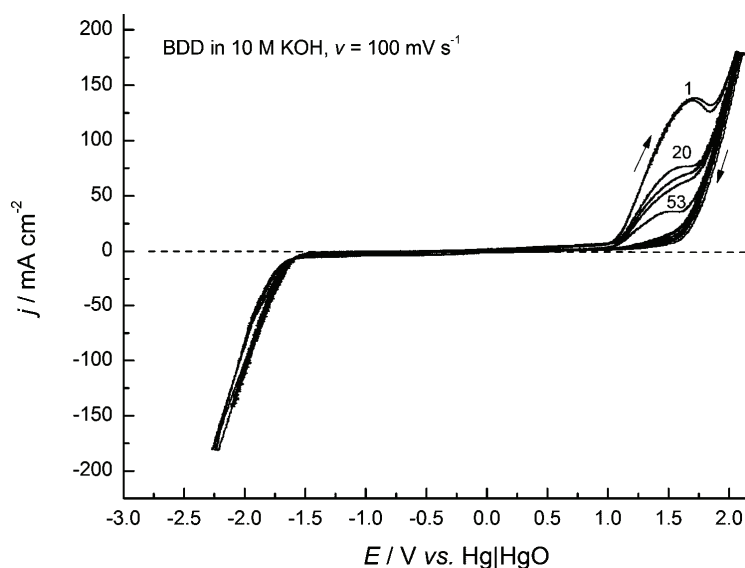
Fig. 2. Cyclic voltammogram of BDD in 10 M KOH, $v = 100$ mV s^{-1}, $E_0 = -0.5$ V *vs.* Hg|HgO after holding potential –1.2 V *vs.* Hg|HgO for 45 min, scan No. 1 to 53.

The cyclic voltammogram of the BDD electrode obtained after an anodic potential scan limit was set before the potential of the current peak is shown in Fig. 3. The gradual increase of the two peaks, A$_1$ and A$_2$, seen in the enlarged segment of cyclic voltammogram, reflects the incomplete anodic oxidation of the >CH$_2$ groups according to Eq. (1). The accumulation of >CH$_2$ groups on the diamond surface is an obvious result of the incomplete oxidation because of the anodic potential scan limit:[15–24]

$$>CH_2 + H_2O \rightleftarrows >C{=}O + 4H^+ + 4e^- \tag{1}$$

The results shown in Figs. 2 and 3 are comparable with data reported by Beck *et al.*[26,27], where the current peak on the cyclic voltammogram of a BDD electrode that appears at the anodic potential scan before the OER potential was explained as being the consequence of the oxidation of both the >CH$_2$ groups and the graphite impurities from the electrode surface.[26,27]

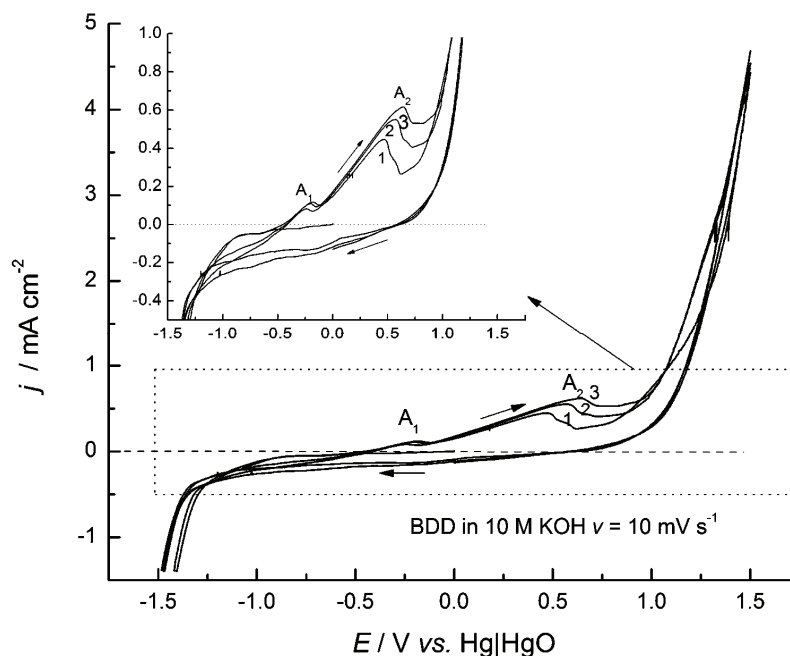Fig. 3. Cyclic voltammogram for BDD electrode in 10 M KOH solution in the cycle that was limited at an anodic potential before the OER, $v = 10$ mV s^{-1}.

The third possibility for the appearance of this anodic peak on the voltammogram shown in Fig. 2 would be a lower OER overvoltage on the C-sp^2 surface inclusions. Therefore, polarization of the BDD electrode at higher overpotential than the OER potential is required to oxidize and remove all of these impurities from the electrode surface.[7,26–39]

Electrochemical oxidation of Fe(III) on BDD

The initial conditions for the electrochemical synthesis of ferrate(VI) by anodic oxidation of ferric species on a BDD electrode in strong alkaline solution were explored by cyclic voltammetry in order to examine the influence of possible parallel processes, such as oxidation of >CH$_2$ and C-sp^2 and oxygen evolution, on ferrate(VI) production.[1,3–15]

The voltammograms in Fig. 4 show the effect of the presence of ferric compounds in the 10 M KOH alkaline solution on the behavior of the BDD electrode. The behavior of BDD electrode in pure solution is shown on CV (1), and behavior in the presence of Fe(III) species on CV (2). Obviously, Fe(III) species in the alkaline electrolyte provoked the appearance of a current hump or shoulder on the voltammogram (2) at anodic potentials higher than 0.7 V against the Hg|HgO electrode, which is less positive with respect to the potential of the OER in Figs. 2 and 3. Hence, this anodic wave could be the result of the oxidation of

the ferric species to ferrate(VI) precursors, *i.e.*, Fe(IV) or Fe(V), according to Eqs. (2) to (7),[40–49] because in the electrolyte preparation process, all ferrous species were oxidized to ferric species. Thus, there should be no doubt that the growth of the anodic current peak at potentials >0.7 V against the Hg|HgO reference electrode was the result of Fe(III) oxidation to higher valence states, Fe(IV) or Fe(V), which are quoted in the relevant literature as ferrate(VI) precursors.[1,22,40–49]
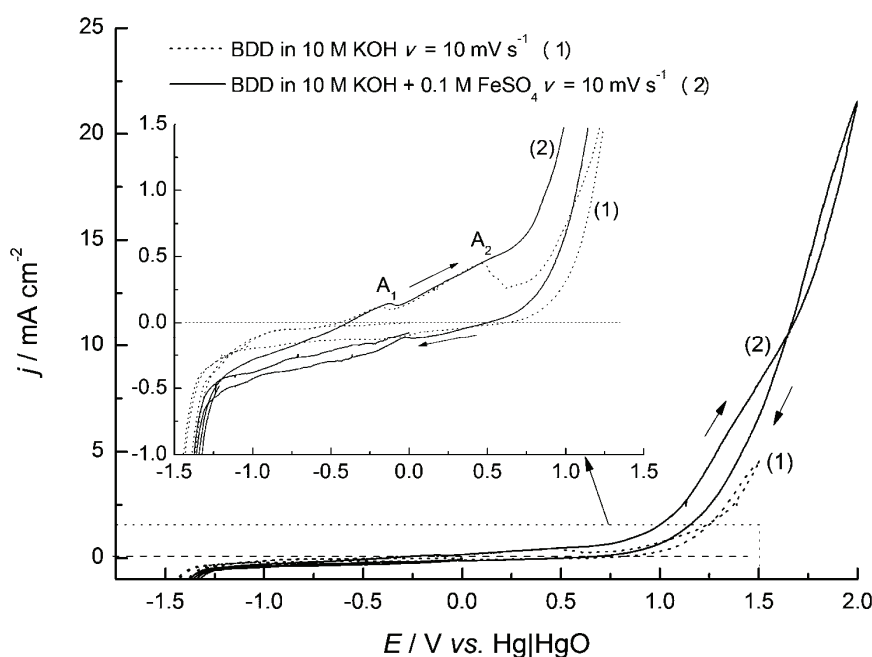

Fig. 4. Cyclic voltammograms of BDD in 10 M KOH (1) and in 10 M KOH + 0.1 M FeSO$_4$ (2), v = 10 mV s^{-1}.

The cyclic voltammogram of the BDD electrode in 5 M KOH electrolyte saturated with Fe(III) hydroxide, presented in Fig. 5, was obtained with a higher potential scan rate and more clearly demonstrates the possibility of ferrate(VI) synthesis at anodic potentials >0.7 V against the Hg|HgO reference. The current shoulder A$_2$ is in the potential region that correlates with ferrate(VI) generation, and the corresponding cathodic wave C$_2$ reflects the reduction of Fe(VI) to Fe(III) and wave C$_1$ reflects the reduction of Fe(III) to Fe(II).[40–49] The relatively low current density of the Fe(VI) reduction is the result of both ferrate(VI) migration from the electrode, which was observed during the experiment as a characteristic red–purple coloring of the solution in the vicinity of the BDD anode, and the decomposition of adsorbed ferrate(VI) in the reaction with water and Fe(III).[40–49]
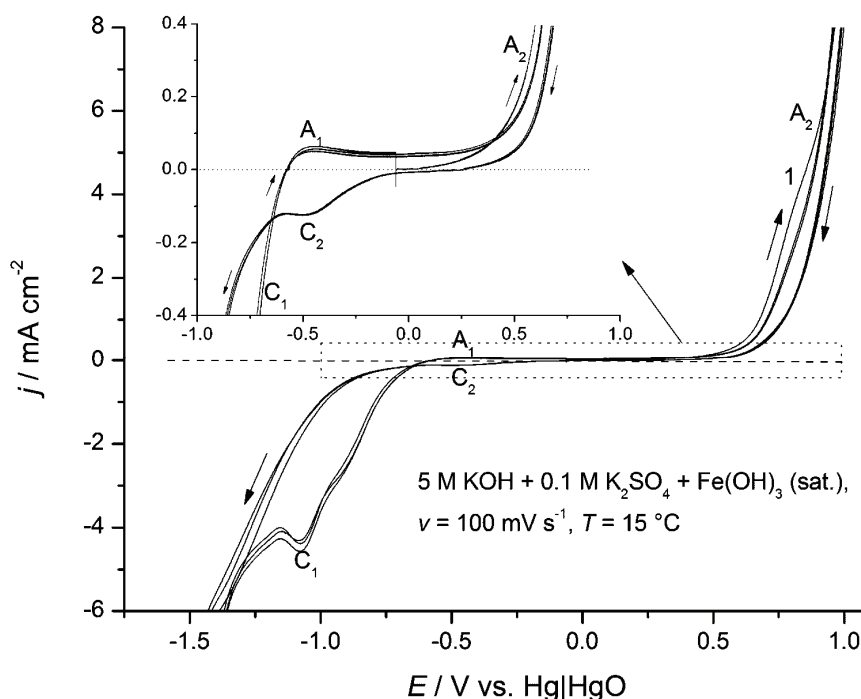
Fig. 5. Cyclic voltammograms of BDD in 5 M KOH + 0.1 M K_2SO_4 + Fe(OH)$_3$ (saturated suspension), v = 100 mV s^{-1}, T = 15 °C.

The cyclic voltammograms in Fig. 6 show the effect of 10 M KOH electrolyte saturated with Fe(OH)$_3$ on the behavior of the BDD electrode. The potential of the current shoulder on voltammogram (1) shows that Fe(III) compounds are oxidized with formation of ferrate(VI) (observed as a red–purple coloration of the electrolyte) at anodic potentials higher than +0.7 V *vs.* the Hg|HgO electrode, while, according to voltammogram (2), oxidation of >CH_2, >C=O and the OER on the BDD electrode commence at anodic potentials higher than 1 V. The shift of HER reaction potential more than 0.5 V towards positive potentials on the voltammogram (1) is a consequence of the lower HER overvoltage on deposited iron from iron containing electrolyte, with respect to voltammogram (2) of a clean BDD electrode obtained in an iron-free electrolyte.

The cathodic current peak that appears within the potential region between –200 and –500 mV *vs.* the Hg|HgO reference electrode that is seen on the voltammograms in Figs. 4, 5 and 7, reflects the reduction of ferrate(VI) ions to Fe(III). Namely, the results from the relevant literature show that these current peaks were recorded only if ferrate(VI) had been detected in the electrolyte.[1,22,40–59] The potential region where the ferrate(VI) reduction peak appears depends on numerous variables, such as the electrode material, the electrolyte pH value, the

ferrate(VI) concentration at the electrode surface, the transport of electrode reactants, rate of potential scan, *etc*.[40–49]
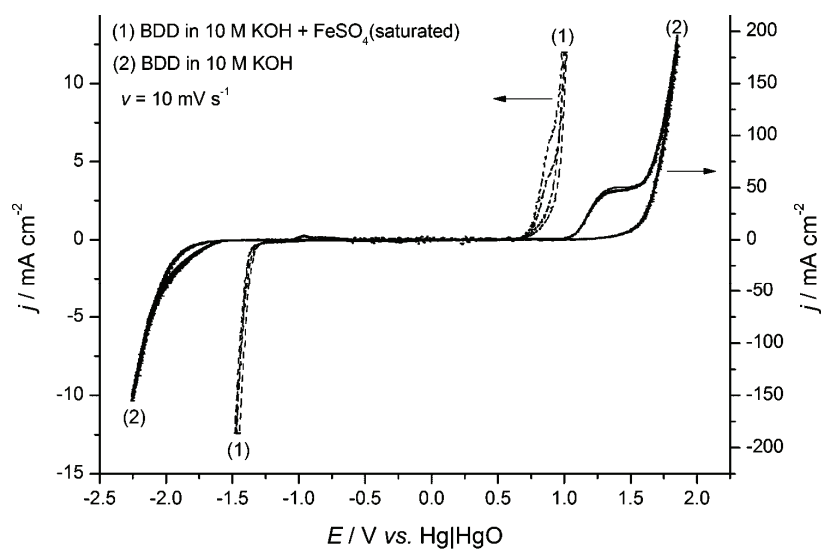

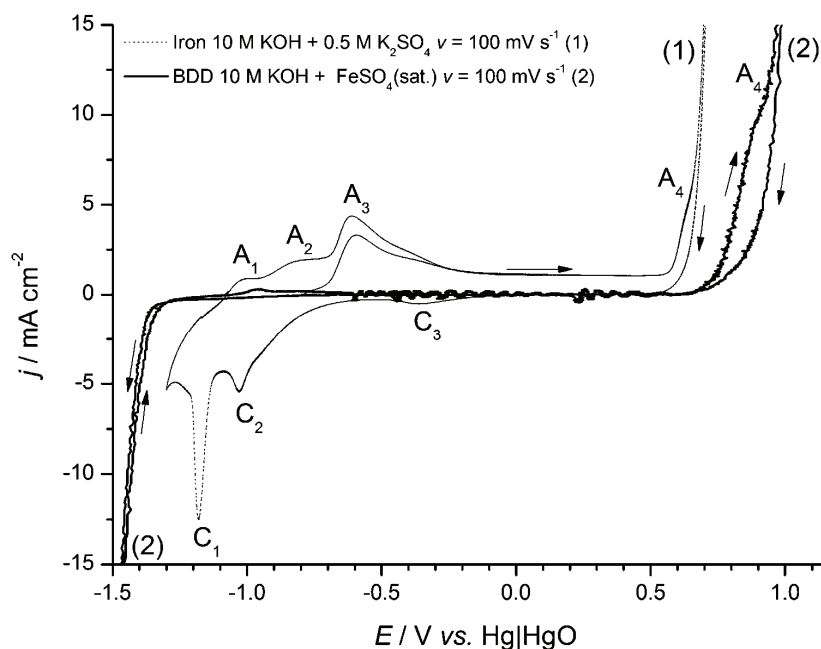Fig. 6. Cyclic voltammogram of BDD in (1) 10 M KOH saturated with $FeSO_4$ and (2) 10 M KOH, $v = 10$ mV s^{-1}.

Fig. 7. Cyclic voltammograms of BDD in 10 M KOH + $FeSO_4$ (saturated) and ARMCO iron (99.99 % Fe) in 10 M KOH, obtained at $v = 100$ mV s^{-1}.

The potentials of the current peaks in the region of the ferrate(VI) generation potential shown in Figs. 4–6 are compatible with the results obtained for the anodic oxidation of FeO_2^- at an SnO_2–Sb_2O_3/Ti electrode,[48] where the authors explained the possibility of ferrate(VI) synthesis at inert electrodes by direct oxidation of ferric compounds.

The cyclic voltammograms in Fig. 7 are given to compare the behavior of an iron electrode in 10 M KOH + 0.5 M K_2SO_4 with behavior of the BDD electrode in 10 M KOH electrolyte saturated with soluble ferric species and aid the discussion concerning the mechanism of ferrate(VI) formation at inert anodes. The current waves or shoulders A_4 of ferrate (VI) formation are visible on both voltammograms in Fig. 7. The cathodic current peaks, C_3 of Fe(VI) to Fe(III) reduction, C_2 of Fe(III) to Fe(II) reduction and C_1 that correspond to Fe(II) to Fe(0) reduction are visible only on the iron electrode voltammogram.[40–49] Peak A_1 at the potential of iron oxidation to Fe(II) was noticed on both voltammograms. Peaks A_2 and A_3, which correlate with the formation of higher valence state iron compounds are seen just on the Fe voltammogram, because ferric compounds are already present in the electrolyte from which ferrate(VI) is formed at a diamond electrode.[40–49]

The overpotential of ferrate(VI) formation by direct anodic oxidation of Fe(III) on a BDD electrode was shifted anodically by approximately 0.2 V with respect to synthesis by transpassive anodic oxidation of iron, as a consequence of a limited availability of soluble Fe(III) reactants at the BDD electrode.[12–15,22,40–49] That is, the rate of ferrate(VI) generation at inert anodes is limited by a low concentration of soluble Fe(III) compounds and hence its low migration rate towards the electrode.

Due to the low solubility product constant of $Fe(OH)_3$, 2.79×10^{-39} in pH 8 solutions, the electrochemical generation of Fe(VI) by oxidation of Fe(III) at a BDD seems improbable, but in solutions with high a concentration of OH^-, $Fe(OH)_3$ and FeOOH behave like weak acids and succumb to acidic ionization according to Eqs. (2) and (3) with the formation of FeO_2^-, the most soluble form of Fe(III).[12–15,40–50] The concentration of FeO_2^- can reach the considerably large values of 0.02 M in 14 M NaOH in the presence of oxidants,[48] which would also be the case in this study because of an oxidative environment:

$$2Fe(OH)_3 + 2OH^- \rightleftarrows 2FeO_2^- + 4H_2O \qquad (2)$$

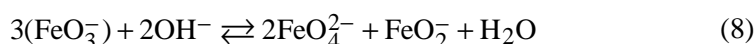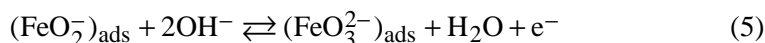$$FeOOH + OH^- \rightleftarrows FeO_2^- + H_2O \qquad (3)$$
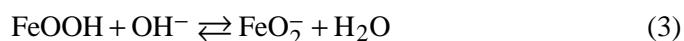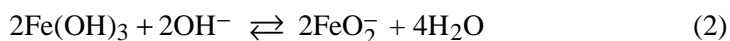
As BDD is a rather inert anode material with low adsorption capacity,[3–15] the adsorption rate of reacting Fe(III) species on the BDD surface, Eq. (4), also controls the rate of ferrate(VI) synthesis:

$$(FeO_2^-)_{sol} \rightleftarrows (FeO_2^-)_{ads} \qquad (4)$$

According to the relevant literature, FeO_2^- will be oxidized in strong alkaline solutions to $Fe^{IV}O_3^{2-}$ according to Eq. (5) or $Fe^{V}O_3^-$ according to Eq. (7), depending on the experimental conditions.[12–15,45–50]

The precursors $Fe^{IV}O_3^{2-}$ and $Fe^{V}O_3^-$ finally disproportionate to ferrate(VI) – $Fe^{VI}O_4^{2-}$ and ferrate(III) – $Fe^{III}O_2^-$, in the processes given by Eqs. (6) and (8), respectively.

$$(FeO_2^-)_{ads} + 2OH^- \rightleftarrows (FeO_3^{2-})_{ads} + H_2O + e^- \tag{5}$$

$$2(FeO_3^{2-})_{ads} \rightleftarrows FeO_4^{2-} + FeO_2^- \tag{6}$$

$$(FeO_2^-)_{ads} + 2OH^- \rightleftarrows (FeO_3^-)_{ads} + H_2O + 2e^- \tag{7}$$

$$3(FeO_3^-) + 2OH^- \rightleftarrows 2FeO_4^{2-} + FeO_2^- + H_2O \tag{8}$$

Adsorption of sulfates, which are formed in the hydrolysis process of ferrous salts, at a BDD electrode may have some weak effect on the adsorbed Fe(III) oxide structure,[50] but as the oxidation of sulfate starts at higher positive potentials than the potential of ferrate(VI) generation, this would not influence its generation.[7,3–21]

At cathodic polarization, ferrate(VI) is reduced to Fe(III) according to reaction given by Eq. (9):

$$FeO_4^{2-} + 2H_2O + 3e^- \rightleftarrows 4OH^- + FeO_2^- \tag{9}$$
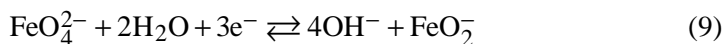
Although ferrate(VI) is relatively stable in strong alkaline solutions, cathodic ferrate(VI) small reduction current peaks on the cyclic voltammograms of BDD Figs. 4, 5 and 7 were visible. This could be a consequence of ferrate(VI) migration from the inert anode and the catalytic effect of FeO_2^- present in the electrolyte on its decomposition, according to the reversible reactions given by Eqs. (6) and (8), and of water oxidation, according to Eq. (10), which together cause a considerable decrease in the surface concentration of ferrate(VI):[1,12–14,22,40–49]

$$4FeO_4^{2-} + 10H_2O \rightleftarrows 4Fe(OH)_3 + 3O_2 + 8OH^- \tag{10}$$
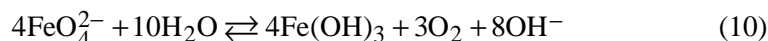
The formation of the ferrate(VI) by anodic oxidation of ferric compounds at the BDD electrode in strong alkaline solution was confirmed by the UV–Vis absorbance spectra of the ferrate(VI) solutions. The UV–Vis absorbance spectrum of a 0.03 mM FeO_4^{2-} solution in 10 M KOH is presented in Fig. 8, on which the characteristic absorbance peak of FeO_4^{2-} at 504 nm is obvious.[51] The 0.03 mM FeO_4^{2-} ferrate(VI) solution was prepared by the anodic polarization of the BDD electrode for 2 h at a potential of 0.9 V *vs.* the Hg|HgO reference electrode in 10 M KOH electrolyte saturated with Fe(OH)$_3$ with an average current intensity of 10 mA. A current efficiency of 25 % was determined by the chromite analytical method.[52–53]

The experimental results and the discussion on a possible mechanism of ferrate(VI) electrochemical synthesis at inert anodes given in this study disagree with the results and discussion of Sánchez-Carretero *et. al.*,[14,15] who explained the formation of ferrate(VI) at a BDD electrode as the result of a mediated Fe(III) oxidation by hydroxyl radicals at high anodic potentials. The results of this study show that an anodic synthesis of ferrate(VI) at a BDD is possible at a lower anodic potential with respect to the potential of the OER. In addition, the formation of hydroxyl radicals is only possible at anodic potential higher than the potential of the OER,[7,36–39] and, especially, higher than the overpotential of Fe(III) oxidation and ferrate(VI) formation.[40–49] Moreover the electro-chemical generation of hydroxyl radicals at BDD electrode pH >9 electrolytes was not evidenced.[39]
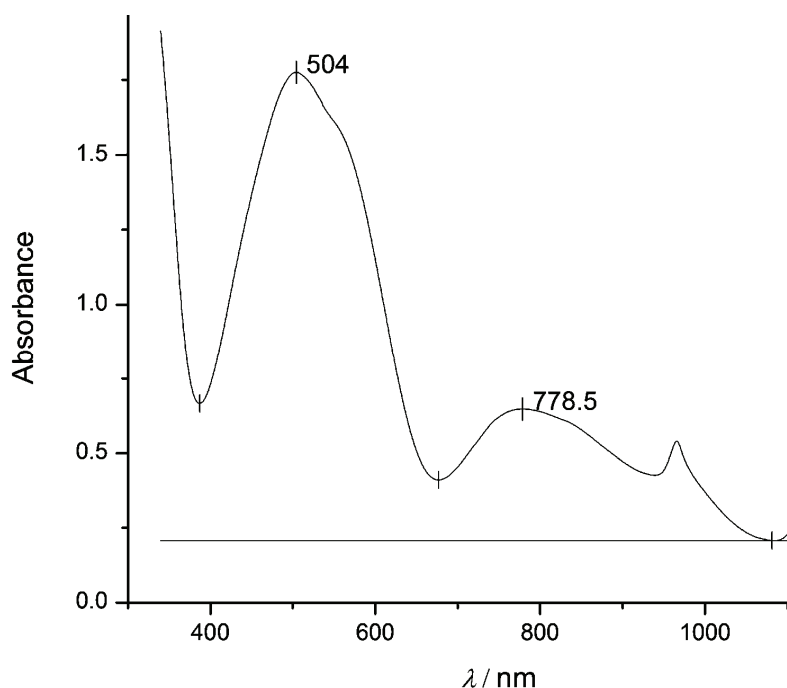

Fig. 8. UV–Vis Absorbance spectra of the ferrate(VI) solution obtained by anodic oxidation of saturated Fe(III) alkaline solution 10 M KOH on BDD electrode at 0.9 V *vs.* Hg|HgO for 2 h and $I \approx 10$ mA. λ is the wavelength.

CONCLUSIONS

The possibility of the direct electrochemical synthesis of ferrate(VI) by oxidation of Fe(III) species in a 10 M KOH solution on a BDD anode was explored by cyclic voltammetry.

The influences of factors such as the surface coverage of the BDD electrode with >CH$_2$ and >C=O, the overpotential of oxygen evolution, as well as the rates

of formation, transport and adsorption on the BDD of soluble Fe(III) compounds, such as FeO_2^-, on the anodic synthesis of ferrate(VI) have been discussed.

Ferrate(VI) formation by direct oxidation of soluble Fe(III) compounds on a BDD electrode is possible at a lower anodic potential with respect to the oxygen evolution reaction potential.

Formation of ferrate(VI) by anodic oxidation of Fe(III) from strong alkaline solution at a BDD electrode was confirmed by the characteristic peak of ferrate(VI) in the UV–Vis absorbance spectra of the synthesized ferrate(VI) solution.

ИЗВОД

СИНТЕЗА ФЕРАТА(VI) НА БОРИРАНОЈ ДИЈАМАНТСКОЈ ЕЛЕКТРОДИ ИЗ НЕУТРАЛНИХ И АЛАКАЛНИХ ЕЛЕКТРОЛИТА

МИЛАН ЧЕКЕРЕВАЦ[1], ЉИЉАНА НИКОЛИЋ-БУЈАНОВИЋ[1], АЊА ЈОКИЋ[2] и МИЛОШ СИМИЧИЋ[1]

[1]*IHIS Techno-experts, Батајнички пут 23, 11080 Београд и* [2]*Универзитет у Приштини, Природно–математички факултет, Косовска Митровица*

Испитивана је оксидација једињења гвожђа на борираној дијамантској електроди у алкалном електролиту 10 M KOH методом цикличне волтаметрије, између потенцијала реакције издвајања водоника и потенцијала реакције издвајања кисеоника, са циљем електрохемијске синтезе фервата (VI). Показано је да врхови анодних струја који се јављају у електролиту без гвожђа при мање позитивним потенцијалима од потенцијала реакције издвајања кисеоника, вероватно одговарају оксидацији >CH2 група и C-sp2 графитних нечистоћа уз настајање >C=O група у C-sp3 дијамантској структури. Додатак Fe(III) једињења у електролит изазива формирање анодног таласа на цикличним волтамограмима у области потенцијала који одговара настајању фервата(VI). Закључено је да је директна електрохемијска синтеза Fe(VI) једињења на борираној дијамантској аноди могућа услед мање позитивног потенцијала формирања фервата(VI) у односу на потенцијал реакције издвајања кисеоника. Присуство фервата(VI) формираног након анодне поларизације бориране дијамантске електроде у електролиту 10 M KOH засићеном једињењима Fe (III) на 0,9 V у односу на Hg|HgO електроду доказано је UV–Vis спектрометријом.

(Примљено 9. марта, ревидирано 16. октобра 2012)

REFERENCES

1. V. K. Sharma. Ed., *Ferrates, ACS Symposium Series* 985, American Chemical Society, Washington, DC, USA, 2008
2. M. I. Čekerevac, L. N. Nikolić-Bujanović, M. B. Mirković, N. H. Popović, *Hem. Ind.* **64** (2010) 423

3. G. M. Swain, A. B. Anderson, J. C. Angus, *MRS Bull.* **23** (1998) 56
4. H. B. Martin, A. Argoitia, U. Landau, A. B. Anderson, J. C. Angus, *J. Electrochem. Soc.* **143** (1996) 133
5. M. Panizza, G. Cerisola, *Electrochim. Acta* **51** (2005) 191
6. A. Kraft, *Int. J. Electrochem. Sci.* **2** (2007) 355
7. B. Marselli, *Electrochemical oxygen transfer reaction on Synthetic boron-doped diamond thin film electrode,* Thèse No. 3057, École Polytechnique Fédérale de Lausanne, Lausanne, 2004
8. G. M. Swain, *J. Electrochem. Soc.* **141** (1994) 3382
9. R. Ramesham, M. F. Rose, *Diamond Relat. Mater.* **6** (1997) 17
10. G. M. Swain, *Adv. Mater.* **5** (1994) 388
11. G. M. Swain, R. Ramesham, *Anal. Chem.* **65** (1993) 345
12. P. Cañizares, M. Arcís, C. Sáez, M. A. Rodrigo, *Electrochem. Commun.* **9** (2007) 2286
13. C. Sáez, M. A. Rodrigo, P. Cañizares, *AIChE J.* **54** (2008) 1600
14. A. Sánchez-Carretero, M. A. Rodrigo, P. Cañizares, C. Sáez, *Electrochem. Commun.* **12** (2010) 644
15. A. Sānchez-Carretero, C. Sáez, P. Cañizares, S. Cotillas, M. A. Rodrigo, *Ind. Eng. Chem. Res.* **50** (2011) 7073
16. K. Arihara, C. Terashima, A. Fujishima, *Electrochem. Solid-State Lett.* **9** (2006) D17
17. A. Kraft, M. Stadelmann, M. Wünsche, M. Blaschke, *Electrochem. Comm.* **8** (2006) 883
18. P. A. Michaud, E. Mahe, W. Haenni, A. Perret, C. Comninellis, *Electrochem. Solid-State Lett.* **3** (2000) 77
19. T. Lehmann, P. Stenner, Degussa A.G., Düsseldorf (DE), US Patent 6503386 (2003)
20. C. Comninellis, P. A. Michaud, W. Haenni, A. Perret, M. Fryda, US Patent 6855242 (2005)
21. M. Panizza, I. Duo, P. A. Michaud, G. Cerisola, C. Comninellis, *Electrochem. Solid-State Lett.* **3** (2000) 550
22. J. Lee, D. A. Tryk, A. Fujishima, S.-M. Park, *Chem. Commun.* (2002) 486
23. J. Duan, J. Gregory, *Adv. Colloid Interface Sci.* **100–102** (2003) 475
24. M. S. Saha, T. Furuta, Y. Nishiki, *Electrochem. Solid-State Lett.* **6** (2003) D5
25. P. Cañizares, F. Larrondo, J. Lobat, M. A. Rodrigo, C. Sáez, *J. Electrochem. Soc.* **152** (2005) D191.
26. F. Beck, H. Krohn, W. Kaiser, M. Fryda, C. P. Klages, L. Schäfer, *Electrochim. Acta* **44** (1998) 525
27. F. Beck, W. Kaiser, H. Krohn, *Electrochim. Acta* **45** (2000) 4691
28. I. Yagi, H. Notsu, T. Kondo, D. A. Tryk, A. J. Fujishima, *J. Electroanal. Chem.* **473** (1999) 173
29. K. Hayashi, S. Yamanaka, H. Watanabe, T. Sekiguchi, H. Okushi, K. Kajimura, *J. Appl. Phys.* **81** (1997) 744
30. M. C. Granger, G. M. Swain, *J. Electrochem. Soc.* **146** (1999) 4551
31. M. C. Granger, M. D. Koppang, M. Witek, J. E. Butler, J. Xu, G. Lucazeau, J. Wang, M. Hupert, M. Mermoux, A. Hanks, J. W. Strojek, G. M. Swain, *Anal. Chem.* **72** (2000) 3793
32. N. Simon, H. Girard, D. Ballutaud, S. Ghodbane, A. Deneuville, M. Herlem, A. Etcheberry, *Diamond Relat. Mater.* **14** (2005) 1179
33. J. Ristein, *Appl. Phys., A* **82** (2006) 377
34. J. H. T. Luong, K. B. Male, J. D. Glennon, *Analyst* **134** (2009) 1965

35. V. Chakrapani, S. C. Eaton, A. B. Anderson, M. Tabib-Azar, J. C. Angus, *Electrochem. Solid-State Lett.* **8** (2005) E4
36. K. J. McKenzie, F. Marken, *Electrochem. Solid-State Lett.* **5** (2002) E47
37. I. Duo, A. Fujishima, C. Comninellis, *Electrochem. Commun.* **5** (2003) 695
38. K. Serrano, P. A. Machaud, C. Comniellis, A. Savall, *Electrochim. Acta* **48** (2002) 431
39. T. A. Enache, A. M. Chiorcea-Paquim, O. Fatibello-Filho, A. M. Oliveira-Brett, *Electrochem. Commun.* **11** (2009) 1342
40. S. Venkatadri, W. F, Wagner, H. H. Bauer, *Anal. Chem.* **43** (1971) 1115
41. F. Beck, R. Kaus, M. Oberst, *Electrochim. Acta* **30** (1985) 173
42. K. Bouzek, I. Roušar, *J. Appl. Electrochem.* **23** (1993) 1317
43. K. Bouzek, I. Roušar, H. Bergmann, K. Hertwig, *J. Electroanal. Chem.* **425** (1997) 125
44. M. De Koninck, D. Belanger, *Electrochim. Acta* **48** (2003) 1435
45. M. I. Čekerevac, L. N. Nikolić-Bijanović, M. V. Simičić, *Hem. Ind.* **63** (2009) 387
46. Z. Mácova, K. Bouzek, V. K. Sharma, *J. Appl. Electrochem.* **40** (2010) 1019
47. Z. A. Mácová, K. Bouzek, *J. Appl. Electrochem.* **41** (2011) 1125
48. C.-Z. Zhang, Z. Liu, F. Wu, L.-J. Lin, F. Qi, *Electrochem. Commun.* **6** (2004) 1104
49. H. B. Shao, J. M. Wang, W. C. He, J. Q. Zhang, C. N. Cao, *Electrochem. Commun.* **7** (2005) 1429
50. R. M. Cornell, U. Schwertmann, *The Iron Oxides: Structure Properties Reactions Occurrences and Uses*, Wiley-VCH, Weinheim, Germany, 2003, p.p. 3, 221–252
51. S. Licht, V. Naschitz, L. Halperin, N. Halperin, L. Lin, J. Chen, S. Ghosh, B. Liu, *J. Power Sources* **101** (2001) 167
52. J. M. Schreyer, L. T. Ockerman, *Anal. Chem.* **23** (1951) 1312
53. W. F. Wagner, J. R. Gump, E. N. Hart, *Anal. Chem.* **24** (1952) 1497.

Journal of the Serbian Chemical Society

Electrochemical behavior of labetalol at an ionic liquid-modified carbon paste electrode and its electrochemical determination

YAN-MEI ZHANG[1], CHENG-QIAN DUAN[1,2] and ZUO-NING GAO[1]*

[1]*College of Chemistry and Chemical Engineering, Ningxia University, Yinchuan, 750021, China and* [2]*Higher Vocational College of Ningxia Medical University, Yinchuan, 750004, China*

Abstract: The electrochemical behavior of labetalol (LBT) at a carbon paste electrode (CPE) and an ionic liquid 1-benzyl-3-methylimidazole hexafluorophosphate ([BnMIM]PF$_6$) modified carbon paste electrode ([BnMIM]PF$_6$/CPE) in Britton–Robinson buffer solution (pH 2.0) was investigated by cyclic voltammetry (CV) and square wave voltammetry (SWV). The experimental results showed that LBT at both the bare CPE and [BnMIM]PF$_6$/CPE showed an irreversible oxidation process, but at [BnMIM]PF$_6$/CPE its oxidation peak current increased greatly and the potential shifted negatively. The electrode reaction process is diffusion-controlled involving a one-electron transfer accompanied by the participation of one proton at [BnMIM]PF$_6$/CPE. In addition, the electrochemical kinetic parameters were determined. Under the optimized electrochemical experimental conditions, the oxidation peak currents were proportional to LBT concentration in the range of 7.0×10^{-6}–1.0×10^{-4} mol L^{-1} with a limit of detection (*LOD*, *S*/*N*=3) of 4.810×10^{-8} mol L^{-1} and a limit of quantification (*LOQ*, *S*/*N* = 10) of 1.60×10^{-7} mol L^{-1}. The proposed method was successfully applied in the determination of the LBT content in commercial tablet samples.

Keywords: labetalol; carbon paste electrode; ionic liquid; electrochemical determination.

INTRODUCTION

Labetalol (LBT) (structure formula is shown in Fig. 1) is used in the treatment of hypertension, now clinically. It is most commonly prescribed as a first line agent for the treatment of hypertensive disorders of pregnancy, including pre-eclampsia.[1] Due to its clinical importance, many analytical techniques has been developed for its determination, including high performance liquid chromatography (HPLC),[2,3] liquid chromatography coupled with mass spectrometry

---

(LC–MS),[4] capillary electrophoresis (CE),[5,6] spectrophotometry[7] and electrochemical methods.[8,9] Among the cited electrochemical methods, they mainly discuss the voltammetric determination of LBT in pharmaceuticals and the spiked human urine at a bare carbon paste electrode[8] and the performance characteristics of labetalol-H on an ion selective membrane electrode.[9] However, its electrochemical behaviors, electrochemical kinetics and electrochemical determination at an ionic liquid 1-benzyl-3-methylimidazole hexafluorophosphate ([BnMIM]PF$_6$) modified carbon paste electrode ([BnMIM]PF$_6$/CPE) have not hitherto been reported.
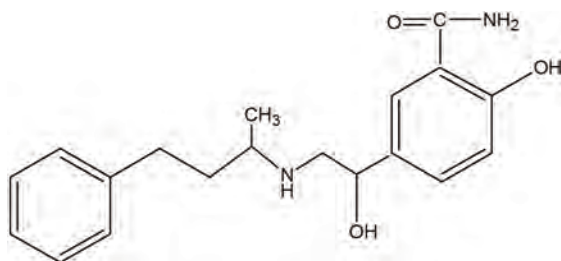

Fig. 1. The structure of labetalol (LBT).

Ionic liquids (ILs) are ionic compounds consisting of organic cations and various kinds of anions, which are liquids at temperatures around 298 K and below. ILs have a number of valuable properties, such as high ionic conductivity, electrochemical thermal stability, negligible vapor pressure and wider electrochemical windows, *etc*.[10,11] Due to their nature, ILs are non-flammable, non-volatile and non-hazardous, which makes them attractive as "green" solvents for many chemical processes on both the industrial and laboratory scale. Meanwhile, they have been widely used as a modifier or binder to fabricate electrodes in the research field of electrochemistry.

As continuations of previous work,[12–15] an IL/CPE was fabricated using 1-benzyl-3-methylimidazole hexafluorophosphate ([BnMIM]PF$_6$) as a modifier and characterized by both cyclic voltammetry (CV) and electrochemical impedance spectroscopy (EIS). The electrochemical behaviors and the electrochemical determination of LBT were investigated at both bare a CPE and [BnMIM]PF$_6$/CPE by CV and the square wave voltammetry (SWV). Its electrochemical kinetic parameters were also determined. Meanwhile, an electrochemical quantitative determination was established which was successfully employed for the determination of LBT content in commercial tablet samples.

EXPERIMENTAL

Apparatus

All electrochemical experiments were performed using an electrochemistry workstation CHI660A (CHI Instrument, USA). A conventional three-electrode system was used, which included a carbon paste electrode (CPE) and 1-benzyl-3-methylimidazole hexafluorophos-

phate ([BnMIM]PF$_6$)-modified carbon paste electrode ([BnMIM]PF$_6$/CPE) as working electrodes, a saturated calomel electrode (SCE) as the reference electrode, and a platinum wire as the auxiliary electrode. All the electrochemical experiments were performed at room temperature with a high purity nitrogen purge for 5 min before the experiments. All potentials measured and reported in this work are *vs.* a SCE.

Chemicals and reagents

Labetalol (batch No. 32780-64-6, purity 99 %) was purchased from Shanghai CpG Biotech Co., Ltd. (Shanghai, China) and used without further purification. LBT tablets (batch No. 110102) were purchased from Jiangsu Tianhe Disainuo Pharmaceutical Co. Ltd. (Jiangsu, China). 1-Benzyl-3-methylimidazole hexafluorophosphate ([BnMIM]PF$_6$) was purchased from Chengjie Chemical Reagent Co., Ltd. (Shanghai, China, Purity 99 %). All of the other chemicals were of analytical grade and double distilled water was used throughout this work.

Preparation of CPE and [BnMIM]PF$_6$/CPE

The bare CPE was prepared by thoroughly mixing 1.2 g of graphite with 0.40 mL of paraffin oil in a mortar to form a homogeneous carbon paste. A portion of the carbon paste was filled firmly into one end of a polytetrafluoroethylene (PTFE) tube, and a copper wire was inserted through the opposite end to establish an electrical contact. The surface of the CPE was polished on a piece of weighing paper to obtain a smooth surface just before use.

The [BnMIM]PF$_6$/CPE was fabricated by dissolving 0.60 g of [BnMIM]PF$_6$ in 0.60 mL of *N*,*N*-dimethylformamide (DMF), and then added in 1.20 g of graphite powder in a mortar, ground until the DMF had totally volatilized, and finally mixed with 0.60 mL of paraffin oil in a mortar. A portion of the so-obtained carbon paste was processed in the same manner as the pure carbon paste.

RESULTS AND DISCUSSION

Characterization of the electrodes

Electrochemical behaviors of the bare CPE and [BnMIM]PF$_6$/CPE were first investigated by CV using K$_3$[Fe(CN)$_6$] as a redox probe. The cyclic voltammograms of both the electrodes in a solution containing 5.0×10^{-3} mol L^{-1} K$_3$[Fe(CN)$_6$] in 1.0 mol L^{-1} KCl in the potential range –0.30 to 0.60 V are shown in Fig. 2. The cyclic voltammogram curve of the bare CPE (Fig. 2, curve a) exhibited a pair of well-defined voltammetric peaks with a cathodic peak potential (E_{pc}) of 0.158 V and an anodic peak potential (E_{pa}) of 0.311 V. The peak-to-peak separation (ΔE_p) is 153 mV. The cyclic voltammogram curve of [BnMIM]PF$_6$/CPE, with an E_{pc} of 0.189 V, E_{pa} of 0.272 V and ΔE_p of 83 mV, is presented in Fig. 2, curve b. Compared with the bare CPE, the redox peak currents of [BnMIM]PF$_6$/CPE were increased dramatically and the peak-to-peak separation obviously decreased. Simultaneously, the peak current ratio R (I_{pa}/I_{pc}) is 1.053, suggesting a reversible electron transference process. The results indicated that the good conducting property of ILs could greatly promote the electron transference rate of [Fe(CN)$_6$]$^{3-}$.

For further characterization of the electrodes, electrochemical impedance spectroscopy (EIS) was used. EIS could reflect the surface properties of the mo-
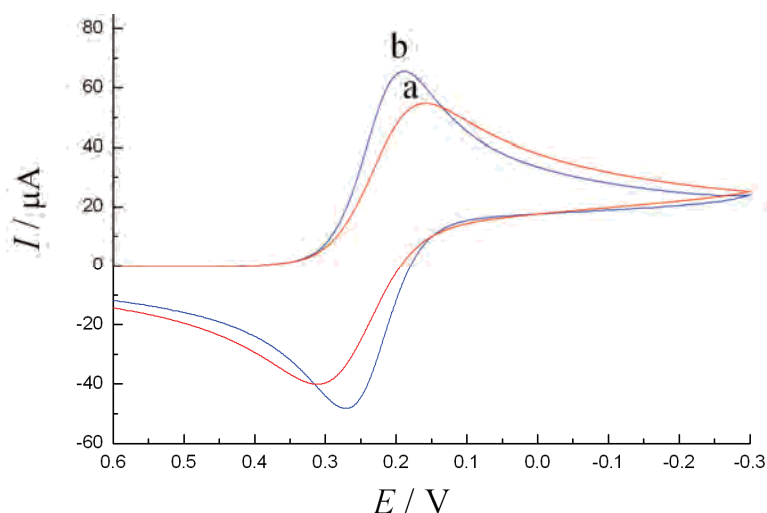
Fig. 2. CVs of the CPE (a) and the [BnMIM]PF$_6$/CPE (b) in 5.0×10^{-3} mol L^{-1} K$_3$[Fe(CN)$_6$] + 1.0 mol L^{-1} KCl. Scan rate: 50 mV s^{-1}.

dified electrodes[16] using the [Fe(CN)$_6$]$^{3-/4-}$ redox couple as an electrochemical probe. The EIS spectra consisted of two sections: one is the linear part at lower frequencies, representing a diffusion-limited process; the other one is a semicircle portion observed at higher frequencies, corresponding to an electron-transfer-limited process.[17] Generally, the diameter of the semicircle is usually equal to the resistance to electron transfer (R_{et}).[18] The Nyquist diagrams of 5.0×10^{-3} mol L^{-1} [Fe(CN)$_6$]$^{3-/4-}$ in 1.0 mol L^{-1} KCl solution at the different electrodes in the frequency range from 1 Hz to 100 kHz are shown in Fig. 3. The bare CPE (Fig. 3, curve a) exhibited a large semicircle in the high frequencies range with a large resistance of electron transference (R_{et}), suggesting a sluggish electrochemical performance of the redox probe on the bare CPE. This might be due to the presence of nonconductive paraffin oil in the carbon paste, which played an important role in hindering the electron transfer and made it more difficult for the electron transfer reaction to occur. Meanwhile, the nonconductive paraffin oil increased the resistance of the Fe(CN)$_6$$^{3-/4-}$ redox couple. However, the [BnMIM]PF$_6$/CPE (Fig. 3, curve b) showed a quasi-semicircle portion of much smaller diameter in the high frequencies range, which was attributed to the good ionic conductivity of ILs and the lower resistance to electron transfer of the [BnMIM]PF$_6$/CPE.[10,11] At low frequencies, [BnMIM]PF$_6$/CPE presented a linearity with a larger slope than that of the bare CPE, which is a characteristic of a diffusion-limited electrochemical process. The experimental results of EIS confirmed that the [BnMIM]PF$_6$/CPE could effectively promote the electron transference rate of [Fe(CN)$_6$]$^{3-/4-}$ and showed properties very different from those of the bare CPE.
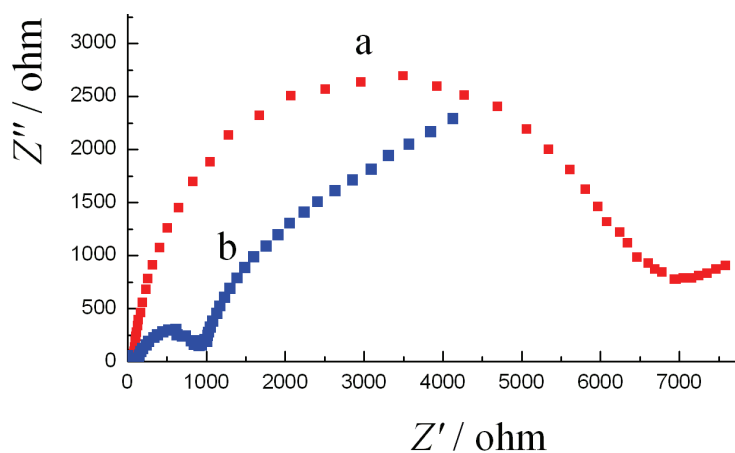
Fig. 3. EIS for the CPE (a) and the [BnMIM]PF$_6$/CPE (b) in 5.0×10^{-3} mol L^{-1} [Fe(CN)$_6$]$^{3-/4-}$ + 1.0 mol L^{-1} KCl. Frequency range: 1–10^5 Hz.

Cyclic voltammetric behavior of LBT

The electrochemical behaviors of 1.0×10^{-4} mol L^{-1} LBT at both the bare CPE and [BnMIM]PF$_6$/CPE were investigated by CV at a scanning rate of 100 mV s^{-1} in Britton–Robinson buffer solution (pH 2.0) over the potential range between 0.20 and 1.20 V (Fig. 4). From Fig. 4, curve a, it can be seen that no
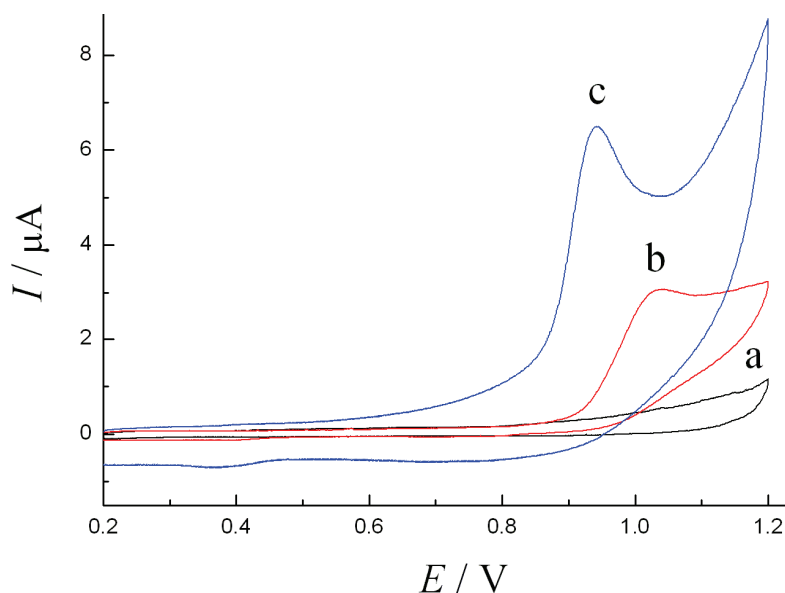

Fig. 4. CVs of the CPE in Britton–Robinson buffer solution (pH 2.0) in the absence (a) and the presence of 1.0×10^{-4} mol L^{-1} LBT (b) and of the [BnMIM]PF$_6$/CPE in the presence of 1.0×10^{-4} mol L^{-1} LBT (c). Scan rate: 100 mV s^{-1}.

oxidation peak could be observed in the blank Britton–Robinson buffer solution (pH 2.0) at the bare CPE. However, at the bare CPE (Fig.4, curve b) and [BnMIM]PF$_6$/CPE (Fig. 4, curve c), irreversible oxidation peaks in the presence of LBT were observed with the oxidation peak potential and the oxidation peak currents of 1.040 V, 2.830×10^{-6} A (CPE) and 0.942 V, 5.956×10^{-6} A ([BnMIM]PF$_6$/CPE), respectively. The oxidation peak potential of LBT at [BnMIM]PF$_6$/CPE was shifted negatively by 98 mV and the oxidation peak current increased significantly by almost two times compared with that of CPE, and exhibited a great response of electrocatalytic activity. The above-mentioned experimental results indicated that the presence of the ionic liquid in the modified electrode showed good electrocatalytic ability, which was attributed to the specific advantages of ILs, including high conductivity and the inherent catalytic ability of ILs.[19]

The effect of the scan rate (v) on the oxidation peak current (I_p) of 1.0×10^{-4} mol L^{-1} LBT at [BnMIM]PF$_6$/CPE was investigated by CV (Fig. 5). With increasing scan rate from 20 to 1000 mV s^{-1}, the oxidation peak currents increased gradually. The oxidation peak currents *vs*. the square root of the scan rate exhibited a good linear relationship, the linear regression equation of which is expressed as $I_p/\mu A = -2.257 + 0.7231v^{1/2}$ (where v is in mV s^{-1}) with the correlation coefficient (R) of 0.9982 and a relative standard deviation (RSD) of 2.8 %. The electrochemical oxidation of LBT at [BnMIM]PF$_6$/CPE was indicated to be a diffusion-controlled electrode reaction process.
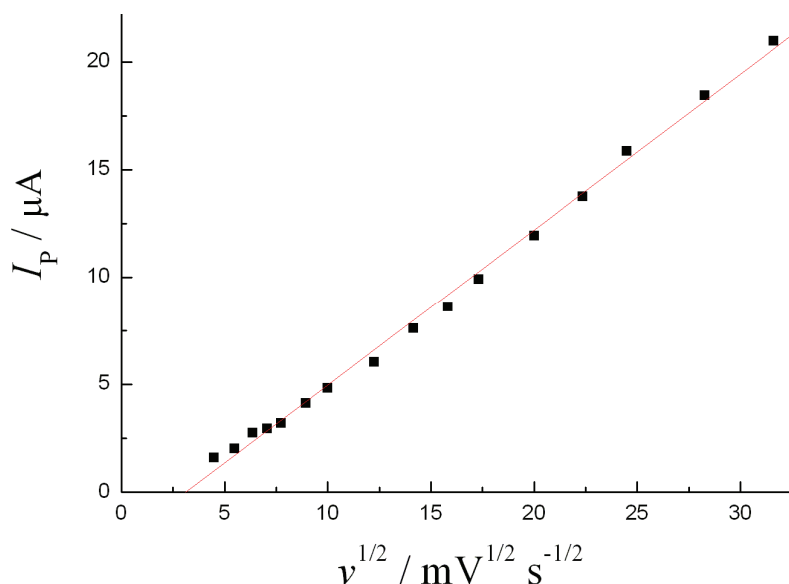

Fig. 5. The relationship of the oxidation peak current I_p *vs*. $v^{1/2}$ at the [BnMIM]PF$_6$/CPE.

The effect of experimental conditions on the peak currents and potentials

The effect of various media on the peak currents and potentials of LBT could be easily observed by CV. The CV of 1.0×10^{-4} mol L^{-1} LBT at a scan rate of 100 mV s^{-1} in different electrolyte solutions, *i.e.*, 0.10 mol L^{-1} KNO$_3$, Na$_2$SO$_4$, NaCl, NaClO$_4$, NaAc, Na$_2$HPO$_4$–NaH$_2$PO$_4$ (PBS) and Britton–Robinson buffer solution was investigated. The experiment results showed that a well-defined electrochemical behavior was obtained in Britton–Robinson buffer solution. Therefore, Britton–Robinson buffer solution was adopted.

The effect of the pH of the Britton–Robinson buffer solution on the electrochemical response of 1.0×10^{-4} mol L^{-1} LBT was investigated in the pH range from 2.0 to 10.0 (Fig. 6), It can be seen from Fig. 6 that the oxidation peak potential (E_p) of LBT decreased gradually with increasing pH from 2.0 to 10.0. A linear regression equation between E_p and pH was obtained as E_p/mV = 1106.4 − −73.0 pH with *R* 0.9987 and *RSD* 1.9 %. The slope of 73.0 mV/pH was close to the theoretical value of 59 mV/pH, which indicates that the number of electrons
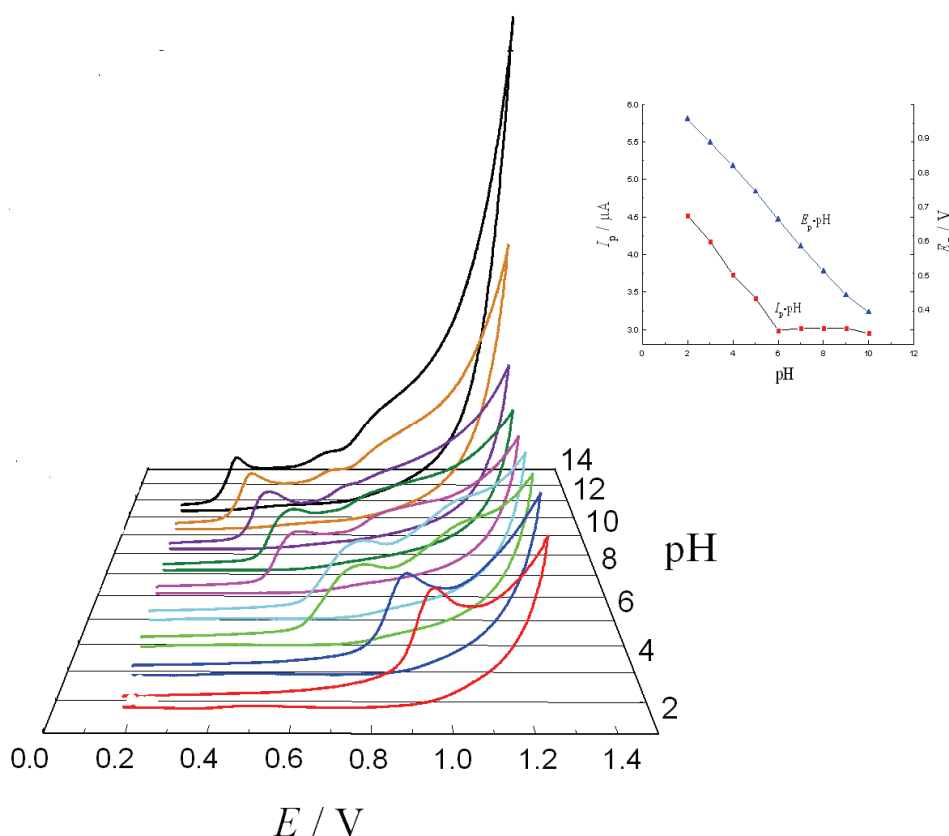

Fig.6 Effect of pH on E_p and I_p at the [BnMIM]PF$_6$/CPE.

and protons involved in the oxidation process of LBT were almost equal. It was also found that the oxidation peak current (I_p) of LBT decreased gradually with the increasing pH from 2.0 to 6.0, after which it remained almost constant. Therefore, Britton–Robinson buffer solution of pH 2.0 was chosen for the determination of LBT.

Electrode reaction kinetics

*Electron transference number (*n*) and proton transference number (*m*).* The effect of scanning rate (v) on the oxidation peak potential (E_p) of 1.0×10^{-4} mol L^{-1} LBT at [BnMIM]PF$_6$/CPE was investigated by CV (Fig. 7). From Fig. 7, it can be seen that the oxidation peak potential shifted positively with increasing scan rate, a linear relationship was obtained in the range of 60–800 mV s^{-1}. The relationship can be expressed by the following equation:[20]

$$E_p \,/\, \text{mV} = 855.2 + 43.60\log (v \,/\, \text{mV s}^{-1}) \tag{1}$$
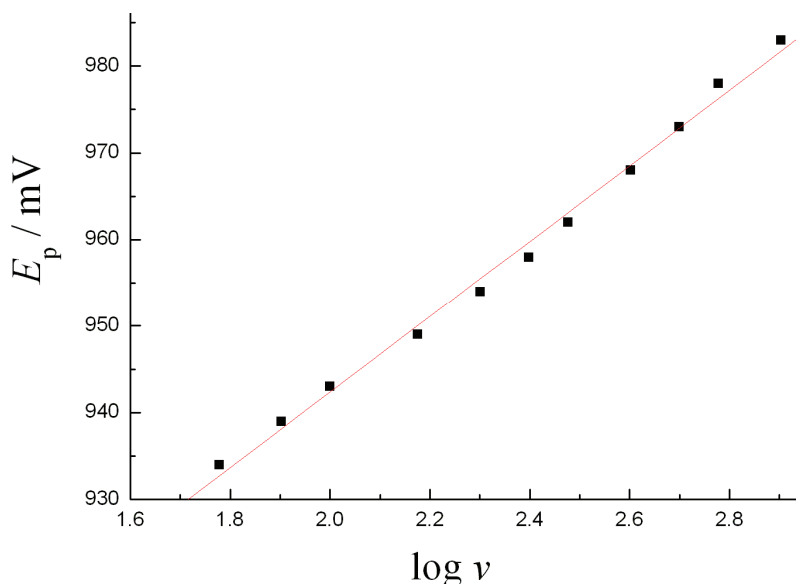$$R = 0.9971,\ RSD = 1.8\ \%$$

Fig. 7. The relationship of the oxidation peak potential E_p *vs.* log v at the [BnMIM]PF$_6$/CPE.

For a totally irreversible electrode process, the relationship between E_p and v is defined by the following equation:[21]

$$E = E^{\circ\prime} + \left(\frac{RT}{\alpha nF}\right)\left[0.780 + \ln\left(\frac{D_R^{1/2}}{k^\circ}\right) + \ln\left(\frac{\alpha nFv}{RT}\right)^{1/2}\right] \tag{2}$$

where $E^{\circ\prime}$ is the formal potential; the k°, the standard heterogeneous rate constant; D_R, the diffusion coefficient of LBT, α, the charge transference coefficient. The other symbols have their usual significance. From Eqs. (1) and (2), one can obtain the slope $(2.303RT/2\alpha nF)$ of the plot of E_p–log v as:

$$0.5 \times 2.303\ (RT\ /\ \alpha nF) = 0.04360 \tag{3}$$

Generally, α in a totally irreversible electrode process is assumed as 0.5.[22] Consequently, one electron is involved in the oxidation of LBT. Therefore, according to the experimental results, the above mentioned showed that the electrochemical oxidation of LBT on [BnMIM]PF$_6$/CPE is a one-electron and one-proton process.

*Diffusion coefficient (*D*).* The geometrical surface (A) for bare CPE and [BnMIM]PF$_6$ modified CPE can be calculated from the slope ($2nFAc\sqrt{D/\pi}$) of the plot of Q *vs.* $t^{1/2}$ by chronocoulometry (CC) using 5.0×10^{-3} mol L^{-1} K$_3$[Fe(CN)$_6$] as the electrochemical model (the diffusion coefficient D of K$_3$[Fe(CN)$_6$] is 7.6×10^{-6} cm^2 s^{-1})[23] from Eq. (4):[24]

$$Q = 2nFAc\sqrt{Dt/\pi} + Q_{dl} + Q_{ads} \tag{4}$$

Based on the slopes of 8.709×10^{-6} ($RSD = 1.3$ %) for CPE and 9.255×10^{-6} ($RSD = 1.9$ %) for [BnMIM]PF$_6$/CPE of the plots of Q *vs.* $t^{1/2}$, A can be calculated as 0.0580 cm^2 for CPE and 0.0617 cm^2 for [BnMIM]PF$_6$/CPE when c (K$_3$[Fe(CN)$_6$] concentration), D (diffusion coefficient of 5.0×10^{-3} mol L^{-1} K$_3$[Fe(CN)$_6$]), and n (electron transfer number) are known.

The diffusion coefficient D of LBT at the bare CPE and [BnMIM]PF$_6$/CPE can also be determined using CC based on Eq. (4). From the slopes of 3.630×10^{-6} ($RSD = 0.27$ %) for CPE and 8.645×10^{-6} ($RSD = 1.2$ %) for [BnMIM]PF$_6$/CPE of the plot of Q *vs.* $t^{1/2}$, D can be obtained as 3.303×10^{-5} cm^2 s^{-1} for CPE and 1.655×10^{-4} cm^2 s^{-1} for [BnMIM]PF$_6$/CPE.

The electrode reaction rate constant k$_f$. The electrode reaction rate constant (k_f) at both the bare CPE and [BnMIM]PF$_6$/CPE were calculated by chronoamperometry (CA) based on Eq. (5):[25]

$$I(t) = nFAk_f c \left[1 - 2H\sqrt{t/\pi} \right] \tag{5}$$

where, $H = k_f\ /\ D_{Ox}^{1/2} + k_b\ /\ D_{Rd}^{1/2}$. For a totally irreversible electrochemical reaction, the value of k_b is 0, therefore, when t approaches 0, the plot of $I(t)$ *vs.* $t^{1/2}$ gives a good straight line (Fig. 8). Thus, k_f can be calculated from the intercept ($nFAk_f c$) of 3.393×10^{-7} ($RSD = 2.1$ %) for CPE and of 8.207×10^{-6} ($RSD = 1.5$ %) for [BnMIM]PF$_6$/CPE of the CA curves. The resulting values for k_f are 6.063×10^{-4} cm s^{-1} for CPE and 1.379×10^{-2} cm s^{-1} for [BnMIM]PF$_6$/CPE.
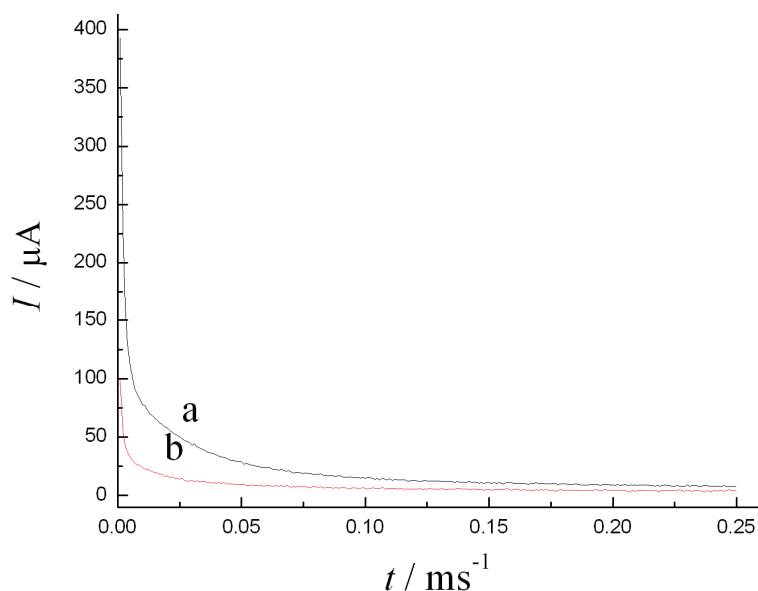
Fig. 8. Plots of the CA curves of 1.0×10^{-4} mol L^{-1} LBT at the CPE (a) and the [BnMIM]PF$_6$/CPE (b).

Application of the electrochemical determination

Square wave voltammetric (SWV) behaviors of LBT. The responses of square wave voltammetry are markedly dependent on the parameters of the exciting signals. Therefore, the optimization of the frequency, the pulse amplitude, and the scanning potential increment were investigated in the experiment. The dependence of the oxidation peak current on the frequency in the range 20–100 Hz was investigated. The peak current increased linearly with frequency from 20 up to 50 Hz, after which, it remained almost constant between 50 and 100 Hz. Thus, a frequency of 50 Hz was chosen. With a 50 Hz frequency, the pulse amplitude was changed in the range of 10–80 mV. It was found that between 10 and 30 mV, the peak current increased linearly with pulse amplitude, after 30 mV, it remained almost constant. A pulse amplitude of 30 mV was chosen. In addition, with a 50 Hz frequency and a pulse amplitude of 30 mV, a scanning potential increment of 5 mV was found to develop well-defined electrochemical behavior.

The SWV behaviors of 1.0×10^{-4} mol L^{-1} LBT at both the bare CPE and [BnMIM]PF$_6$/CPE in Britton–Robinson buffer solution (pH 2.0) under the optimized experimental conditions (frequency 50 Hz, pulse amplitude 30 mV, and scanning potential increment 5 mV) are shown in Fig. 9. From Fig. 9, curve a, it can be seen that no oxidation peak could be observed in the blank Britton–Robinson buffer solution (pH 2.0) at the bare CPE. While at the bare CPE (Fig. 9, curve b) and [BnMIM]PF$_6$/CPE (Fig. 9, curve c), irreversible oxidation peaks in

the presence of LBT were observed with the oxidation peak potential and the oxidation peak currents of 1.005 V, 7.414×10^{-6} A (CPE) and 0.940 V, 1.734×10^{-5} A ([BnMIM]PF$_6$/CPE), respectively. The oxidation peak potential of LBT at [BnMIM]PF$_6$/CPE was shifted negatively by 65 mV and the oxidation peak current was significantly increased by almost two times compared with that at bare CPE, which confirmed its great electrocatalytic activity. These experimental results were in quite good agreement with those of CV.
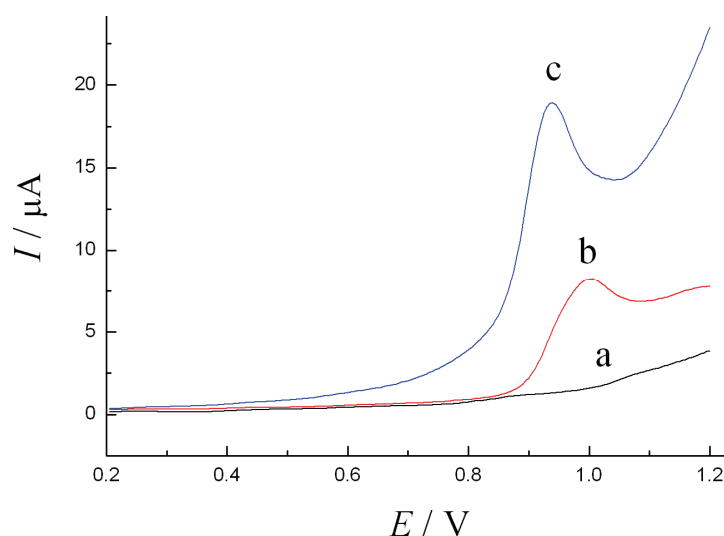

Fig. 9. SWV curves of the CPE (a) in Britton–Robinson buffer solution (pH 2.0) in the absence and the presence of 1.0×10^{-4} mol L^{-1} LBT (b) and of the [BnMIM]PF$_6$/CPE in the presence of 1.0×10^{-4} mol L^{-1} LBT (c).

The relationship between oxidation peak currents and LBT concentration were investigated at [BnMIM]PF$_6$/CPE. The oxidation peak currents increased linearly with increasing LBT concentration in the range of 7.0×10^{-6}–1.0×10^{-4} mol L^{-1}. The linear regression equation is expressed as:

$$I_p\ (\mu A) = 2.214 + 60.59c\ (c\ \text{is in mM})$$
$$R = 0.9986,\ RSD = 2.1\ \%$$

Under the optimized experimental conditions, an *LOD*, (*S/N* = 3) of 4.810×10^{-8} mol L^{-1} and an LOQ (*S/N* = 10) of 1.60×10^{-7} mol L^{-1} were obtained.

Reproducibility, stability and interference

After each experiment, the used carbon paste was carefully removed from the end cavity of the modified electrode, and then another new [BnMIM]PF$_6$/ /CPE was fabricated. The reproducibility of [BnMIM]PF$_6$/CPE was estimated by

comparing the oxidation peak current of 1.0×10^{-4} mol L^{-1} LBT. The relative standard deviation (*RSD*) was 2.4 % for 10 determinations, revealing that the modified electrode had good reproducibility. After the modified electrode had been stored at room temperature for ten days, the current response obtained was within ±5 % the immediately obtained response, which shows the excellent stability of the modified electrode.

Moreover, some common excipients were tested to check their levels of interference in the LBT determination. The results suggest that 100-fold concentrations of glucose, sucrose, amylum, magnesium stearate and dextrin had no influence on the signals of LBT with *RSD* below ±5 %.

Analytical applications

In order to ascertain the potential application in commercial tablet samples analysis, the proposed method was used to determined LBT content in LBT tablets. Ten tablets of LBT with the labeled amount of 50.00 mg per tablet were homogeneously ground into powder in a mortar, and then an appropriate amount of the powder was accurately weighed, dissolved in doubly distilled water, transferred quantitatively into a 100 mL volumetric flask and doubly distilled water added to scale line. Finally, a known-amount of sample solution was added into pH 2.0 Britton–Robinson buffer solution and determined by SWV. The content of LBT in the sample solution, which was measured by the standard addition method, is given in Table I. An acceptable reproducibility with an *RSD* of 1.2–2.1 % for commercial tablet samples was obtained for six parallel measurements. By using the standard addition method, the recoveries for the determination LBT were in the range of 98.30–104.2 %, indicating that the proposed method has good accuracy and could be used as an effective quantitative electrochemical determination of LBT in commercial tablet samples.

Table I. Determination results of the samples ($n = 6$)

Samples	Labeled	Found, mg	*RSD* / %	Added, mg	Determined, mg	Recover, %
1	50.00 mg tablet^{-1}	49.69	2.1	13.00	63.24	104.2
2		50.07	1.2	25.00	74.65	98.30
3		50.49	1.8	50.00	99.80	98.60

CONCLUSIONS

A modified carbon paste electrode ([BnMIM]PF$_6$) was successfully fabricated and characterized by CV and EIS. The electrochemical behaviors of LBT at the both a bare CPE and a [BnMIM]PF$_6$/CPE were investigated by CV and SWV. Compared with the bare electrode, the oxidation peak current of LBT increased greatly and the oxidation peak potential shifted negatively at the [BnMIM]PF$_6$//CPE, which revealed some advantages of [BnMIM]PF$_6$/CPE over CPE, such as high conductivity and inherent catalytic ability. The electrochemical behavior of

LBT at [BnMIM]PF$_6$/CPE is a diffusion-controlled electrode reaction process involving one electron transfer accompanied by the participation of one proton. Moreover, the electrochemical kinetic parameters (diffusion coefficient D and the electrode reaction rate constant k_f) of LBT were determined at the both the electrodes by CV, CC and CA. The oxidation peak currents increased linearly with the increasing LBT concentration in the range of 7.0×10^{-6}–1.0×10^{-4} mol L^{-1}. The linear regression equation was expressed as I_p (μA) = 2.214 + 60.59c/10^{-3} mol L^{-1} ($R = 0.9986$ and RSD of 2.1%). The limit of detection (LOD, $S/N = 3$) was 4.810×10^{-8} mol L^{-1} and the limit of quantification (LOQ, $S/N = 10$) was 1.60×10^{-7} mol L^{-1}. A comparison of the present experimental results with those already existing in literature[8] for similar electrochemical procedures, in which the LOD values were 1.0×10^{-6} mol L^{-1} for LSV and 1.0×10^{-8} mol L^{-1} for DPV, and the linear calibration curve ranges were 2.5×10^{-6}–1.0×10^{-5} mol L^{-1} for LSV and 2.5×10^{-8}–1.0×10^{-5} mol L^{-1} for DPV, shows that that the method presented herein is quite good and no preconcentration/medium exchange steps are necessary. Thus, the proposed method was successfully applied in the determination of the LBT content in commercial tablet samples with satisfactory results.

ИЗВОД

ЕЛЕКТРОХЕМИЈСКО ПОНАШАЊЕ И ОДРЕЂИВАЊЕ ЛАБЕТАЛОЛА НА ЕЛЕКТРОДИ ОД УГЉЕНИЧНЕ ПАСТЕ КОЈА ЈЕ МОДИФИКОВАНА ЈОНСКОМ ТЕЧНОШЋУ

YAN-MEI ZHANG[1], CHENG-QIAN DUAN[1,2] и ZUO-NING GAO[1]

[1]*College of Chemistry and Chemical Engineering, Ningxia University, Yinchuan, 750021, People's Republic of China u* [2]*Higher Vocational College of Ningxia Medical University, Yinchuan, 750004, People's Republic of China*

Испитивано је електрохемијско понашање лабеталола (ЛБТ) на електроди од угљеничне пасте са и без модификације јонском течношћу 1-бензил-3-метилимидазол хексафлуорофосфатом ([BnMIM]PF$_6$) у Бритон−Робинсоновом пуферском раствору pH 2,0. У поређењу са немодификованом електродом, електрода модификована [BnMIM]PF$_6$ је показује повећану струју за електрохемијску оксидацију ЛБТ, као и добро дефинисан и осетљив оксидациони пик. Одређени су и кинетички параметри електрохемијске оксидације ЛБТ. Под оптимизованим условима електрохемијског експеримента струјни пик оксидације линеарно зависи од концентрације у опсегу $7,0\times10^{-6}$–$1,0\times10^{-4}$ M уз границу детекције ($S/N = 3$) од $4,81\times10^{-8}$ M и границу квантификације ($S/N = 10$) од $1,60\times10^{-7}$ M. Предложена метода је успешно примењена за одређивање количине ЛБТ у узорцима комерцијалних лекова.

REFERENCES

1. D. Kernaghan, G. McKay, *Pract. Diab. Int.* **28** (2011) 139
2. J. M. Dakers, D. W. Boulton, J. P. J. Fawcett, *J. Chromatogr., B* **704** (1997) 215
3. C. Ceniceros, M. I. Maguregui, R. M. Jimenez, R. M. Alonso, *J. Chromatogr., B* **705** (1998) 97

4. T. M. D. J. P. Carvalho, R. D. C. Cavalli, M. P. Marques, S. P. D. Cunha, C. D. O. Baraldi, V. L. Lanchote, *Chirality* **21** (2009) 738
5. T. V. Goel, J. G. Nikelly, R. C. Simpson, B. K. Matuszewski, *J. Chromatogr., A* **1027** (2004) 213
6. L. Potier, S. L. Tamisier-Karolak, P. Morin, F. Megel, M. Taverna, *J. Chromatogr., A* **829** (1998) 341
7. N. Rahman, H. Rahman, S. N. H. Azmi, *J. Chin. Chem. Soc.* **54** (2007) 185
8. A. Radi, Z. El-Sherif, A. Wassel, *Chem. Pap*. **58** (2004) 242
9. Voulgaropoulos, M. Sofoniou, E. Kazakou, *Electroanal*ysis **5** (1993) 525
10. E. K. Goharshadi, M. Moosavi, *J. Mol. Liq*. **142** (2008) 41
11. M. C. Buzzeo, C. Hardace, R. G. Compton, *Anal. Chem*. **76** (2004) 4583
12. L. H. Liu, C. Q. Duan, Z. N. Gao, *Croat. Chem. Acta* **83** (2010) 409
13. Q. Duan, Y. M. Zhang, Z. N. Gao, *Croat. Chem. Acta* **85** (2012) 27
14. L. H. Liu, Z. N. Gao, *Chin. J. Pharm. Anal*. **30** (2010) 438
15. L. H. Liu, C. Q. Duan, Z. N. Gao, *J. Serb. Chem. Soc*. **77** (2012) 483
16. J. J. Feng, G. Zhao, J. J. Xu, H. Y. Chen, *Anal. Biochem*. **342** (2005) 280
17. X. G. Kong, J. W. Zhao, J. B. Han, D. Y. Zhang, M. Wei, X. Duan, *Electrochim. Acta* **56** (2011) 1123
18. E. Katz, I. Willner, *Electroanal*ysis **15** (2003) 913
19. W. Sun, Y. Z. Li, Y. Y. Duan, K. Jiao, *Biosens. Bioelectron*. **24** (2008) 988
20. M. Golabi, H. R. Zare, *Electroanalysis* **11** (1999) 1293
21. A. J. Bard, L. R. Faulkner, *Electrochemical Methods Fundamentals and Applications*, Wiley, New York, 1980, p. 223
22. K. B. Wu, Y. Y. Sun, S. S. Hu, *Sens. Actuators, B* **96** (2003) 658
23. R. N. Adams, *Electrochemistry at solid electrode*, Marcel Dekker, New York, 1969, p. 220
24. F. C. Anson, *Anal. Chem.* **38** (1966) 54
25. A. J. Bard, L. R. Faulkner, *Electrochemical Methods Fundamentals and Applications*, Wiley, New York, 1980, p. 167.

Electroanalytical determination of metronidazole in tablet dosage form

SELEHATTIN YILMAZ[1], ESRA BALTAOGLU[1], GULSEN SAGLIKOGLU[1],
SULTAN YAGMUR[1], KAMRAN POLAT[2] and MURAT SADIKOGLU[3*]

[1]*Onsekiz Mart University, Faculty of Science and Arts, Department of Analytical Chemistry, 17020, Canakkale, Turkey,* [2]*Ankara University, Faculty of Science, Department of Chemistry, 06100, Ankara, Turkey and* [3]*Gaziosmanpasa University, Faculty of Education, Department of Science Education, 60100, Tokat, Turkey*

Abstract: In this study, the electrochemical reduction and determination of metronidazole were easily realized in Britton–Robinson buffer (pH 4.01) using an UTGE by cyclic voltammetric (CV) and differential pulse voltammetric (DPV) techniques. In this acidic medium, one irreversible and a sharp cathodic peak were observed. A linear calibration curve for DPV analysis was constructed in the metronidazole concentration range 3×10^{-6}–9×10^{-5} mol L^{-1}. The limit of detection (*LOD*) and limit of quantification (*LOQ*) were 1.42×10^{-7} and 4.76×10^{-7} mol L^{-1} respectively.

Keywords: metronidazole; determination; voltammetry; UTGE; dosage form.

INTRODUCTION

Metronidazole is a nitroimidazole anti-infective medication (Fig. 1) used mainly in the treatment of infections caused by susceptible organisms, particularly anaerobic bacteria and protozoa.[1–7]
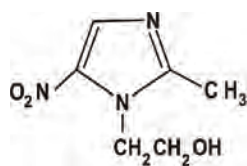

Fig. 1. Chemical structure of metronidazole.

Methods for the assay of metronidazole in pharmaceutical dosage forms are usually based on high performance liquid chromatographic (HPLC)[8] and spectrophotometric[9] techniques. For such applications, however, the analyses are time consuming and are of high cost.

Hitherto, only a few papers have been published about the electroanalytical determination of metronidazole based on its reduction behaviour.[1–7] The determination of metronidazole on an ultra trace graphite electrode (UTGE) based on its detailed electrochemical reductive behaviour has to date not yet been reported. Therefore, it was considered of interest to investigate the properties of the reduction process and determination of metronidazole in tablet dosage form using a UTGE.

EXPERIMENTAL

Apparatus

A Model Metrohm 757 VA trace analyzer (Herisau, Switzerland) was used for the voltammetric measurements, with a three-electrode system consisting of an ultra trace graphite working electrode (UTGE, disc diameter; $R = 2$ mm, Metrohm), a platinum wire auxiliary electrode and Ag/AgCl (KCl 3 mol L^{-1}, Metrohm) reference electrode. Firstly, deoxygenation of the supporting electrolyte solutions was performed with argon gas for 5 min before all experiments. Then, the argon gas was also passed through the solutions for 60 s after the addition of each sample solution in the experiments. All pH measurements were made with Model Metrohm 744 pH meter (Herisau, Switzerland).

Reagents

Metronidazole as pure active material and its Nidazole® tablets (labelled as containing 250 mg metronidazole per tablet) was kindly supplied by I. E. Ulugay (Istanbul, Turkey). A stock solution of 1.0×10^{-2} mol L^{-1} of metronidazole was prepared by dissolving an accurate mass of the drug in an appropriate volume of ethanol and kept in a refrigerator. Britton–Robinson buffer solutions (0.04 mol L^{-1}, pH 2.09–12.00); acetic acid, Riedel, Seelze, Germany, 100 mas. %; boric acid, Merck, Darmstadt, Germany, and phosphoric acid, Carlo Erba, Rodeno, France, 85 mas. %, were used for the supporting electrolyte solution.

Calibration graph for quantitative determination

The stock solution of metronidazole was diluted with ethanol to obtain different metronidazole concentrations. Using the optimum conditions described in the experimental section, a linear calibration curve for DPV analysis was constructed in the metronidazole concentration range 3×10^{-6}–9×10^{-5} mol L^{-1} (Fig. 2). The repeatability, accuracy and precision were checked (Table I).

Working voltammetric procedure of spiked tablet dosage forms

Ten tablets were weighed and ground to a fine powder. An adequate amount of this powder, corresponding to a stock solution of concentration 1×10^{-2} mol L^{-1} was weighed and transferred into a 10 mL volumetric flask and the volume was adjusted with ethanol. The contents of the flask were centrifuged for 20 min at 4000 rpm to affect complete dissolution and then diluted to volume with the same solvent. Appropriate solutions were prepared by taking suitable aliquots of the clear supernatant liquor and diluting with selected supporting electrolyte solutions. Each solution was transferred into the voltammetric cell. The nominal content of the corresponding regression equations was compared with previously plotted calibration plots (Table II).
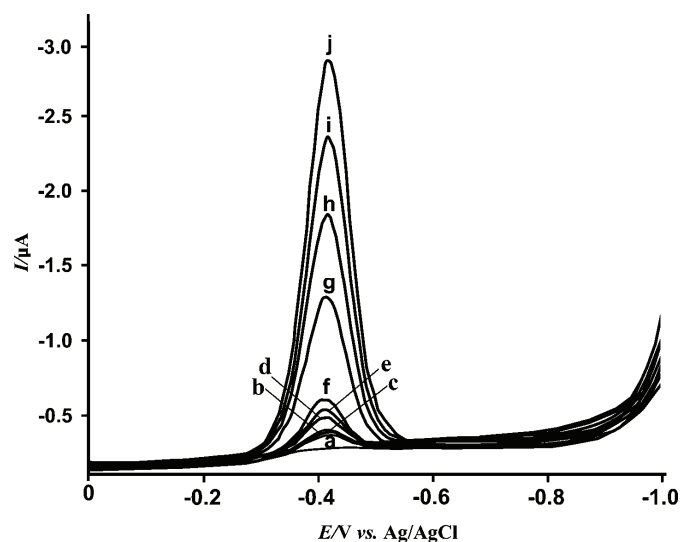
Fig. 2. The calibration voltammograms at different concentrations (b–j) of metronidazole in 0.04 mol L^{-1} BR buffer (pH 4.01) on an UTGE by DPV; a) blank; b–j) increasing concentrations of metronidazole.

TABLE I. Regression data of the calibration lines for the quantitative determination of metronidazole. The calibration plots were obtained in 0.04 mol L^{-1} BR buffer (pH 4.01) on an UTGE using the DPV technique

Parameter	Results
Measured potential, mV	–0.432
Linear concentration range, mol L^{-1}	3.0×10^{-6}–9.0×10^{-5}
Slope, µA M^{-1}	2.96×10^{4}
Intercept, µA	1.35
Correlation coefficient, r	0.0233
SE of slope	16.48
SE of intercept	0.9989
Number of measurements, N	10
LOD / mol L^{-1}	1.42×10^{-7}
LOQ / mol L^{-1}	4.76×10^{-7}
Repeatability of the peak current, *RSD* / %	0.47
Reproducibility of the peak current, *RSD* / %	0.41
Repeatability of the peak potential, RSD / %	0.69
Reproducibility of the peak potential, *RSD* / %	0.61

RESULTS AND DISCUSSION

Electrochemical reduction behaviour of metronidazole

The electrochemical reduction process and determination using this electrode were first realized using the CV and DPV techniques. The CV measurements performed with a 1×10^{-4} mol L^{-1} metronidazole solution at scan rates

between 10–1000 mV s^{-1} on a UTGE in 0.04 mol L^{-1} BR buffer (pH 4.01) are shown in Fig. 3.

TABLE II. Application of the DPV technique for the assay of metronidazole in commercial spiked Nidazole® tablets and mean recoveries on an UTGE

Parameter	Results
Labelled, mg	250.00
Amount found, mg	255.14
RSD / %	1.24
Bias, %	2.05
Metronidazole spiked, mg	20.00
Found, mg	19.20
Recovery, %	96.00
RSD of recovery , %	0.29
Bias / %	4.00

Fig.3. The cyclic voltammograms of 1×10^{-4} mol L^{-1} metronidazole in 0.04 mol L^{-1} Britton–Robinson (BR) buffer (pH 4.01) on an UTGE. Scan rate, mV s^{-1}: a) blank, b) 10, c) 25, d) 50, e) 100, f) 150, g) 250, h) 500, i) 750 and j) 1000.

As can be seen from Fig. 3, metronidazole exhibited one well-defined cathodic peak at different scan rate values. By reversing to 1.00 V, no anodic oxidation peak corresponding to the cathodic response was observed in the anodic region. This indicated that the reduction process of metronidazole had an irreversible nature.

Scan rate studies were then performed to assess whether the processes on the UTGE were under diffusion or adsorption control.[10–20] Two tests were employed for this procedure. One of them was the linear relationship obtained on the UTGE between the peak current and square root of the scan rate between 10–1000 mV s^{-1} as follows:

$$I_p/\mu A = 0.2423\nu^{1/2}\ (mV\ s^{-1}) + 0.04\ (r = 0.991) \tag{1}$$

Correlation coefficient was found very close to 1.0 showing that the reduction process was diffusion-controlled.

Another important test is the plot of the logarithm of the peak current *vs.* the logarithm of the scan rate that gave a straight line with a slope of 0.52, which is nearly the same as the theoretical value of 0.5 that is expected for an ideal reaction of solution species.[10–20] The equation obtained on the UTGE was:

$$\log I_p / \mu A = 0.5221 \log \nu\ (mV\ s^{-1}) - 0.6358\ (r = 0.998) \tag{2}$$

Therefore, a diffusion component must be taken into account. Other studies were conducted in line with this phenomenon.

Next, in order to obtain the optimum experimental conditions, the effect of pH on peak potential and peak intensity were studied on the UTGE using DPV techniques. The DPV results for the reduction reaction of metronidazole are given as *E*–pH and *I*–pH graphs in Figs. 4a and 4b, respectively, for the UTGE. The voltammetric response was strongly pH dependent. The peak potential of the cathodic peak was shifted to more positive values with increasing pH (Fig. 4a).

As can be seen from Fig. 4a, highly linear segments of potential were found between pH values of about 2–8. In acid and neutral media, the reduction was pH dependent, although for pH values higher than 8, the reduction was pH independent, in agreement with Brett and Leach.[6,7]

This indicates that metronidazole shows basic properties in acidic and neutral media (pH 2–8). The differential pulse and cyclic voltammograms of metronidazole at pH 4.01 are shown in Figs. 2 and 3, respectively. This peak corresponds to reduction of the nitro group to form the hydroxylamine, involving 4 electrons and 4 protons followed by a two-electron reduction of the hydroxylamine to amine.[6] However, metronidazole shows weakly basic (or strong acid) properties at pH values higher than 8, meaning a decrease in the protonation of hydroxylamine with increasing pH.[6]

Validation parameters for the quantitative analysis

Validation of the procedure for the quantitative determination of metronidazole was examined by the DPV technique *via* evaluation of the limit of detection (*LOD*), limit of quantification (*LOQ*), repeatability, reproducibility, accuracy and precision (Tables I and II).
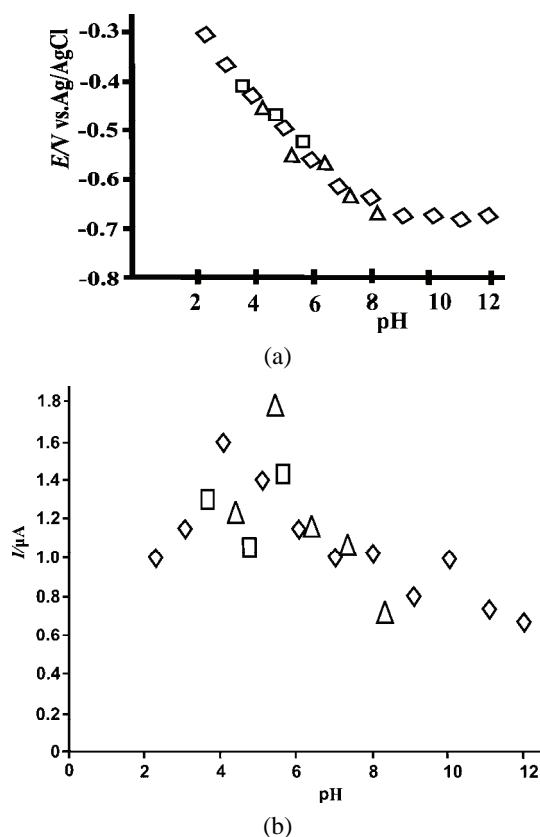
Fig. 4. Effect of pH on the DPV peak potential (a) and peak current (b) of 5×10^{-5} mol L^{-1} metronidazole; □) acetate (0.2 mol L^{-1}); Δ) phosphate (0.067 mol L^{-1}); ◊) Britton–Robinson buffer (0.04 mol L^{-1}).

LOD and *LOQ* were calculated from the electro-reduction peak current using the following equations: *LOD* = 3 *s*/*m* and *LOQ* = 10 *s*/*m* (*s* is the standard deviation of the peak currents (ten runs), *m* is the slope of the calibration curve):[10–20]

$$LOD = 3\ s/m = 3 \times 1.4 \times 10^{-3}/2.96 \times 10^{4} = 1.42 \times 10^{-7}\ \text{M} \qquad (3)$$
$$LOQ = 10\ s/m = 10 \times 1.4 \times 10^{-3}/2.96 \times 10^{4} = 4.73 \times 10^{-7}\ \text{M} \qquad (4)$$

The precision and accuracy of the developed method were checked by recovery studies in tablet dosage form. The procedures are given in the pharmaceutical application section (Table II).

A UTGE and three different electrodes (a DNA-modified glassy carbon electrode, a mercury thin film electrode and a glassy carbon electrode) showed a similar trend in the reduction mechanism for metronidazole, dependent on pH in acid and neutral media and independent in alkaline media.[6] One irreversible and a sharp cathodic peak at –0.432 V were observed in agreement with Brett and Leach (–0.465 V).[6,7]

Pharmaceutical applications

The amount of metronidazole in nidazole commercial tablets was calculated by reference to the appropriate calibration plots. The results obtained are given in Table II.

To determine whether excipients in the tablets interfered with the analysis, the accuracy of the proposed methods were evaluated by recovery tests after the addition of a certain amount of pure drug to pre-analyzed formulations of metronidazole (Table II). The results showed the validity of the proposed techniques for the quantitative determination of metronidazole in tablets.

И З В О Д

ЕЛЕКТРОАНАЛИТИЧКО ОДРЕЂИВАЊЕ МЕТРОНИДАЗОЛА
У ТАБЛЕТНИМ ДОЗИРАНИМ ОБЛИЦИМА

SELEHATTIN YILMAZ[1], ESRA BALTAOGLU[1], GULSEN SAGLIKOGLU[1], SULTAN YAGMUR[1], KAMRAN POLAT[2]
и MURAT SADIKOGLU[3]

[1]*Onsekiz Mart University, Faculty of Science and Arts, Department of Analytical Chemistry, 17020, Canakkale, Turkey,* [2]*Ankara University, Faculty of Science, Department of Chemistry, 06100, Ankara, Turkey u* [3]*Gaziosmanpasa University, Faculty of Education, Department of Science Education, 60100, Tokat, Turkey*

У овом раду су приказани електрохемијска редукција и одређивање метронидазола у Бритон–Робинсоновом пуферу (pH 4,01) применом цикличне волтаметрије (ЦВ) и диференцијалне пулсне волтаметрије (ДПВ). У киселој средини запажен је иреверзибилан и оштар катодни пик. Конструисана је калибрациона крива за ДПВ, линеарна у опсегу 3×10^{-6}–9×10^{-5} mol L^{-1} метронидазола. Граница детекције (ГД) и квантификације (ГК) износе $1,42\times10^{-7}$ одн. $4,76\times10^{-7}$ mol L^{-1}.

(Примљено 11. јануара, ревидирано 3. маја 2012)

REFERENCES

1. E. Bishop, W. Hussein, *Analyst* **109** (1984) 759
2. S. A. Özkan, Y. Özkan, Z Şentürk, *J. Pharm. Biomed. Anal*. **17** (1997) 3299
3. M. A. La-Scalea, S. H. P. Serrano, I. G. R. Gutz, *J. Braz. Chem. Soc.* **10** (1999) 127
4. P. N. Bartlett, E. Ghoneim, G. El-Hefnawy, I. El-Hallag, *Talanta* **66** (2005) 869
5. E. Baltaoglu, master thesis, Çanakkale Onsekiz Mart University, Institute for Natural & Applied Sciences. Canakkale, 2007
6. A. M. O. Brett, S. H. P. Serrano, I. G. R. Gutz, M. A. La-Scale, *Electroanalysis* **9** (1997) 110
7. S. C. Leach, R. D. Weaver, K. Kinushita, W. Lee, *J. Electroanal Chem.* **129** (1981) 213
8. B. M. Tashtoush, E. L. Jacobson, M. K. Jacobson, *Drug Dev. Ind. Pharm.* **34** (2008) 840
9. O. Adegoke, O. Umoh, *Acta Pharm.* **59** (2009) 407
10. S. Yilmaz, B. Uslu, S. A. Ozkan, *Talanta* **54** (2001) 351
11. B. Uslu, S. Yılmaz, S. Ö. Özkan, *Pharmazie* **56** (2001) 629
12. B. T. Demircigil, S. A. Özkan, Ö. Çoruh, S. Yılmaz, *Electroanalysis* **14** (2002) 122

13. S. A. Ozkan, B. Uslu, *Anal. Bioanal. Chem.* **372** (2002) 582
14. S. Skrzypek, W. Ciesielski, A. Sokołowski, S. Yilmaz, D. Kazmierczak, *Talanta* **66** (2005) 1146
15. M. Çıtak, S. Yılmaz, Y. Dilgin, G. Türker, S. Yagmur, H. Erdugan, N. Erdugan, *Current Pharm. Anal*. **3** (2007) 141
16. S. Skrzypek, W. Ciesielski, S. Yilmaz, *Chem. Anal. (Warsaw)* **52** (2007) 1071
17. S. Yılmaz, S. Skrzypek, Y. Dilgin, S. Yagmur, M. Coskun, *Curr. Anal. Chem*. **3** (2007) 41
18. S. Yilmaz, M. Sadikoglu, G. Saglikoglu, S. Yagmur, G. Askin, *Int. J. Electrochem. Sci.* **3** (2008) 1534
19. S. Yılmaz, *Colloids Surfaces., B* **71** (2009) 79
20. M. Sadikoglu, G. Saglikoglu, S. Yagmur, E. Orta, S. Yilmaz, *Curr. Anal. Chem.* **7** (2011) 130.

Removal and recovery of phosphorus during anaerobic digestion of excess sludge by the addition of waste iron scrap

WEI ZHENG[1], XIAO MING LI[1,2]*, DONG BO WANG[1], QI YANG[1], KUN LUO[1], GUO JING YANG[1] and GUANG MING ZENG[1]

[1]College of Environmental Science and Engineering, Hunan University, Changsha 410082, P. R. China and [2]School of the Environment, Guangxi University, Nanning 530004, P. R. China

Abstract: In the current investigation, the feasibility of phosphorus removal in the anaerobic digestion of excess sludge by the addition of waste iron scrap (WIS) was studied. The results showed that the removal efficiency of phosphorus increased with increasing amount of WIS, and the maximum removal efficiency of 39, 93 and 99 % could be reached at WIS dosages of 1, 2 and 3 g L^{-1}, respectively. Sterilization greatly decreased the removal efficiency of phosphorus, being only –6, 53 and 64 % at WIS dosages of 1, 2 and 3 g L^{-1}, respectively. This means that iron-reducing bacteria and hydrolytic bacteria enhance 45, 40 and 35 % of the phosphorus removal at WIS dosages of 1, 2 and 3 g L^{-1}, respectively. The first and most important mechanism of phosphorus removal using WIS involves hydrolytic bacteria, which reduce the pH of the sludge to corrode the WIS, followed by precipitation of phosphorus by ferrous iron generated by iron-reducing bacteria. Phosphorus adsorption onto the WIS is the second probable mechanism. The removed phosphorus is recovered by up to 56 % using magnet. This method is characterized by high removal efficiency, easy and steady operation, low cost, recovery and reuse, making it better than other physical and chemical treatments.

Keywords: waste iron scrap; phosphorus removal; excess sludge; anaerobic digestion.

INTRODUCTION

An excessive presence of phosphate in freshwater affects the water quality and the ecosystem balance negatively through a process known as eutrophication. To diminish the negative effects of phosphorus in effluents from municipal wastewater treatment plants (MWWTP), treatment processes are becoming more stringent. Today, the main commercial processes for phosphorus removal from

---

wastewater effluents are chemical precipitation with iron, alum, lime and magnesium[1–6] and, to a lesser extent, biological removal.[7]

An efficient phosphate removal technique is precipitation involving struvite;[8] however, the crystallization rate of struvite is low. Another method, chemical precipitation, is a very flexible and speedy process for phosphorus removal using ferric chloride and ferrous sulfate.[9] However, this process is not generally favored because of high costs.[10]

In contrast to the majority of research dedicated to the removal of phosphorus, including chemical[11–14] and biological methods,[15–20] phosphorus is removed from the aqueous phase to the solid phase, especially in biological methods. Phosphorus is transferred from the water to the sludge, and in the process of sludge treatment, abundant phosphorus is released from the sludge to the aqueous phase. The whole process consumes large amounts of energy and cannot fundamentally solve the problems.

Currently, the removal of phosphorus in the process of sludge digestion has not yet been studied. In the present study, investigated the feasibility of phosphorus removal in the process of excess sludge digestion using waste iron scrap (WIS) was investigated. The effects of sterilization and adsorption were also studied to understand the mechanisms of phosphorus removal. The phosphorus recovery was also investigated.

MATERIALS AND METHODS

Composition of anaerobic sludge and WIS

The anaerobic sludge used in this study was obtained from a MWWTP in Changsha, China. The sludge was filtered through a 1×1 mm metal sieve and stored at 4 °C for later use. The total solids (TS) content, total volatile solids (TVS), dissolved phosphate, total iron ions, and pH were 11.1, 7.5, 93.6 and 125 mg L^{-1} and 6.8, respectively. The WIS, which was collected from a grinding workshop near Hunan University, China, was 4–8 mm in length and 3 mm in width. The WIS was first degreased in 10 % NaOH solution and then cleaned using deionized water.

Experimental setup

Experiments on the influence of dosage of WIS on phosphorus removal were performed in 10 identical glass reactors, each having a liquid volume of 500 mL. The WIS was added into the reactors (*i.e*., unsterilized, sterilized sludge and prepared phosphate solution) at dosages of 0, 1, 2 and 3 g L^{-1}. Subsequently, the reactors were air-bath mixed at 120 rpm to blend the contents, at a temperature maintained at 25±1 °C. Each reactor was purged with nitrogen gas for 5 min and sealed to ensure anaerobic conditions. To investigate the adsorption performance of WIS onto phosphorus, a phosphate solution of definite concentration was prepared to which WIS at the above-mentioned dosages was added. All the reactors were run for 10 d. At predetermined time intervals, samples were collected and analyzed. All tests were performed in triplicate and the average results are presented in this study.

Analytical methods

The values of TS, TVS, and dissolved phosphate were determined according to standard methods.[21] The pH was determined using a Multiline 330i pH meter standardized using buffer solutions of different pH values. The concentration of total iron was measured using the phenanthroline spectrophotometric method.[22]

The volatile fatty acids (VFAs) were analyzed using an Agilent 6890N GC with a flame ionization detector and equipped with a 30 m×0.25 mm×0.25 μm DB-FFAP column. Nitrogen was used as the carrier gas at a flux of 5.6 mL min^{-1}. The injection port and the detector were maintained at 250 and 300 °C, respectively. The oven of the GC was programmed to start at 70 °C for 3 min, then to increase at a rate of 20 °C min^{-1} to 250 °C, at which temperature, it was held for 3 min. The sample injection volume was 1.0 μL.

RESULTS AND DISCUSSION

Effect of WIS dosage

The amounts of phosphorus removed as a function of the amount of WIS are shown in Fig. 1. The amount removed increased with increasing amount of WIS, except for the control test because of the phosphorus released in the process in excess of the sludge digestion. The highest phosphorus removal efficiency at WIS dosages of 1, 2 and 3 g L^{-1} were 39, 93 and 99 %, respectively, because higher dosages of WIS have larger surface areas available for reaction with phosphate. The chemical removal of phosphate was accompanied by the adsorption of phosphate ions and dissolved organic phosphorus on ferric hydroxide flocs.[13,23] The
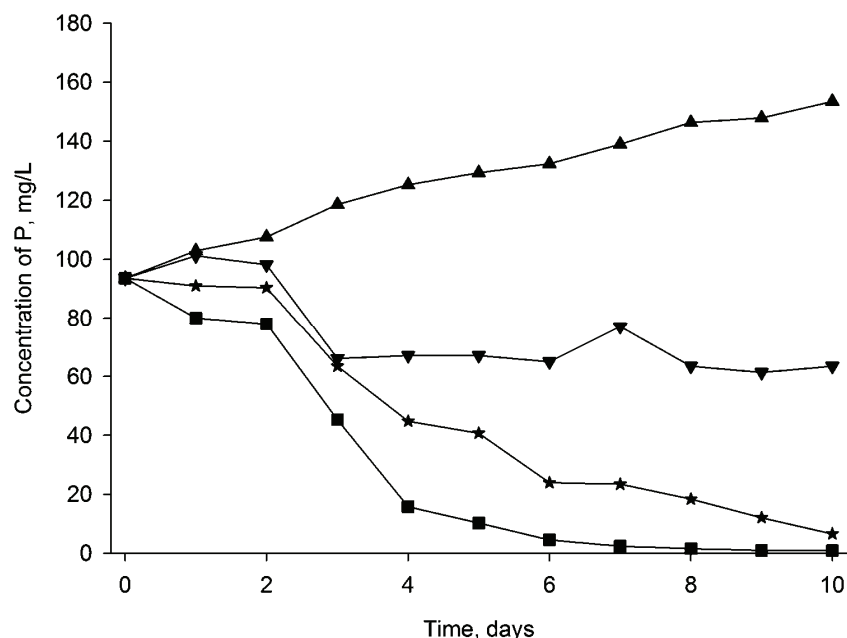

Fig. 1. Effect of WIS dosage on the removal of phosphorus (▲, 0; ▼, 1; ★, 2; ■, 3 g L^{-1}).

removed phosphorus, Fig. 1, was not released with extended time, indicating that the WIS had a high affinity for phosphorus. The final concentration of phosphate at a WIS dosage of 3 g L^{-1} was 0.8 mg L^{-1}, which is lower than the permitted level of phosphate in MWWTP effluent in China.

The removal of phosphorus from excess sludge prior to supernatant recycling in aerobic tanks can significantly reduce the phosphorus load in the main stream of the MWWTP effluent, thereby preventing the eutrophication of aquatic systems and deterioration of water quality.[13,24] Another benefit of this technology is that it can recover phosphorus used as a fertilizer in agriculture.

pH Variation and total production of volatile fatty acids

The pH variations at different WIS dosages during sludge digestion are shown in Fig. 2, from which it can be seen that the pH of the sludge in the presence and absence of WIS exhibited a similar trend: an initial decrease followed by an increase. This trend is caused by the production of organic acids during the digestion of the excess sludge and the bacterial conversion of the organic acids into methane and carbon dioxide. Higher WIS dosages can shorten the time during which the pH decreases, which may be attributed to the bioreduction of WIS (Eqs. (1) and (2)) and the corrosion of WIS (Eqs. (3)and (4)).
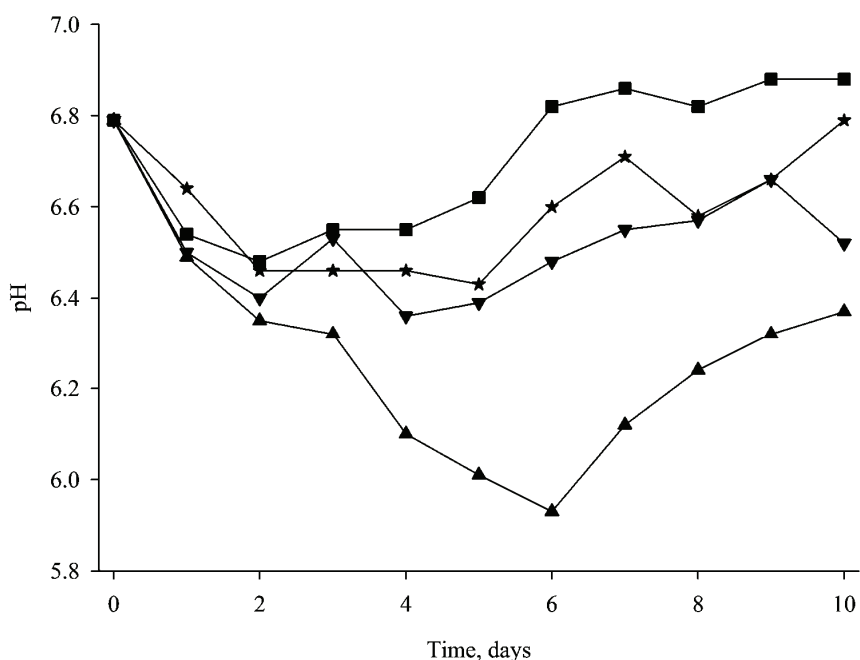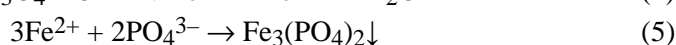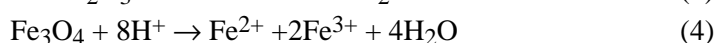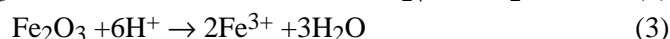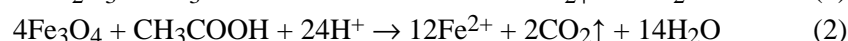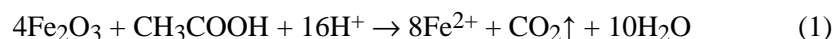

Fig. 2. Variation in pH at different WIS dosages during sludge digestion
(▲, 0; ▼, 1; ★, 2; ■, 3 g L^{-1}).

An anaerobic digester contains many types of iron-reducing bacteria.[25] With acetate as the electron donor, the reduction of WIS, which is mainly composed of Fe_2O_3 and Fe_3O_4, and the precipitation of phosphorus by ferrous irons can be described by the following equations:

$$4Fe_2O_3 + CH_3COOH + 16H^+ \rightarrow 8Fe^{2+} + CO_2\uparrow + 10H_2O \qquad (1)$$

$$4Fe_3O_4 + CH_3COOH + 24H^+ \rightarrow 12Fe^{2+} + 2CO_2\uparrow + 14H_2O \qquad (2)$$

$$Fe_2O_3 + 6H^+ \rightarrow 2Fe^{3+} + 3H_2O \qquad (3)$$

$$Fe_3O_4 + 8H^+ \rightarrow Fe^{2+} + 2Fe^{3+} + 4H_2O \qquad (4)$$

$$3Fe^{2+} + 2PO_4^{3-} \rightarrow Fe_3(PO_4)_2\downarrow \qquad (5)$$

$$Fe^{3+} + PO_4^{3-} \rightarrow FePO_4 \qquad (6)$$

However, Ca^{2+} and Mg^{2+} are released in the process of excess sludge digestion. The results of Gao and Mucci[26] further indicated that the formation of Mg^{2+}, Ca^{2+} and ternary cation–phosphate surface complexes ($\equiv$FeOMg$^+$, $\equiv$FeOCa$^+$, $\equiv$FeOMgHPO$_4^-$, $\equiv$FeOMgH$_2$PO$_4^0$, $\equiv$FeOCaHPO$_4^-$ and $\equiv$FeOCaH$_2$PO$_4^0$) affect phosphate adsorption by WIS.

The effects of WIS dosage and hydrolysis time on the total production of VFAs are shown in Fig. 3. The individual VFAs were converted to chemical oxygen demand (*COD*) values using appropriate conversion factors. The total VFA concentration was greatly affected by the WIS dosage. The fermentation time to
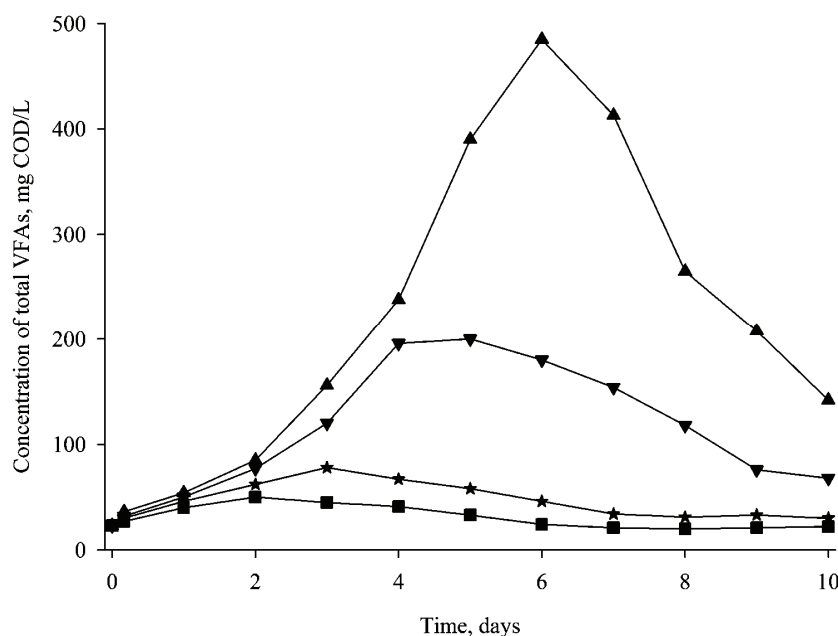

Fig. 3. Production of VFAs at different WIS dosages during sludge digestion ($\blacktriangle$, 0; $\blacktriangledown$, 1; $\bigstar$, 2; $\blacksquare$, 3 g L^{-1}).

reach the maximum VFA concentration was also affected by the WIS dosage. For example, the maximum VFA concentration was 485 mg COD L^{-1} on the 6th day in the blank test, 200 mg COD L^{-1} on the 5th day at a WIS dosage of 1 g L^{-1}, 78 mg COD L^{-1} on the 3rd day at 2 g L^{-1} and 50 mg COD L^{-1} on the 2nd day at 3 g L^{-1}. Moreover, as shown in Fig. 3, the concentration of the VFAs decreased with increasing WIS dosage because the VFAs were consumed, according to Eqs. (1)–(4).

Effect of adsorption

The important mechanisms involved in phosphorus removal using steel slag are specific adsorption on metal hydroxides and precipitation.[27] To determine the effect of adsorption, three 140 mg L^{-1} phosphorus solutions were prepared. The phosphorus removal efficiency by WIS as function of the WIS dosage and contact time are presented in Fig. 4, which shows that phosphorus removal first increases with the increasing contact time, then there was no obvious increase when the contact time was longer than 9 and 7 d at WIS dosages of 3 or 2 and 1 g L^{-1}, respectively. This finding indicates that the adsorption reaction of phosphorous onto WIS mainly occurred within the first 9 and 7 d, respectively. When the contact time reached 9 and 7 d, phosphorus removal was 38, 34 and 16 % at WIS
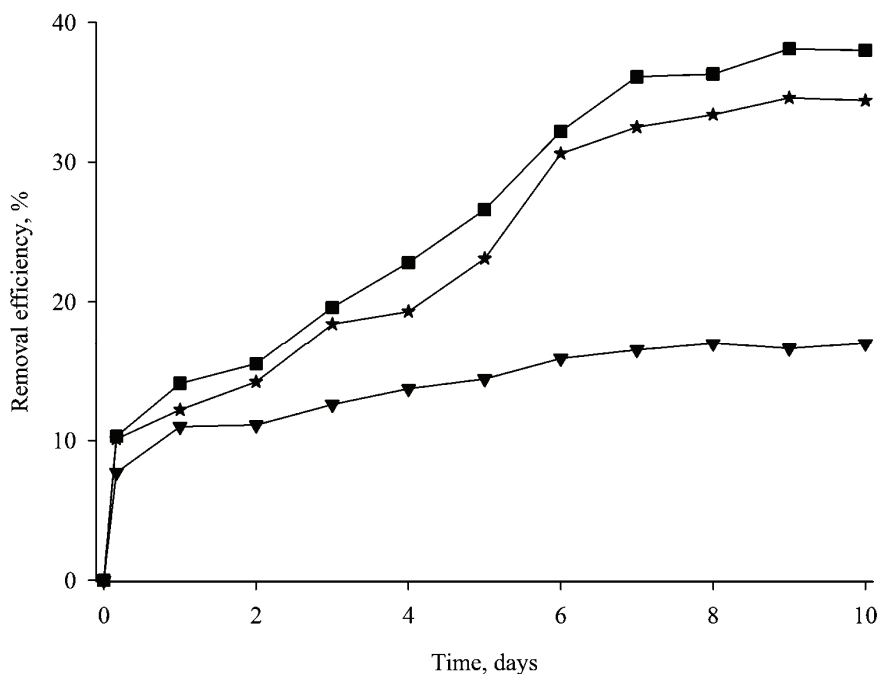

Fig. 4. Effect of the adsorption of phosphorus at different WIS dosages ($\blacktriangledown$, 1; $\bigstar$, 2; $\blacksquare$, 3 g L^{-1}).

dosages of 3, 2 and 1 g L^{-1}, respectively. The presence of Ca^{2+}, Mg^{2+} and other heavy metals in the excess sludge led to decreases in phosphorus removal by the sludge phase. Thus, adsorption removal of phosphorus in the process of excess sludge digestion was less than 16, 34 and 38 % at WIS dosages of 1, 2 and 3 g L^{-1}, respectively. The contribution of iron-reducing bacteria and hydrolytic bacteria (hyrolyze complex organics (carbohydrates, proteins and lipids to monosaccharides, amino acids, higher fatty acids and alcohols) in phosphorus removal was more than 32, 61 and 61 % at WIS dosages of 1, 2 and 3 g L^{-1}, respectively.

Effect of sterilization

Sterilization was used to determine the effect of iron-reducing bacteria and hydrolytic bacteria. As shown in Fig. 5, the concentration of phosphorus first increases and then decreases. However, the concentration of phosphorus in the reactor of unsterilized sludge decreases with the increase in time at all WIS dosages (Fig. 1). This finding indicates that sterilization can inhibit phosphorus removal, especially at the low WIS dosages. As shown in Figs. 1 and 5, the removal efficiencies of phosphorus are –6, 53 and 64 % in sterilized sludge and 39, 93 and 99 % in unsterilized sludge at WIS dosages of 1, 2 and 3 g/L, respectively. This finding indicates that iron-reducing bacteria and hydrolytic bacteria enhance 45, 40 and 35 % of phosphorus removal at WIS dosages of 1, 2 and 3 g/L, respectively.
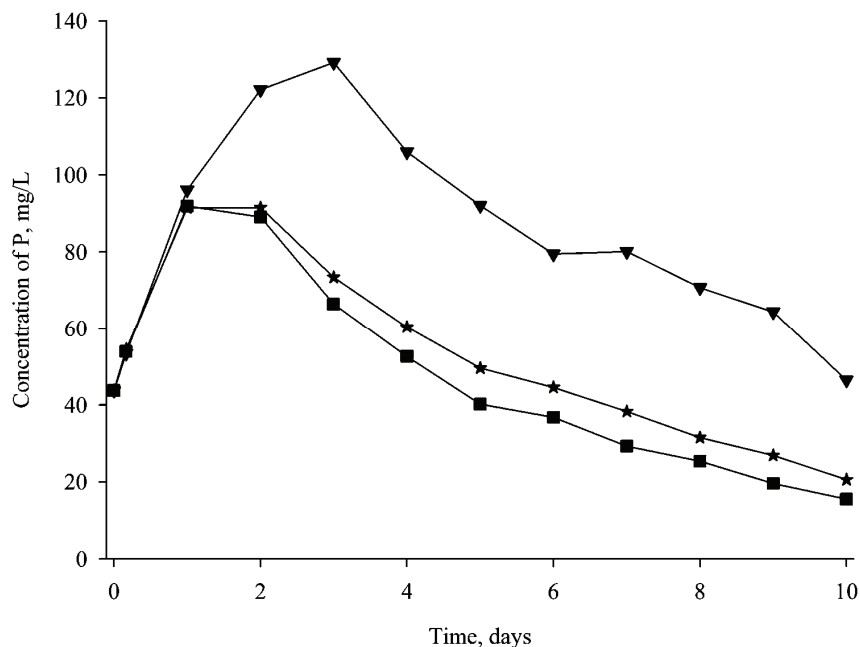

Fig. 5. Effect of sterilization on the removal of phosphorus (▼, 1; ★, 2; ■, 3 g L^{-1}).

Recovery of phosphate

Currently, fertilizer utilizes 80 % of the world's phosphate production. The production of phosphorus fertilizer from ores is non-renewable and should be considered unsustainable.[28] Thus, recycling phosphorus resources and gaining political and economic priority are important in the long term. A magnet is used for the removal of phosphorous from the sludge (3g L^{-1}) *via* three cycles of attraction for a 10-day treatment. During this process, WIS and the adsorbed phosphate can be fully attracted, while $Fe_2(PO_4)_2$ and $FePO_4$ are partially attracted due to their weak magnetism. The attracted substance was cleaned using distilled water and then transferred to a clean beaker. The attracted substance was dissolved using hydrochloric acid (1 mol L^{-1}). The results show that 56 % of phosphate was recovered. The attraction between the magnet and the removed phosphorus was (P+WIS) > $Fe_3(PO_4)_2$ > $FePO_4$. Thus, the recovered phosphorus was mainly in the form of phosphate adsorbed by WIS and partially in the form of $Fe_3(PO_4)_2$ and $FePO_4$.

Economic estimation

The iron scrap in the present study was waste and obtained free. No reagents were added in the entire process, except WIS. This method is characterized by high removal efficiency, easy and steady operation, low cost, recovery and reuse, making it better than other physical and chemical treatments.

CONCLUSIONS

The results of the current study indicate that WIS could effectively remove phosphorus from excess sludge. The highest phosphorus removal efficiencies at WIS dosages of 1, 2 and 3 g L^{-1} were 39, 93 and 99 %, respectively. The mechanisms of phosphorus removal by WIS were surface adsorption onto WIS, hydrolysis and bioreduction of WIS and precipitation of phosphorus by ferrous ions resulting from the action of hydrolytic and iron-reducing bacteria. The first and the most important mechanism of phosphorus removal using WIS is hydrolytic bacteria, which reduce the pH of the excess sludge that corrodes the WIS, followed by precipitation of phosphorus using ferrous ions. Phosphorus adsorption to WIS is the second mechanism, which is less than 16, 34 and 38 % at WIS dosages of 1, 2 and 3 g L^{-1}. This type of material may have broader applications because of its high phosphorus removal efficiency, abundant supply, and low cost. Using a magnet, 56 % of the removed phosphorus is recovered. This method is characterized by high removal efficiency, easy and steady operation, low cost, recovery and reuse, making it better than other physical and chemical treatments.

И З В О Д

УКЛАЊАЊЕ И САКУПЉАЊЕ ФОСФОРА ТОКОМ АНАЕРОБНЕ ОБРАДЕ ОТПАДНОГ МУЉА ДОДАВАЊЕМ ОТПАДА ГВОЖЂА

WEI ZHENG[1], XIAO MING LI[1,2], DONG BO WANG[1], QI YANG[1], KUN LUO[1], GUO JING YANG[1] и GUANG MING ZENG[1]

[1]*College of Environmental Science and Engineering, Hunan University, Changsha 410082, P.R. China* и [2]*School of the Environment, Guangxi University, Nanning 530004, P.R. China*

У овом истраживању проучавана је изводљивост уклањања фосфора при анаеробној преради отпадног муља додавањем отпада гвожђа (ОГ). Резултати показују да се ефикасност уклањања фосфора побољшава са количином ОГ, достижући ефикасност од 39, 93 и 99 % при дозама ОГ од 1, 2, односно 3 g L^{-1}. Стерилизација знатно умањује ефикасност уклањања фосфора, достижући само 6, 53 и 64 % при дозама ОГ од 1, 2, односно 3 g L^{-1}. Ово значи да бактерије које уклањају гвожђе и хидролитичке бактерије побољшавају уклањање фосфора за 45, 40 и 35 % при дозама ОГ од 1, 2, односно 3 g L^{-1}. Први и најважнији механизам уклањања фосфора помоћу ОГ су хидролигичке бактерије, које смањују pH муља да би нагризла ОГ, након чега следи таложење фосфора феро-јонима које генеришу бактерије које редукују гвожђе. Други могућ механизам је адсорпција фосфора на ОГ. До 56 % уклоњеног фосфора се сакупи помоћу магнета. Овај метод карактерише висока ефикасност уклањања, лак и континуалан рад, економичност и рециклабилност, што га чини бољим од других физичких и хемијских поступака.

(Примљено 5. фебруара, ревидирано 11. јуна 2012)

REFERENCES

1. D. Donnert, M. Salecker, *Environ. Technol*. **20** (1999) 735
2. L. E. de-Bashan, Y. Bashan, *Water Res.* **38** (2004) 4222
3. Y. Q. Wang, T. W. Han, Z. Xu, G. Q. Bao, T. Zhu, *J. Hazard. Mater.* **B121** (2005) 183
4. A. O. Babatunde, Y. Q. Zhao, *Chem. Eng. J.* **152** (2009) 8
5. C. J. Li, J. Ma, J. M. Shen, P. Wang, *J. Hazard. Mater.* **166** (2009) 891
6. T. Zhang, L. L. Ding, H. Q. Ren, Z. T. Guo, J. Tan, *J. Hazard. Mater.* **176** (2010) 444
7. I. Stratful, S. Brett, M. B. Scrimshaw, J. N. Lester, *Environ. Technol.* **20** (1999) 681
8. L. Pastor, N. Marti, A. Bouzas, A. Seco, *Bioresour. Technol.* **99** (2008) 4817
9. Y. N. Zhou, X. H. Xing, Z. H. Liu, L. W. Cui, A. F. Yu, Q. Feng, H. J. Yang, *Chemosphere* **72** (2008) 290
10. G. K. Morse, S. W. Brett, J. A. Guy, J. N. Lester, *Sci. Total Environ.* **212** (1998) 69
11. Y. Fu, S. L. Yu, *Desalination* **247** (2009) 442
12. K. Kaikake, T. Sekito, Y. Dote, *Waste Manag.* **29** (2009) 1084
13. N. Karapinar, *J. Hazard. Mater.* **170** (2009) 1186
14. J. A. Rentz, I. P. Turner, J. L. Ullman, *Water Res.* **43** (2009) 2029
15. Y. Liu, Y. G. Chen, Q. Zhou, *Chemosphere* **66** (2007) 123
16. D. B. Wang, X. M. Li, Q. Yang, G. M. Zeng, D. X. Liao, J. Zhang, *Bioresour. Technol.* **99** (2008) 5466
17. H. J. Li, Y. G. Chen, G. W. Gu, *Bioresour. Technol.* **99** (2008) 4400

18. D. B. Wang, X. M. Li, Q. Yang, W. Zheng, J. B. Cao, G. M. Zeng, X. Yue, T. T. Shen, T. J. Zeng, Y. Ding, *Sci. China, Ser. B Chem.* **52** (2009) 2358
19. D. B. Wang, X. M. Li, Q. Yang, W. Zheng, Z. Y. Liu, Y. L. Liu, J. B. Cao, X. Yue, T. T. Shen, G. M. Zeng, J. H. Deng, *Bioresour. Technol.* **100** (2009) 4005
20. C. Zhang, Y. G. Chen, *Environ. Sci. Technol.* **43** (2009) 6164
21. APHA, Standard Methods for the Examination of Water and Wastewater, 20th ed., Washington DC, 1998
22. EPA, *Water quality-Determination of Iron-phenanthroline spectrophotometry (HJ/T 345-2007)*, P. R China, 2007
23. I. Takacs, S. Murthy, S. Smith, M. McGrath, *Water Sci. Technol.* **53** (2006) 21
24. C. H. Guo, V. Stabnikov, V. Ivanov, *Bioresour. Technol.* **101** (2010) 3992
25. J. L. Nielsen, S. Juretschko, M. Wagner, P. H. Nielsen, *Appl. Environ. Microbiol.* **68** (2002) 4629
26. Y. Gao, A. Mucci, *Chem. Geol.* **199** (2003) 91
27. A. Drizo, C. Forget, R. P. Chapuis, Y. Comeau, *Environ. Sci. Technol.* **36** (2002) 4642
28. H. Mattenberger, G. Fraissler, T. Brunner, P. Herk, L. Hermann, I. Obernberger, *Waste Manage.* **28** (2008) 2709.